UNIVERSITY OF NAPLES PARTHENOPE

Department of Science and Technologies

PH.D. PROGRAMME IN ENVIRONMENTAL RISKS AND PHENOMENA
COORDINATOR: PROF. ENRICO ZAMBIANCHI
XXX Cycle

IOLANDA NUZZO

Ph.D. Thesis

Use of Low-damage Structural Systems in Loss-based Earthquake Engineering

TUTOR PROF. ENG. NICOLA CATERINO
CO-TUTOR PROF. ENG. STEFANO PAMPANIN
PROF. ENG. GIORGIO SERINO

2018

To my grandmother, hoping that one day I could
be 1/10 of the wonderful person she is

Acknowledgements

My PhD program has been continuously inspired by dynamism, that I believe is a keyword not only in the scientific approach of research study, but in life as general truth. I feel a very lucky person in having had the possibility of working with many different brilliant minds and no words can be found to acknowledge all of them.

First of all, my tutor, Professor Nicola Caterino, who has been constantly leading my way, teaching me the scientific method and providing important prompts for the achievement of better works. His meticulousness and dedication have become contagious, generating in me the wish of always reaching higher goals. I would like to thank him for the fundamental support he gave me and for the patience he had with me and my "obstinacy".

The presence of Professor Giorgio Serino in my professional and personal growth since, by now, several years, is of crucial importance for me. His capacity of decomposing complex and knotty issues in easier and user-friendly sub-components represents a very important teaching for me, not only in approaching scientific problems, but also in the everyday life problems. His positivity, passion, honesty and humility continuously encourage me in doing better, making him my mentor.

My research work has received a significant added value after meeting Professor Stefano Pampanin, at the University of Canterbury, in New Zealand. He is dynamism in person, always being everywhere around the world to share his great expertise and precious ideas. A special thank is dedicated to him, for the possibility he gave me in widening my knowledge and opening my mind in a so stimulating context, such as New Zealand is.

I also would like to express my gratitude to Engineer Luis Bozzo, suggesting new ideas for the development of interesting projects, looking for the fundamental meeting point between theory and practice.

A special thanks is for my colleague and friend Daniele Losanno, helping me to deepen my knowledge in specific fields and also supporting me when I was doubtful.

During these years I particularly appreciated to share my everyday adventures with all my numerous colleagues and friends Nicolò Vaiana, Donatella De Silva, Anna Bozza, Carolina Aiello, Piera Salzano, Valeria Iannuzzella, Giancarlo Ramaglia, Roberto Gentile, Fabio Palermo, Claudio D'Ambra, Houman Hadad, Umberto Vitiello, Stefano Belliazzi, Fabrizia Cilento, Claudio Balestrieri, Marta Del Zoppo…I would need too much pages to mention all of them. Thank you guys, also for all the regenerative coffee breaks!

The real engine of my force is my family. I would like to thank my parents, for all the love that they make me feel in happy and sad moments of our lives. They are always ready to support and encourage me, particularly in most difficult moments. A particular thanks is to my lovely sister, who is my best and special friend, present in all moments of my life.

I cannot miss to mention some of my dearest friends, Giuliana and Fabrizia, for all good moments we spend together, forgetting problems and just enjoying life together.

Last but not least, all my effort in overtaking any challenge would not exist without my best supporter and life team-mate, Lanfranco. I want to thank him for his love, sweetness and patience in taking always care of me.

Index

List of figures

List of tables

List of abbreviations and acronyms

ADAS = Added Damping And Stiffness

ADRS = Acceleration-Displacement Response Spectrum

B = Brace

BI = Base Isolated

BIM = Building Information Modeling

BF = Braced Frame

C = Contents

C_c = Contruction Cost

CBF = Concentrically Braced Frame

CDF = Cumulative Distribution Function

CP = Collapse Prevention

DB = Damped Brace

DDBA = Direct Displacement-Based Assessment

DDBD = Direct Displacement-Based Design

DM = Damage Measure

DV = Damage Variable

DS = Damage State

EAL = Expected Annual Loss

EBF = Eccentrically Braced Frame

EDP = Engineering Demand Parameter

EQ = Earthquake record

F = Frame

FF = Fixed-Fixed

FBD = Force-Based Design

FNF = Fixed-Not-Fixed

HDRB = High Damping Rubber Bearing

HYB = Hybrid (Re-centering/Dissipative Rocking system)

HVAC = Heating Ventilation and Air Conditioning

IDA = Incremental Dynamic Analysis

IDR = Interstorey Drift Ratio

IM = Intensity Measure

IM_d = Design Intensity Measure

IO = Immediate Occupancy

LDRB = Low Damping Rubber Bearing

LD-HYB = Low-Damage Hybrid

LOSD = Loss Optimization Seismic Design

LS = Life Safety

LTR = Loss ThReshold

MAF = Mean Annual Frequency

MBA = Moment Beam Analogy

MDF = Mean Damage Factor

MDOF = Multi-Degree Of Freedom system

MR = Magneto-rheological damper

MRF = Moment Resisting Frame

NS = Non Structural

NSASS = Non Structural Acceleration Sensitive System

NSDSS = Non Structural Drift Sensitive System

PACT = Performance Assessment Calculation Tool

PBEE = Performance-Based Earthquake Engineering

PBD = Performance-Based Design

PFA = Peak Floor Acceleration

PFA_fa = Peak Floor Acceleration of the floor above

PFA_If = Peak Floor Acceleration of the first floor

PFA_sf = Peak Floor Acceleration of the supporting floor

PGA = Peak Ground Acceleration

PGV = Peak Ground Velocity

PML = Probable Maximum Loss

PML_k = Characteristic Probable Maximum Loss

PP= Performance Point

Pre-Lam = Prestressed Laminated timber

PRESSS = PREcast Seismic Structural System

PSHA = Probabilistic Seismic Hazard Analysis

PT = Post-Tensioning

RC = Repair Cost

RC_{tot} = Total Repair Cost

RCR = Repair Cost Ratio

RDDI = Residual Deformation Damage Index

RPLV = RePLacement Value

RIDR = Residual Interstorey Drift Ratio

S = Structural

SA = Semi-Active control system

SDOF = Single Degree Of Freedom system

SEL = Scenario Expected Loss

SEWS = Seismic Early Warning System

SL = Shear Link

SPD = Shear Panel Damper

SSD = Steel Slit Damper

SUL = Scenario Upper Loss

SYC = Scorpion Yielding Connector

TADAS = Triangular Added Damping And Stiffness

VE = Visco-Elastic

CHAPTER 1

INTRODUCTION

The current seismic design approach pursues the achievement of specific performance objectives, according to the earthquake intensity and the facility's occupancy. This intent, at the base of the Performance-Based Earthquake Engineering (PBEE) framework, comes from the necessity of opportunely distributing socio-economic resources, thus investing more in structures important for the whole community rather than for individualities. The performance objectives, generally corresponding to a qualitative description of the structural state of damage, are translated into engineering parameters' limits, that are properly calibrated to accomplish the specific performance level. The structural seismic resistance is commonly achieved through the well-known concept of capacity design, according to which energy dissipation is provided by non-linear behavior of ductile systems.

The drawbacks of this design approach, typically targeting Life Safety under the design-level earthquake (i.e. 500 years return period for an ordinary building) have been highlighted during recent seismic events, such as the Canterbury sequence 2010-2011 in New Zealand. It was observed that many buildings reached the expected performance level, although generating huge repair costs or even irreparable tags. It emerged the urgent need of introducing design parameters allowing to gain controllable socio-economic losses. To this aim, many recent studies were

addressed to the investigation of new design damage indexes, commonly identified in the maximum drift, maximum residual drift and maximum acceleration, attempting to describe damage of both structural and different non-structural elements. Although, even when assuming that a global damage can be actually and reliably quantified, the challenge still remains that of defining an appropriate threshold corresponding to reasonable (i.e economically convenient) repair costs. Moreover damage's technical definition would always keep a communicative gap between the stakeholder, expecting for an earthquake-proof structure, and the designer, working towards an earthquake-resistant system. A different seismic design approach, overcoming the above mentioned issues, consists in directly assuming loss parameters as new performance measures, thus leading to the design of a system characterized by pre-defined, limited losses in case of seismic event, once recognized the impossibility of realizing a zero-loss facility.

To this aim, this work of thesis proposes a new multi-objective loss performance matrix, according to which the performance levels to be achieved are not identified any more by qualitative description of structural damage nor by specific engineering parameters (such as maximum drift or acceleration), but rather by the Probable Maximum Loss (PML). This indicator is the result of an intensity-based loss estimation analysis and describes which is the expected loss and the corresponding level of reliability, under the design hazard load. Inspired by the traditional PBEE approach, the herein proposed framework identifies different loss performance goals according to the intensity measure and the facility's occupancy. The employment of the suggested loss performance matrix requires the implementation of a new cost-based design methodology, proposed in this work, attempting to pursue the loss performance objectives.

If on one hand, in the aftermath of reality-check earthquakes, it is evident the need to take into account losses at the seismic design stage, on the

other hand it is obvious that the current design approach yields too damaged or irreparable facilities. Indeed, the excursion of structural elements into non-linearity unavoidably provides detrimental residual deformations. Accordingly, it emerges the necessity of upgrading performance targets to higher goals, that means generating reasonable repair costs of a structure under potential seismic loads that it is likely to experience. In last decades, research communities have provided a very important contribution to the investigation of innovative seismic design technologies, working with the intent of avoiding structural damage. Their implementation into real applications is generally discourage due to their higher construction cost. Although, if the initial investment is compared to the economy achieved in terms of repair costs caused by the design earthquake's occurrence, then the economic convenience of such technologies would be highlighted.

In light of all the motivations described above, the present thesis develops the design of a 5-storey-3-bay case-study structure, through the proposed cost-based approach, adopting different seismic control systems, namely traditional and low damage technologies. Intensity-based loss estimation analysis are performed for each technology through a numerical approach based on the use of Monte Carlo simulations. The different seismic solutions are then examined within a loss performance matrix, finding out the possible direct loss performance goals achievable by each of them. Finally, PML values are compared to the construction cost, analyzing if the initial investment is balanced out by the reduced repair costs.

This work of thesis is structured into several Chapters, organized as follows.

Chapter 2 presents, first of all, a wide overview on the PBEE concept, starting from the first seismic codes introducing a correlation between multi-objective performance levels and seismic intensities and, finally, describing literature proposals of challenging performance matrixes

explicitly including damage indexes. Earthquake loss estimation assessment is then introduced, focusing on its role in seismic risk classification. Traditional and innovative seismic control systems are presented, highlighting main issues concerning capacity design approach and describing different families of seismic control techniques, identifiable as active, semi-active, passive or hybrid systems.

Chapter 3 describes the existing literature concerning the definition and quantification of losses. In particular, both rigorous and simplified approaches are presented. Many existing software, performing loss estimation analysis, are mainly based on the use of numerical Monte Carlo simulations. Among them, the Performance Assessment Calculation Tool (PACT) is introduced, widely describing its mode of operation.

Chapter 4 first provides a literature review about possible uses of loss estimation analysis results, both as design parameters or critical measures for the optimization of alternative design criteria of new constructions or strengthening interventions of existing buildings. Then, an evolution of the traditional PBEE framework is proposed through a 3D loss performance matrix, that employs the PML as performance measure. The three axes of the new loss performance matrix show the seismic Intensity Measure (IM), the probability of loss, corresponding to the probability of exceeding a certain level of loss given a seismic intensity, and the Repair Cost Ratio (RCR), that is the repair cost (RC), caused by a certain IM, over the total RePLacement Value (RPLV) of the building/facility. Defining RCR and its probability of exceedance practically means defining PML, that is therefore briefly indicated herein as a new performance measure. In the perspective of suggesting a multi-objective loss performance matrix, several performance goals are associated to different PML values, that is pairs of Repair Cost Ratio (RCR)-Probability of loss-exceedance, according to the seismic intensity and the facility's social importance. The

employment of the proposed multi-objective loss performance matrix well suits with the application of a cost based-design framework, widely described in this Chapter, according to which specific loss performance goals have to be achieved.

In Chapter 5 the case-study building is introduced. It consists in a 5-storey-3-bay structure located in Norcia, where the Central Italy Earthquake stroke in 2016 (Mw 6.5). The structure is designed through the Direct Displacement-Based Design (DDBD) approach, supposing to employ different seismic solutions: a traditional Moment Resisting Frame, designed in the respect of the capacity design principle, a HYBrid re-centering rocking dissipative system (HYB), the same hybrid solution adopting Low-Damage non-structural components (LD-HYB), a dissipative Braced Frame (BF) characterized by the adoption of a particular shear link device and, finally, a Base Isolated (BI) system employing high damping rubber bearings. First, each of the innovative technologies is introduced, describing its working principle. Then the DDBD is applied, differentiating it according to the seismic control system. In particular, while consolidated DDBD approaches are employed for MRF and HYB solutions, a new methodology is proposed for the application to the dissipative BF system. Literature methods are instead applied to the BI case-study. The intensity-based loss estimation analysis is performed for 500yrs return period events, implementing a numerical approach through PACT and monitoring direct losses. Structural, non-structural and contents fragility components are selected from PACT database or literature studies. A specific fragility component is proposed for the shear link damper adopted in BF system, developing it from recent experimental tests. Main loss results are analyzed selecting specific values of PML, finally comparing the trend of Construction Costs and Repair Costs in correspondence of each seismic solution. Loss performances

achieved through the different control technologies are investigated within the proposed loss performance matrix.

CHAPTER 2

NEW CHALLENGES OF PERFORMANCE-BASED EARTHQUAKE ENGINEERING

This chapter presents, first of all, an overview on the Performance-Based Earthquake Engineering (PBEE) concept, starting from the first seismic codes introducing a correlation between multi-objective performance levels and seismic intensities and finally describing the current PBEE. The importance of introducing damage and associated loss in the designing framework is outlined. A literature review analysis of performance matrixes explicitly including damage indexes is addressed. Loss estimation assessment is then introduced, focusing on its role in seismic risk classification. Traditional and innovative seismic control systems are presented, highlighting main issues concerning capacity design approach and describing different families of seismic control techniques, identifiable as active, semi-active, passive or hybrid systems.

2.1 The Performance-Based Earthquake Engineering and accepted risk

Performance-Based Earthquake Engineering (PBEE) is a conceptual approach pursuing the design and construction of facilities satisfying pre-defined performance objectives under frequent and rare seismic loads

(Krawinkler and Miranda 2004). The choice of a specific structural achievement represents the need of satisfying the owner's expectations about the construction's protection against earthquakes, the meeting of the society minimum requirements in preventing excessive damage and human live losses and the designer's capacity of fulfilling these necessities within reasonable economic initial investment. The PBEE framework implies the need not only of properly defining the seismic action, but also of quantifying performance goals into engineering parameters and providing prescriptive measurements to meet them. The first seismic guideline indicating minimum performance objectives was the SEAOC Blue Book (1959), which correlated the intensity of earthquake ground motion to an accepted level of damage. Design criteria definition were still empirical and purely elastic, but the concept of the actual capacity design criterion was introduced, since performance objectives were mainly achieved providing sufficient ductility through detailing of local elements, in such a way maximizing the global dissipation capacity.

The milestone of PBEE was set by the Structural Engineers Association of California in the Vision 2000 report, cited as SEAOC (1995). They proposed the well-known framework given in Figure 1, according to which a discrete performance level corresponds to a discrete seismic design level depending on the importance of the building. In particular the report distinguished "basic", "essential/hazardous" and "safety critical" objectives, imposing more restrictive performance goals for constructions of higher importance and impact on society, such as hospitals and firemen stations (essential building) or nuclear power plants (safety critical structure). Performance levels were classified as "Fully Operational", "Operational", "Life Safe" and "Near Collapse", providing both a qualitative description of damage to structural, non-structural and content elements and quantitative limits of inter-story drifts in correspondence of each of them. Earthquake design level were differentiated in "Frequent", "Occasional", "Rare" and "Very rare" according to the return period

identified respectively in 43 years, 72 years, 475 years and 970 years. The key concept of PBEE consists in the definition of multiple performance objectives, given the facility's importance, associating structural and non-structural performance goals to different seismic intensities.

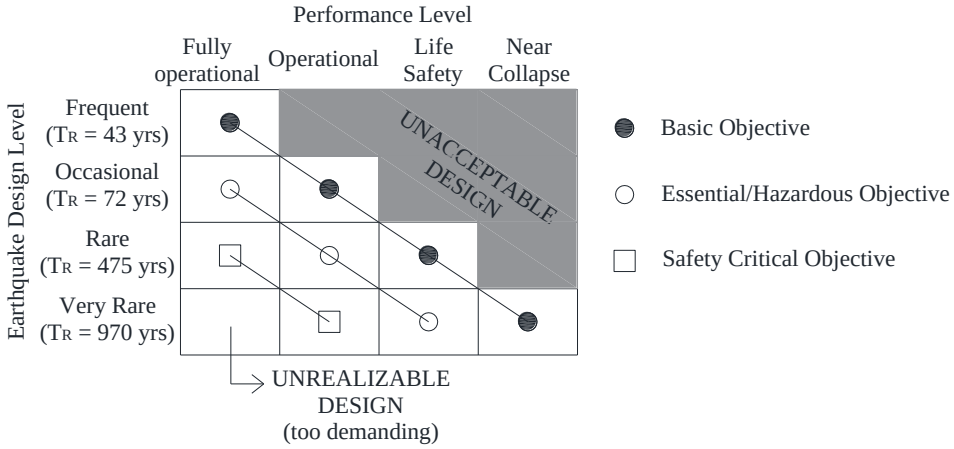

Figure 1 Performance objectives for buildings, recommended in SEAOC (1995)

During the same years the U.S. Federal Emergency Management Agency (FEMA) produced national guidelines for the seismic rehabilitation of buildings, known as FEMA 273 and FEMA 274 (1996), based on the discrete performance framework proposed by SEAOC (1995), but different from it, since considering respectively "operational", "Immediate Occupancy" (IO), "Life Safety" (LS) and "Collapse Prevention" (CP) limit states. These guidelines provided a great effort in traducing the performance levels into engineering demand parameters limits, delivering many quantitative rules and prescriptive acceptance criteria. The ATC-40 document (1996) was developed as seismic evaluation and retrofit guidelines of existing reinforced concrete constructions. It was based on the PBEE approach of the Vision 2000, introducing new analysis methods for the determination of target displacements, such as the capacity spectrum method.

All these American guidelines were defining the earthquake intensity through a probabilistic hazard analysis, but the performance assessment was purely deterministic since nominal values of strength, stiffness and deformation were employed. Conversely, several factors can influence the structure's functioning conditions during its nominal life, making its performance affected by aleatory condition: materials' resistance, for instance, can significantly vary during time due to ageing or to the interaction with atmospheric agents. Similarly, also vertical load actions can be quite different during the service life of a facility if we only think about accidental or snow loads. Thus the performance of a structure cannot be determined deterministically, but it must be associated to a certain level of reliability, that is the probability that the structure fulfils the specified requirements for which it has been designed within the working life. The complementary to 1 of the structural reliability represents the probability of failure, indicated as P_f. This means that each structural design implies a certain probability of collapsing, indicated as accepted risk, which must be kept very low but cannot be exactly zero, because this would be economically unfeasible. Thus the calibration of its maximum admissible limit, P_f^*, depends on the richness of the country and should be the result of political and socio-economic studies. Actually, safer structures correspond to lower values of P_f^*, unavoidably implying higher construction costs, and vice versa. The evaluation of the probability of failure represents the resolution of a reliability problem and it can be mathematically expressed introducing a performance function $G(x_1,.., x_n)$, depending on the vector $\overline{X}$ of aleatory variables $(x_1,.., x_n)$ influencing the structure's performance. A structure is considered to survive if $G > 0$ and to fail if $G \leq 0$. If R is the resistance and E the effect of actions, the performance function G is: $G = R - E$ with R, E and G random variables. An alternative measure of reliability is conventionally defined by the reliability index β, defined as the ratio between the mean value μ_G and the standard deviation σ_G of G when it is normally distributed, so that

$$\mu_G-\beta\sigma_G=0 \quad (1)$$

Thus

$$P_f=P(G\leq 0)=P\left(G\leq \mu_G-\beta\sigma_G\right)=\Phi(-\beta) \quad (2)$$

where Φ indicates the cumulative distribution function. For other distributions of G, β is only a conventional measure of the reliability.

According to European code for construction of earthquake resistant structures - EC8-Part1 (2003), "structures in seismic regions shall be designed and constructed in such a way that no-collapse and damage limitation requirements are met, each with an adequate degree of reliability". The performance criteria are intended to achieve two objectives, that are protecting human lives and minimizing repair costs. The first objective is achieved primarily by the provision of adequate strength and ductility, ensuring the structural protection from full or partial collapse during large, rare earthquakes occurring within building's design life. The second objective limits building's damaging caused by more frequent seismic events of lower intensity, which may occur in design life of structures, in order to minimize economic losses. Thus EC8 suggests design criteria based on the PBEE approach previously defined, but it introduces the concept of reliability, associating the satisfaction of a certain performance requirement in correspondence of a given seismic intensity to an "adequate degree of reliability". The reliability problem is discussed in EC0 (2002), which gives indications about acceptable reliability index values to be pursued in the performance-based design. Moreover it introduces the concept of "reliability differentiation", according to which the acceptable reliability index depends on the social importance of the facility and on the consequences' impact of its failure or malfunction. Indeed, allowing P_f^* values of basic constructions higher than values associated to buildings susceptible of large crowds, makes possible

an optimization of socio-economic resources to be used for construction works. The code classifies three consequences classes (CC1, CC2 and CC3), as indicated in Table 1, associating a reliability class to each of them (respectively RC1, RC2 and RC3). A minimum value of β is then indicated for each reliability class considering 1 and 50 years return periods, as given in Table 2.

Table 1 Definition of consequences classes - recommended in EC0 (2002)

Consequences Class	Description	Examples of buildings and civil engineering works
CC3	**High** consequence for loss of human life, *or* economic, social or environmental consequences **very great**	Grandstands, public buildings where consequences of failure are high (e.g. a concert hall)
CC2	**Medium** consequence for loss of human life, economic, social or environmental consequences **considerable**	Residential and office buildings, public buildings where consequences of failure are medium (e.g. an office building)
CC1	**Low** consequence for loss of human life, *and* economic, social or environmental consequences **small or negligible**	Agricultural buildings where people do not normally enter (e.g. storage buildings), greenhouses

Table 2 Recommended minimum values for reliability index (ultimate limit states) in EC0 (2002)

Reliability class	Minimum values for β	
	1 year reference period	50 years reference period
RC3	5.2	4.3
RC2	4.7	3.8
RC1	4.2	3.3

Finally, in order to assess if the performance reliability is "adequate", that means respectful of the minimum requirements provided by the code, it would be necessary to evaluate the probability of failure and compare it to the limit value. The P_f can be expressed as

$$P_f = \int_F f_{\overline{X}}(x_1, \ldots, x_n) d\overline{x} \tag{3}$$

where F is the failure domain, $f_{\overline{X}}$ is the Probability Distribution Function PDF of the vector $\overline{X}$. The resolution of a reliability problem, given its probabilistic approach, is not easy and it is believed incompatible to

professional applications. Consequently, EC0 (2002) introduced the semi-probabilistic approach, according to which both resistance R and effects of actions E are multiplied by partial factors indirectly accounting for uncertainties, thus providing design values R_d and E_d, corresponding to specific percentiles. This simplification leads the reliability problem to the comparison of scalar quantities that have to satisfy the relation $R_d > E_d$. If it happens, then the structure designed according to the use of given partial factors and in the respect of other prescriptions contained in Eurocodes, is generally considered to have a satisfactory β value (greater than the minimum limit).

2.2 Limitations of traditional PBEE and new perspectives

The challenge of realizing earthquake-proof structures is a worldwide matter which involves the interests of many countries throughout the globe. Since the last 40-50 years, when the first seismic codes were introduced both in Europe and overseas, important evolutions of the studies concerning Seismic Engineering have been pursued. The choice of a specific seismic structural system represents the result of an awkward balance between economic, political, societal and technical features. From an engineering point of view it could be possible to realize very stiff and massive infrastructures, hence limiting structural movement and damages. It is obvious that the unfeasibility of this solution stands in the high cost that would arise, as well as in the architectural cons concerning a bad organization of habitable spaces. It is from these considerations that the traditional PBEE framework, outlined in SEAOC (1995) and introduced in the previous section, associates several performance objectives to different seismic levels according to the facility's use, in the perspective of the multi-objectives PBEE. In particular, the more intense is the earthquake the lower is the reachable performance objective. More in detail, according to the earthquake design level and to the occupancy of the

structure, i.e. its social importance, it is suggested to design an earthquake-resistant system able to certain performance objective, but far away of being an earthquake-proof system. This implicates that an amount of damage is generally accepted. Most structures are designed according to the basic objective at Life Safety (LS) performance level, considering 475 years return period events. This essentially means preventing human life losses, but allowing significant structural damage. The conventional seismic design approach is based on the concept of capacity design: some structural elements are designated to be "sacrificial" fuses within the whole system, providing energy dissipation through their plasticization. The most common example of this type of designing method is the moment resisting frame (MRF), where the fuses are given by beam elements, since they are more ductile than columns and even because if yielded a global collapsing mode is generated, avoiding fragile soft stories. The main drawback of this sort of system is the residual damage which results after severe earthquakes in correspondence of structural elements. In recent seismic events, as 2010 and 2011 Christchurch earthquakes in New Zealand (Pampanin 2012, Mayes et al. 2013), but even oldest ones, as 1994 Northridge (California) and 1995 Kobe (Japan) earthquakes, several systems accomplished the performance objectives for which they were designed. Although, the result was the formation of irreparable plastic hinges within the end of beams, generating the necessity of demolishing the structures. Buildings owners' expectations about structural performances were largely higher, particularly considering that the cost of construction of the facilities was only a small fraction of the cost of disrupted operations and/or lost equipment and materials (Christopoulus and Filiatrault, 2006).

These observations highlight many problems concerning PBEE approach: even if the structure survives to earthquakes preventing human life losses and achieving the design performance objective, its irreparability represents the cause of high economic losses, due both to demolition and

reconstruction costs and to downtime. The term downtime indicates the amount of time necessary to recover the structural functionality and it is an important economic indicator, particularly in the case of industrial buildings or offices. Therefore, given the seismic intensity and the building's occupancy, the performance level should be enhanced to a repairable performance threshold in the PBEE framework. Consequently, several questions arise: what does reparability mean? Which crack width can be defined acceptable and which not? Past research studies have tried to find a definition of a damage index, which is generally defined as a number between 0 (undamaged condition) and 1 (collapse condition), and can be classified into two main classes: local and global indices. The former concerns damage in correspondence of structural elements or joints, while the latter refers to the state of the whole structure, and can be defined as a weighted average of local damage indices or through the comparison of respectively damaged and undamaged structural modal properties. First definitions of the local damage index used to simply associate damage with the ductility demand, so not taking into account the cumulative effect of repeated cycles of deformation, i.e. the absorbed hysteretic energy. More advanced local index expressions presented deformation-based and energy-based cumulative relations, in which damage was respectively correlated to the ductility concept covering repeated loading, and to the energy accumulated during the seismic action. Among them, the best-known and widespread one is the Park and Ang index (1985), resulting from the regression analysis of test data relative to more than 400 RC elements, reported in USA and Japan. Further proposals came from other authors, such as Cosenza et al. (1993), Stone and Taylor (1993), who proposed a damage index relation, expressed as a function of moment and curvature, analyzing 82 tests on CALTRANS circular bridge columns. Williams and Sexsmith (1995) suggested a damage categorization based on damage index classification. Pampanin et al. (2002) highlighted that deformation and energy-based damage index

can efficaciously predict structural failure performance level, but it is unable to properly describe the whole system reparability since most damage sustained by buildings during earthquakes is due to non-structural elements and contents. Conversely, a Residual Deformation Damage Index (RDDI) was proposed (Christopoulus et al. 2003, Pampanin et al. 2003), resulting to be an effective measure of the actual extent and reparability of damage when interpreted by means of a maximum-residual performance-matrix, as shown in Figure 2.

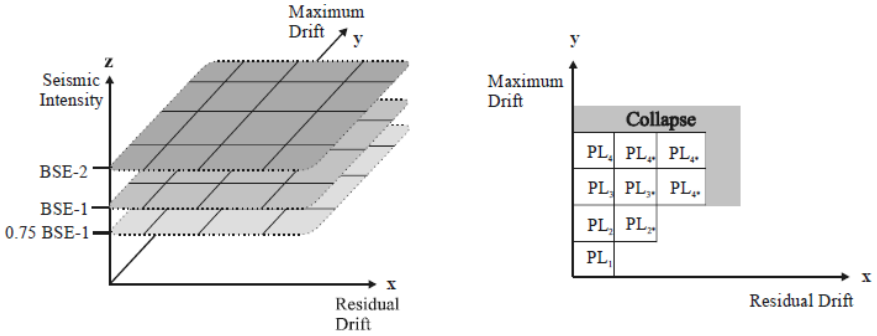

Figure 2 Residual Drift-based performance matrix for different intensity levels - Pampanin et al. 2002

Christopoulus and Pampanin (2004) proposed a Direct Displacement-based Design approach directly including expected residual deformation within the design framework.

Kam et al. (2010) proposed a 3D performance objective matrix considering maximum drift, residual drift and maximum acceleration on its axis (Figure 3). In this way, given the seismic intensity and the building's type and function, it is possible to define both the structural and non-structural performance levels, identified respectively by maximum drift - residual drift and maximum drift - maximum acceleration.

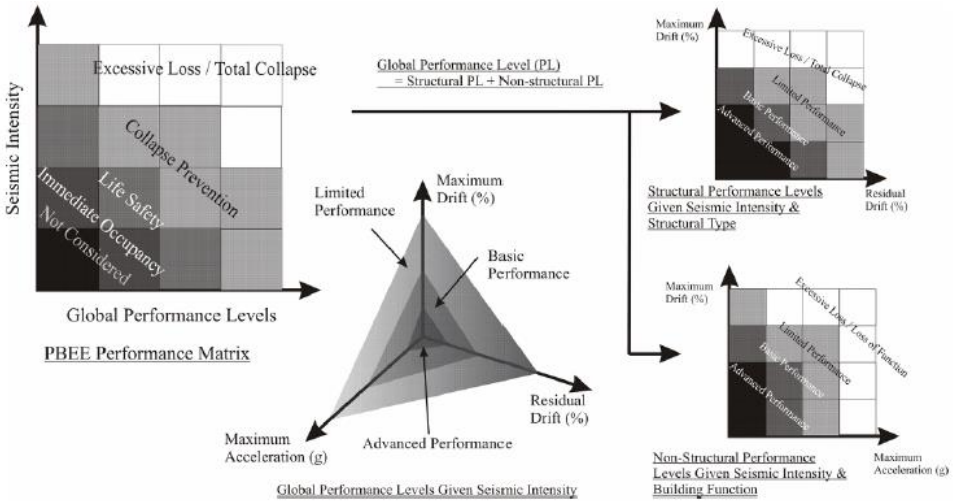

Figure 3 Global performance levels identified by structural and non-structural performance objectives - Kam et al. 2010

Actually, no codes account for maximum admissible floor accelerations, relevant indicators of damage to some non-structural components and contents.

Even when assuming that a global structural damage can be actually and reliably quantified, the challenge still remains that of defining an appropriate threshold corresponding to reasonable (i.e economically convenient) repair costs. Moreover damage's technical definition would always keep a communicative gap between the stakeholder and the designer.

Contrarily, a very different approach can be represented by the introduction of new performance measures within the PBEE framework, according to which losses caused by the design earthquake's occurrence are directly considered in the designing procedure. Indeed, damage measures can be expressed not only as discrete objectives, e.g. interstorey drift or other Engineering Demand Parameters (EDP) associated to different limit states, but also as continuum variables representative of losses, as qualitative indicated in Figure 4. In particular, economic losses,

expressed as percentage of replacement cost, casualty rate or length of downtime can be functional representation of losses, allowing to directly characterize economical and societal risks associated to the design of a certain construction under pre-defined seismic levels. The assessment of such performance measures, is the result of a complex probabilistic problem introduced in the following section and better characterized in Chapter 3.

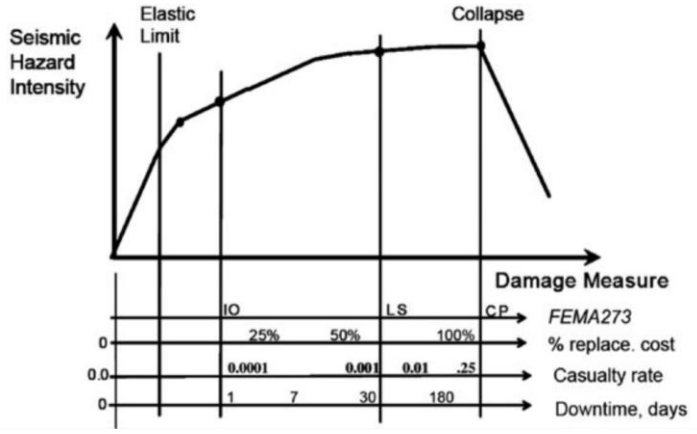

Figure 4 Conceptual comparison of different damage measures – Krawinkler and Miranda (2004)

2.3 Introduction to loss estimation assessment

Loss estimation analysis has the main objective of evaluating different loss parameters, defined as Decision Variables (DV). Its rigorous evaluation consists in the resolution of a multi-level integral, known as PEER equation (Cornell and Krawinkler 2000), addressed to Chapter 3.

If the loss analysis is performed for a given seismic intensity level, i.e. intensity-based analysis, the final DV will be the Probable Maximum Loss (PML). It corresponds to the Cumulative Distribution Function (CDF) of a certain loss parameter. Differently, if the loss analysis is repeated in correspondence of several intensity levels, a multitude of intensity-based

analysis is performed, thus realizing a time-based loss analysis. In this case, the final DV would correspond to the Expected Annual Loss (EAL), that describes the annual loss of the facility, independently from the specific earthquake that could occur.

Loss estimation is at the base of several buildings' rating systems which attempt to classify structures according to the seismic risk associated to them. The USRC (U.S. Resiliency Council) rating system (Platinum, Gold, Silver and Bronze) delivers information on building's expected safety, damage and recovery. The REDiTM (Resilience-based Earthquake Design Initiative) rating system distinguishes three different resilience-based classes (Platinum, Gold and Silver) according to functional recovery and financial loss, proposing a set of qualitative guidelines intended to minimize building damage (Almufti and Willford 2013, 2014). Italian guidelines (DM 65 2017) propose a simplified method to define buildings' seismic risk class (from A+ to G), based on EAL and on the Safety Index (IS-V), defined as the ratio between capacity and demand peak ground acceleration. Rating systems can increase market value of high class rated buildings and provide a better understanding of long-term risks, allowing governments and institutions to identify safe buildings and make strategic plans for reducing reconstruction costs and recovery time following major disasters. Finally, a further advantage gained from a loss estimation study is the fundamental support it can provide to insurance companies in order to define premium against earthquakes. Nowadays, the only countries where it is possible to get this type of insurance for the buildings are New Zealand, Turkey, Japan and California. Although, New Zealand is the only country where the 90% of people buy it, mainly because insurance against fire is mandatory for timber constructions, which are quite widespread in this region, and it automatically protects also against earthquakes. There is a flat premium to be paid by the client, while the rest is provided by the State. The choice of introducing the mandatory insurance against

earthquakes is a complex topic, which involves political, economic, societal and technical features, and goes beyond the scope of this work.

2.4 Innovative technologies in the PBEE framework

The PBEE framework sets the seismic design philosophy at the base of modern earthquake engineering. Current seismic design practice mainly promotes the capacity design concept. The general design approach aims to provide ductility, so energy dissipation, in correspondence of opportunely selected structural regions, able to undergoing nonlinear excursions without causing brittle failure mechanisms, such as soft-storey collapse (Figure 5). This principle was first introduced by professors Park and Pauley at the University of Canterbury in late 1960s, and is described by the well-known concept of the "weakest link of the chain" (Paulay and Priestley, 1992 - Figure 6).

Figure 5 Soft storey collapse mechanism - L'Aquila after the earthquake of April the 6th, 2009

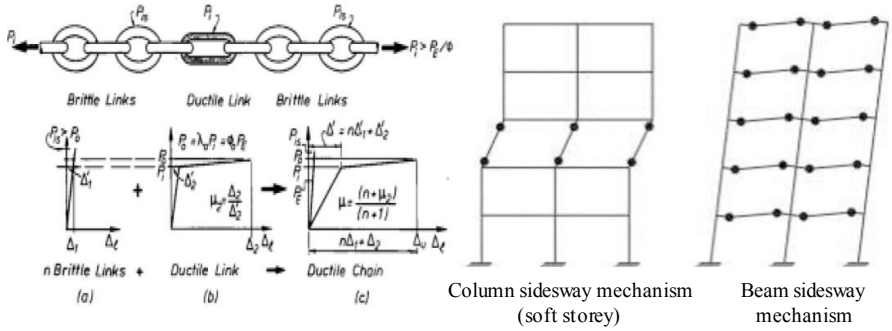

Figure 6 Capacity design philosophy - Paulay and Priestley 1992

The key words of the capacity design philosophy are ductility and structural redundancy. Indeed the higher is the number of static indeterminacy, the greater will be the number of possible plastic hinges forming in the structure. It is for this reason that moment resisting frames are able to dissipate wide amount of energy.

The structural ductile behaviour can be ensured respecting several requirements concerning material characteristics, details of longitudinal and transversal steel reinforcement in elements, type of elements collapse and hierarchy of strength among elements. The result is the design of cheaper structures, able to preserve human life losses with the compromise of allowing permanent deformations, which usually generate damages in the structural and non-structural elements. Indeed inelastic behaviour in critical regions of the structure often results in significant damages to the structural members. Critical regions have to be well detailed because hysteretic behaviour will degrade with repeated inelastic cycling. Further, the large inter-storey drifts, required to achieve significant hysteretic energy dissipation in critical regions, usually result in substantial damage to non-structural elements, such as infill walls, partitions, doorways and ceilings.

The PBEE recommends the minimum performance objectives to be achieved according to the earthquake intensity and the structure's occupancy or importance level. Consequently, performance levels are

associated to the maximum acceptable extent of damage and the subsequent losses, under a given earthquake intensity. This correlation results from the obvious impossibility of realizing a global earthquake-proof society and the consequent necessity of distributing capital resources, giving priority to essential buildings for the communities. Although, if losses in the post-event environment are considered, the socio-economical balance defining the performance objectives can be altered. In this perspective, the use of modern seismic control technologies, generally - but not necessarily - more expensive than traditional systems, can result economically convenient, comparing the initial, eventually, higher investment and the significant advantage of savings in terms of losses caused by an earthquake. The implementation of low-damage systems can "raise the bar" (Pampanin 2012, Kam and Pampanin 2012) of the targeted performance objectives, reducing structural and non-structural damages, as synthetically represented in Figure 7 (Pampanin 2009).

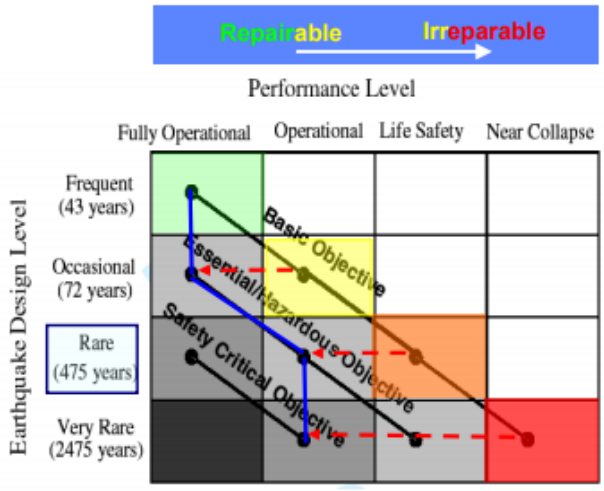

Figure 7 Arrangement of the traditional PBEE (Vision 2000) towards a damage-control approach - Pampanin 2009

Innovative structural control systems may be employed as alternative to the traditional seismic design. They are based on the installation of supplemental devices, typically aiming at reducing seismic demand to the main, hosting structure (Soong and Spencer 2002, Symans et al. 2008, Christopoulus and Filiatrault 2006). Different control strategies can be grouped into three main categories: passive, active or semi-active.

Passive systems, encompassing a range of materials and devices for enhancing structural damping, stiffness and strength, generally operate on principles such as frictional sliding, yielding of metals, deformation of visco-elastic (VE) solids or fluids and fluid orificing. According to FEMA 273, energy dissipation devices are classified as either displacement-dependent (friction or metallic devices), velocity-dependent (solid or fluid visco-elastic devices and fluid viscous devices), or other (superelastic materials, friction-spring assemblies with re-centring capability and fluid restoring force-damping devices).

While passive control systems are activated by the structural deformation induced by the earthquake, other types of seismic control need an external source of energy. In particular, in the case of active control, the enhancement of the structural performance is obtained by means of external forces, whose intensity varies during the earthquake, aiming at reducing the structural demand. A large amount of energy is needed to make the actuators work. Semi-active (SA) control systems are based on the use of variable devices, i.e. devices whose mechanical characteristics (typically stiffness and/or dissipating capacity) can be changed in real time during the excitation. The decision about the instantaneous calibration of such devices is taken through a control algorithm, according to the instantaneous characteristics of earthquake demand or structural response. This control system also requires a source of energy, however much smaller than that needed for active systems. In order to detect the earthquake input (feed-forward approach) or the structural response (feed-back approach), and to modify the device's properties, a framework of

sensors and a computer are required as well, as for active systems. This makes active and SA control systems quite more expensive than passive ones. Among the main advantages of SA control devices there is the fact that, with respect to a passive system, they can be adapted according to the characteristics of the incoming seismic event, so optimizing the structural response. Moreover, if a plausible black-out occurred during the earthquake, while an active system would fail because of the lack of energy, a SA system would work as a passive one, thus ensuring anyway a form of control.

In some cases, the introduction of a control system may improve the structural response from a point of view, while causing a worsening of other performance criteria. For instance, in the case of base-isolated structures, the installation of a flexible base system provides an elongation of the vibration period and thus a reduction of base moment and shear. On the other hand, it generates an increase of displacements, with consequent possible pounding problems for adjacent structures. In order to reduce the incidence of such disadvantages, different control devices can be installed to work together in a so-called hybrid control system. Dissipative devices are generally adopted for the aforementioned case of base-isolated structures (Kelly 1999).

Recent innovative studies have shown the possible use of SA control strategy in combination with a Seismic Early Warning System (SEWS). A SEWS can reveal in advance information about the intensity of an incoming seismic event: P-waves, faster than the destructive S-waves, are the first detected by the SEWS, so giving the possibility of predicting, on the basis of their characteristics, the main features of the latter. The first applications of the SEWSs were addressed to give the alarm and let immediate rescue operations. Today research is pushing in order to get important technical information about seismic events, like PGA (peak ground acceleration) or PGV (peak ground velocity), from a SEWS: these data can be used in order to adjust in real time mechanical properties of a

SA protection system installed on a given structure. This kind of combination has been firstly explored by Kanda et al. (1994), then by Pnevmatikos et al. (2004) and by De Iuliis et al. (2008), introducing the idea of modifying structural properties on the basis of an incoming earthquake's intensity measure, forecasted by a SEWS available at the site. Occhiuzzi et al. (2004, 2006, 2008a, 2008b) have developed an integrated seismic protection system where smart magnetorheological (MR) devices are calibrated on the basis of the incoming earthquake's entity given by a SEWS, through a control algorithm.

The combination of smart passive devices with the SEWS prediction allows to gain an important simplification of the SA framework, since the on-line continuous acquisition and processing of the structural response is not needed: no additional sensors are required. Nevertheless, the use of such a type of smart control system remains still quite more complex than other (passive) control systems. Although, its use allows the achievement of structural enhancement not only in terms of mean response against a set of seismic records (as seismic codes typically strictly require), but for any possible seismic input expected in the area of interest (Nuzzo et al. 2017).

CHAPTER 3

EARTHQUAKE LOSS ESTIMATION ANALYSIS

The present chapter describes the rigorous approach for the definition and quantification of losses, through the multi-level PEER integral. Main attention is given to the description of the mode of operation of the Performance Assessment Calculation Tool (PACT - FEMA P-58-1). This software, specific for buildings, is based on the use of numerical Monte Carlo simulations and allows to perform Scenario-based, Intensity-based or Time-based loss analysis. In the following chapter main required input data for a correct operating of the tool are described. Finally, some literature analytical simplified approaches are presented.

3.1 Rigorous approach to perform loss estimation analysis

In the attempt of developing a quantitative performance based methodology able to provide better informed decisions to stakeholders in assessing adequacy of a structure or its new design, PEER (Pacific Earthquake Engineering Research Center) community provided a probabilistic description of seismic performance assessment through the introduction of Decision Variables (DV). The latter generally refer to loss parameters, that could be direct or indirect. In particular, direct DV represents economic losses due to repair and/or reconstruction costs, while indirect losses are associated to injuries/casualties and downtime, that is

the time necessary to recover the facility's functionality after the occurrence of an event. Indeed, the disruption of activities, particularly in the case of commercial offices, can significantly influence losses. The DVs are often indicated as the 3Ds, that are Dollars, Deaths and Downtime.
Cornell and Krawinkler (2000) proposed a probabilistic evaluation of DV, providing the mean annual frequency λ (MAF) of economic loss exceeding a certain amount of dollars, through a disaggregation in terms of structural Damage Measures (DM) and ground motion Intensity Measures (IM):

$$\lambda(DV)=\iint G(DV|DM)\, dG(DM|IM)\, d\lambda(IM) \qquad (4)$$

where

G(DV|DM) is the conditional probability that DV exceeds a specified value given that DM is equal to a certain value
G(DM|IM) is the conditional probability that DM exceeds a specified value given that IM is equal to a certain value
λ(IM) is the mean annual frequency of IM.

The above multi-level integral, known as PEER equation, is nothing more than an application of the Total Probability Theorem. Its scope is to evaluate the mean annual frequency of DV (losses), from the analysis of the probabilistic distribution of it given observed DM (damages), which in turn are characterized by a certain probabilistic distribution given observed IM, having a certain annual frequency λ(IM).
A modified version was proposed by Krawinkler (2002), distinguishing structural response, indicated as Engineering Demand Parameters (EDP), from DM:

$$\lambda(DV)= \iiint G(DV|DM)\, dG(DM|EDP)\, dG(EDP|IM)\, d\lambda(IM) \quad (5)$$

where all the four variables (IM, EDP, DM, DV) are continuous independent random variables. Thus the probabilistic distributions of DM given EDP and of EDP given IM are introduced.

Each parameter involved in the PEER equation is the object of study of different disciplines: λ(IM) is the result of a conventional Probabilistic Seismic Hazard Analysis (PSHA) provided by seismologists and geotechnical engineers, G(EDP|IM) and G(DM|EDP) are the output of structural engineers work and require the knowledge of fragility functions for each potential damage state of each structural and non-structural component, while G(DV|DM) comes from cost estimators.

The value of λ(DV), relative to the whole building, can be computed as the sum of the MAF of economic loss exceedance of each j-th structural and non-structural component within the facility, indicated as $E[L_j]$ (Miranda and Aslani, 2002):

$$\lambda(DV)=E\left[L_{Bldg.}\right]=\sum_{i=1}^{n} E\left[L_j\right] \quad (6)$$

where n is the total number of components in the building, while $E[L_j]$ is the expected loss of the j-th component, and can be computed as

$$E\left[L_j\right]=\sum_{i=1}^{m}\int_{0}^{\infty} E\left[L_j|DM=dm_i\right]\, P\left(DM|EDP_j=edp\right)\, P\left(EDP_j>edp|IM=im\right)\left|\frac{dv(IM)}{dIM}\right| dEDP\, dIM \quad (7)$$

where m is the total number of damage states in j-th component and i is the indicator of the i-th damage state.

The PEER equation has been developed for mainshock, supposing that after its occurrence the damaged building is repaired to its original

condition (which is assumed to be non-deteriorating due to age). Actually, since the consideration of mainshock-damaged buildings in the aftershock environment can significantly influence economic loss and functional recovery, some studies have been proposed to include aftershocks in the seismic performance assessment (Yeo and Cornell 2005).

3.2 Implementation of numerical methods for loss estimation analysis

As introduced in the previous section, in order to perform a loss estimation analysis, first it is necessary to implement a PSHA study and get the hazard curve, representative of the mean annual frequency of IM. Then, a probabilistic evaluation of the response of the structure under the hazard load has to be determined, in terms of EDP. In particular, the demand indicators to be investigated have to be significant for the analysis of damage DM in the subsequent step, consisting in the probabilistic study of damage caused by that EDPs under IM. In order to achieve this result, fragility curves of all possible damageable components within the facility (structural, non-structural elements and contents) should be defined. Finally, a probabilistic study of losses distribution provides DVs.

Given the high dimensionality of the several random variables involved in the evaluation of the PEER equation, closed form solution are not always possible and consequently alternative numerical methods, such as Monte Carlo simulations, can be preferable (Baker and Cornell 2008). Such simplified approach allows to implement the integration using inferred statistical distributions of building response obtained from limited suites of analyses (Yang et al. 2009), which is at the basis of FEMA P-58 methodology.

Nowadays there are many tools which can be implemented in order to perform a loss estimation study, such as PACT (FEMA P-58-1 and FEMA-P-58-2, 2012), SLAT (Bradley 2009), SP3 (Baker et al. 2016) or others. In this work of thesis the PACT software is implemented. For this

reason, a description of its mode of operation and integrated methodology is provided.

3.2.1 Performance assessment calculation tool (PACT)

In order to solve the PEER equation, FEMA P-58 (2012) has developed a loss assessment framework integrated in the software PACT (Performance Assessment Calculation Tool). In order to implement it, main input information concerning each variable involved in the PEER integral must be provided by the user, i.e. seismic hazard curve, structural response, fragility curves, describing damage states of components within the facility, and finally consequences function, quantifying loss associated to each damage state. Through the use of Monte Carlo simulations the software randomly assesses, for each realization, the amount of repair cost, repair time and casualties.

Further data to be provided are the structural geometry, the total replacement cost and time to recover the structure's functionality, the total loss threshold, corresponding to the maximum loss over which it is economically preferable to re-build the structure. Main issues are discussed in the following sub-sections.

3.2.1.1 Seismic hazard definition

The user can choose to perform a scenario, intensity or time based seismic loss analysis. In a scenario-based analysis magnitude and earthquake specific location relative to the building site must be defined; then, through the application of an appropriate attenuation relationship, the target spectrum can be evaluated. Differently, in the case of an intensity-based simulation the user can choose any target spectrum consistent with the geologic characteristics of the site. Finally, the time-based analysis requires the definition of a seismic hazard curve (Figure 8), so providing

the MAF of exceedance of earthquake intensity; in this case at least 8 points of this curve should be selected and in correspondence of each of them the target spectrum has to be defined. Therefore, this case corresponds to the performance of multiple intensity-based analysis.

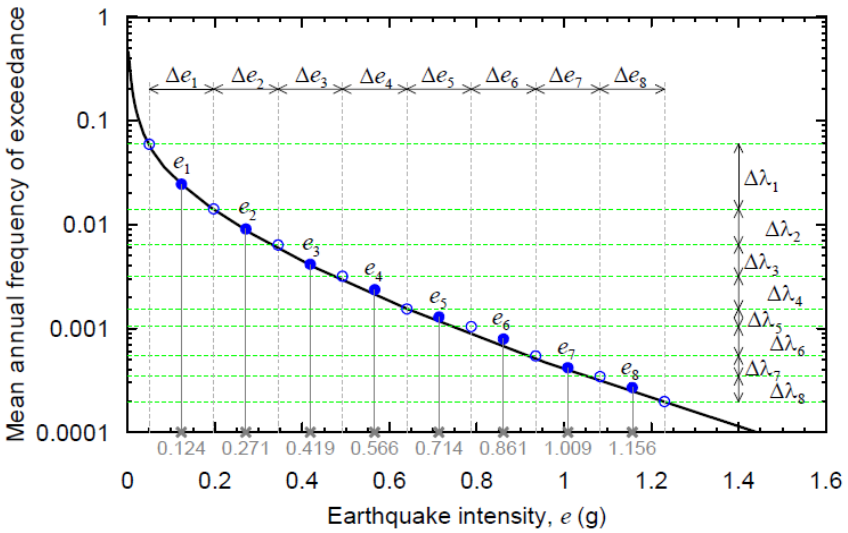

Figure 8 Seismic hazard curve (from FEMA P-58-1, 2012)

3.2.1.2 Engineering demand parameters evaluation

Once the target spectrum has been established according to the type of seismic hazard analysis, as previously commented, linear or nonlinear analysis has to be performed in order to get a set of EDP (generally inter-storey drifts, floor acceleration or velocity, in a particular direction at each level). In the perspective of realizing a non-linear dynamic analysis, for instance, a set or vector of EDP values could be calculated in correspondence of each record event considered. Collecting results relative to more records, a matrix of EDP would then be determined. Although, since the adoption of a limited number of EDP vectors would not be statistically significant and, at the same time, the realization of a higher number of analysis would require too computational effort, the

software generates N simulated vectors of EDP, where N is the total number of realizations in the Monte Carlo simulation, characterized by the same statistical distribution of the limited number of EDP vectors provided by the user's analysis (Figure 9).

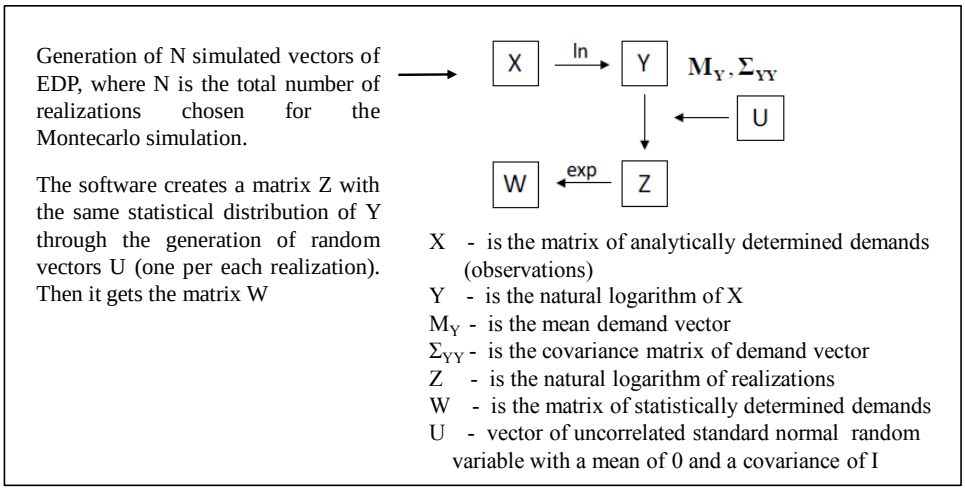

Figure 9 Generation of N simulated EDP values

3.2.1.3 Identification of damage measures: fragility components and performance groups

The user has to identify all the structural and non-structural (including furnishings) elements which may contribute to determine losses and define for each of them possible damage states and corresponding fragility curves. In particular, for each component sequential, mutually exclusive or simultaneous damage states (DS) can be defined. In the first case, DS can only occur sequentially, one after the other (e.g. Figure 10: beam-column joint).

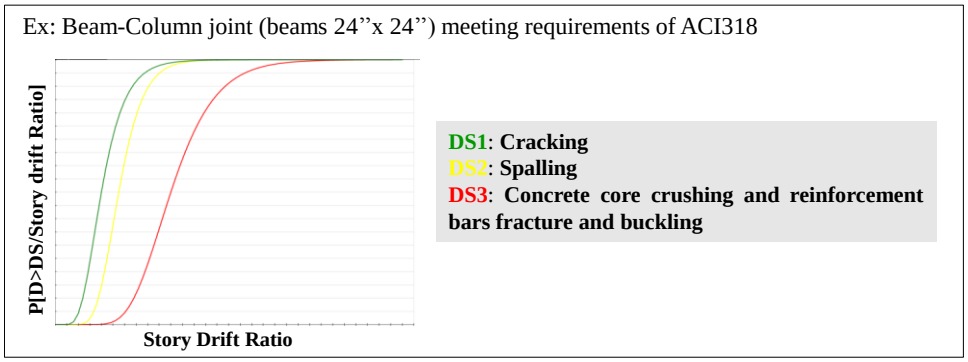

Figure 10 Example of sequential damage states fragility curves

Mutually exclusive DS exist when the occurrence of one damage state precludes the occurrence of another damage state. The probabilities for all mutually exclusive DS must sum to 100% (e.g. Figure 11).

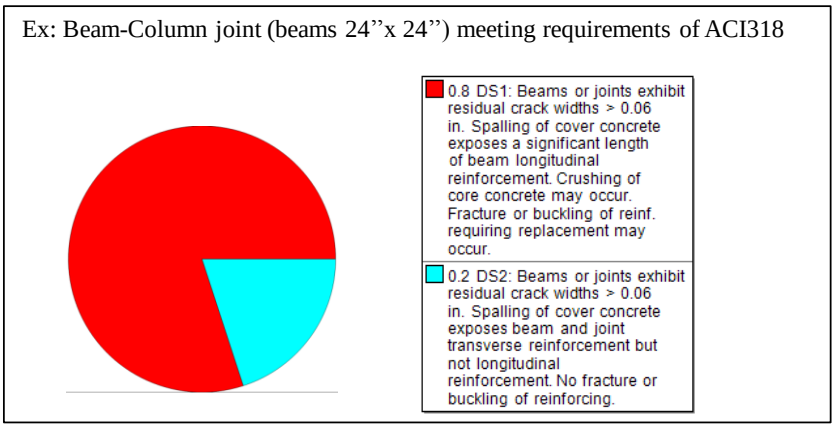

Figure 11 Example of mutually exclusive damage states

Finally simultaneous DS are independent and unrelated; the sum of the probabilities for all simultaneous DS will generally exceed 100% (e.g. Figure 12.

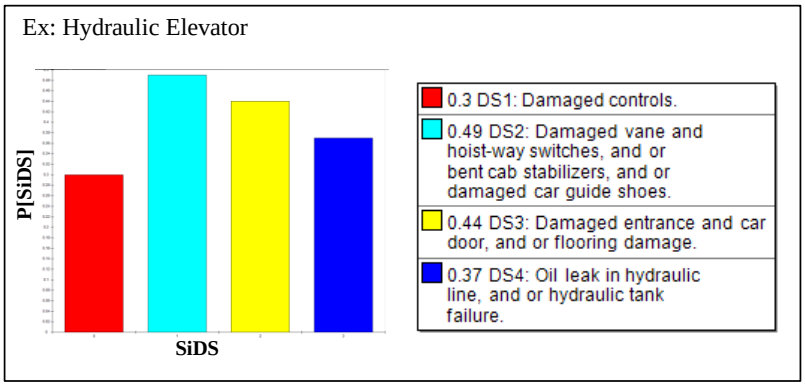

Figure 12 Example of simultaneus damage states

More than 700 fragility components are integrated in PACT software. All the fragility components which are subjected to the same EDP have to be assigned to the same performance group (Figure 13). A performance group is indeed a subset of fragility group components that are subjected to the same earthquake demands (e.g., story drift, floor acceleration, or velocity, in a particular direction, at a particular floor level). For each of them it is necessary to define the quantity per floor.

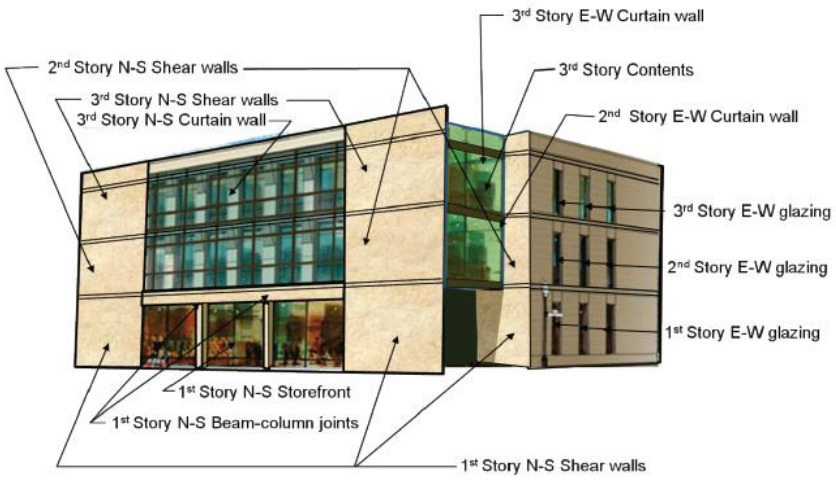

Figure 13 Performance groups identification

Moreover, also the whole structure fragility curve must be assigned by the user, in order to allow the consideration of eventual total structural collapse. This condition would, obviously, correspond to repair activities of site clearance and reconstruction. Finally, the structural irreparability curve should also be provided, as a function of the residual drift ratio. Indeed, there is a limit value of deformation over which the structure is deemed irreparable. This eventuality would correspond to a total replacement cost as well.

3.2.1.4 Definition of loss consequences

In correspondence of each fragility component, and in particular each DS, the consequences in terms of repair cost and time (Figure 14) has to be defined by the user. This allows the quantification of loss consequences when, at the end of a certain realization, a specific component is deemed to be in a given DS condition.

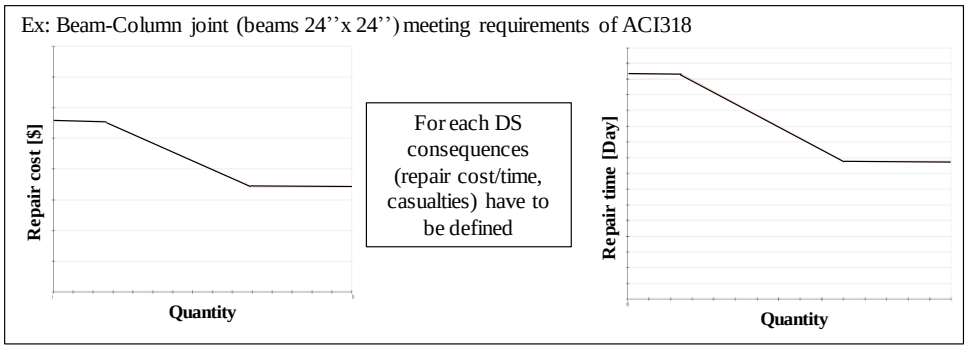

Figure 14 Repair cost and time consequence functions

Finally, in order to estimate casualties, the user must assign an occupancy population model (Figure 15), which provides the number of occupants per floor along with time.

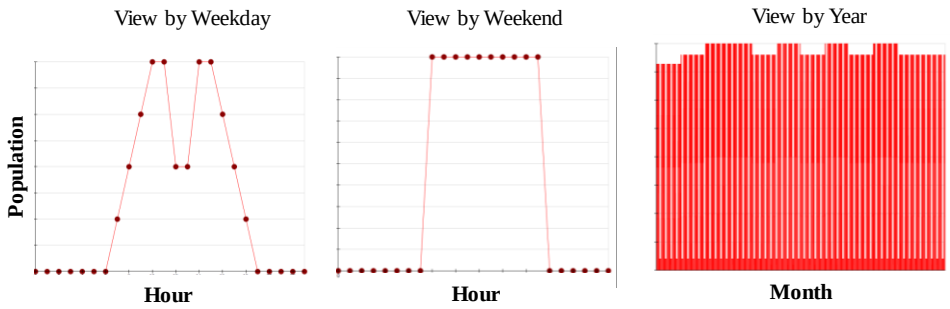

Figure 15 Occupancy population model

3.2.1.5 Loss assessment through PACT

Once all the above input data have been specified, the methodology framework, illustrated in Figure 16, allows to estimate repair cost, repair time and casualties in correspondence of the i-th realization.

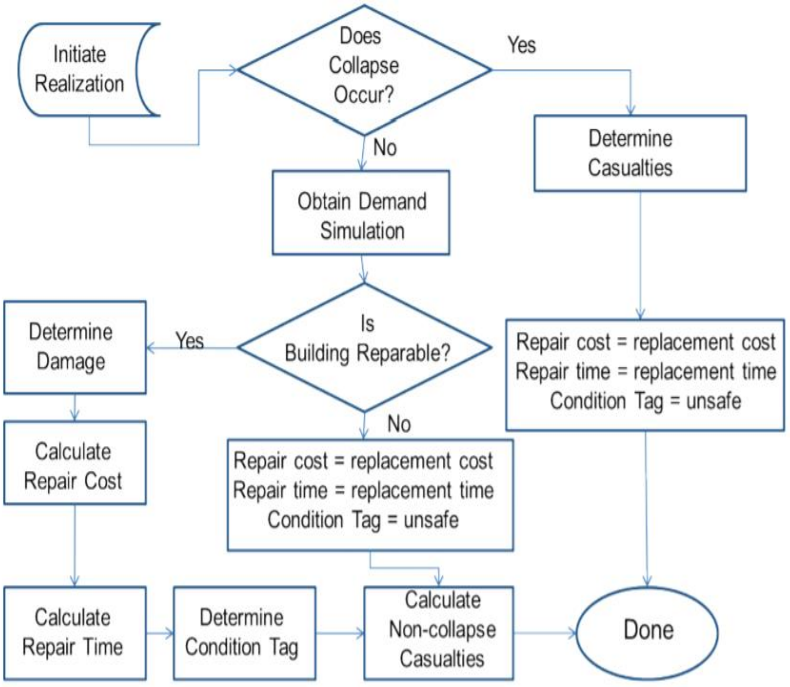

Figure 16 Methodology assessing a performance outcome in each realization (from FEMA P-58-1, 2012)

At the initiation of each realization, one vector of EDPs is selected among the N generated. The first step of the analysis consists in the eventual assessment of the structural collapse In order to assess this, the software employs the structural collapse fragility curve, providing the probability of collapse P_c, and randomly generates a number $1 \leq R_d \leq 100$ and establishes that:

- If $R_d \leq P_c$ → COLLAPSE
- Otherwise → NO COLLAPSE

This statement can be better understood considering the Venn diagram of Figure 17: knowing P_c, the collapse and non-collapse spaces can be distinguished. Through the random number generation, it is possible to statistically observe if the extracted number falls into the collapse or non-collapse range.

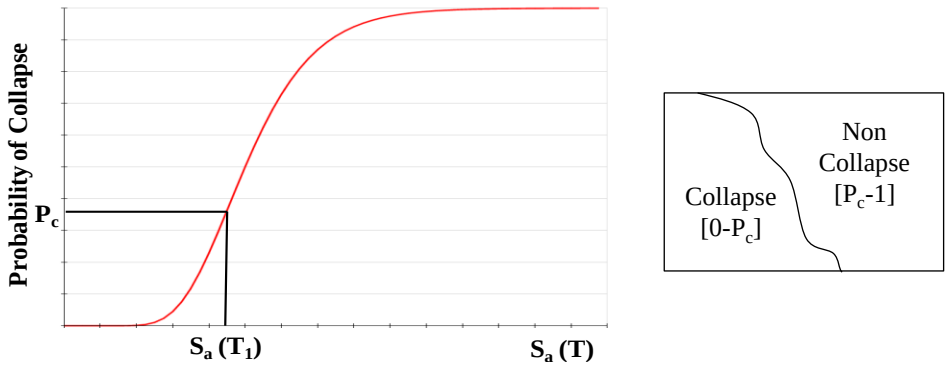

Figure 17 Evaluation of collapse and non-collapse condition

If collapse occurs, the software evaluates:

- Repair cost = total repairing cost
- Repair time = total downtime

If collapse does NOT occur, the software evaluates if the building is repairable or not: it enters in the irreparability curve in correspondence of

the maximum residual story drift and gets which is the corresponding probability of irreparability P_R. Again, it generates a random number $1 \leq R_d \leq 100$ and compares it to P_R:

- If $R_d \leq P_R$ → the structure is IRREPAIRABLE:
  - Repair cost = total repairing cost
  - Repair time = total downtime
- Otherwise → the structure is REPAIRABLE

In this latter case, in order to establish which are the reparability cost and downtime, it is first necessary to determine which is the level of damage in each component. More in detail, if the structure is repairable, knowing the EDPs, the software generates random numbers $1 \leq R_d \leq 100$ for each performance group. In correspondence of each fragility component belonging to a specific performance group, the software evaluates which is the level of damage comparing R_d with the probability of the component of being in a certain DS. As instance, if damage states are sequential, the software states that (Figure 18):

- If $R_d \leq (1\text{-}P_{DS1})$ → NO DAMAGE
- If $(1\text{-}P_{DS1}) < R_d \leq (1\text{-}P_{DS2})$ → DS1
- If $(1\text{-}P_{DS2}) < R_d \leq (1\text{-}P_{DS3})$ → DS2
- If $R_d > (1\text{-}P_{DS3})$ → DS3

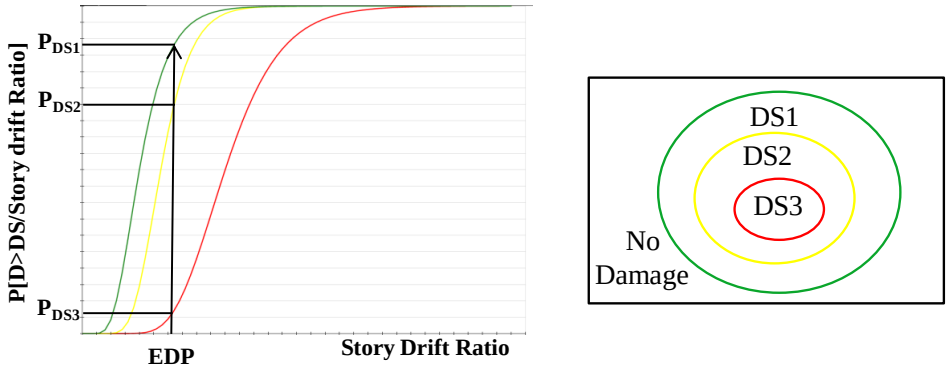

Figure 18 Evaluation of the DS in correspondence of a specific componenet

Once it has been established which is the DS, the corresponding consequences in terms of money, time and casualties are determined. This operation is repeated:

- in the same performance group for each component belonging to it if damage has been defined uncorrelated (it means that components of the same performance group can be subjected to different damage states);
- for each performance group.

At the end of each realization the corresponding loss in terms of money, time to repair and casualties will be determined, summing the contributions of all elements, and stored. The process is repeated for a high number of realizations (at least N=500); then loss data evaluated for each realization are sorted in ascending (or descending) order, finally getting the Cumulative Distribution Function (CDF) of loss (Figure 19) representing the probability of loss, hereafter defined as loss curve.

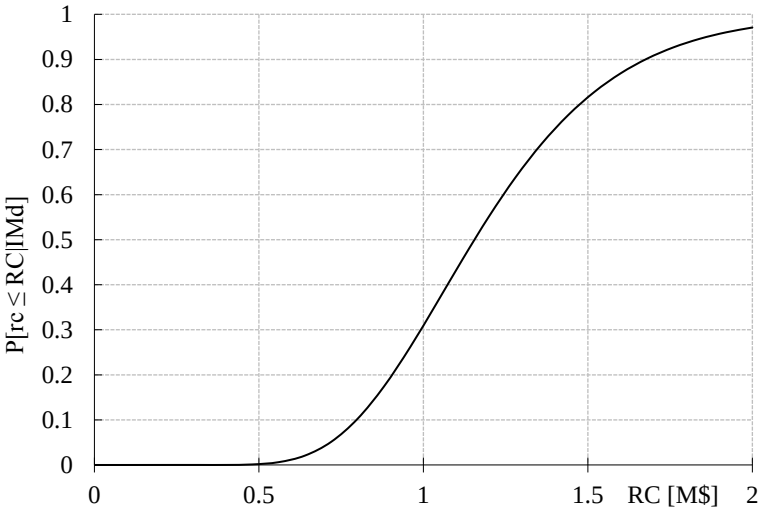

Figure 19 Example of Cumulative Distribution Function (CDF) of Repair Costs (RC), in output from PACT loss analysis

The loss curve is the output of an intensity-based loss estimation analysis and provides the Probable Maximum Loss, that is the loss under a specific intensity associated to a certain probability of not-being exceeded. In literature, specific values of PML, corresponding to particular probability of non-exceedance, have been defined (FEMA P 58-1), such as the Scenario Expected Limit (SEL), corresponding to the median value, or the Scenario Upper Limit (SUL), that is the 90° percentile. The mean loss is known as Mean Damage Factor (MDF). In this thesis a further indicator is introduced, that is the characteristic PML (PML_k), corresponding to the 95° percentile.

A time-based loss estimation analysis consists in the realization of a multitude of intensity-based analysis in correspondence of different intensity measures λ_{IM}. Evaluating the MDF value relative to each intensity-based analysis, allows to build the plot (λ_{IM} - MDF), as given in Figure 20. The hatched area under the curve is defined an Expected Annual Loss, consisting in the likely loss for any given year.

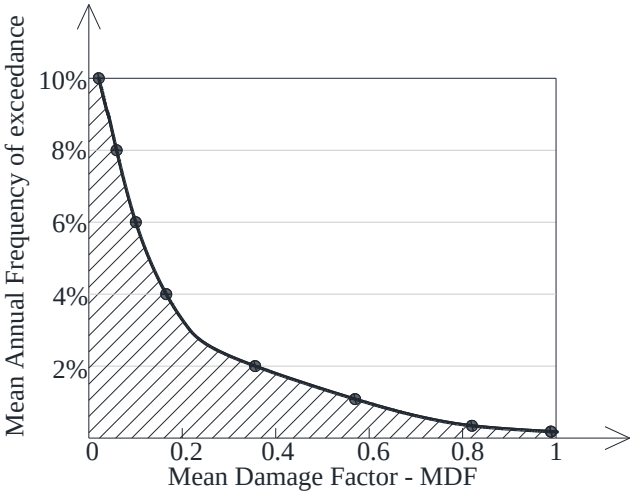

Figure 20 Expected Annual Loss (hatched area)

3.3 Simplified approaches to perform loss estimation analysis

In literature many simplified approaches attempting to estimate losses have been proposed. Among them, Welch et al. (2012, 2014) proposed a Direct Displacement-Based Assessment (DDBA) for simplified loss estimation of existing structures. In particular, the DDBA (Sullivan and Calvi 2011) allows a prompt evaluation of deformation demands in correspondence of different performance levels, with no need of executing non-linear analysis. The methodology aims to evaluate the Expected Annual Loss (EAL) through the definition of the Mean Damage Factor (MDF) in correspondence of different Limit States (LS), that are zero loss, operational, damage control and near collapse. The bounding LS are assumed to determine 0 and 1 MDF values respectively. Differently, MDF values corresponding to the two intermediate LS are evaluated through the EDP-DV functions proposed by Ramirez and Miranda (2009), once EDP have been estimated as an output of the DDBA procedure. These functions allow to associate damage and repair costs considering the expected inventory of components within the facility, according to its occupancy,

structural system and number of storeys. The EDPs considered are Interstorey Drifts Ratio (IDR) and Peak Floor Acceleration (PFA). Since the DDBA provides considerations only about deformation demand parameters, rough estimation of PFA is obtained through empirical approximations described within the ATC-58 (ATC, 2011). Each LS is associated to a specific hazard level: at zero loss LS the intensity is such to make the expected loss to commence; operational and damage control LS correspond to the transition region between frequent, low-intensity and rarer, high-intensity events; near collapse LS correspond to intensity level very rare, such to cause a total loss. The identification of the pair of points MAF (Mean Annual Frequency) and MDF allows to build the curve of Figure 21, in which the hatched area represents the approximated value of EAL.

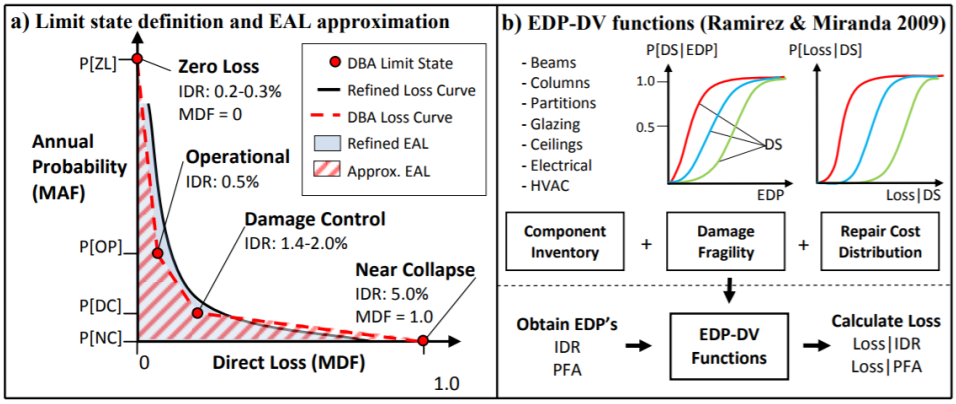

Figure 21 Evaluation of the EAL through the DDBA approach and implementation of EDP-DV functions - Welch et al. (2012)

The methodology provides only one set of EDPs through the DDBA approach, so the uncertainty of the likely structural response for a given intensity is not intrinsically considered. For this reason authors proposed corrective factors for the incorporation of uncertainty.

Vitiello et al. (2016) proposed a simplified loss assessment approach based on the use of static non-linear analysis. In particular, through the N2 method, in correspondence of each step of the pushover curve the PGA value, assumed to represent the hazard intensity causing that specific level of deformation, is identified. This simplification allows to promptly define the relation between the hazard intensity and the structural response (EDPs). Then, after identifying structural (beams, columns and beam-column joints) and non-structural (drywall partitions, electric and hydraulic systems) components, fragility curves and consequent direct losses at different damage states DS_j are selected from literature (Pagni and Lowes 2006, Aslani and Miranda 2005, Ruiz-Garcia and Negrete 2009) and assigned to them. The final EAL is estimated through the following expression:

$$EAL=\sum_{i=1}^{n}\sum_{DS_j}\bar{C}_{i,DS_j}\int P\left[DS_j|\overline{EDP}_j(IM)\right]g[IM|D]dIM \tag{8}$$

where n is the number of fragility components, $C_{i,DSj}$ is the functionality's recovering cost of damaged component at damage state DS_j, $P[DS_j|EDP_j(IM)]$ is the probability of occurrence of DS_j given EDP_j at the i-th component, g[IM|D] is the derivative of the seismic hazard curve given the site location's characteristics D.

CHAPTER 4

IMPLEMENTATION OF A COST-BASED DESIGN FRAMEWORK WITHIN A MULTI-OBJECTIVE LOSS PERFORMANCE MATRIX

This chapter is addressed to the proposal of an innovative PBEE framework, based on a 3D loss performance matrix employing the Probable Maximum Loss (PML) as new performance measure. The Repair Cost Ratio (RCR) is adopted as loss parameter, and corresponds to the repair cost (RC) over the total RePLacement Value (RPLV) of the building/facility. A qualitative multi-objective loss performance matrix is presented, suggesting several performance goals according to the seismic intensity and the facility's social importance. The employment of the proposed multi-objective loss performance matrix well suits with the application of a new cost based-design framework, widely described in this chapter through several main steps. The methodology first requires the application of a Direct Displacement-based Design (DDBD) approach. Main differences between Force-Based and Displacement-Based design methods are presented. Then, in order to apply the cost-based design framework and check the achievement of the loss performance objectives, an intensity-based loss estimation analysis has to be performed.

4.1 Introduction

The Performance-Based Earthquake Engineering (PBEE) framework, outlined in SEAOC Vision 2000 (1995), provides the seismic design philosophy at the base of modern earthquake engineering. Although, there is an urgent need of involving considerations about expected damage and economical losses along the service life of the structure in the design process. To this aim, many important contributions have been proposed, as commented at §2.2. Although, the challenge of defining the maximum acceptable threshold (i.e. allowable repair costs) of such damage parameters, to be associated to various performance levels, is still open. Moreover, the damage index reparability limit would probably be not univocal for different structural typologies. For example, suppose that both a reinforced concrete Moment Resisting Frame (MRF) and a Base Isolated (BI) systems are subjected to the same amount of residual top displacement in the post event scenario of a severe earthquake. The MRF system is severely damaged, optimistically according to a global mechanism failure, presenting plastic hinges at the base of ground floor columns, deformed in such a way to cause the top residual displacement. Differently, the BI system probably presents failure in correspondence of base isolators, that did not re-centred properly, causing the top residual displacement. Both systems would be accordingly red-targeted, but implying repair intervention activities so different that it would be very difficult to state that damage observed in the two cases would yield the same economic consequences. After all, Ghobarah (2015), after collecting analytical and experimental data to study the correlation between drift and damage of various reinforced concrete structural elements and systems, found out that the dispersion of drifts at different damage levels was significant among members and systems analysed.

Moreover, in order to take into account damage of structural but also non-structural elements and contents it is necessary to introduce several

parameters, and then define for each of them the acceptable threshold corresponding to allowable losses.

The PBEE framework, defining design performance objectives as a function of specific discrete parameters, either explicitly accounting for damage or not, creates a gap between stakeholder's expectations about seismic structural performance and the reality.

A prompt way of by-passing the above mentioned issues consists in the assumption of direct (repair costs) and/or indirect (injuries/casualties and downtime) loss performance measures. Indeed, the latter can be converted into economic losses through local socio-economic relations, quantifying monetary value of downtime and loss of human lives. As a matter of fact, lost money identifying different performance levels would be univocal, all-encompassing if properly evaluated, and univocally understood by non-technical stakeholders, such as owners, insurers and decision-makers.

In order to perform Performance-Based Design (PBD) adopting loss performance measures, it is necessary to provide useful prescriptions so that the loss performance assessment yields desired results, becoming more a verification than an iterative design. From this observation, Krawinkler and Miranda (2004) introduced a design approach based on acceptable losses, according to which a design alternative is chosen if able to satisfy target demand values, corresponding to acceptable monetary loss, for a spectral acceleration $S_a(T_1)$ at a given hazard level (Figure 22). In particular, the authors proposed to split the whole facility in three subsystems, respectively representing Structural System (SS), Non-Structural Drift Sensitive System (NSDSS) and Non-Structural Acceleration Sensitive System (NSASS). The total loss corresponds to the summation of the three parts. In correspondence of each subsystem the function relating expected loss to Engineering Demand Parameter (EDP) is assumed to be known. The first step of the proposed procedure is to choose the design acceptable loss in correspondence of a specific hazard level. Then, entering in the expected loss-EDP function (lower portion of

Figure 22) in correspondence of the design expected loss, the corresponding EDP is known. Similarly, from the hazard curve (upper left portion of Figure 22) it is possible to read the spectral acceleration corresponding to the design hazard level (i.e. the one relative to the acceptable loss). The intersection of the two estimated quantities defines the design target in the upper right portion of Figure 22: all systems crossing S_a to the left of the target design are feasible because the associated EDP, hence loss, is lower than the maximum limit.

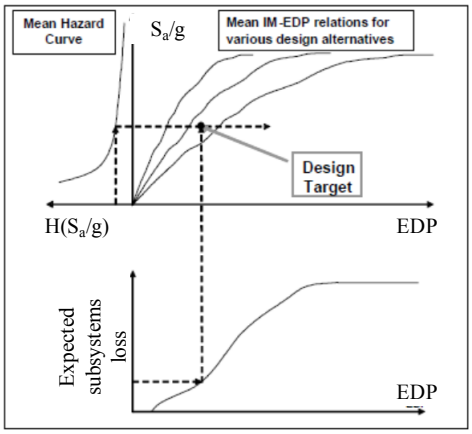

Figure 22 Designing for acceptable monetary loss - Krawinkler and Miranda (2004)

According to this approach, statistical state-of-art results and engineering judgement are employed in order to get expected loss directly as a function of EDP. Indeed, there is an important lack of data that makes the application of this method, albeit conceptually straightforward, even impossible.

More recently, Dhakal (2011) suggested a multi-objective seismic design procedure, defined as LOSD, "Loss Optimization Seismic Design", that considers the minimization of financial loss in addition to Life-Safety performance criteria. In particular, the author proposes to express performance goals through the RDI format, consisting in the definition of three parameters, that are the allowable mean values of repair (R) cost of

damaged components and replacement cost of damaged content (expressed as a percentage of the total replacement value of the building), the number of days to recover the facility's functionality (D) and the injury vector (I). Each arrangement of allowable RDI parameters correspond to a specific seismic intensity.

In many studies loss performance measures are assumed as critical decision parameters for the optimization of alternative design criteria of new constructions (Bradley et al. 2009, Cutfield et al. 2014, Cimellaro et al. 2015, Dang et al. 2015, Bovo et al. 2017) or strengthening interventions of existing buildings (Aslani and Miranda 2005, Marriott et al. 2009, Beetham 2013, Ligabue 2015, Vitiello et al. 2016), often representing a crucial measure in Life-Cycle Cost or decision-making analysis. In some applications loss indicators are used to quantify the environmental impact of building wastes, in the aftermath of an earthquake scenario, within a life cycle environmental assessment (Alirezaei et al. 2016).

Baker et al. (2016) implemented the FEMA P-58 procedure in relation to 10 buildings belonging to Christchurch's Central Business District (CBD), comparing estimated economic loss and recovery time to data collected after 2010 and 2011 earthquakes. A similar study, concerning the validation of loss assessment of existing reinforced concrete buildings that experienced the 2009 L'Aquila earthquake, has been developed by Del Vecchio et al. (2017).

In the present work, an evolution of the traditional PBEE framework is proposed through a 3D loss performance matrix that employs the Probable Maximum Loss (PML) as performance measure. The PML is the result of an intensity-based loss assessment analysis and provides the probable repair cost induced by a specific earthquake intensity. The three axes of the new loss performance matrix respectively show the seismic Intensity Measure (IM), the probability of loss, corresponding to the probability of exceeding a certain level of loss given a seismic intensity, and the Repair

Cost Ratio (RCR), that is the repair cost (RC) over the total RePLacement Value (RPLV) of the building/facility. Defining RCR and its probability of exceedance practically means defining PML, that is therefore briefly indicated as new performance measure herein.

The qualitative shape of the loss performance matrix is illustrated in the following section, discussing the expected trend of RCR as a function of the probability of loss, for a given earthquake intensity level. The use of the proposed approach allows to associate building's damage directly to the consequent economic loss. The maximum allowable damage state can be correlated to the maximum amount of repair cost that the stakeholder or the insurance accept to provide. According to the accuracy of the loss analysis performed, both direct and indirect losses can be considered. In this way, a direct communication between the stakeholder and the designer is possible, providing higher awareness about the (expected) amount of repair costs (time and money) to face in case of a seismic event. Although, in this work only direct losses are considered.

Through the use of a loss performance matrix, it is possible to implement a cost-based design in which the designer selects the allowable RCR and the maximum (acceptable) probability of loss associated to it. Consequently, the PML can become a key design parameter. The design process would be iterated until the design loss conditions are satisfied (Nuzzo et al. 2018). Accordingly, the proposed approach appears more as an iterative cost-based design procedure or cost-based assessment. Future research developments should be able to provide the engineers with dedicated charts associating PML to EDP (Engineering Demand Parameters) and IM, thus allowing for a direct control/design of the building system economic performance.

4.2 A new loss performance matrix

A new loss performance matrix is proposed in the attempt to provide higher awareness of economic losses involved in the case of a severe seismic event. Generally, in traditional PBEE framework, performance levels correspond to a qualitative description of structural and non-structural damage and are associated to discrete performance measures through Engineering Demand Parameters, EDP, such as interstorey drifts, floor acceleration, or others. Instead, in the herein proposed approach, the PML, Probable Maximum Loss, is assumed as key and overarching performance measure. In order to determine the PML, an intensity-based loss estimation analysis should be performed, that means assessing loss at a given seismic intensity level, e.g. design hazard level. Differently, if the loss analysis is repeated in correspondence of several intensity levels, a multitude of intensity-based analysis is performed, thus realizing a time-based loss analysis. In this case, the final DV would correspond to the Expected Annual Loss (EAL). This latter parameter provides a broad and important set of information, as it describes the annual loss of the facility independently from the specific earthquake that could occur. On the other hand, the parameter PML is strictly correlated to the seismic intensity used to perform the assessment, thus provides knowledge about expected loss during the service life of the facility under the design-level earthquake. Although less complete, PML is also less computationally demanding than EAL. Moreover it provides a very important information, that is the probable maximum loss to face in case of the design earthquake's occurrence, against which the structure has been specifically designed. These data can be very useful for government's institutions in preparing urban emergency plans. For these reasons, PML is assumed in this work as key performance measure in the loss matrix. An integrated version of the same matrix, out of the scope of this thesis, would combine both PML and EAL as loss indicators.

The 3D loss performance matrix (Figure 23 - left side) associates different PML values, that is pairs of Repair Cost Ratio (RCR)-Probability of loss-exceedance, to different loss performance design levels, according to the seismic intensity IM. In particular, the lower are both RCR and corresponding probability of loss, the better is the facility's performance in terms of losses under the design earthquake level, yielding towards an ideal design. Conversely, when a system provides low probability of loss in correspondence of high values of RCR, it means that it is susceptible of significant damage, as well as a system characterized by high probability of loss associated to small repair cost values. When PML values are not satisfactory because RCR and/or its probability of exceedance are too high, the building's design is defined unacceptable, since economically unrepairable. The gradual passage from ideal to unacceptable design is progressively less severe as the design seismic intensity (IM_d) level increases.

Given a fixed level of seismic intensity, the 3D loss performance matrix is reduced to a 2D version, as shown in Figure 23 - right side. Actually, a PML or loss curve, i.e. the curve associating the probability of loss to RCR, corresponds to a specific level of Intensity Measure. Considering the 2D loss matrix, the probability of exceeding a certain loss given a fixed intensity level is reported on the vertical axis. Conversely, on the horizontal axis RCR is presented within a range between 0% (no loss) and 50%, considered as the maximum loss threshold for which it is economically feasible to repair the facility (FEMA P-58-1 2012).

Superimposing the loss curve to the 2D loss performance matrix is the way suggested herein to check the achievement of a performance objective.

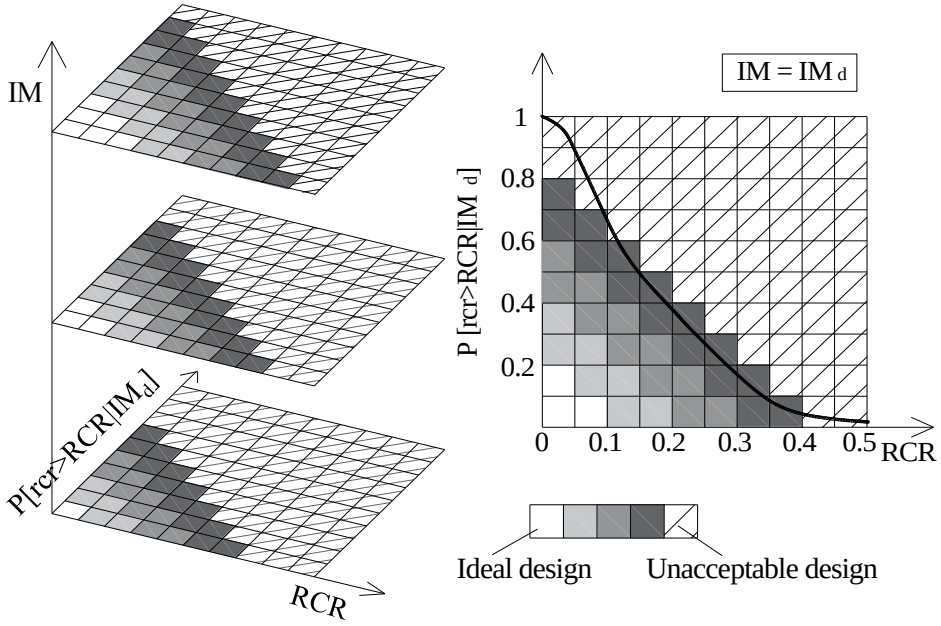

Figure 23. Loss performance matrix in 3D (left side) and 2D (right side) views

This approach could be usefully involved within a cost-based design framework, introduced in the next section. According to such methodology, a building would be designed for a certain seismic hazard such that the maximum acceptable repair cost is associated to a minimum defined level of probability of loss (Nuzzo et al. 2018). As a matter of fact, through a loss analysis, it is possible to appreciate the (expected) probability of loss associated to the design RCR value and decide if it is deemed acceptable. The lower the RCR the higher the probability of exceeding it under the given level of earthquake intensity. An ideal design corresponds to a system able to provide low probability of loss (e.g. lower than 10%) associated to low design repair cost (e.g. RCR ≤ 10-15%). As the IM increases, the PML curve is shifted to higher values of loss (left side of Figure 24).

In some cases it could happen that there is no correspondence between the allowable RCR value and the acceptable probability of loss, given IM. Then it can be necessary to implement low-damage technologies to reduce

the probability of loss. For example, consider the right side of Figure 24, where alternative technology-based performance-objectives are represented within a loss performance matrix for two different technologies, e.g. a traditional (TR) solution and a low-damage (LD) system respectively. In correspondence to a certain RCR=rcr the probability of loss of the LD system is significantly lower than the TR one, given the design seismic intensity (IM_d):

$$P[rcr > RCR \mid IM_d]_{LD} < P[rcr > RCR \mid IM_d]_{TR} \quad (9)$$

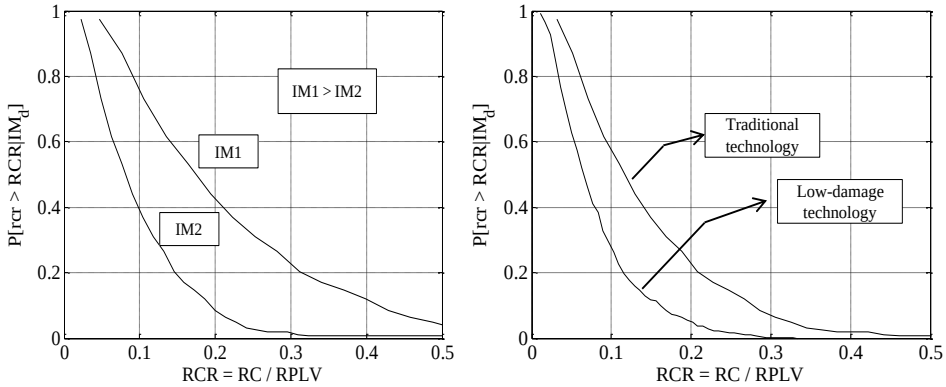

Figure 24 PML curve within a loss-performance matrix for different IM values (left). Alternative technology-based performance objectives, within a loss-performance matrix (right).

Vice versa, a certain confidence on the design in terms of probability of achieving that loss for a given earthquake intensity would result to higher RCR in the traditional TR solution when compared to the low-damage solution LD.

The loss performance matrix can be customized according to the facility's occupancy for different intensity hazard levels. In Figure 25 three different intensity levels, namely $IM_{d1}<IM_{d2}<IM_{d3}$, e.g. corresponding to occasional, rare and very rare seismic events, and three importance levels

(basic, essential/hazardous and critical safety of Vision 2000 PBEE matrix) are considered.

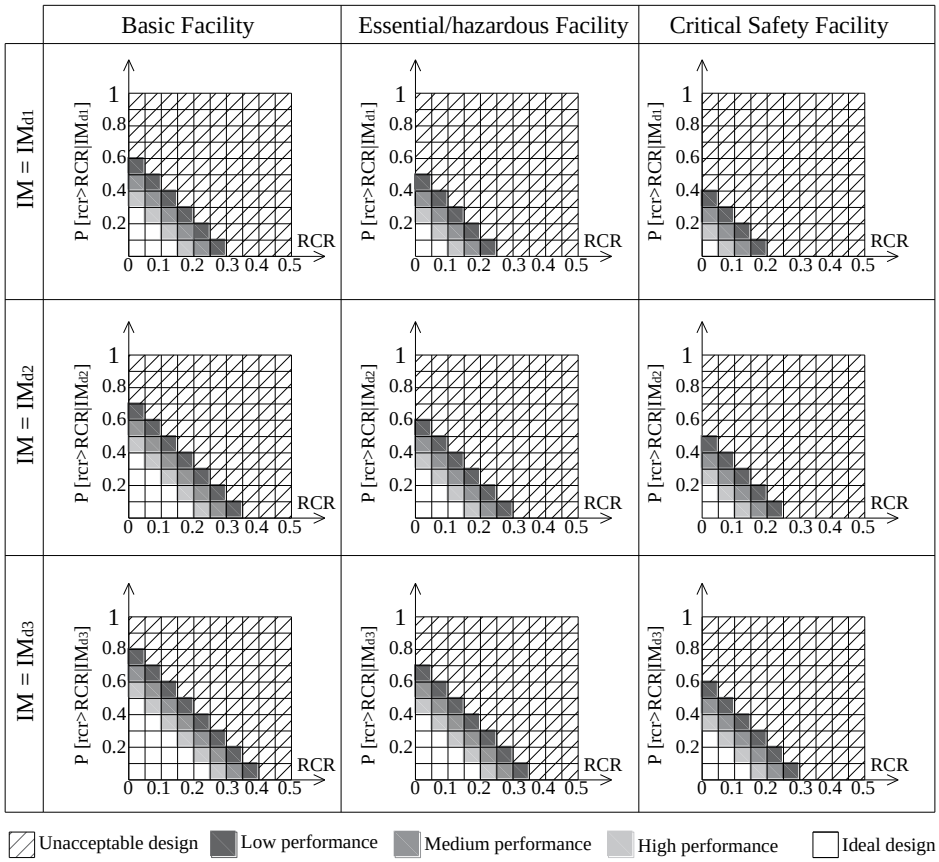

Figure 25 Particularization of the loss performance matrix according to IM and facility's occupancy

The qualitative trend of the loss performance matrix for each combination of the facility's occupancy and intensity hazard shows the evolution of the design performance level (high, medium and low), as a function of PML. In particular, for a specific occupancy, the admitted loss in correspondence of each performance level is gradually less restrictive for increasing values of the intensity. Similarly, as the facility's importance level increases from a basic to a critical safety building, the acceptable loss limit decreases to

more conservative thresholds, given the seismic intensity level. Conceptually there is a diagonal correspondence between the different combinations of building's importance level and intensity measure: indeed note that loss thresholds identifying loss performance levels of a basic facility designed at intensity measure IM_{d1} correspond to the same limits for an essential/hazardous facility designed at IM_{d2}, as well as to a critical safety facility designed at IM_{d3}. In this perspective, the loss performance framework identified in Figure 25 can be re-written in the arrangement of Figure 26, more similar to a traditional multi-objective performance-based matrix. Each loss performance matrix identifying possible loss performances (from ideal to unacceptable) for a specific building's occupancy and intensity measure level, can be considered as a "macro" loss performance objective, to be associated to a certain intensity level according to the facility's occupancy.

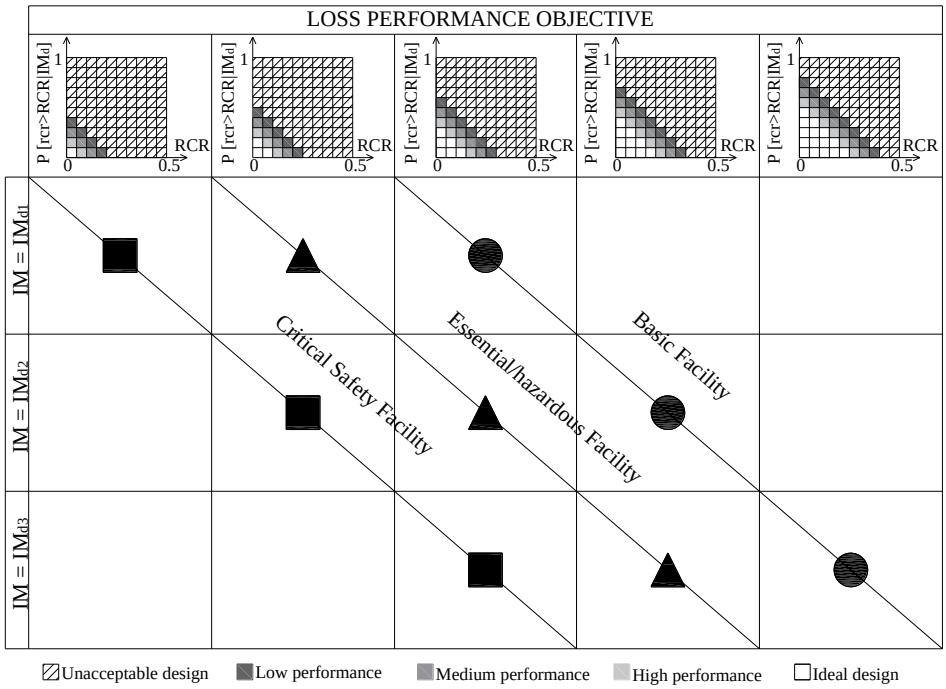

Figure 26 Loss performance matrix in the traditional PBEE shape

In the same way as the traditional PBEE, multi-objective loss performance levels can be required within a cost-based design framework, as it will be clarified in the next section. In particular, the design of a specific facility could require different loss indicator levels according to the severity of the considered seismic entity. An important advantage achieved employing loss indicators, as in the proposed framework, is that they are continuum parameters, thus allowing wide ranges of design options. Conversely, in the traditional PBEE there are some "gaps" in between different (discrete) performance levels, that in some cases have been considered too large (Priestley 2000).

The use of this new loss performance matrix could imply that seismic design might not necessarily be carried out in order to limit a specific EDP, as it is in the traditional PBEE, rather it will pursue pre-defined level of economic losses associated to a certain level of confidence. In more practical terms, a combination of an EDP-based design approach (i.e. Displacement-Based Design) and loss-based charts/spectra would allow to integrate the two approaches and enhance the current mechanical-based approach with some more explicit economic considerations.

4.3 A cost-based design framework

For the implementation of the loss performance matrix and fulfilment of a controllable loss design, a new cost-based design framework is proposed. Design parameters involved are the initial Construction Cost C_c, the maximum allowable repair cost $RC_{allowable}$ and the maximum probability of loss to be associated to it, $P=P[RC > RC_{allowable}|IM=IM_d]$, given the occurrence of design seismic intensity. Indeed, while the initial budget for the realization of the construction can be considered as deterministic, the maximum allowable repair cost is affected by aleatory events and so it must be associated to a certain probability of loss. The designing process can be iterated until the Cumulative Distribution Function (CDF) resulting

from the loss estimation analysis crosses $RC_{allowable}$ at least in correspondence of P.
This approach allows to design a new building knowing that, in case of seismic event of a given intensity (i.e. the design seismic hazard), a maximum repair cost with a certain probability of occurrence will be faced.

The proposed framework can be summarized through the following steps:

1) given the initial available budget, pre-dimensioning of the structural system, with subsequent evaluation of the construction cost C_c, can be promptly performed through the use of Direct Displacement-Based Design method;
2) definition of the total replacement cost value (RPLV), that is the total cost for demolition, site clearance and reconstruction. It is the maximum "repair" cost that occurs in case of collapse or irreparability of the structure. It can be defined as the initial cost increased of the 20-30% to include the cost for demolition and site clearance (FEMA P-58-1, 2012);
3) definition of the performance objective, that consists in selecting the allowable Repair Cost Ratio and corresponding probability of loss $\underline{P}$, given that the design seismic intensity is occurring:

$$RCR_{allowable}=\frac{RC_{allowable}}{RPLV} \tag{10}$$

$$\underline{P}=P[RCR > RCR_{allowable}|IM=IM_d] \tag{11}$$

where $RC_{allowable}$ is the maximum cost the owner is willing to spend to repair the structure damaged after an earthquake. This amount of money can be reasonably fixed, according to the

stakeholders' wish, to a certain percentage of the initial cost of the construction or to the maximum cost covered by insurance;

4) loss estimation analysis, providing the CDF of repair cost. It is suggested to consider the ratio of RC with respect to RPLV, thus obtaining the CDF of RCR, expressing $P[RCR \leq rcr|IM=IM_d]$. Then, it can be converted into the probability of loss $P[RCR > rcr|IM=IM_d]$, corresponding to the complementary to 1 of it;
5) once the loss curve is obtained, it is possible to read which is the probability of loss corresponding to the value of $RCR_{allowable}$. If it results to be lower or equal to the maximum allowable value $\underline{P}$, it means that the structural system designed achieves the performance objective and hence the designing process can be considered completed. Otherwise, the framework should be iterated from step 1, improving the structural and non-structural design so as to limit damage. In some cases, it could be necessary to modify the whole structural system.

The proposed cost-based framework is illustrated in the flowchart of Figure 27, while an applicative example follows.

Consider that in correspondence of the design of a certain facility at a given hazard intensity IM_d (step 1), whose construction cost C_c and replacement value RPLV are known (step 2), the maximum allowable repair cost ratio and corresponding probability of loss are chosen to be $RCR_{allowable}=0.3$ and $\underline{P}=0.05$ (step 3). Accordingly, this means choosing a loss design parameter PML equal to the 95° percentile of not-being exceeded, that is the characteristic value, PML_k, corresponding to 0.3. The intensity-based loss analysis is performed in correspondence of the design seismic intensity IM_d (step 4). Finally, at step 5, if the designed structural system in correspondence of IM_d yields the loss curve indicated as technology A in Figure 28, it means that the system is not sufficiently limiting damage to satisfy the maximum acceptable loss threshold. Indeed,

in correspondence of the maximum allowable RCR value, the corresponding probability of loss is higher than 0.05.

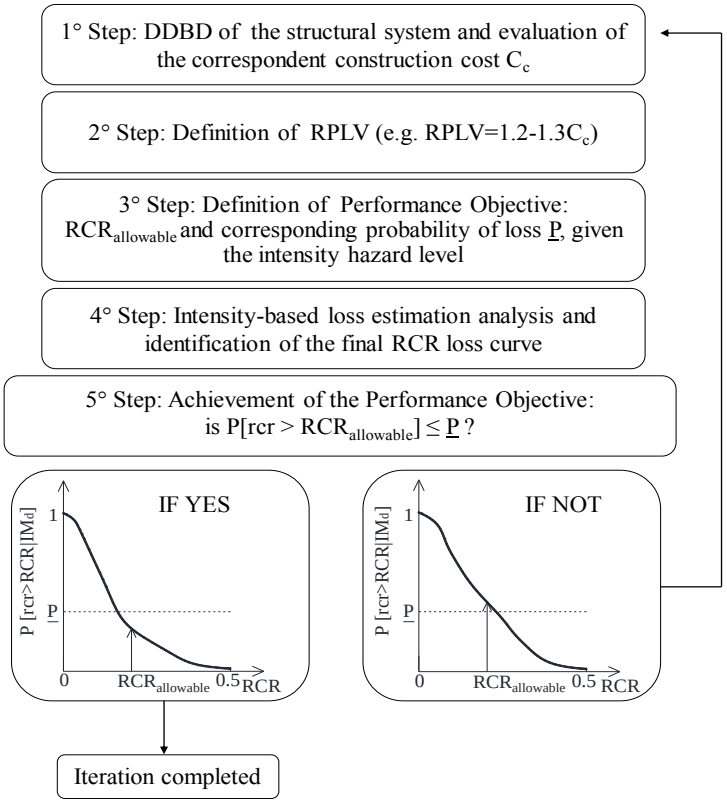

Figure 27 Flowchart of the cost-based design framework

Consequently, stricter technical solutions should be adopted to reduce losses, such as limiting the maximum design drift, adopting low-damage non-structural components able to accommodate higher deformations or choosing an alternative seismic control system, finally obtaining a satisfying loss curve (technology B of Figure 28).

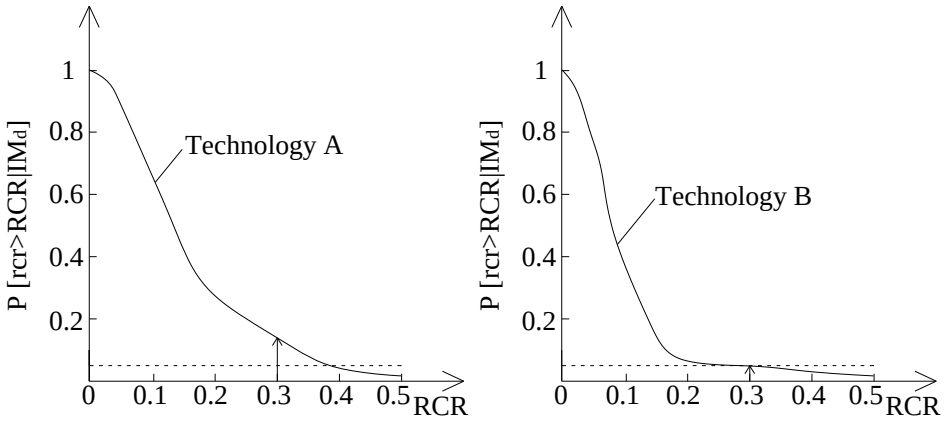

Figure 28 Applicative example of the proposed cost-based design framework

In the attempt of realizing a multi-objective loss performance design, the loss analysis (step 4) should be repeated in correspondence of different intensity measures, representative of earthquakes in between frequent-low intensity and rare-high intensity events. Supposing that loss curves of Figure 28 corresponds to an intensity measure IM_{d2}, suppose that lower (IM_{d1}) and higher (IM_{d3}) intensity levels are considered, yielding loss curves for technologies A and B overlapped on the loss performance matrixes in Figure 29.

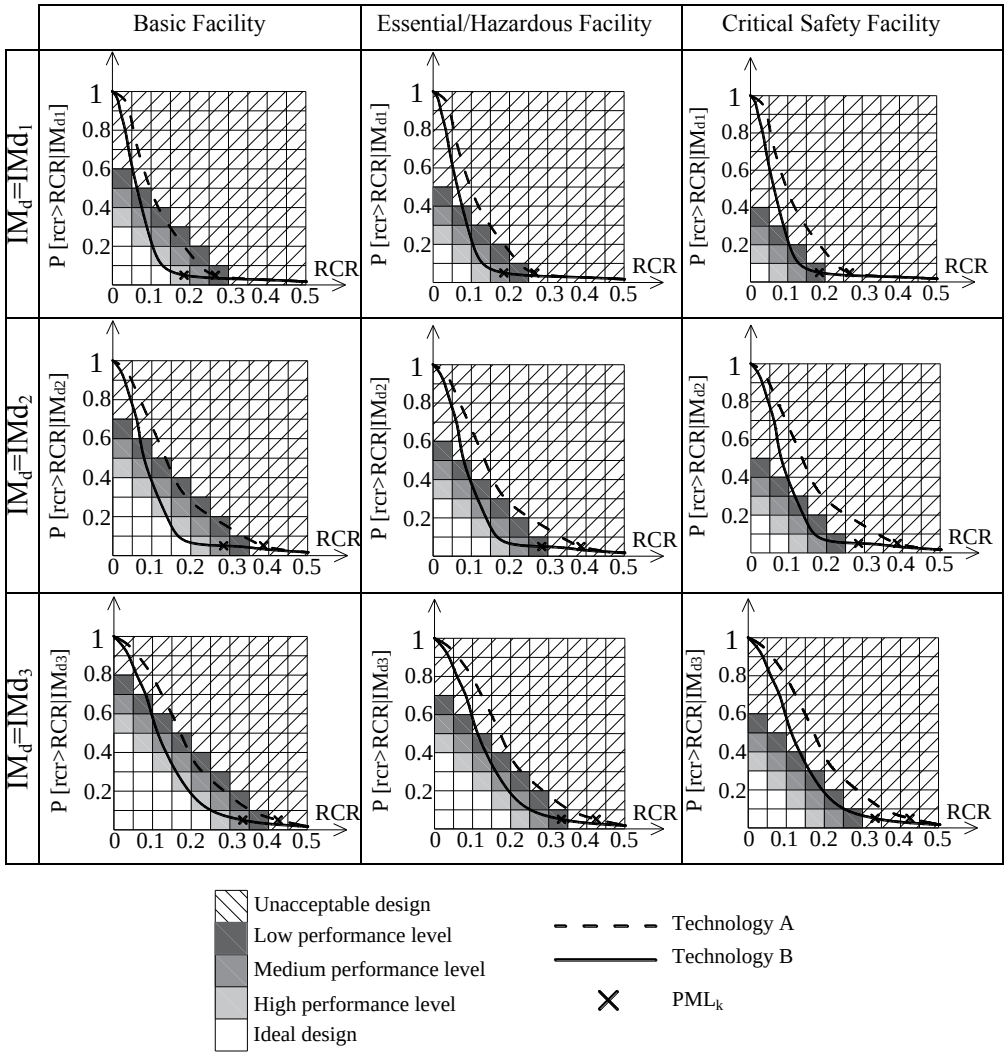

Figure 29 Overlapping of the applicative example loss curves within loss performance matrixes for different occupancies and intensity measure levels

In accordance with the loss indicator adopted for the applicative example of the cost-based design framework, assume PML_k as loss parameter: at IM_{d2} technologies A and B must satisfy the maximum threshold PML_k=0.3. Differently, in correspondence of other intensity levels no requirements are imposed, but the use of the loss performance matrix can

allow to identify which loss performance level can be achieved by each technology.

The interpretation of obtained results is that in correspondence of the design loss parameter PML_k=0.3 at IM_{d2}, that is $RCR_{allowable}$=0.3 and 5% of probability of loss given IM_{d2}, the technology A is never satisfactory. Indeed, it provides values of PML_k higher than the maximum allowable of 0.3, moreover always falling in the unacceptable design area for all the possible occupancies. Differently, at IM_{d2} technology B yields a PML_k value lower than 0.3, so satisfying the loss performance requirement of the cost-based design framework. Although, in accordance to performance levels described by the matrix at the design IM, technology B would correspond to a medium, low and unacceptable design respectively for a basic, essential or critical facility. These results, are synthetically illustrated in Table 3 where, in correspondence of IM_{d2} row, it is possible to read that technology A provides, for all possible occupancies, not satisfactory loss results given that PML_k=0.38, that is higher than the maximum allowable value of 0.3 required in the cost-based design framework. Moreover, in correspondence of the characteristic value of PML, this structural solution always yields an unacceptable loss performance design level.

Differently, technology B, as commented above, can supply satisfactory loss (PML_k=0.28), yielding medium, low and unacceptable performance levels respectively for basic, essential and critical occupancies at IM_{d2}. At other intensity levels, where no loss requirements have been imposed, it is possible to read the loss performance levels that can be achieved by each specific technology, according to the facility's occupancy.

Table 3 Loss performance levels achieved in the multi-objective loss performance matrix, supposing different occupancies for technology A and B

	Technology A		
	Basic	Essential	Critical
IMd_1	Low	Unaccept.	Unaccept.
IMd_2	Unaccept. - NS	Unaccept. - NS	Unaccept. - NS
IMd_3	Unaccept.	Unaccept.	Unaccept.

	Technology B		
	Basic	Essential	Critical
IMd_1	High	Medium	Low
IMd_2	Medium - S	Low - S	Unaccept. - S
IMd_3	Medium	Low	Unaccept.

*S=Satisfactory; NS=Non Satisfactory

4.4 Methodology

The main issues relative to the proposed cost-based design framework concerns step 1 and step 4, that are the structural design and loss estimation analysis, respectively. As far as the structural design is concerned, a prompt dimensioning of elements can be achieved through the implementation of a Direct Displacement-Based Design (DDBD) approach. Indeed, as it will clarify in the following section, this procedure directly considers deformations, thus avoiding the displacement check required, retrospectively, in a Force-Based Design (FBD) method. Moreover, not of secondary importance, it is acknowledged that DDBD is more suitable to a PBEE approach, due to the higher associability of displacement parameters to damage (Priestley 1998, Priestley 2000, Cardone et al. 2009, Kam and Pampanin 2012). Central differences between force-based and displacement-based design approaches are provided in the following section, focusing on the DDBD methodology.
The use of Monte Carlo numerical analysis is suggested to perform the intensity-based loss estimation analysis, adopting PACT software, widely described in Chapter 3.

The methodology required to implement the new cost-based design framework is described through the following main steps, summarized in Figure 30:

- Structural design through DDBD approach;

- Dynamic non-linear analysis: EDPs evaluation;
- Analysis of cost: definition of the Construction Cost (C_c), total RePLacement Value (RPLV) and maximum Loss ThReshold (LTR), this latter corresponding to the limit ratio of the loss over RPLV, beyond which it is believed to be economically convenient to demolish and rebuild the facility;
- EDPs selection: generally Interstorey Drift Ratio (IDR), Peak Floor Acceleration (PFA) and Residual Interstorey Drift Ratio (RIDR) are required, but in some applications other EDPs could be necessary, depending on the structural typology;
- Definition of the structural probability of failure;
- Structural (S), Non-structural (NS) and Contents (C) fragility components selection and performance groups definition.

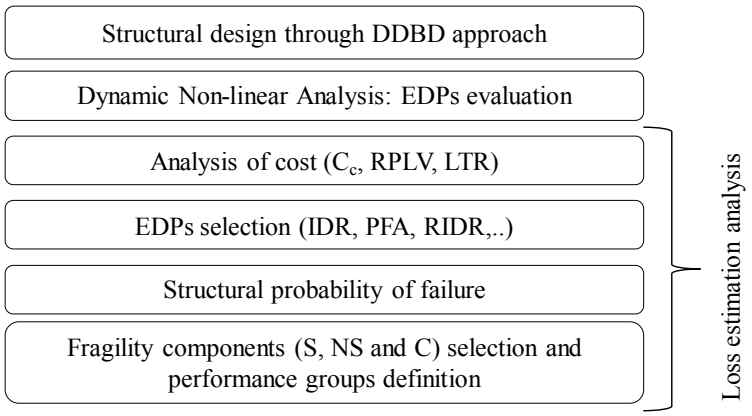

Figure 30 Description of the methodology to perform a cost-based analysis

In particular, in the next sections some considerations about structural response and probability of failure are discussed.

4.4.1 Force-Based Design (FBD) vs Direct Displacement-Based Design (DDBD)

Both Force-Based Design (FBD) and Direct Displacement-Based Design (DDBD) approaches aim to determine the design base shear, to be then distributed along the building in order to pre-dimension structural elements. Although, according to the Force-Based Design (FBD) approach, generally implemented within seismic design codes, the base shear is evaluated through the following expression:

$$V_b = S_{ad}(T_1) \cdot m \tag{12}$$

where m is the total mass and $S_{ad}(T_1)$ is the design spectral acceleration in correspondence of the elastic period of vibration of the structure. In particular, the design spectrum is determined through the selection of the design ductility and the consequent definition of the behaviour factor. Thus, in order to apply equation (12), it is necessary to first define the elastic period of vibration. For some structural typologies, such as reinforced concrete or masonry structures, it is not easy to properly define it because cracked sections should be considered, despite of gross cross-section of members. Moreover, an important inconsistency highlighted by Priestley (1998) is that the definition of stiffness (necessary for the estimation of the elastic period) is not an intrinsic property of section's geometry, while depending also from its strength that, at this step of the design procedure, is still unknown. Sporn and Pampanin (2013) suggested both an iterative FBD procedure and a closed-form "retrofit" FBD methodology, trying to overcome this discrepancy between initial assumed stiffness (depending from the choice of the elastic period) and the actual stiffness, looking instead for a compatibility between structural design strength and stiffness.

A further limit of the FBD approach is that it does not take into account any consideration about displacements, so making necessary a retrospective displacement check.
Differently, according to DDBD (Priestley et al. 2007) the base shear can be determined through the knowledge of the effective secant stiffness K_e at the design target displacement Δ_d of the equivalent Single Degree of Freedom (SDOF) system, that is the "substitute structure" (Shibata and Sozen 1976):

$$V_b = K_e \cdot \Delta_d \tag{13}$$

The target displacement is calculated through the definition of the design displaced shape of the structure, while the effective stiffness is determined from the effective period of vibration of the equivalent SDOF system entering in the design displacement response spectrum. The latter is derived introducing the equivalent damping, combination of viscous and hysteretic damping. Accordingly, the DDBD approach does not require the definition of the elastic stiffness, neither implies the retrospective displacement check, since it starts from deformation considerations. Indeed the first part of the procedure consists in the definition of the normalized inelastic mode shape of the MDOF system, from which the yield and design displaced profiles are then estimated, according to relations provided in Figure 31. In particular the yielding and design drifts depend on the structural typology. Further insights will be provided in the case-study section.

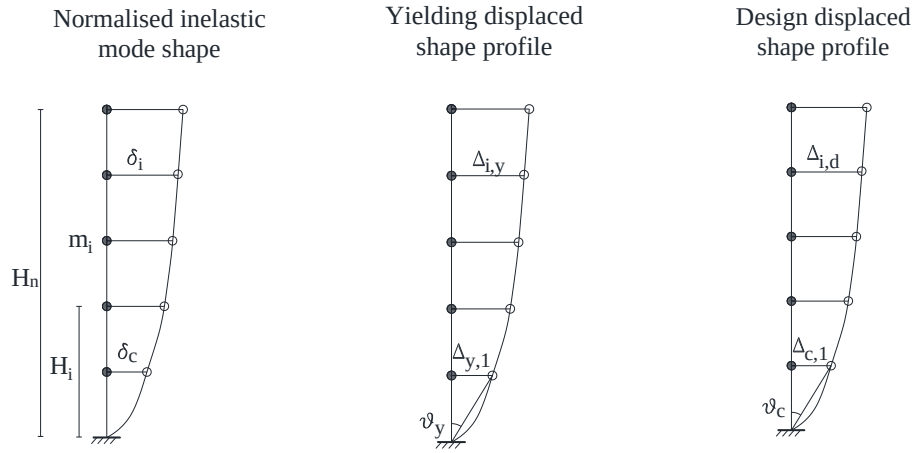

Figure 31 Identification of yield and design displaced profiles

Consequently, the equivalent SDOF system is determined, estimating its yielding displacement, design displacement, equivalent mass and height respectively through the following expressions:

$$\Delta_y = \frac{\sum_{i=1}^{n}\left(m_i \Delta_{i,y}^2\right)}{\sum_{i=1}^{n}\left(m_i \Delta_{i,y}\right)} \tag{14}$$

$$\Delta_d = \frac{\sum_{i=1}^{n}\left(m_i \Delta_i^2\right)}{\sum_{i=1}^{n}\left(m_i \Delta_i\right)} \tag{15}$$

$$m_e = \frac{\sum_{i=1}^{n} m_i \Delta_i}{\Delta_d} \tag{16}$$

$$H_e = \frac{\sum_{i=1}^{n} m_i \Delta_i H_i}{\sum_{i=1}^{n} m_i \Delta_i} \tag{17}$$

Then, knowing the ductility as the ratio between design and yielding displacements, the equivalent damping ξ_e can be formulated according to

different relations which depend from the dissipative system (Pampanin et al. 2010). Entering into the design displacement response spectrum in correspondence of the target displacement Δ_d, the SDOF equivalent period can be read, finally determining the secant equivalent stiffness and the base shear:

$$K_e=\frac{4\pi^2 m_e}{T_e} \tag{18}$$

$$V_b=K_e\cdot\Delta_d \tag{19}$$

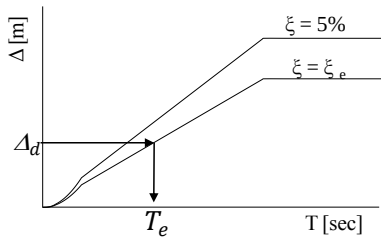

Figure 32 Definition of the SDOF equivalent period in the DDBD approach

Thus, the base shear is distributed along the levels according to the floor mass and displacement, adding an increment of 10% at the last level to account for additional storey shear due to higher modes:

$$F_i=\left(0.9\cdot\frac{m_i\Delta_i}{\sum_{i=1}^{n}(m_i\Delta_i)}\right)\cdot V_b, \text{ for } i \leq (n-1) \tag{20}$$

$$F_i=\left(0.1+0.9\cdot\frac{m_i\Delta_i}{\sum_{i=1}^{n}(m_i\Delta_i)}\right)\cdot V_b, \text{ for } i = n \tag{21}$$

It is now possible to evaluate the distribution of internal actions and design then the connections.

4.4.2 Intensity-based loss estimation analysis

There are numerous simplified methodologies adoptable to perform the intensity-based loss estimation analysis. Although the numerical approach based on the use of Monte Carlo simulations, as the one integrated in the PACT software, is believed to be one of the most effective, so its implementation is recommended. While main issues relative to the software have been discussed in Chapter 3, some indications about data to be given in input into PACT are addressed to the following section.

4.4.2.1 Evaluation of engineering demand parameters

According to FEMA P-58-1 (2012), the evaluation of Engineering Demand Parameters (EDP), necessary for the analysis of damage in correspondence of each component and of the facility as a whole, can be performed both through static and dynamic linear or nonlinear analysis. Although, given the higher reliability of dynamic nonlinear analysis and the powerful support of computer-aided design, their implementation is strongly recommended.

4.4.2.2 Probability of collapse: record selection and IDA analysis

In order to get the fragility curve of the whole structure, the most complete tool is given by Incremental Dynamic Analysis - IDA (Vamvatsikos and Cornell 2002). The main concern consists in the choice of the Engineering Demand Parameter (EDP) to observe and the Intensity Measure to employ. In most applications, the Interstorey Drift Ratio (IDR) is a significant indicator to be used as EDP, even though its representativeness mainly depend on the structural typology. As far as the IM selection is concerned, often the 5% spectral acceleration at the fundamental period of

vibration, $S_a(T_1)$, is adopted. This parameter allows a better characterization of the record frequency content near the structural first-mode frequency (Vamvatsikos and Cornell 2002) and yields to be more efficient (lower EDP dispersion) than PGA in the case of drift response (Iervolino and Manfredi 2008). Although, for tall, long period buildings, because of their significant higher modes, $S_a(T_1)$ may have less prediction power than the case of first-mode dominated structures. In several studies the sufficiency of $S_a(T_1)$ with respect to magnitude M and epicentral distance R has been discussed, highlighting that the choice of $S_a(T_1)$ makes EDP variable conditionally independent of M and R (Shome and Cornell 1998, Shome et al. 1998, Bazzurro and Cornell 2002, Iervolino and Cornell 2005). Moreover, in the case of SDOF structures where displacement-related response measures are investigated, $S_a(T_1)$ has been proved to be sufficient with respect to the ground motion duration as well (Iervolino et al. 2006). Since $S_a(T_1)$ may be insufficient on soft soil, it is prudent to avoid the selection of events on this type of soil or of near source records (Iervolino and Manfredi 2008). The efficiency (small dispersion of EDP given IM) of $S_a(T_1)$ diminishes with increasing level of nonlinearity and when used to evaluate large nonlinear deformations in MDOF structures (Miranda et al. 2017). As a matter of fact, the period lengthening during the shaking due to nonlinear structural behaviour makes the structure susceptible to a range of periods beyond T_1 and this is not contemplated by $S_a(T_1)$ as IM (Iervolino and Manfredi 2008). For this reason, many enhanced IM quantities have been proposed, in the attempt of considering a wider range of periods. For example Baker and Cornell (2006) suggested an IM consisting of $S_a(T_1)$ combined with the ground motion parameter ε (defined as the difference between a record's spectral acceleration at a certain period and the mean of a ground motion prediction equation at the given period). Differently Haselton et al. (2009) proposed a procedure where the collapse capacity is corrected by means of a factor depending of the ε value for each record. Eads et al. (2015)

introduced a new IM corresponding to the geometric mean of spectral acceleration values defined in a given range of periods, demonstrating an evident reduction in the record-to-record variability. Cordova et al. (2001) proposed an IM quantity corresponding to $S_a(T_1)$ corrected by a factor function of the 5% spectral acceleration at the fundamental period and of the 5% spectral acceleration at a higher period accounting the reduced structural stiffness due to nonlinear behaviour.

However the investigation about the optimization of records' selection in the context of IDA analysis lies outside the aim of the present work of thesis. Valid and exhaustive readings about this topic can be found in literature, some of them just cited above.

4.5 Limitations and future developments

The implementation of the proposed cost-based design framework within the multi-objective loss performance matrix environment, currently presents some limitations, if not some interesting cause for reflection of future research developments.

First of all, it is necessary to promote the procedure from an iterative design approach (looking for the system satisfying pre-defined loss performance levels), that is more similar to a cost-based assessment, towards a more reliable methodology promptly yielding the desired loss indicators. To this aim, it would be very useful to provide relations correlating design parameters to Damage Variables (DV), so allowing a pre-dimensioning of the structure directing the final seismic solution towards the satisfaction of required loss performances. This correlation would be more direct and efficient if a displacement-based approach would be implemented. Indeed deformation parameters are surely more explicit indicators of damage, and then of losses, with respect to parameters implementable in a force-based approach, such as the behaviour factor. Accordingly, even if it is known that the use of higher

values of it indicate higher ductility demand and so higher levels of damage, no information helping to quantify the latter are provided. Consequently, a displacement-based design approach is strongly suggested at step 1 of the procedure.

Moreover, the provision of design parameters - DVs relations should be differentiated for different seismic technical solutions, in order to provide a wide range of choice to the designer on one hand, and to promote the use of alternative low-damage solutions on the other hand. As a matter of fact, today in some countries, such as Italy, the implementation of alternative seismic control systems is generally not preferred to the traditional (capacity design) structures, due to their higher initial costs. On the contrary, if losses caused by the occurrence of design seismic events would be accounted for, the economic advantages of the low-damage technologies would stand out.

A further insight to be investigated consists in the definition of the allowable socio-economic limits identifying the loss performance levels in the multi-objective matrixes. Indeed, the trend herein assumed is qualitative, but it should be characterized as the result of a wide socio-economic study, that lies outside engineering expertise and the scope of this thesis. For this reason, economic parameters involved at step 2 and 3 of the proposed procedure are not further discussed in this work, simply adopting plausible quantities coherent with the state-of-art assumptions.

As far as the step 4 is concerned, several approaches could be implemented for the intensity-based loss assessment. Indeed, as illustrated in Chapter 3, many simplified or numerical methodologies for the resolution of the loss estimation analysis exist today. Although, one of the main concerns corresponds to the identification of all the damageable structural, non-structural components and contents, and the definition of fragility curves and consequence functions for each of them. This part of the procedure is very important for the achievement of reliable loss results and should be carefully executed. In particular, it would be unreasonable

to realize specific studies for each component in the context of the designing stage, since it would be extremely time-consuming. Differently, a wide database of fragility curves covering common typologies of components should be formulated and made available to designers for a prompter implementation of the loss analysis. A similar fragility database has been collected and provided by American guidelines FEMA P58, including more than 700 components. Even if typical of U.S. building stock, this would represent a good starting point for the inclusion of Italian characteristic elements.

Also the identification of all the structural, non-structural components and contents that could be susceptible of damage can be quite onerous in terms of time. Although, in the perspective of performing structural design in the Building Information Modeling (BIM) environment (Eastman et al. 2011), that seems to be an actual direction of engineering design approach in many countries, the definition of performance groups could become much easier (Vitiello et al. 2016). Actually, through BIM platform it is possible to collect a wide range of information concerning different features of the analyzed building, encompassing foundations and structures, installations of equipment and water and wastewater systems, equipment, heating, ventilation and air conditioning (HVAC) and facilities, equipment and electrical systems (Maia et al. 2015).

Alirezaei et al. 2016 has proposed an integration of loss assessment within a BIM designing process, simply exporting structural properties from BIM environment to a structural analysis software in order to evaluate the structure's response under specific loading condition. Then, the obtained EDPs data are used to perform a loss analysis through PACT software, employing its fragility database. Differently, if a fragility database would be already integrated within the BIM environment, implying that the selection of a specific element would directly provide the corresponding fragility curves, a powerful enhancement would be achieved. Indeed, exporting fragility data from BIM platform to a loss estimation tool would

extremely simplify the loss assessment and the implementation of a cost-based design.

CHAPTER 5

LOSS-BASED COMPARISON OF ALTERNATIVE LOW-DAMAGE SOLUTIONS VIA A CASE-STUDY APPLICATION

In the present chapter the cost-based design approach proposed in the previous section is applied to five different seismic technologies, namely a traditional Moment Resisting Frame (MRF), a dissipative rocking re-centering system (HYBrid - HYB), a HYB system employing Low-Damage non-structural components (LD-HYB), a dissipative Braced Frame (BF) and a Base Isolated system (BI). In particular all the technologies are applied to the same case-study structure, each time designed according to a DDBD approach. The intensity-based loss estimation analysis is performed for 500yrs return period events through numerical Monte Carlo simulations, employing the American software known as PACT - Performance Assessment Calculation Tool. Loss curves are compared in a loss performance matrix. Main results are analyzed selecting specific values of PML, finally comparing the trend of Construction Costs and Repair Costs in correspondence of each seismic solution.

5.1 Passive control systems

Passive control systems, already introduced at §2.4, are comprehensive of a wide range of devices generally designed to provide added stiffness, strength and damping through several mechanism, as frictional sliding, yielding of metals, deformation of visco-elastic (VE) solids or fluids and fluid orificing.

In the present thesis, some specific passive control systems are selected as alternative seismic solutions of a case-study structure, comparing them to the performances of a traditional Moment Resisting Frame (MRF). In particular, the passive technologies adopted are dissipative rocking system (HYB), dissipative Braced Frame (BF) and Base Isolated system (BI). In the following section, each of them is presented, focusing on main characteristics and working principle.

5.1.1 Self-centering dissipative rocking system

The self-centering passive rocking system (synthetically indicated hereafter as HYB, standing for hybrid) was first studied in the late 1990s in the U.S. PRESSS (PREcast Seismic Structural System) program at the University of California, San Diego (Priestley 1991, Priestley 1996, Priestley et al. 1999). It consists of precast concrete elements jointed through dry ductile connections given by unbonded post-tensioning (PT) tendons/bars and longitudinal mild steel (Figure 33). In this way both energy dissipation and self-centering capacities are provided, leading to negligible residual deformation. In particular, the grounted mild steel rebars, inserted in corrugated metallic ducts, present a small unbonded length in correspondence of the connection interface, so avoiding a premature mild steel's rupture at the gap opening.

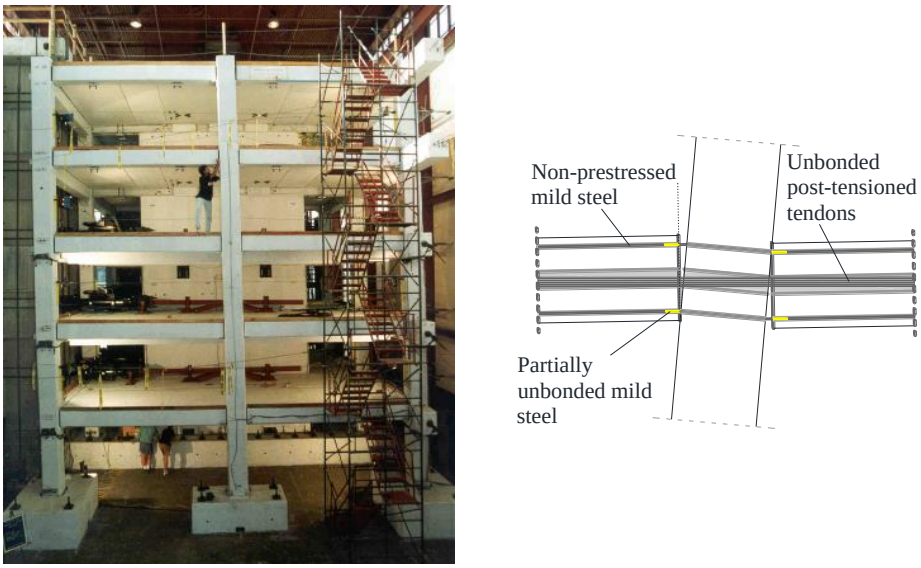

Figure 33 HYB technology: the PRESSS building (left) tested at the Univertity of San Diego (Priestley et al. 1999). Beam-column HYB connection (right)

These characteristics make the system belong to the low-damage category, given that after a strong event the presence of PT cables ensures structural self-centring, practically eliminating detrimental residual displacements. Although, mild steel rebars' damage, generated by energy dissipation, could imply the necessity of substituting internal steel. This repair intervention would be quite invasive, economically onerous and time consuming. Accordingly, Pampanin (2005) has proposed an interesting advancement of the PRESSS technology, consisting in the use of external dissipation devices, given by simple steel bars working extensionally, known as plug&play. After the occurrence of a severe seismic event, the eventually damaged elements could be easily substituted, implying a lower economic repair impact. The concept of the re-centring/dissipative hybrid system has been extended from precast concrete also to timber frames and walls, in what is known as Pres-Lam (Prestressed Laminated timber) system (Palermo et al. 2005, Pampanin et al. 2006). Some real applications of the Pres-Lam technology in Christchurch (New Zealand)

are shown in Figure 34: on the left there are plag&play dampers at the base of a column and at the beam-column connection; on the right there is a coupled Pres-Lam wall with visible PT cables and plug&play devices. Moreover note that in between the two coupled walls there are U-shape Flexural Plate dampers.

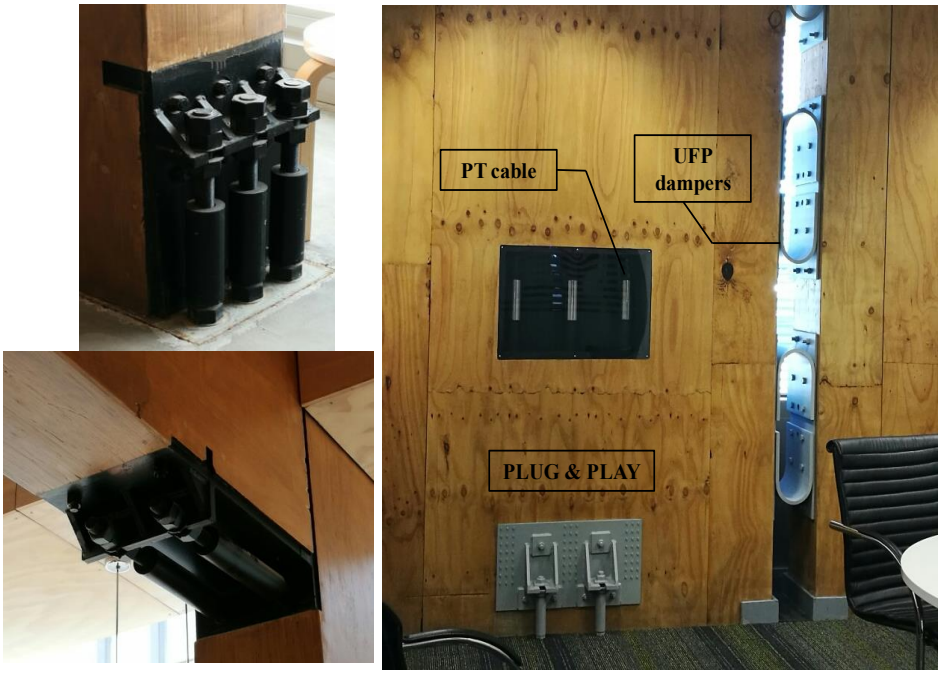

Figure 34 Real applications of the Pres-Lam technology: Victoria street building (on the left) and Trimble building (on the right). Christchurch, NZ (2016)

The typical cyclic hysteresis of a HYB connection is described by a flag-shape curve (Figure 35), given by the combination of re-centring capacity, provided by post-tensioning elastic nonlinear behaviour (M_{PT}) and axial load (M_N), and dissipation capacity given by mild steel (or external dampers) plastic nonlinear performance (M_S). The ratio between the two contributions is defined by λ factor, while parameters α and β represent the values of each contribution with respect to the total:

$$\lambda=\frac{M_{PT}+M_N}{M_s} \tag{22}$$

$$\alpha=\frac{M_{PT}+M_N}{M_{total}}=\frac{\lambda}{\lambda+1} \tag{23}$$

$$\beta=\frac{M_s}{M_{total}}=\frac{1}{\lambda+1} \tag{24}$$

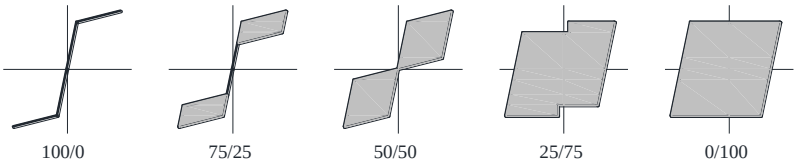

Figure 35 Typical HYB connection flag-shape for different λ values (after Pampanin et al. 2010)

5.1.2 Dissipative braced frame through a shear link energy dissipation device

Shear link dampers belong to the family of hysteretic passive control devices. They can provide additional source of energy dissipation through metals yielding mechanism, when properly introduced within a frame structure. The first versions of this type of device was used for eccentrically braced frames (EBF) (Popov and Engelhardt 1988). This latter were conceived as intermediate steel structure systems between dissipative but excessive deformable moment resisting frames (MRFs) and stiff and brittle concentrically braced frames (CBFs). EBF systems are significantly stiffer than MRFs, due to the introduction of braces, and supply an additional source of energy dissipation through shear and/or bending in a portion of beam called “link”. The longer or shorter link’s length respectively identifies a moment or shear link primary behavior.

Many different steel dampers have been proposed and investigated, considering different materials, geometric shapes, manufacturing process and connection configurations to the structure (Christopoulos and Filiatrault 2006, Symans et al. 2008). The simplest shear link is a single steel plate, generally welded to the structure, indicated in literature as shear panel damper, SPD (Choi and Abebe 2013, Liu et al. 2013). Low-yield steel (Nakashima 1995) or aluminum materials (Rai and Wallaces 2010, Sahoo and Rai 2010) have been used for alternative SPD. Actual dissipation capacity mainly depends on inelastic excursions that the device can sustain even for small vibrations.

The family of flexural steel dampers is wider, including the most popular ADAS, TADAS, slit dampers, honeycomb dampers. Added Damping And Stiffness (ADAS) device was first investigated by Bergman and Goel (1987) and Whittaker and Bertero et al. (1991). It is composed by steel X-shape plates connected in parallel at the top and at the bottom to rigid elements so that the rotation is not allowed. The particular shape of steel plates ensures a uniform flexural yielding in the element. Alternatively, Triangular Added Damping And Stiffness (TADAS) device is a triangular steel plate (Tsai et al. 1993) that subjected to a perpendicular lateral force undergoes uniform yielding along the height thanks to linearly increasing moment. The steel slit damper (SSD) is a standard I-section with a number of slits cut from the web. The final shape is an alternation of struts and slits, achieving a vierendeel truss arrangement (Chan and Albermani 2008, Climent et al. 1998). Honeycomb steel damper was developed by Kobori et al. (1992) with the aim of increasing energy absorption of high-rise buildings. This device consists in a steel plate with honeycomb-shaped openings, which generate X-shaped struts.

All above mentioned devices are generally placed between chevron braces and upper beam. In some cases yielding dampers can be placed in series with diagonal braces, so providing energy dissipating element in concentrically braced frames. This is the case of a particular cast steel

yielding fuse, also known as scorpion yielding connector, SYC (Gray et al. 2014), which dissipates energy through the cyclic inelastic flexural deformation of the SYC's cast steel yielding fingers. The overall fuse's aspect resembles ADAS or TADAS device, with the difference that SYCs are manufactured through steel casting process.

A different group of yielding dampers dissipate cyclic loads-induced energy through axial deformation. This is the case of Buckling Restrained Braces (BRB), developed by Clark et al. (1999), which consists in an unbonded core steel brace encased in a concrete-filled steel tube to avoid buckling mechanism when compressed.

A wide number of experimental tests performed on both shear and flexural dissipative links has shown that the formers shear links can achieve larger plastic rotations and greater energy dissipation than the latter (Popov and Engelhardt 1988). In general, shear links' common features are stable hysteretic curves, significant strain hardening and energy dissipation capacity. These remarkable characteristics encourage further investigation of this kind of passive device, on one hand trying to optimize some important features such as the manufacturing process and the cost of the device, on the other hand promoting its use with experimental campaigns that highlight the actual effectiveness of such dampers for structural control.

A particular shear link damper (Figure 36), also known as Shear Link Bozzo, consisting in a metallic yielding device first advanced at the University of Girona, Spain, in 1997 (Cahis et al. 1997 and 2000, Bozzo et al. 1999, Hurtado and Bozzo 2008) is implemented in this thesis within the Braced Frame (BF) case-study system. This damper, briefly indicated as SL in the following, is particularly advantageous thanks to its flexibility in covering a wide range of force capacities, that makes it adaptable to different levels of demand. It consists of a metallic hysteretic damper realized from a hot laminated steel plate which is generally modelled so that to obtain an I-shape. The flanges of the device represent the stiffer

parts and are employed to realize the connection to structural elements. Differently, energy dissipation is concentrated at the web where some "dissipative windows" with reduced thickness are generated through a milling manufacturing process (Bozzo et al. 1998). Wide ranges of SL's dissipation capacities can be obtained simply varying the height, width and thickness of the dissipative windows and web stiffeners.

The basic idea behind the SL damper is providing local ductility, while avoiding local buckling in a simple, manufactured controlled and cheap way. The simplicity of SL dampers' geometry makes them particularly suitable to be adapted to different arrangements within the structure. The typical and most used installation mode for SLs is between chevron braces and upper beam, as schematically shown in Figure 36. Although, the first use of such devices was to protect infill masonry walls (Bozzo et al. 1998). The alternative use of SL dampers to protect precast reinforced concrete structures, inserting devices within diagonal braces (Figure 37) has also been investigated (Nuzzo et al. 2014).

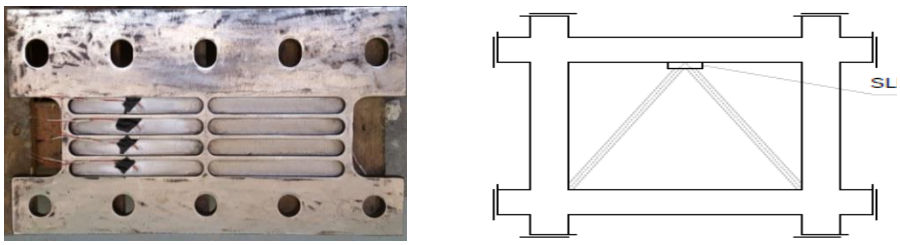

Figure 36 SL damper and its typical configuration within the structure

Figure 37 Shear link energy dissipation device allocated in tubular braces

Nowadays, several applications have been developed and carried out using these devices: more than one thousand of SL dampers have been installed worldwide, mainly in reinforced concrete buildings in Mexico, Peru and Ecuador, for new constructions (Figure 38) as well as for seismic retrofitting of existing ones (Figure 39).

Figure 38 Installation of a SL for the new construction of Torre Ixtapa (Mexico)

Figure 39 Installation of a SL for the seismic retrofit of hotel Ceibo Dorado after October 2016 earthquake in Ecuador

The connection is totally bolted, in order to avoid welding and make easier installation and replacement process during lifetime of the building. Moreover the upper side of the connection is realized through slotted holes, with the aim to avoid axial load transferred from the upper beam to the device. The performance of SL dampers has been recently tested at the Laboratory of Federico II University (Nuzzo et al. 2017). In particular five different geometries have been investigated, selecting for each of them two specimens, for a total of ten tests. Seven specimens were tested cyclically, while three of them were subjected to monotonic load, measuring reaction forces up to 1000 kN. Experimental results and data processing are given in Appendix A.

5.1.3 Base isolation system

Base isolation represents a consolidated effective way to reduce seismic demand in buildings: the horizontally flexible and dissipative interface at the base of the building, between foundation system and superstructure, allows to decouple the building from the soil movement. The structure rests on special isolation devices capable of significant relative displacements and energy dissipation, thus producing a lengthening of the structural period of vibration and a reduction of the spectral demand. Actually, the effectiveness of such protection system is decreased in case of high-rise buildings, already characterized by high values of the fundamental period of vibration.

Isolation could also interest just a part of the structure, such as it is the case of factories hosting vibrating machines.

Added damping is an inherent property of most isolators, but may also be provided by supplemental energy dissipation devices installed across the isolation interface.

This technology considerably limits structural damage, given that the building mainly moves rigidly on isolators, maintaining itself essentially undeformed (maximum drifts of 0.3-0.4%), while all the deformation is concentrated in correspondence of devices. Moreover it is gained the advantage that reduced forces acting on the structure are constant with the height, thus the overturning moment at the base is reduced as well. The use of this technology is not very common because its cost is higher with respect to other types of passive seismic protection systems. Although, recent studies demonstrated the possibility of employing low-cost recycled rubber isolators (Spizzuoco et al. 2014).

Base isolation can be employed both for the design of new constructions (Figure 40) or the retrofit of existing ones (Figure 41). The presence of seismic joints and flexible systems is a fundamental issue for the proper success and functionality of a base isolated structure.

Figure 40 Base isolation device between foundation and superstructure systems

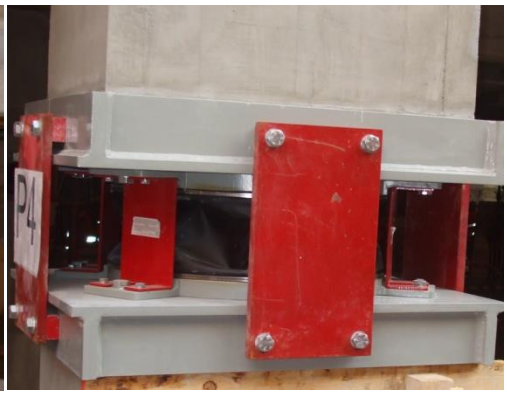

Figure 41 Base isolation device between foundation system and a column (building retrofitted in L'Aquila after the earthquake of April the 6th, 2009)

The first type of base isolation device investigated in last decades is the rubber bearing isolator: it consists in circular, square or rectangular cross section elements, constituted by the alternation of neoprene and steel shits that provide an impediment to the lateral rubber bulging (Figure 42). In fact, it is well-known that rubber is an incompressible material, characterized by a Poisson modulus ν=0.5; so, subjected to the gravitational load of the building, the bearing could bulge.

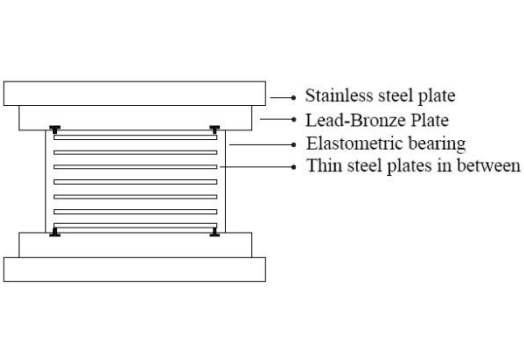

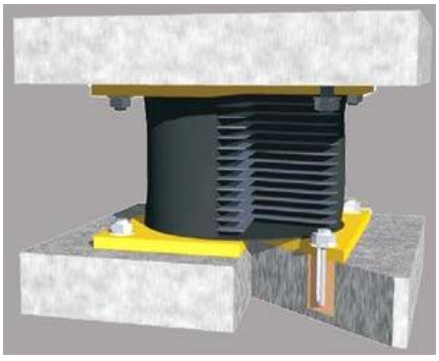

Figure 42 Rubber bearing isolation device

This element can deform just horizontally, thus there is no isolation in vertical direction; generally this is not a problem since the most danger and damaging demand is due to the horizontal component of ground motions.

Bolted or dowelled rubber bearings can be distinguished according to the kind of connection between the device and the foundation. In the first case the rubber bearing element is inserted between two thicker steel plates, that allow the connection to the rest of the structure through bolting. The dowelled bearing, on the other hand, provides a shear connection since the bearing is inserted in a steel element. Thus the main difference between these two types of connection is that the bolted one works both in tension and in compression, while the dowelled bearing cannot sustain tension loads. For this reason, in the case of very high-rise buildings, in which the overturning moment is significant, bolted bearings are necessary.

A further distinction can be done between High Damping steel laminated Rubber Bearing (HDRB) and Low Damping steel laminated Rubber Bearing (LDRB), that respectively provide a damping ratio around 10-15% in the first case, and 5% in the second.

Other types of isolation system are given by Lead Rubber Bearing (LRB) and Friction Pendulum Systems (FPS). In the first case, energy dissipation capacity of a typical rubber bearing is enhanced introducing an internal lead core, thus allowing a better base displacement's control. Differently, friction isolation devices consist of sliding rollers in which frictional forces, opposing to the structural movement, are generated. In particular, there are two sliding plates characterized by curved surfaces covered with a layer of stainless steel; between them there is an articulated slider that can move on the curved surfaces. The side of the slider in contact with the spherical surfaces is coated with a low friction material. Friction pendulum bearings use characteristics of a pendulum to lengthen the natural period of the isolated structure so that to reduce earthquake forces. The curved shape of FPS surfaces enables the structure to return to its

initial position after the action of an earthquake, using the weight of the structure itself. This is an advantage with respect to other devices, not having a restoration force allowing the structure to go back to its original position, thus causing significant permanent displacements.
The last case-study system analyzed in the present thesis is a HDRB base isolated structure.

5.2 Case-study

In this section a case-study building is introduced. The same structure will be designed in different seismic configurations, i.e. adopting four technologies that are Moment Resisting Frame (MRF), dissipative rocking system (HYB), Braced Frame (BF) and Base Isolated (BI) systems. Moreover, a further technology employing HYB structural configuration and assuming low-damage non-structural components will be analyzed as well (LD-HYB). Intensity-based loss estimation analysis will be performed for each structural typology, according to FEMA-P58 methodology and employing PACT software. Finally, loss performances will be compared in a loss-based earthquake engineering framework.
Main features of the case-study building are presented in the following sections, addressing details and specifications relative to each system respectively to §5.3, §5.4, §5.5, §5.6 and §5.7.

5.2.1 Geometry

The case-study building is a new 5-storey-3-bay reinforced concrete structure, with interstorey height of 3.2 m and bay's width of 7.5 m. The building's occupancy is supposed to be commercial office and its structural plan and elevation are given in Figure 43.

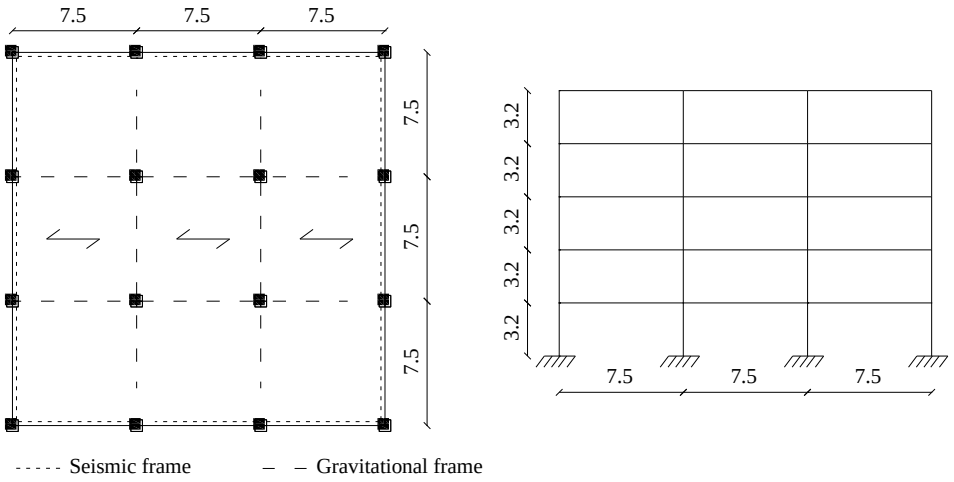

Figure 43 Case-study building: plan and front view (dimensions in meters)

The structure has a symmetric configuration in order to simplify the 3D analysis, allowing to consider only the transversal frame. The lateral resistance to seismic action is provided by external frames along the perimeter, while internal frames are designed only for gravitational loads. This choice comes from the aim of selecting a structural configuration compatible with all technical solutions to compare. In the case of the hybrid or braced structures, the seismic system would not be adopted for both longitudinal and transversal internal frames because this would lead to excessive stressed columns, in addition to being architecturally unfeasible. For this reason, only perimetral frames are demanded to withstand lateral actions. Actually, in this configuration columns in the corners are anyway loaded both longitudinally and transversally. Hence it would be preferable to have a gravitational beam separating the external orthogonal frames, or to adopt a structural wall in the transverse direction. Although, in order to keep the comparison among the four systems (MRF, HYB, BF, BI) as purer as possible, it is assumed the simplification of the symmetrical structural configuration.

5.2.2 Structural design approach for the case-study building

The case-study structure is designed several times, assuming each of the seismic solutions to be compared, through the Direct Displacement-based Design (DDBD) approach (Priestley 1998, Priestley et al., 2007) and considering 500yrs return period event as seismic action. Details about the adopted procedure and outcomes will be given in the next sections, where each seismic protection system is focused. Herein the reader can find the main input data and the description of the general approach.

The structure is assumed to be located in Norcia, where the Central Italy Earthquake stroke in 2016 (Mw 6.5), on a site class B, topography class T2. The elastic pseudo-acceleration and displacement response spectra, corresponding to a probability of exceedance of 10% in 50 years and class of use II, are constructed according to Italian seismic code provisions (NTC-08) and are given in Figure 44.

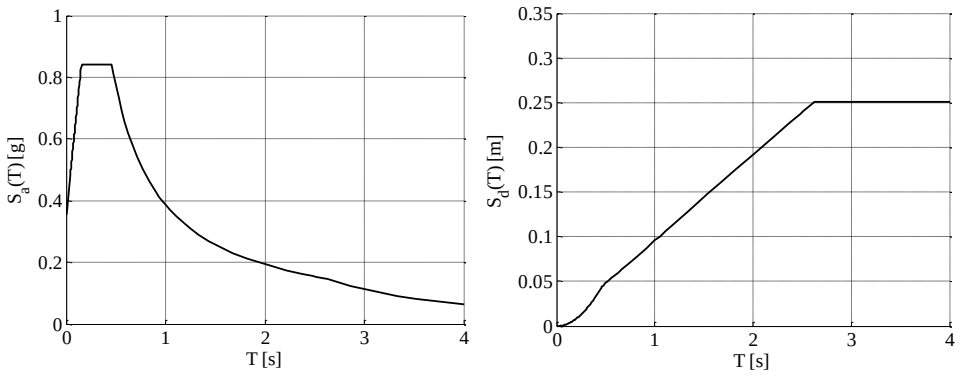

Figure 44 Elastic pseudo-acceleration and displacement response spectrum (ξ=5%)

Design drifts adopted are typical for each seismic technology. In particular MRF and HYB systems are designed for drifts of 2%, while BF and BI structures for drifts of 0.5% and 0.4% respectively. The DDBD, introduced at §4.4.1 is specialized for each structural typology.

Ribbed slab with steel reinforcement is assumed; gravitational structural, non-structural and live loads are given in Table 4.

Table 4 Gravitational loads' definition

Load [kN/m^2]		Structural self-weight	Non-structural self-weight	Live load
Level	1 to 4	2.25	3.84	3
	5	2.25	1.5	0.5

5.2.3 Record selection for dynamic non-linear and IDA analyses

Non-linear models are created through OpenSees software (McKenna 1997) to launch non-linear dynamic analysis using an OpenSees-Matlab platform. Specific employed elements are differentiated according to the structural typology, so they will be described in each dedicated section. The main objective of nonlinear dynamic analysis is to check the structural design on one hand, and to provide EDP quantities necessary to perform loss estimation analysis on the other hand. A set of 7 couples of records spectrum-compatible to the target elastic spectrum have been selected from SIMBAD database (Smerzini et al. 2013) using Rexel v.3.5 software (Iervolino et al. 2009). The SIMBAD database (Selected Input Motions for displacement-Based Assessment and Design) assembles records of engineering relevance for the most frequent design conditions in Italy from strong ground motion database worldwide. From the disaggregation analysis (Figure 45) it is possible to select ranges of moment magnitude Mw and epicentral distance R characterizing the records significant in the hazard contribution of the target spectrum. In particular values of Mw and R ranging respectively between 5 and 7 and 0 and 30 km are selected. Scaled records, with a maximum mean scale factor of 2, are selected and listed in Table 5.

Spectrum matching of scaled spectra is provided in the range of period between 0.15 s and 4 s, as shown in Figure 46.

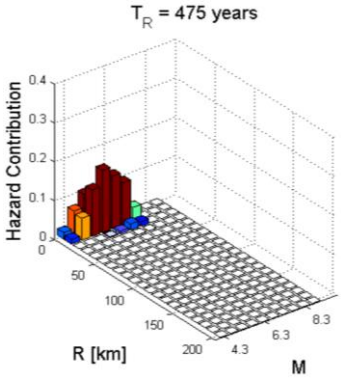

Figure 45 Disaggregation analysis of events significant in the hazard contribution of the target spectrum

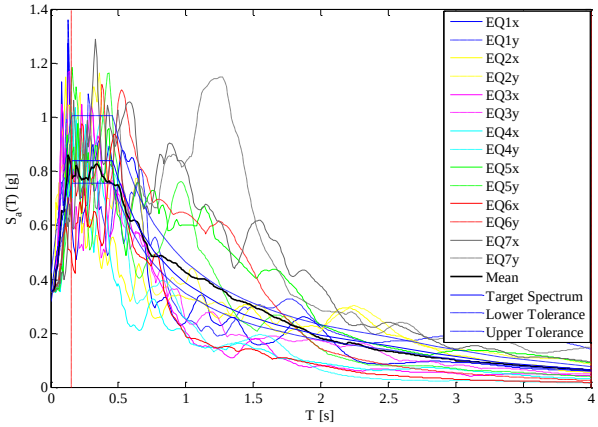

Figure 46 Spectro-compatible scaled spectra

Table 5 Set of 7 couples of spectro-compatible records

EQ	Waveform ID	EQ ID	Earthquake Name	Mw	PGA_x [g]	PGA_y [g]	Scaling Factor_x	Scaling Factor_y
1	242	111	Eastern Fukushima pref	6.6	0.19	0.18	1.84	1.95
2	139	51	Southern Iwate prefecture	6.9	0.30	0.22	1.18	1.59
3	243	111	Eastern Fukushima pref	6.6	0.13	0.10	2.73	3.55
4	432	83	Parkfield	6	0.36	0.23	0.98	1.54
5	438	83	Parkfield	6	0.14	0.23	2.50	1.54
6	146	54	S Suruga Bay	6.2	0.42	0.26	0.85	1.38
7	421	46	Irpinia	6.9	0.18	0.16	2.02	2.24

Fragility curve of each structural system is estimated through Incremental Dynamic Analysis (IDA), performing a wide number of dynamic non-linear analysis (Vamvatsikosand Cornell 2002). In particular, the Intensity Measure (IM) employed is the 5% damped spectral acceleration at the fundamental period of vibration $S_a(T_1)$. The Engineering Demand Parameter (EDP) selected is the interstorey drift for MRF, HYB and BF structures, while it is the base displacement for the BI system. A wide number of ground motions is selected again from SIMBAD database, in the attempt of reducing uncertainties of the collapse fragility curve. In particular a total of 42 records is selected on soil type B (Table 6),

covering a range of moment magnitude Mw between 5 and 7 and epicentral distance R between 15 km and 35 km (so including mid-to-far field events).

Table 6 Selected records for Incremental Dynamic Analysis

EQ	Waveform ID	EQ ID	Earthquake Name	Mw	R [km]	PGA_x [g]	PGA_y [g]
1	146	54	S Suruga Bay	6.2	25	0.42	0.26
2	422	72	Friuli 1st shock	6.4	22	0.32	0.35
3	432	83	Parkfield	6	20	0.36	0.23
4	438	83	Parkfield	6	15	0.14	0.23
5	272	122	Mid Niigata pref	6.2	21	0.25	0.28
6	144	54	S Suruga Bay	6.2	23	0.31	0.32
7	443	89	Imperial Valley	6.5	25	0.16	0.17
8	184	68	L'Aquila aftershock	5.6	17	0.28	0.25
9	427	74	Friuli 3rd shock	5.9	17	0.21	0.26
10	424	73	Friuli 2nd shock	5.6	26	0.23	0.13
11	169	64	L'Aquila mainshock	6.3	18	0.15	0.15
12	14	8	Near Miyakejima Island	6.4	22	0.13	0.20
13	395	150	Christchurch	5.2	15	0.28	0.24
14	284	125	MT Fuji region	5.9	20	0.14	0.16
15	61	23	Kyushu	5.7	17	0.36	0.22
16	252	114	Easter Fukushima pref	5.9	24	0.18	0.16
17	236	54	S Suruga Bay	6.2	31	0.10	0.23
18	286	125	MT Fuji region	5.9	20	0.24	0.17
19	138	50	Off Noto Peninsula	6.7	27	0.40	0.54
20	441	87	Tabas	7.1	21	0.41	0.33
21	456	94	Loma Prieta	6.9	28	0.32	0.51
22	454	94	Loma Prieta	6.9	29	0.36	0.33
23	412	35	Hector Mine	7.1	29	0.34	0.27
24	139	51	Southern Iwate Prefecture	6.9	23	0.30	0.22
25	463	99	Northridge	6.7	19	0.28	0.47
26	304	94	Loma Prieta	6.9	19	0.59	0.97
27	140	51	Southern Iwate Prefecture	6.9	19	0.36	0.38
28	421	46	Irpinia	6.9	19	0.18	0.16
29	22	12	W Tottori Prefecture	6.6	19	0.27	0.16
30	208	39	Duzce	7.1	27	0.50	0.91
31	242	111	Easter Fukushima pref	6.6	26	0.19	0.18
32	414	46	Irpinia	6.9	22	0.19	0.13
33	455	94	Loma Prieta	6.9	16	0.39	0.45
34	310	39	Duzce	7.1	30	0.12	0.16
35	429	75	Friuli 4th shock	5.9	17	0.33	0.35
36	37	15	N Miyagi Prefecture	6.1	25	0.20	0.15
37	115	41	South Iceland	6.5	17	0.38	0.25
38	118	42	South Iceland	6.4	21	0.11	0.17
39	42	16	Mid Niigata Prefecture	6.6	21	0.87	1.71
40	54	20	NE Fukuoka Prefecture	5.4	28	0.13	-
41	418	47	Umbria-Marche 3rd shock	5.6	20	0.13	-
42	220	104	E Off Izu Peninsula	5.6	24	0.21	-

Ground motion records are scaled considering an IM step of 0.1g covering a range between 0 to 2.5g for MRF, HYB and BF systems. Differently, for the BI case-study IM is made vary between 0 to 0.5g, considering that this structural typology is conceived to have large fundamental period of vibration and thus limited spectral acceleration. Consistently with recent IDA applications (Miano et al. 2016), for each record only one of the two horizontal components is selected, i.e. the one giving the higher spectral acceleration at the fundamental period of vibration. The structural fragility curve is derived from IDA curves in correspondence of the EDP value believed to cause collapse, which is, obviously, different for each seismic technology and will be specified in the next dedicated sections.

5.2.4 Loss estimation analysis

The intensity-based loss estimation analysis is performed through PACT software, widely illustrated in Chapter 3. In particular a total of 500 realizations of a Monte Carlo simulation are performed for each analysis. Only direct losses, that are costs caused by components' damage, structural irreparability or structural collapse, are considered in this work.
The analysis of costs is performed employing Italian pricing list catalogues and converting euros in dollars according to the 2011 currency exchange rate (1€ = 1.44$). Indeed, all costs implemented in PACT software as consequence functions of components' damaging refer to 2011. Once the construction cost of the MRF system is defined, as it will be clarified later, the cost of all other considered alternative solutions is evaluated increasing the MRF structural construction cost, estimated to be the 20% of the total (Krawinkler et al. 2004), due to increased construction materials quantity. More details about the analysis of cost of each case-study system is addressed to next sections.
A total loss threshold of 50% is set: it means that if in correspondence of a certain realization the sum of all components' repairing costs is higher than

the 50% of the total RePLacement Value (RPLV), the software considers RPLV as final output (the structure is demolished and rebuilt).
The population model integrated within PACT software for office destination of use is adopted in the present study. Although, note that this piece of information is needed to define casualties and injuries, that won't be analyzed as output in the present work, focusing only on direct losses.

5.2.4.1 Non-structural components and furnishings fragility

In order to perform the loss estimation analysis it is necessary to identify all the structural and non-structural (including furnishings) elements which may contribute to determine losses and define for each of them possible damage states and corresponding fragility curves. Structural components adopted depend on the seismic system in consideration and are specified in the next. Differently, non-structural (NS) components and contents (C) are the same for all the alternative technologies analyzed (except the HYB system employing low-damage non-structural components, defined later), and are listed in Table 7. In particular, given the lack of a fragility curves database typical of the Italian building stock elements, all of them have been selected from PACT database, each identified by a specific code. The EDP defining employed NS and C fragility components are the Interstorey Drift Ratio (IDR), the Peak Floor Acceleration of the floor above (PFA_fa), the Peak Floor Acceleration at the first floor (PFA_If) and the Peak Floor Acceleration of the supporting floor (PFA_sf). All the fragility components which are subjected to the same EDP have to be assigned to the same performance group. The user has to define the quantity of components per floor belonging to each performance group, according to the software units.

Table 7 Fragility components in MRF case-study

Type	Definition	Fragility component	Unit	Quantity per floor	Direction X	Direction Y	EDP
NS	Exterior glass window system	B2022.082	30SF	58.58	√	√	IDR
NS	Gypsum partition	C1011.001a	100LF	5.45	√	√	IDR
NS	Prefabricated steel stairs ; no seismic joint	C2011.001b	EA	0.54	√	-	IDR
NS	Suspended Ceiling	C3032.002b	600SF	8.17	-	-	PFA_fa
NS	Independent pendant lighting	C3034.001	EA	10.00	-	-	PFA_fa
NS	Hydraulic elevator	D1014.021	EA	1	-	-	PFA_If
NS	Cold Water Distribution Piping, SDC C	D2021.012a	1000LF	0.08	-	-	PFA_fa
NS	Hot Water Distribution Piping, SDC C	D2022.012a	1000LF	0.46	-	-	PFA_fa
NS	Hot Water Distribution Bracing, SDC C	D2022.012b	1000LF	0.16	-	-	PFA_fa
NS	Sanitary Waste Piping (flexible couplings), SDC C	D2031.012b	1000LF	0.31	-	-	PFA_fa
NS	HVAC Ducting - SDC C	D3041.011b	1000LF	0.41	-	-	PFA_fa
NS	HVAC drops/diffusers in suspended ceilings - SDC C	D3041.031b	EA per 10 gsf	4.90	-	-	PFA_fa
NS	Variable Air Volume (VAV) Box - SDC C	D3041.041b	EA per 10 gsf	2.72	-	-	PFA_fa
NS	Packaged Air Handling Unit	D3052.013b	EA per 10 gsf	1.00	-	-	PFA_sf
NS	Sprinkler Piping, old style victaulic - SDC D, E, F	D4011.023a	1000LF	1.09	-	-	PFA_fa
NS	Sprinkler drop	D4011.032a	100 EA	0.49	-	-	PFA_fa
NS	Motor control center unanchored	D5012.013a	EA	1.00	√	√	PFA_sf
NS	Low voltage switchgear	D5012.021a	EA	1.00	√	√	PFA_sf
C	Modular office workstation	E2022.001	EA	40.00	-	-	PFA_sf
C	Electronic equipment on wall mount brackets	E2022.021	EA	5.00	-	-	PFA_sf
C	Desktop electronics	E2022.023	EA	40. 00	-	-	PFA_sf

*Legend: IDR=Interstorey Drift Ratio; PFA_fa=Peak floor acceleration of the floor above; PFA_If=Peak floor acceleration at the first floor; PFA_sf=Peak floor acceleration of the supporting floor

5.2.4.2 Residual drift

In order to assess if the damaged facility is repairable or not, maximum residual drifts should be defined as input data of PACT software. In the specific case-study, residual drifts are calculated as output of a free vibration condition of the structure after shaking induced by each seismic record. The median irreparable residual story drift is assumed equal to 1%,

in accordance with FEMA P-58-1 (2012) recommendations and literature assumption (Welch et al. 2014).

5.3 The case-study structure designed as Moment Resisting Frame (MRF) system

The first technology adopted for the case-study structure is the traditional Moment Resisting Frame (MRF), based on the concept of capacity design criterion (Figure 47).

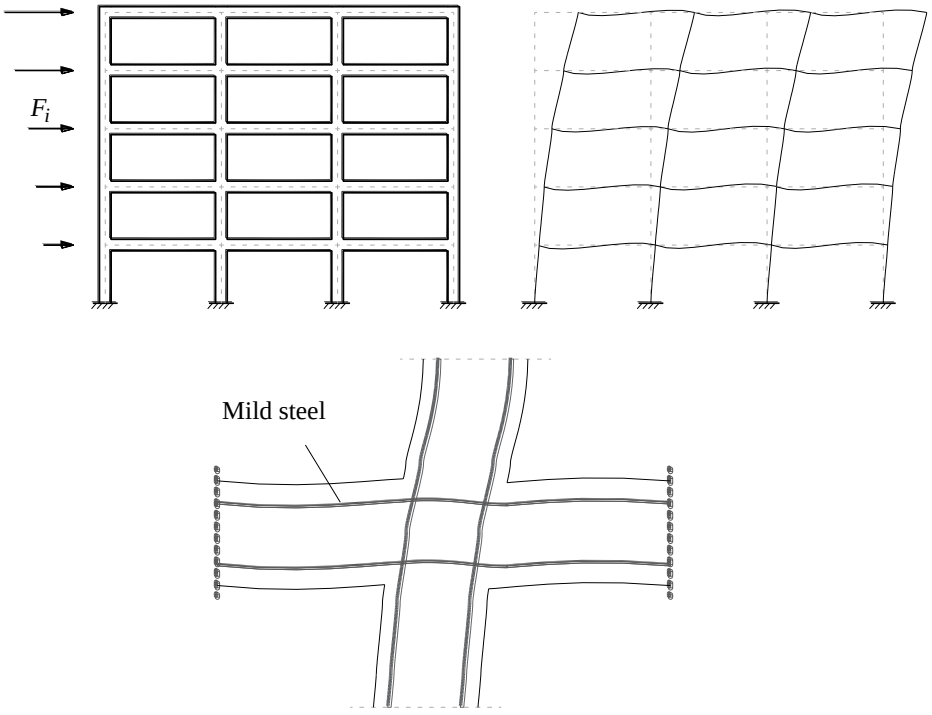

Figure 47 MRF system typical deformed shape

Beams and columns transversal sections are respectively 400x600 mm and 600x600 mm. The following sub-sections describe the application of the DDBD to the specific case-study and its main results, outputs of dynamic

non-linear analysis, definition of fragility curve and finally the development of the intensity-based loss analysis.

5.3.1 Materials

Concrete class employed is C25/30, characterized by the characteristic compressive strength at 28 days f_{ck}=25 MPa. Assuming safety partial factor according to the Italian seismic code provisions (NTC08), in the respect of the semi-probabilistic approach, the design value f_{cd}=14.17 MPa is obtained. The concrete modulus of elasticity is 30000 MPa. Steel reinforcement is B450C, corresponding to the characteristic and design strength values f_{yk}=450 MPa and f_{yd}=391.3 MPa respectively.

5.3.2 Application of DDBD

The Direct Displacement-Based Design (DDBD) is applied to the MRF system according to the indications provided at §4.4.1 and §5.2.2.
The yielding drift has been determined through the following expression:

$$\theta_y = 0.5 \cdot \varepsilon_y \cdot \frac{L_b}{h_b} \tag{25}$$

where ε_y is the yielding strain of steel reinforcement, L_b and h_b are respectively the beam's length and cross section's height.
The design drift is 2% assuming the first storey as critical. This limit is generally suggested by codes and guidelines for 10/50 hazard level (Krawinkler et al. 2004). The displacement profile in correspondence of yielding and at the design drift are evaluated, providing results summarized in Table 8 and Table 9 respectively.

Table 8 Evaluation of the yielding displacement profile - MRF system

Yielding parameters at critical storey	
ε_y [-]	0.0019
ϑ_y [-]	0.0116
$\Delta_{c,y}$ [m]	0.0373

Level [-]	H_i [m]	δ_i [-]	$\Delta_{i,y}$ [m]	m_i [tons]	$m_i\Delta_{i,y}$ [-]	$m_i\Delta_{i,y}^2$ [-]
5	16	1.000	0.147	280	41	6.05
4	12.8	0.853	0.126	464	58	7.31
3	9.6	0.680	0.100	464	46	4.64
2	6.4	0.480	0.071	464	33	2.31
1	3.2	0.253	0.037	464	17	0.64
				2134	**196**	**21**

Table 9 Evaluation of the design displacement profile - MRF system

Design parameters at critical storey	
ϑ_d [-]	0.02
H_c [m]	3.2
δ_c [-]	0.253
Δ_c [m]	0.064

Level [-]	H_i [m]	δ_i [-]	Δ_i [m]	m_i [tons]	$m_i\Delta_i$ [-]	$m_i\Delta_i^2$ [-]	$m_i\Delta_i H_i$ [-]
5	16	1.000	0.253	280	71	18	1131
4	12.8	0.853	0.216	464	100	22	1279
3	9.6	0.680	0.172	464	80	14	765
2	6.4	0.480	0.121	464	56	7	360
1	3.2	0.253	0.064	464	30	2	95
				2134	**336**	**62**	**3630**

Applying equations (14) to (17), the equivalent SDOF system parameters are determined. Its main properties are given in Table 10. Once the equivalent ductility μ is evaluated, the equivalent damping ratio is estimated according to the following equation (Pampanin et al. 2010):

$$\xi_s = 5\% + 30 \cdot \left(1 - \frac{1}{\sqrt{\mu}}\right)\% \tag{26}$$

The spectrum reduction factor is determined according to Italian seismic code (NTC08) formulation:

$$\eta = \sqrt{\frac{10}{5+\xi}} \tag{27}$$

Entering the reduced displacement response spectrum in correspondence of the equivalent SDOF displacement Δ_d (Figure 48), the equivalent period

can be estimated. Consequently, the equivalent stiffness and the final base shear are known.

Table 10 Application of the DDBD: evaluation of the equivalent SDOF properties, reduction factor, equivalent period and final base shear - MRF system

m_e	H_e	Δ_y	Δ_d	μ	ξ	η	T_e	K_e	Base Shear
[tons]	[m]	[m]	[m]	[-]	[%]	[-]	[s]	[kN/m]	[kN]
1829	10.80	0.107	0.184	1.72	12.11	0.76	2.51	11459	2107

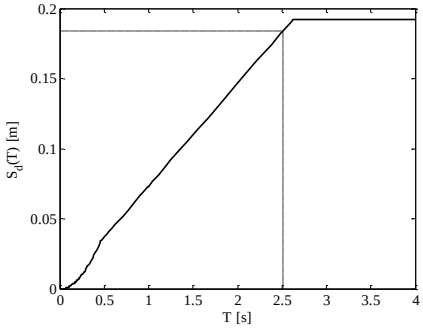

Figure 48 Reduced displacement response spectrum (ξ=12.1%) - MRF system

Table 11 Lateral forces distributed along levels - MRF system

Level	Δ_i [m]	m_i [tons]	$m_i\Delta_i$ [-]	F_i/V_{base} [-]	F_i [kN]
5	0.253	280	71	0.289	**305**
4	0.216	464	100	0.268	**282**
3	0.172	464	80	0.213	**225**
2	0.121	464	56	0.151	**159**
1	0.064	464	30	0.079	**84**
		2134	**336**	**1**	**1053**

The base shear is divided by the number of seismic lateral frames (two) and then distributed along the levels according to equations (20) and (21), obtaining lateral forces given in Table 11.
Descending internal actions are employed to dimension beams and columns longitudinal reinforcement.

5.3.3 Structural design and modeling

Beams and columns steel reinforcement quantity is chosen as a consequence of internal actions coming from the DDBD. Final configurations are represented in Figure 49.

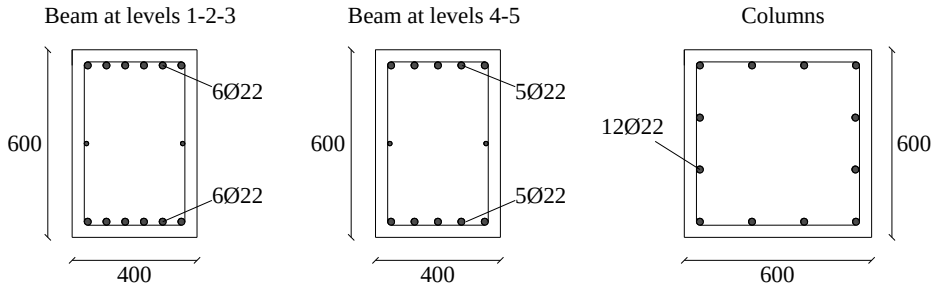

Figure 49 Beams and columns cross sections - MRF system

Mechanical characteristics of beam-column connections in terms of moment M and rotation θ have been estimated in correspondence of yielding (θ_y, M_y) and ultimate capacity (θ_C, M_C) according to Italian and European code prescriptions:

$$\vartheta_y = \chi_y \cdot \frac{L_v}{3} \tag{28}$$

$$\vartheta_u = \vartheta_y + \left(\chi_u - \chi_y\right) \cdot L_{pl} \cdot \left(1 - 0.5 \cdot \frac{L_{pl}}{L_v}\right) \tag{29}$$

where χ_y and χ_u are yielding and ultimate curvature values respectively, L_{pl} is the plastic lenght (Pampanin et al. 2010) and L_v is the shear length.
The choice of adopting the above expressions, thus neglecting shear and bond-slip contributions to yielding rotation and ignoring regression expressions for the evaluation of failure rotation (Eurocode 8 - part 1, 2003), allows coherent assumptions in accordance with the HYB case-study, as it will be clarified in the following sections. Final results are summarized in Table 12.

Table 12 Mechanical characteristics of MRF connections

Element type	Section	# Rebars	Axial load [kN]	θ_y [rad]	M_y [kNm]	θ_C [rad]	M_C [kNm]
Beam at level 1-2-3	40x60	12Φ22	0	0.0067	436	0.0671	453
Beam at level 4-5	40x60	10Φ22	0	0.0065	364	0.0669	379
External column	60x60	12Φ22	323	0.0047	445	0.0505	524
Internal column	60x60	12Φ22	1163	0.0042	556	0.0308	642

An Opensees (McKenna 1997) lumped plasticity finite element model has been constructed adopting "elasticBeamColumn" element for beams and columns. As far as plastic hinges modeling is concerned, elements of zero length with "uniaxialMaterial Hysteretic" has been defined at the end of beams and at the base of columns, assuming values of Table 12 and a degrading unloading stiffness factor of 0.3 and 0.5 respectively. Actually, since the elastic chord rotation is already accounted within the deformability of the elasticBeamColumn elements, deformations of the connection are deducted from the elastic part of them, corresponding to the deformation until cracking is observed.

5.3.4 Dynamic non-linear analysis

The first vibrational period of the 2D MRF system is T_1=0.94s. Actually the frame is reasonably deformable due to large bays' width. Note that the modal analysis is performed considering all nodes rotationally fixed, given that in the elastic range no plastic hinge is formed. Moreover, since the seismic action is demanded only to external frames, the seismic mass is distributed in each direction only between the two resisting frames, so contributing to increase the value of the period.

Dynamic nonlinear analysis are performed in correspondence of the set of records introduced in paragraph 5.2.3. An OpenSees-Matlab code is created in order to both check the structural design and get EDP values needed for the loss estimation analysis, that are maximum Interstorey Drifts Ratio (IDR), Peak Floor Accelerations (PFA) and maximum

Residual Intersotrey Drifts Ratio (RIDR). The displacement profile envelope in correspondence of each record is plotted in Figure 50, showing also the mean trend. Similarly, IDR, PFA and RIDR envelopes are given in Figure 51, Figure 52 and Figure 53 respectively.

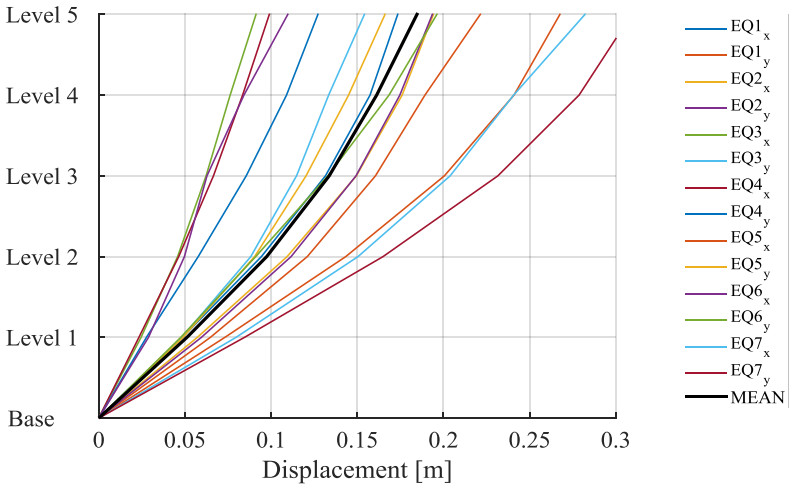

Figure 50 Displacement profile envelope of MRF system

It is verified that in correspondence of beams and columns the mean of maximum internal actions over the 14 records is never greater than elements' capacity. Moreover the global failure mechanism is checked through the comparison of columns and beams flexural capacity, according to Italian and European codes' prescriptions.

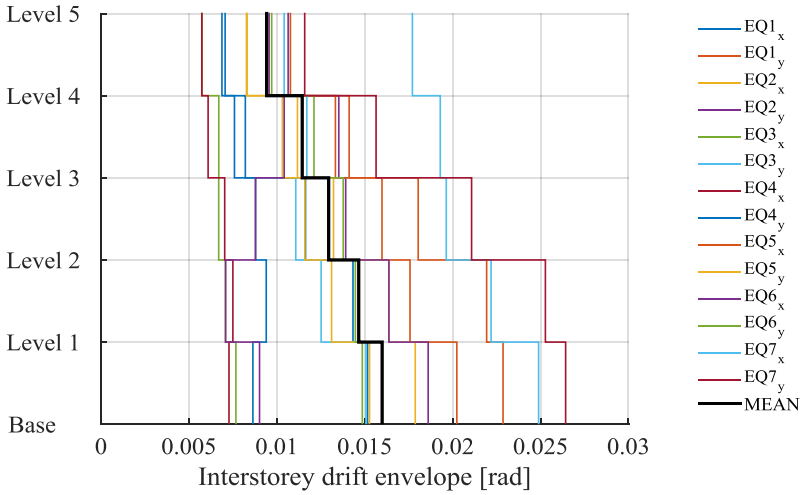

Figure 51 IDR envelope of MRF system

Table 13 Maximum IDR values of MRF system

Level	Base-1	1-2	2-3	3-4	4-5
EQ1x	1.52%	1.43%	1.16%	0.82%	0.71%
EQ1y	2.02%	1.76%	1.60%	1.41%	1.08%
EQ2x	1.79%	1.64%	1.32%	1.12%	0.83%
EQ2y	1.86%	1.64%	1.39%	1.35%	1.06%
EQ3x	0.77%	0.71%	0.67%	0.67%	0.58%
EQ3y	1.51%	1.25%	1.11%	1.17%	1.04%
EQ4x	0.73%	0.75%	0.70%	0.61%	0.57%
EQ4y	0.86%	0.94%	0.88%	0.76%	0.69%
EQ5x	2.29%	2.19%	1.80%	1.33%	0.95%
EQ5y	1.53%	1.31%	1.16%	1.03%	0.83%
EQ6x	0.90%	0.71%	0.88%	1.04%	0.96%
EQ6y	1.49%	1.45%	1.38%	1.21%	0.97%
EQ7x	2.49%	2.22%	1.96%	1.93%	1.77%
EQ7y	2.64%	2.53%	2.11%	1.56%	1.16%
MEAN	**1.60%**	**1.47%**	**1.29%**	**1.14%**	**0.94%**

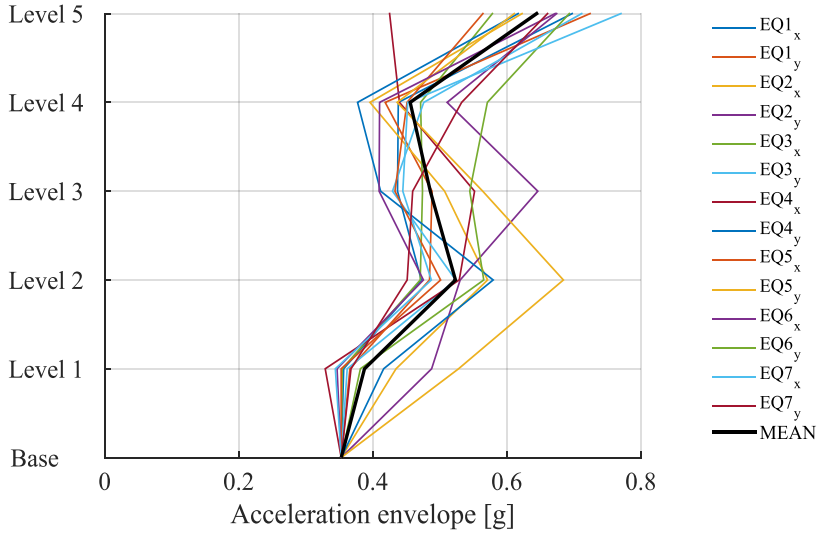

Figure 52 PFA envelope of MRF system

.

Table 14 PFA values of MRF system (in g)

Level	Ground	1	2	3	4	5
EQ1x	0.35	0.36	0.47	0.44	0.44	0.70
EQ1y	0.35	0.37	0.48	0.49	0.42	0.72
EQ2x	0.35	0.43	0.57	0.51	0.40	0.62
EQ2y	0.35	0.49	0.53	0.65	0.51	0.67
EQ3x	0.35	0.35	0.47	0.47	0.47	0.58
EQ3y	0.35	0.36	0.52	0.43	0.48	0.71
EQ4x	0.35	0.33	0.53	0.55	0.44	0.43
EQ4y	0.35	0.42	0.58	0.41	0.38	0.62
EQ5x	0.35	0.35	0.50	0.43	0.45	0.56
EQ5y	0.35	0.53	0.68	0.56	0.44	0.61
EQ6x	0.35	0.35	0.48	0.41	0.41	0.67
EQ6y	0.35	0.38	0.57	0.54	0.57	0.69
EQ7x	0.35	0.34	0.49	0.44	0.45	0.77
EQ7y	0.35	0.37	0.45	0.46	0.53	0.66
MEAN	**0.35**	**0.39**	**0.52**	**0.49**	**0.46**	**0.64**

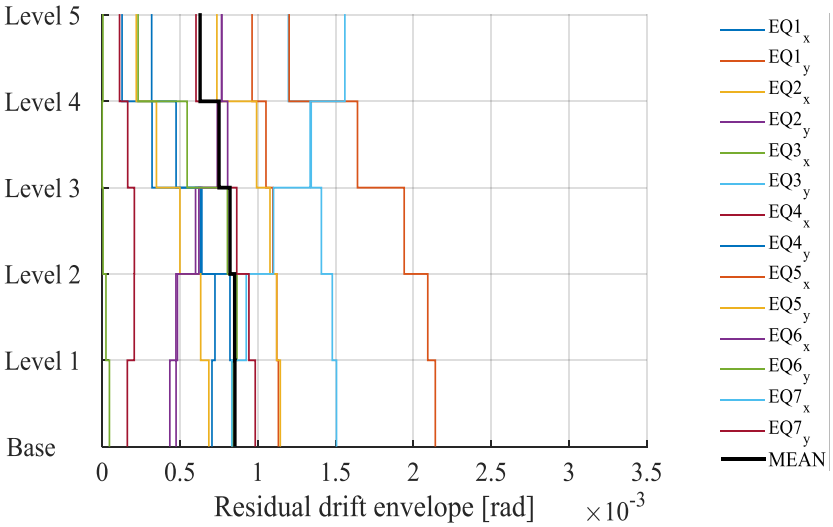

Figure 53 RIDR envelope of MRF system

Table 15 Maximum RIDR values of MRF system

Level	Base-1	1-2	2-3	3-4	4-5
EQ1x	0.01%	0.03%	0.06%	0.08%	0.09%
EQ1y	0.10%	0.11%	0.11%	0.11%	0.11%
EQ2x	0.07%	0.10%	0.11%	0.11%	0.11%
EQ2y	0.08%	0.07%	0.06%	0.05%	0.04%
EQ3x	0.00%	0.00%	0.00%	0.00%	0.00%
EQ3y	0.12%	0.13%	0.14%	0.15%	0.15%
EQ4x	0.01%	0.02%	0.02%	0.02%	0.02%
EQ4y	0.03%	0.05%	0.06%	0.07%	0.07%
EQ5x	0.12%	0.16%	0.19%	0.21%	0.21%
EQ5y	0.02%	0.03%	0.05%	0.06%	0.07%
EQ6x	0.08%	0.08%	0.06%	0.05%	0.05%
EQ6y	0.02%	0.05%	0.08%	0.09%	0.08%
EQ7x	0.16%	0.13%	0.11%	0.09%	0.08%
EQ7y	0.06%	0.07%	0.09%	0.09%	0.10%
MEAN	**0.06%**	**0.08%**	**0.08%**	**0.09%**	**0.09%**

5.3.5 IDA analysis and fragility curve

Incremental Dynamic Analysis (IDA) are performed employing the 42 records introduced in §5.2.3 and adopting interstorey drift as EDP (Figure 54). The fragility curve (Figure 55) is constructed selecting the IM values that cause collapse and plotting the relative Cumulative Distribution

Function (CDF). In particular, the attainment of failure is considered when an interstorey drift of 5% is reached, as suggested in previous works (Welch et al. 2014, Garro 2017). This assumption, generally accepted, is coherent with the value of drift generating collapse of the structural component beam-column connection, stored in the PACT fragility components database.

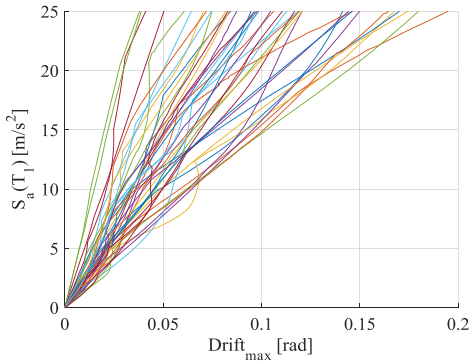

Figure 54 IDA curves for MRF system

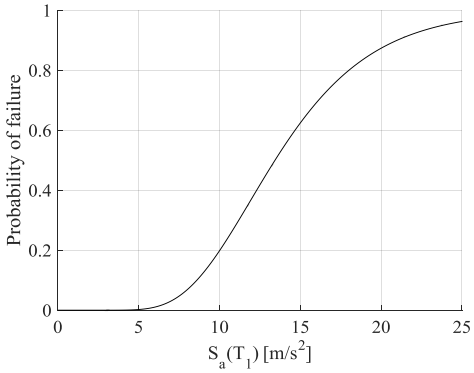

Figure 55 Fragility curve for MRF system

5.3.6 Structural fragility components

The structural fragility components adopted for the MRF case-study building consist in beam-column connections with beam just on one side (external joint) or on both sides (internal joint). The fragility component is integrated within PACT software database. Three different Damage States (DS) are distinguished: at Damage State 1 (DS1) beams or joints exhibit residual crack widths greater than 0.06 inches, there is no significant spalling nor fracture or buckling of steel reinforcing. The median drift corresponding to the achievement of this damage state is θ=2.00%, while dispersion is β=0.4. When spalling of cover concrete exposes beam and joint transverse reinforcement, but not longitudinal reinforcement, Damage State 2 (DS2) is reached, corresponding to median drift θ=2.75% and dispersion β=0.3. Finally, at Damage State 3 (DS3) spalling of cover

concrete exposes a significant length of beam longitudinal reinforcement, crushing of core concrete may occur, as well as fracture or buckling of reinforcing. At this level the median drift is θ=5.00% and dispersion β=0.3. The probability of failure of the structural beam-column joint in correspondence of the three damage states is shown in Figure 56.

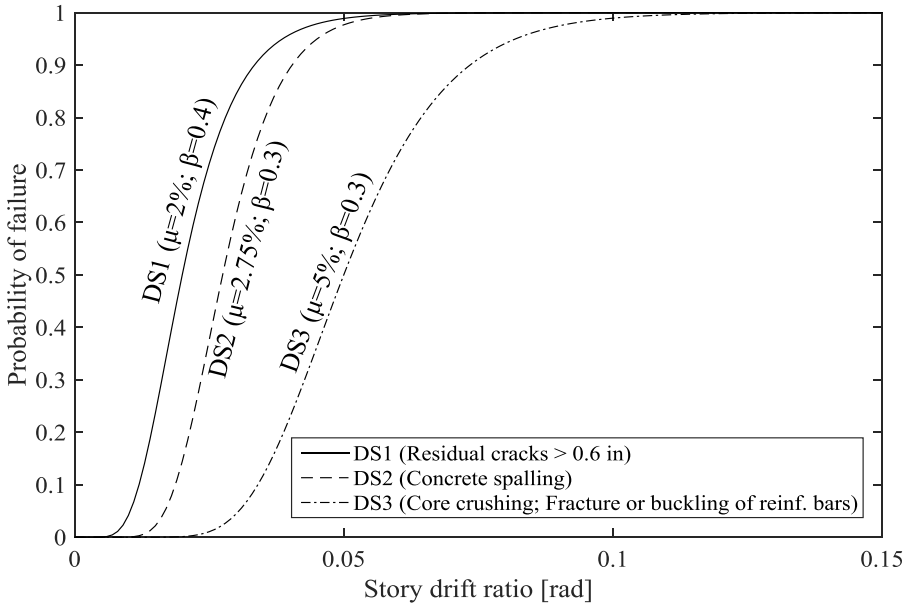

Figure 56 MRF beam-column joint fragility function

Economic consequences corresponding to each damage state are evaluated taking into consideration all repair activities necessary to recover the specific damage state and bring back the system to its original state. As far as MRF beam-column joints are concerned, all DSs require a preliminary repair activity consisting in removing furnishings, ceilings and mechanical, electrical and plumbing systems. Then, at DS1 it is necessary to replace and repair finishes or, as necessary, to prepare cracks to receive epoxy injection. At DS2, after cleaning the area adjacent to the damaged concrete, it is necessary to prepare spalled concrete and cracks to be patched with grout and to receive epoxy injection. Differently, at DS3,

after cleaning the area adjacent to the damaged concrete, it is required to remove it, place concrete forms, place concrete and, finally, remove forms. If fracture or buckling of steel reinforcing occurs, prior to treating damaged concrete as explained above, it is necessary to remove damaged components, place and splice new reinforcement bars to existing, undamaged ones. Finally, for all DSs it is required to replace furnishings, ceilings and mechanical, electrical and plumbing systems. Economic consequences relating to each DS are given in Figure 57 and are in accordance with PACT library and Fitzgerald et al. (2016) indications.

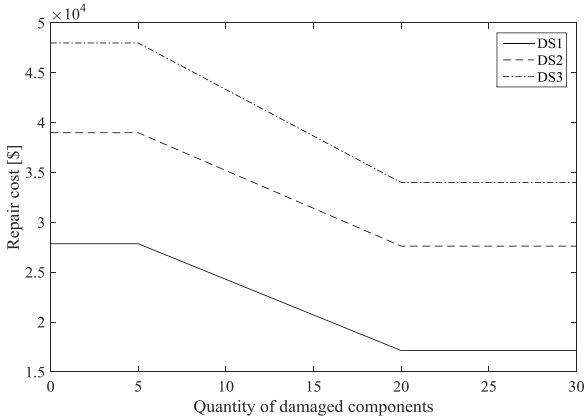

Damage States	Low quantity [$]	High quantity [$]
DS1	27846	17136
DS2	38978	27610
DS3	47978	33985

Figure 57 MRF beam-column joint consequence function

5.3.7 Loss estimation analysis and results

In order to perform the loss estimation analysis it is necessary to evaluate the total replacement cost of the facility. The construction cost of the reinforced concrete MRF system addressed to office use is estimated to be around 1728 $/m^2, according to literature review (De Mare et al. 2002, Garro 2017). The demolition and site clearance cost is estimated according to indications of Italian provisions after the Central Italy Earthquake of 2016 (Prezzario Unico del Cratere del Centro Italia, 2016), predicting a cost of 449 $/m^2, corresponding to the 26% of the construction cost. This

result is coherent with indications of FEMA P-58-1 (2012), suggesting that the reconstruction and site clearance cost is around 20-30% of the initial construction cost. Therefore the total replacement cost is finally set to be 2177 $/m^2$, which is in accordance with state-of-art indications (Saborío Romano et al. 2017) and corresponds to a total of 6.61 M$. The construction cost of the only structural part of the building (concrete and steel reinforcement), including cost of labour, is estimated through the use of Central Italy construction price list (Bollettino ufficiale della Regione Umbria, 2014). For this case-study this cost corresponds to a total of 86'878 $, considering only elements of the external frames, that provide seismic resistance.

Assuming indications provided at paragraph §5.2.4, together with EDP, probability of collapse and structural fragility components given respectively in §5.3.4, §5.3.5 and §5.3.6, intensity-based loss estimation analysis is performed.

Repair Costs (RC) corresponding to each realization of the Monte Carlo simulation are plotted in Figure 58-a, showing also the amount of repair costs provided by each component's category. It is evident that in correspondence of a generic realization the more significant contribution comes always from non-structural components, followed by structural elements and contents. Note that in no simulation the structure is collapsed, while in a few number of them the structure is deemed to be irreparable, causing the total replacement cost corresponding to the demolition, site clearance, and reconstruction. Moreover, in some simulations the sum of repairing costs of damaged components is higher than the 50% of the RPLV, that is the total loss threshold, thus generating again the total replacement cost. This is why the total repair cost curve (dashed curve in Figure 58-a) is higher than RC profile. The total sum of RCs corresponds to the fictitious total amount of money required to repair the structure over 500 realizations, and it is equal to 821 M$. The area beneath the repair cost curve corresponding to structural and non-

structural components, contents and demolition/reconstruction contributions is compared to the total area, providing the pie chart of Figure 58-b. Data observed confirm that the main part of repair costs is attributed to non-structural components, which cover a percentage of 56% of the total, followed by structural components (31%), contents (8%) and demolition/reconstruction cases (4%).

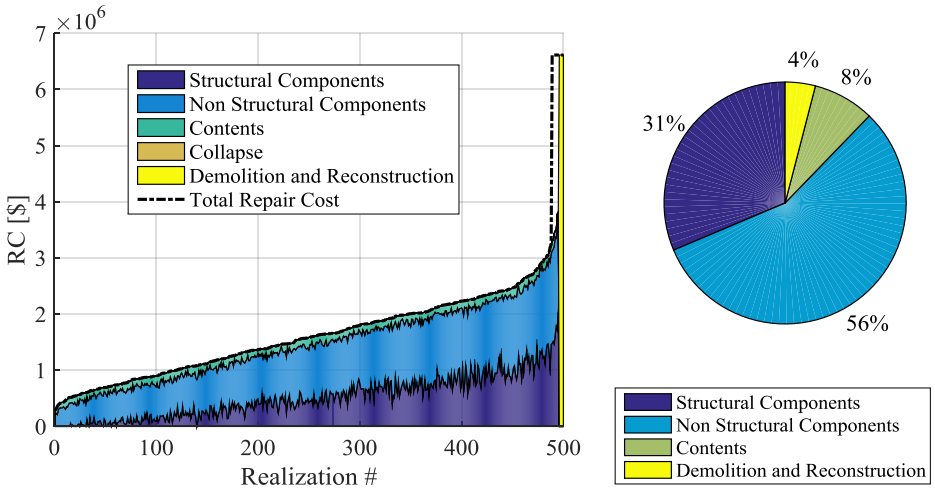

(a) (b)

Figure 58: a) Repair cost over realizations - MRF system; b) Contribution of different categories to the overall repair cost (821 M$) for MRF system

The Mean Damage Factor (MDF) of RC is 1.69 M$, the Scenario Expected Loss (SEL) is 1.59 M$ and the Scenario Upper Loss (SUL) is 2.46 M$. The characteristic value PML_k is 2.82 M$

Repair costs are binned and shown in the bar plot of Figure 59, while the Cumulative Distribution Function (CDF) of Repair Cost is given in Figure 60. Figure 61 and Figure 62 show respectively the CDF of Repair Cost Ratio (RCR), corresponding to RC over the total RPLV of the building, and its complementary to 1, defined as probability of loss.

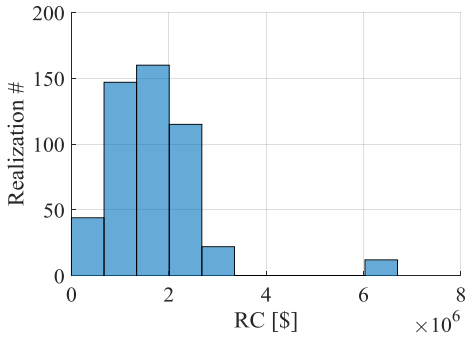

Figure 59 Binned repair costs resulting from the Intensity-based loss estimation analysis of the MRF system

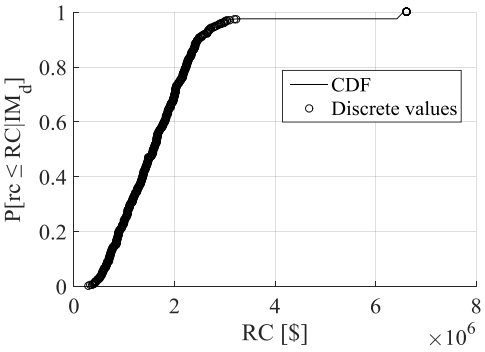

Figure 60 Cumulative distribution function of repair cost (RC) - MRF system

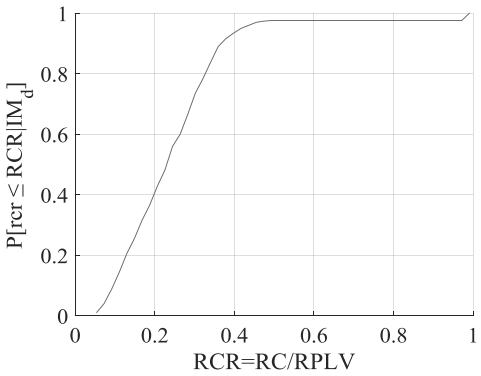

Figure 61 Cumulative distribution function of repair cost ratio (RCR) - MRF system

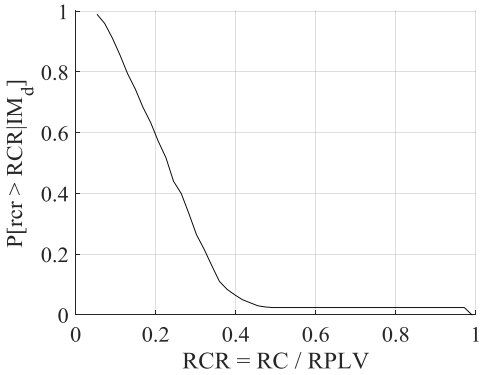

Figure 62 Probability of loss - MRF system

5.4 The case-study structure designed as Hybrid (HYB) system

The case-study building is designed again assuming a rocking dissipative (hybrid) system as seismic technology (HYB). The typical deformed shape of this structural typology is illustrated in Figure 63.

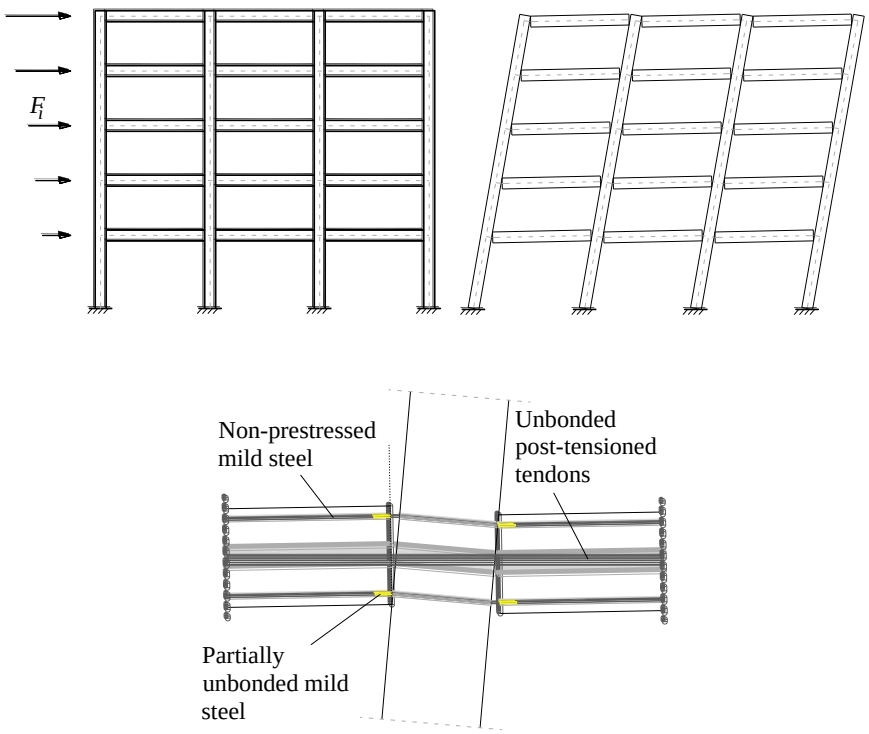

Figure 63 Typical deformed shape and beam-column connection of the HYB system

Beams and columns transversal sections are respectively 400x600 mm and 600x600 mm, as in the MRF case-study. The following sub-sections describe the application of the DDBD to the HYB case-study and its main results, outputs of dynamic non-linear analysis, definition of fragility curve and finally the development of the intensity-based loss analysis.

5.4.1 Materials

Concrete class is higher than MRF case-study due to the presence of post-tensioning cables. In particular it corresponds to C28/35, characterized by the characteristic compressive strength at 28 days f_{ck}=28 MPa. Assuming safety partial factor according to the Italian seismic code provisions (NTC08), in the respect of the semi-probabilistic approach, the design

value f_{cd}=16 MPa is obtained. The concrete modulus of elasticity is 30000 MPa. Steel reinforcement is B450C, corresponding to the characteristic and design strength values f_{yk}=450 MPa and f_{yd}=391.3 MPa respectively, modulus of elasticity E_s=210000 MPa. Post-tensioned cables are characterized by yielding and collapse resistances respectively f_{pty}=1670 MPa and f_{ptu}=1860 MPa, and modulus of elasticity E_{pt}=201000 MPa. Strand's nominal diameter is 15.2 mm, while the section is 139 mm^2.

5.4.2 Application of DDBD

The Direct Displacement-Based Design (DDBD) is applied to the HYB system according to the indications provided at §4.4.1 and §5.2.2. The design drift is 2% assuming the first storey as critical, while the yielding drift is defined through the following equation (Priestley 2002):

$$\theta_y = 0.004 \cdot \frac{L_b}{h_b} \tag{30}$$

where L_b and h_b are the beam's length and cross section's height, respectively.

The design re-centering ratio is selected as λ=1.25. The displacement profiles in correspondence of yielding and at the design drift are respectively summarized in Table 16 and Table 17.

Table 16 Evaluation of the yielding displacement profile - HYB system

Yielding parameters at critical storey	
ε_y [-]	0.0019
ϑ_y [-]	0.0050
$\Delta_{c,y}$ [m]	0.0160

Level [-]	H_i [m]	δ_i [-]	$\Delta_{i,y}$ [m]	m_i [tons]	$m_i\Delta_{i,y}$ [-]	$m_i\Delta_{i,y}^2$ [-]
5	16	1.000	0.063	280	18	1.12
4	12.8	0.853	0.054	464	25	1.35
3	9.6	0.680	0.043	464	20	0.86
2	6.4	0.480	0.030	464	14	0.43
1	3.2	0.253	0.016	464	7	0.12
				2134	**84**	**4**

Table 17 Evaluation of the design displacement profile - HYB system

Design parameters at critical storey	
ϑ_d [-]	0.02
H_c [m]	3.2
δ_c [-]	0.253
Δ_c [m]	0.064

Level [-]	H_i [m]	δ_i [-]	Δ_i [m]	m_i [tons]	$m_i\Delta_i$ [-]	$m_i\Delta_i^2$ [-]	$m_i\Delta_i H_i$ [-]
5	16	1.000	0.253	280	71	18	1131
4	12.8	0.853	0.216	464	100	22	1279
3	9.6	0.680	0.172	464	80	14	765
2	6.4	0.480	0.121	464	56	7	360
1	3.2	0.253	0.064	464	30	2	95
				2134	**336**	**62**	**3630**

Applying equations (14) to (17), the equivalent SDOF system parameters are determined. Its main properties are given in Table 18. After evaluating the SDOF equivalent ductility μ, the equivalent damping ratio is estimated according to the following equation (Pampanin et al. 2010):

$$\xi_{hybrid}=5\%+30\cdot\frac{\left(1-\frac{1}{\sqrt{\mu}}\right)}{(1+\lambda)}\% \tag{31}$$

Entering the reduced displacement response spectrum in correspondence of the equivalent SDOF displacement Δ_d (Figure 64), the equivalent period can be estimated. Consequently, the equivalent stiffness and the final base shear are known. The base shear is divided by the number of seismic lateral frames (two) and then distributed along the levels, obtaining lateral forces given in Table 19. Descending internal actions are employed to dimension beams and columns longitudinal reinforcement.

Table 18 Application of the DDBD: evaluation of the equivalent SDOF properties, reduction factor, equivalent period and final base shear - HYB system

m_e [tons]	H_e [m]	Δ_y [m]	Δ_d [m]	μ [-]	ξ [%]	η [-]	T_e [s]	K_e [kN/m]	Base Shear [kN]
1829	10.80	0.046	0.184	4	11.67	0.77	2.48	11738	2158

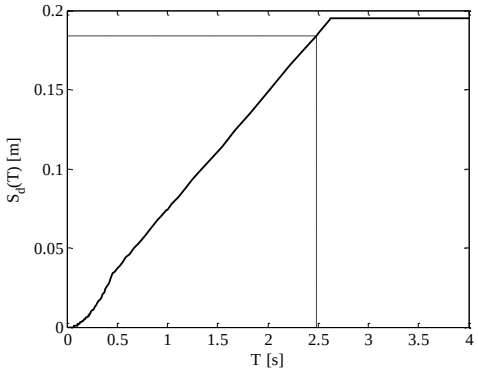

Figure 64 Reduced displacement response spectrum (ξ=11.7%)

Table 19 Lateral forces distributed along levels - HYB system

Level	Δ_i [m]	m_i [tons]	$m_i\Delta_i$ [-]	F_i/V_{base} [-]	F_i [kN]
5	0.253	280	71	0.289	**312**
4	0.216	464	10	0.268	**289**
3	0.172	464	80	0.213	**230**
2	0.121	464	56	0.151	**162**
1	0.064	464	30	0.079	**86**
		2134	**336**	**1**	**1079**

5.4.3 Structural design and modeling

The design of mild steel and post-tensioning in beams and columns can be rapidly performed considering the internal actions estimated through the DDBD procedure and factoring it respectively by α and β parameters. Final configurations are represented in Figure 65.

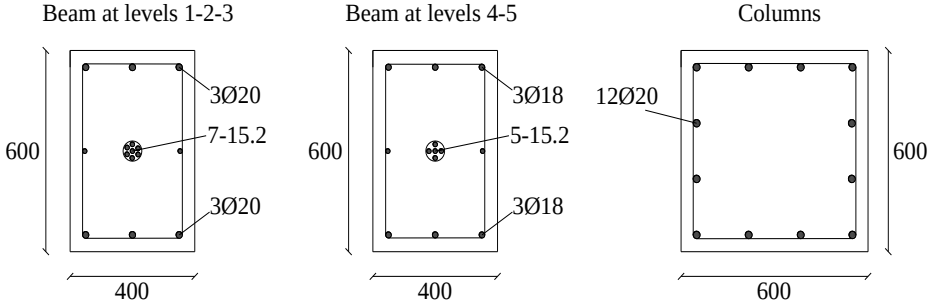

Figure 65 Beams and columns cross sections - HYB system

Mechanical characteristics of beam-column connections in terms of moment M and rotation θ have been estimated in correspondence of decompression (θ_{DEC}, M_{DEC}), yielding (θ_y, M_y) and ultimate capacity (θ_C, M_C). In particular, rotation at decompression is zero, since is represents

the opening of the gap in the rocking mechanism. The corresponding moment is evaluated through elastic relation, considering that the stress at the outer most fibre is equal to zero. Moment and rotation at yielding and failure are calculated through the hypothesis of Moment Beam Analogy (MBA), as introduced by Pampanin et al. (2001). Indeed, in order to evaluate the moment capacity, it is not possible to adopt the typical section analysis approach since the strain compatibility between steel and concrete is not valid any more due to unbonded reinforcement. Consequently, the concept of Monolithic Beam Analogy (MBA) has been proposed in order to introduce an alternative compatibility condition. An iterative procedure allows to get both yielding and ultimate moments (Pampanin et al. 2010). Final results are summarized in Table 20.

Table 20 Mechanical characteristics of HYB connections

Element type	Section [cm^2]	Rebars	Axial load [kN]	M_{DEC} [kNm]	θ_y [rad]	M_y [kNm]	θ_C [rad]	M_c [kNm]
Beam at level 1-2-3	40x60	6Φ20; 7-15.2 Super Strands (A=139mm^2 - $T_{PT,initial}$=900kN)	0	90	0.0015	391	0.0447	468
Beam at level 4-5	40x60	6Φ18; 5-15.2 Super Strands (A=139mm^2 - $T_{PT,initial}$=400kN)	0	40	0.0012	258	0.0616	376
External column	60x60	12Φ20	265	27	0.0012	403	0.0635	518
Internal column	60x60	12Φ20	1163	116	0.0015	574	0.0332	652

An Opensees (McKenna 1997) lumped plasticity finite element model has been constructed adopting “elasticBeamColumn” element for beams and columns. As far as plastic hinges modeling is concerned, elements of zero length characterized by two springs in parallel have been defined within beam-column connections and at the base of columns. The first spring corresponds to mild steel and is described by "uniaxialMaterial Hysteretic", as already employed for MRF system. The other represents

the elastic nonlinear post-tensioning behavior, modeled by "uniaxialMaterial ElasticMultiLinear", assuming values of Table 20.

5.4.4 Dynamic non-linear analysis

The first vibrational period of the 2D HYB system is T_1=0.94s, consistently with modal result of the MRF case-study. Indeed, the two structures, MRF and HYB, have the same elastic performance prior MRF cracking or HYB decompression points are reached.

Dynamic nonlinear analysis are performed in correspondence of the set of records introduced in paragraph 5.2.3. An OpenSees-Matlab code is created in order to both check the structural design and get EDP values needed for the loss estimation analysis. The displacement profile envelope in correspondence of each record is plotted in Figure 66, showing also the mean trend.

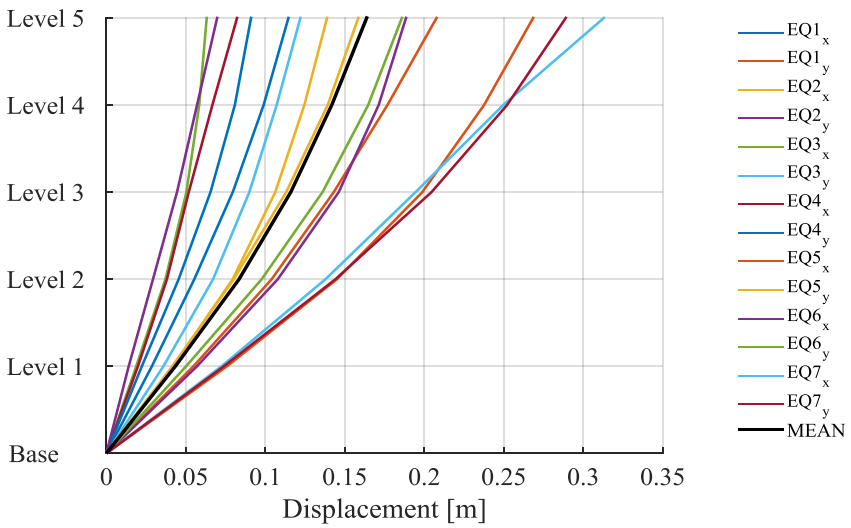

Figure 66 Displacement profile envelope of HYB system

It is verified that in correspondence of beams and columns the mean of maximum internal actions over the 14 records is never greater than elements' capacity.

EDPs required for the loss estimation analysis are IDR, PFA and RIDR. In particular, the maximum in correspondence of each record is selected and recalled in the following tables and figures.

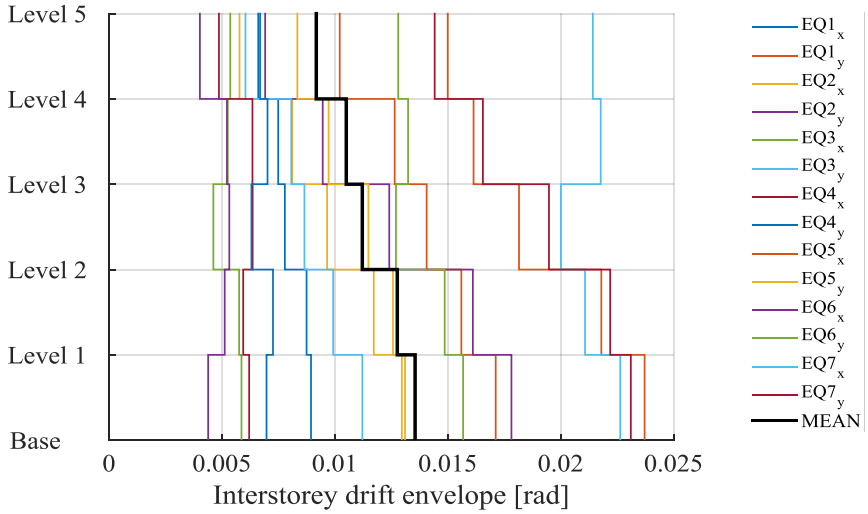

Figure 67 IDR envelope of HYB system

Table 21 Maximum IDR values of HYB system

Level	Base-1	1-2	2-3	3-4	4-5
EQ1x	0.89%	0.88%	0.78%	0.75%	0.66%
EQ1y	1.71%	1.56%	1.41%	1.27%	1.02%
EQ2x	1.31%	1.17%	0.97%	0.81%	0.58%
EQ2y	1.78%	1.61%	1.24%	0.95%	0.69%
EQ3x	0.59%	0.58%	0.46%	0.53%	0.54%
EQ3y	1.12%	0.99%	0.87%	0.81%	0.60%
EQ4x	0.62%	0.59%	0.64%	0.64%	0.49%
EQ4y	0.70%	0.73%	0.63%	0.70%	0.67%
EQ5x	2.37%	2.18%	1.82%	1.61%	1.50%
EQ5y	1.30%	1.26%	1.15%	0.97%	0.83%
EQ6x	0.44%	0.51%	0.53%	0.52%	0.40%
EQ6y	1.57%	1.49%	1.27%	1.32%	1.28%
EQ7x	2.26%	2.11%	2.00%	2.18%	2.14%
EQ7y	2.31%	2.22%	1.95%	1.66%	1.44%
MEAN	**1.36%**	**1.28%**	**1.12%**	**1.05%**	**0.92%**

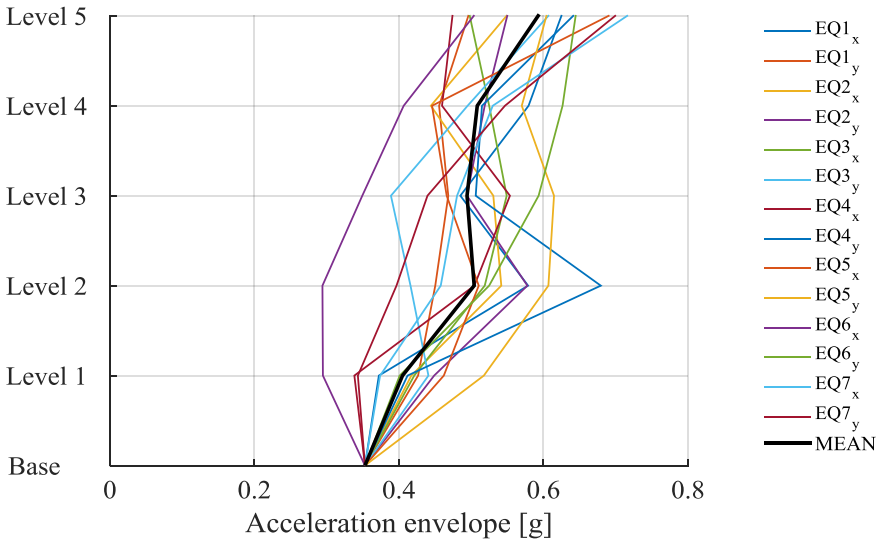

Figure 68 PFA envelope of HYB system

Table 22 PFA values of HYB system (in g)

Level	Ground	1	2	3	4	5
EQ1x	0.35	0.37	0.58	0.48	0.58	0.62
EQ1y	0.35	0.43	0.45	0.47	0.46	0.50
EQ2x	0.35	0.42	0.54	0.53	0.44	0.55
EQ2y	0.35	0.45	0.58	0.49	0.52	0.55
EQ3x	0.35	0.42	0.52	0.55	0.52	0.50
EQ3y	0.35	0.44	0.42	0.39	0.50	0.61
EQ4x	0.35	0.34	0.50	0.55	0.46	0.47
EQ4y	0.35	0.41	0.68	0.51	0.51	0.64
EQ5x	0.35	0.46	0.51	0.47	0.45	0.69
EQ5y	0.35	0.52	0.61	0.61	0.57	0.60
EQ6x	0.35	0.29	0.29	0.35	0.41	0.50
EQ6y	0.35	0.40	0.52	0.59	0.63	0.64
EQ7x	0.35	0.37	0.46	0.48	0.53	0.72
EQ7y	0.35	0.34	0.40	0.44	0.55	0.70
MEAN	**0.35**	**0.40**	**0.50**	**0.49**	**0.51**	**0.59**

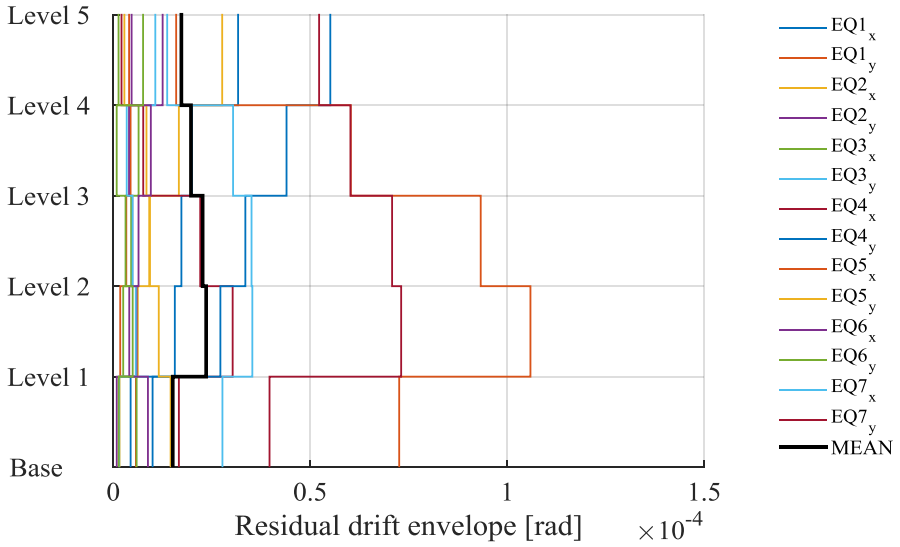

Figure 69 RIDR envelope of HYB system

Table 23 Maximum RIDR values of HYB system

Level	Base-1	1-2	2-3	3-4	4-5
EQ1x	0.00%	0.00%	0.00%	0.00%	0.00%
EQ1y	0.00%	0.00%	0.00%	0.00%	0.00%
EQ2x	0.00%	0.00%	0.00%	0.00%	0.00%
EQ2y	0.00%	0.00%	0.00%	0.00%	0.00%
EQ3x	0.00%	0.00%	0.00%	0.00%	0.00%
EQ3y	0.00%	0.00%	0.00%	0.00%	0.00%
EQ4x	0.00%	0.00%	0.00%	0.00%	0.00%
EQ4y	0.01%	0.00%	0.00%	0.00%	0.00%
EQ5x	0.00%	0.01%	0.01%	0.01%	0.01%
EQ5y	0.00%	0.00%	0.00%	0.00%	0.00%
EQ6x	0.00%	0.00%	0.00%	0.00%	0.00%
EQ6y	0.00%	0.00%	0.00%	0.00%	0.00%
EQ7x	0.00%	0.00%	0.00%	0.00%	0.00%
EQ7y	0.01%	0.01%	0.01%	0.01%	0.00%
MEAN	**0.002%**	**0.002%**	**0.002%**	**0.002%**	**0.002%**

5.4.5 IDA analysis and fragility curve

Incremental Dynamic Analysis (IDA) are performed employing the 42 records introduced at §5.2.3 and adopting interstorey drift as EDP. Resulting IDA curves are plotted in Figure 70. The fragility curve, given in Figure 71, is constructed selecting the IM values that cause collapse and

plotting the relative Cumulative Distribution Function (CDF). In particular the attainment of failure is considered when an interstorey drift of 6.9% is reached. This assumption corresponds to the value of drift generating collapse of the structural component hybrid beam-column joint, proposed by Fitzgerald et al. (2016) and estimated through the analysis of experimental results of 12 specimens reported in previous studies.

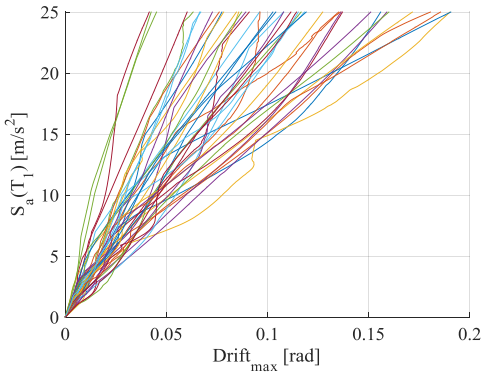

Figure 70 IDA curves for HYB system

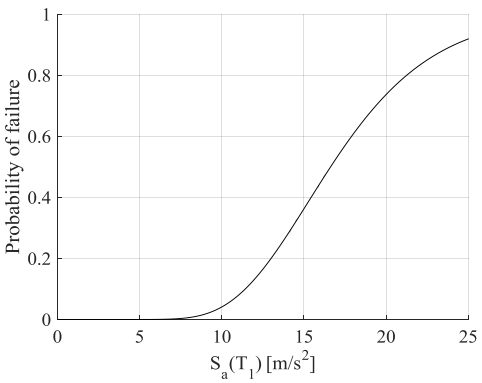

Figure 71 Fragility curve for HYB system

5.4.6 Structural fragility components

The beam-column joint fragility component adopted for the HYB case-study building has been developed by Haselton Baker Risk Group (Fitzgerald et al., 2016). Three different Damage States (DS) are distinguished: at Damage State 1 (DS1) spalling of cover concrete exposes beam and possibly column's transverse reinforcement, but not longitudinal reinforcement. The median drift corresponding to the achievement of this damage state is θ=2.60%, while dispersion is β=0.4. At Damage State 2 (DS2), corresponding to median drift θ=3.70% and dispersion β=0.3, one or more mild steel continuity bars fracture in or near the region of the beam-column interface, such that the strength of the beam-column element is decreased by 20-25%. Finally, at Damage State 3 (DS3) post-tension

cables yield when the median drift is θ=6.90% and dispersion β=0.35. It is interesting to note that cracking damage state is neglected given that it was experimentally observed that cracks close when load is removed from the system (Fitzgerald et al. 2016).The probability of failure of the hybrid beam-column joint in correspondence of the three damage states is shown in Figure 72.

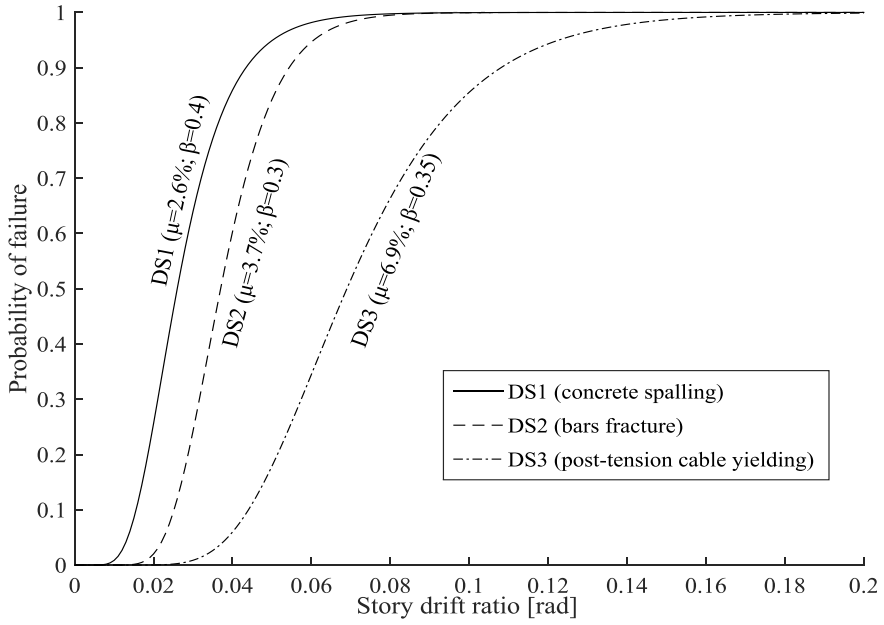

Figure 72 HYB beam-column joint fragility function

Economic consequences corresponding to each damage state are evaluated taking into consideration all repair activities necessary to recover the specific damage state and bring back the system to its original state. As far as HYB beam-column joints are concerned, all DSs require a preliminary repair activity consisting in removing furnishings, ceilings and mechanical, electrical and plumbing systems, as it happens also for the MRF system. Then, at DS1, after cleaning the area adjacent to the damaged concrete, it is necessary to prepare spalled concrete and eventual cracks to be patched with grout and to receive epoxy injection. At DS2 it

is required to remove damaged mild steel trying to leave the core of the beam intact as possible, in order to allow the PT stress to be maintained through the repair process. Then replace mild steel through the joint and provide mechanical coupling to remaining bar anchored in beam. Finally, pour concrete to place the mass spalled and chipped out. Repair activities required if DS3 is reached are similar to DS2 in relation to mild steel bars substitution. Then, as far as PT strand is concerned, first it is necessary to remove end caps and determine the level of damage. Subsequently, if necessary replace PT strand, else re-tension PT strand to obtain the desired stress level. Finally, for all DSs it is required to replace furnishings, ceilings and mechanical, electrical and plumbing systems. Economic consequences relating to each DS are given in Figure 73 and are in accordance with Fitzgerald et al. (2016) indications.

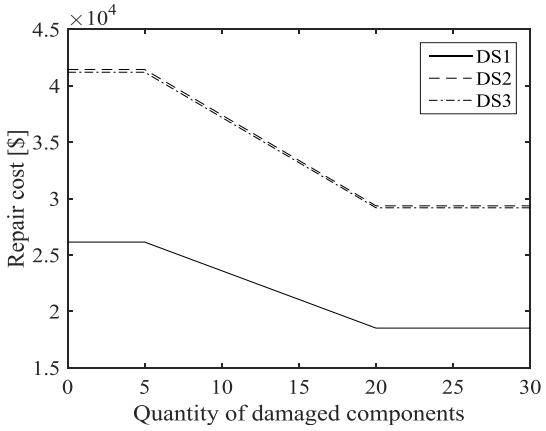

Damage States	Low quantity [$]	High quantity [$]
DS1	26146	18520
DS2	41448	29359
DS3	41206	29187

Figure 73 HYB beam-column joint consequence function

5.4.7 Loss estimation analysis and results

In order to perform the loss estimation analysis it is necessary to evaluate the total replacement cost of the facility. As already introduced in §5.2.4, the construction cost of HYB system is estimated starting from MRF's one and opportunely increasing it according to the comparison of both systems

structural costs. In particular the construction cost of the only structural part of the HYB building (concrete, steel reinforcement and PT strands), including cost of labour, is estimated through the use of Central Italy construction price list (Bollettino ufficiale della Regione Umbria, 2014) to be 105'833 $. The total replacement cost is assumed to be 2272 $/m^2.

The intensity-based loss estimation analysis is finally performed.

Repair Cost (RC) corresponding to each realization of the Montecarlo simulation is plotted in Figure 74-a, showing also the amount of repair costs provided by each component's category. It is evident that in correspondence of a generic realization the more significant contribution comes always from non-structural components, followed by structural elements and contents. Note that in no simulation the structure is collapsed and never irreparability is reached, so the total replacement cost is never observed. The area beneath the total repair cost curve (dashed curve in Figure 74-a) correspond to the fictitious total amount of money required to repair the structure over 500 realizations, and it is equal to 590 M$. The area beneath the repair cost curve corresponding to structural and non-structural components and contents is compared to the total area, providing the pie chart of Figure 74-b. Data observed confirm that the main part of repair costs is attributed to non-structural components, which cover a percentage of 71% of the total, followed by structural components (17%) and contents (12%).

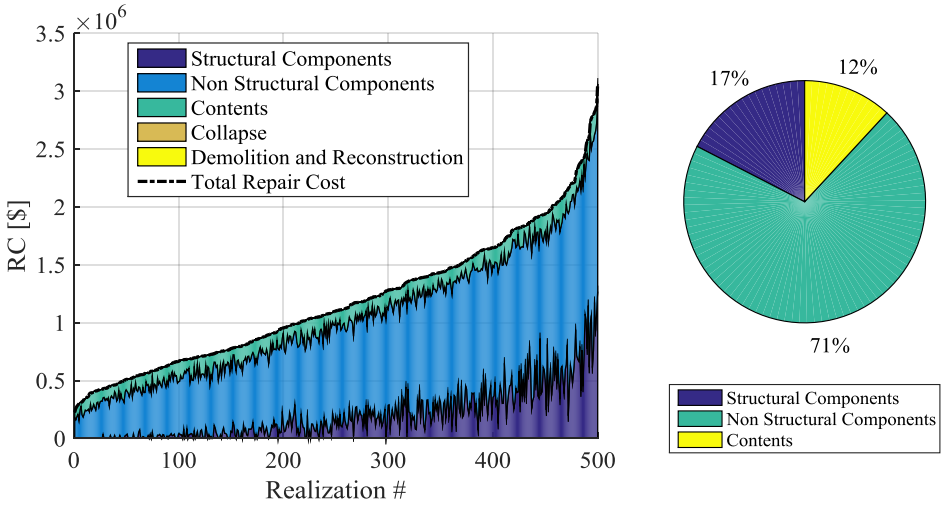

(a) (b)

Figure 74: a) Repair cost over realizations - HYB system; b) Contribution of different categories to the overall repair cost (590 M$) for HYB system

The Mean Damage Factor (MDF) of RC is 1.18 M$, the Scenario Expected Loss (SEL) is 1.10 M$ and the Scenario Upper Loss (SUL) is 1.94 M$. The characteristic PML value (PML_k) is 2.20 M$.

Repair costs are binned and shown in the bar plot of Figure 75. The Cumulative Distribution Function (CDF) of Repair Cost is given in Figure 76, while Figure 77 shows the CDF of repair cost over the total RePlacement Value (RPLV), defined as Repair Cost Ratio (RCR). The probability of loss, expressed as the probability of exceeding a certain RCR value, given the intensity measure, is plotted in Figure 78.

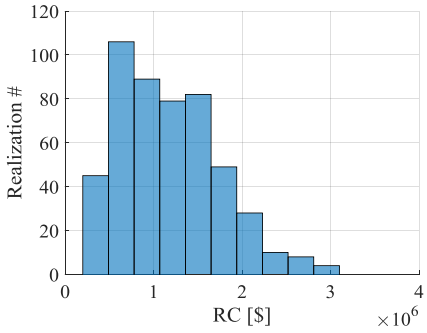

Figure 75 Binned repair costs resulting from the Intensity-based loss estimation analysis of the HYB system

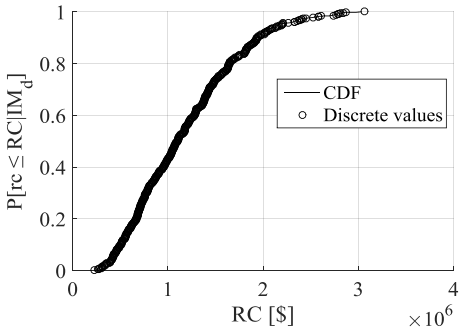

Figure 76 Cumulative distribution function of repair cost (RC) - HYB system

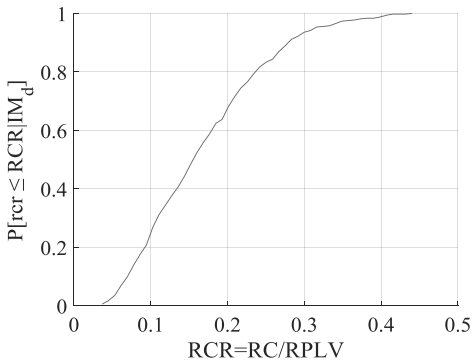

Figure 77 Cumulative distribution function of repair cost ratio (RCR) - HYB system

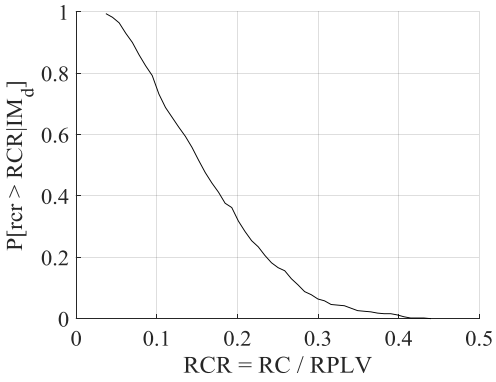

Figure 78 Probability of loss - HYB system

From the analysis of plots from Figure 74 to Figure 78, it is evident that non-structural components generate a significant rate of loss, causing a worsening of the overall performance. Indeed the pie-chart of Figure 74-b shows that the 71% of the overall economic loss is due to non-structural elements, while 17% is due to structural components. Actually, the HYB technology provides structural elements that can undergo deformations comparable to MRF's, but significantly reducing damage, as observable from the comparison of MRF and HYB pie-charts costs of Figure 58-b and Figure 74-b respectively. Consequently, since this structural system does not limit deformations, non-structural elements will suffer a level of

damage of the same entity observed in the MRF case-study. For this reason, in order to further improve the performance of the HYB system in terms of losses and avoid excessive damage to non-structural components, low-damage exterior curtain walls and internal partitions are adopted, introducing the Low-Damage HYBrid system (LD-HYB).

5.5 The case-study structure designed as a Low-Damage Hybrid (LD-HYB) system

The LD-HYB system differs from the previous analyzed HYB case-study only for the assumption of low-damage non-structural components, with the aim of enhancing the overall loss performance. In particular curtain walls and internal partitions are significantly affecting the total loss result because their damage is governed by interstorey drifts, which is not limited by the specific HYB system, instead similar to the MRF case. The description of the LD non-structural components is provided in the following section. Final loss analysis output are then commented.

5.5.1 Low-Damage non-structural fragility components

The low damage curtain wall fragility component, belonging to PACT library, is characterized by 11mm glass-frame clearance, against the 6mm of the previous component used (left-side of Figure 79 shows a simplified curtain wall system from Memari et al. 2007). This allows a wider range of movement to the glass system before initiating of damage. The low-damage curtain wall system can suffer three different damage states that are the gasket failure (DS1), glass cracking (DS2) or glass falling out (DS3), as shown in the right-side of Figure 79.

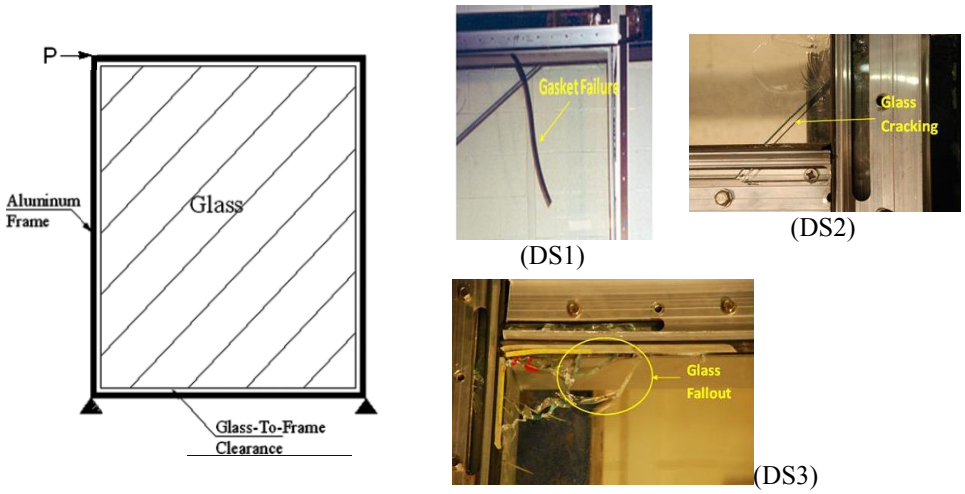

Figure 79 Curtain wall scheme (left-side, from Memari et al. 2007) and damage states (right-side, from PACT library)

Comparison of fragility curves for traditional and low-damage glass curtain wall systems, considering different levels of damage state, is shown in Figure 80.

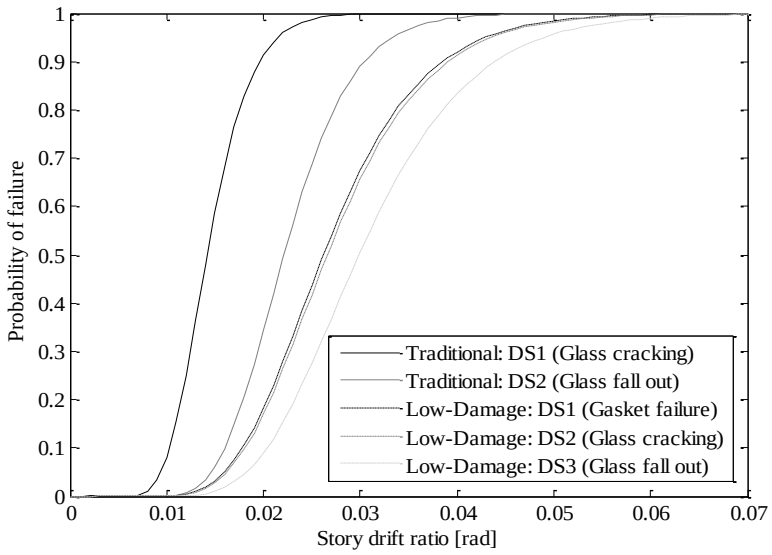

Figure 80 Fragility curves for traditional and low-damage curtain wall systems at different damage states

Median μ and dispersion β values of IDR corresponding to each damage state for both traditional and low-damage curtain wall systems are given in Table 24.

Table 24 Curtain wall system damage states

Type	Definition	Fragility component	EDP	DS1 (Median / Dispersion)	DS2 (Median / Dispersion)	DS3 (Median / Dispersion)
NS	Traditional glass window system	B2022.082	IDR	μ=0.0142; β=0.25	μ=0.0221; β=0.25	-
NS	Low-Damage glass window system	B2022.072	IDR	μ=0.0262; β=0.3	μ=0.0266; β=0.3	μ=0.0299; β=0.3

Differently, fragility curves of the low damage gypsum internal partition considered in this study are suggested in Tasligedik et al. (2014) and refers to light systems characterized by a gap around the gypsum linings, that allows free sliding.

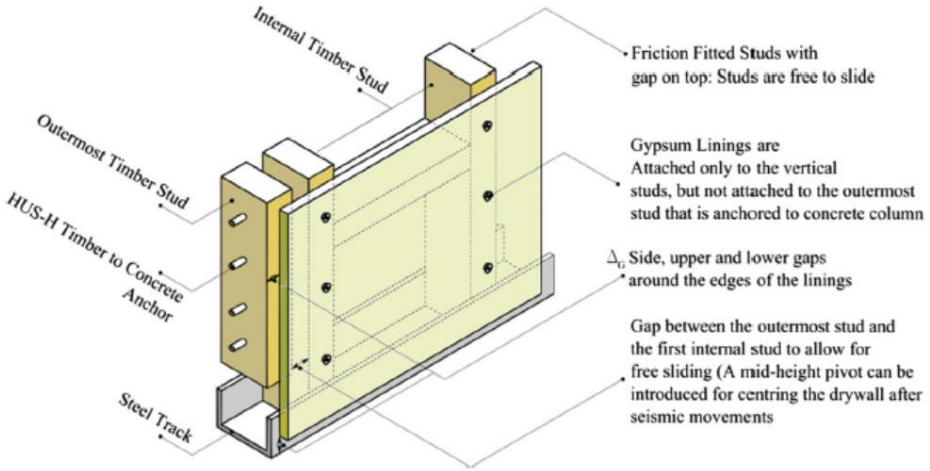

Figure 81 Generalized low damage drywall solution (the studs can either be steel or timber) - from Tasligedik et al. 2014

Fragility curves of traditional and low-damage partitions are plotted in Figure 82.

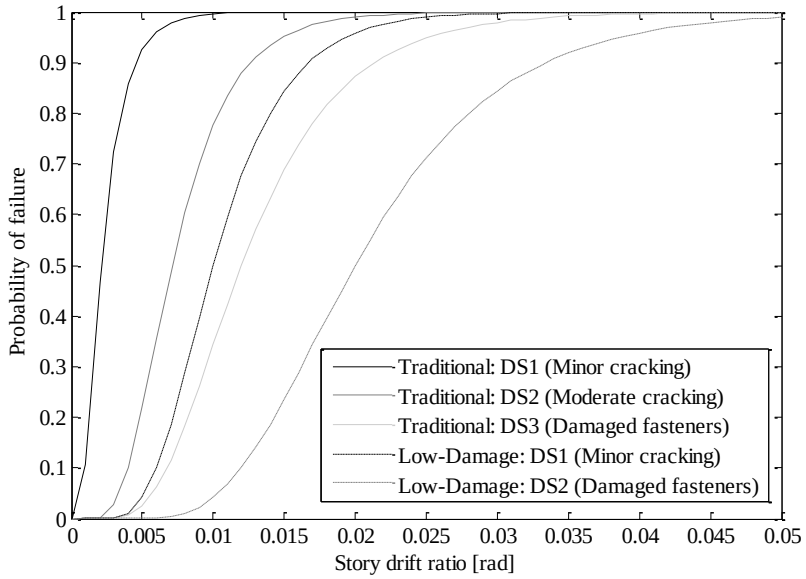

Figure 82 Fragility curves for traditional and low-damage partitions at different damage states

Median μ and dispersion β values of IDR corresponding to each damage state for both traditional and low-damage internal partition systems are given in Table 25.

Table 25 Internal partion system damage states

Type	Definition	Fragility component	EDP	DS1 (Median / Dispersion)	DS2 (Median / Dispersion)	DS3 (Median / Dispersion)
NS	Traditional Gypsum partition	C1011.001a	IDR	μ=0.0021; β=0.6	μ=0.0071; β=0.45	μ=0.012; β=0.45
NS	Low-Damage gypsum partition	C1011.001g	IDR	μ=0.01; β=0.4	μ=0.02; β=0.4	-

Economic consequence functions of LD non-structural components are kept unvaried with respect to traditional ones, assuming that the eventual increase of cost of LD element itself is reasonably not significantly higher.

5.5.2 Loss estimation analysis and results

The replacement cost value of LD-HYB system is supposed to be equal to HYB system's one since the incidence of low-damage partitions and curtain walls costs are not considered significant with respect to the total construction cost.

Intensity-based loss estimation analysis is performed and results are herein described. Repair Costs (RC) corresponding to each realization of the Monte Carlo simulation are plotted in Figure 83-a, showing also the amount of repair costs provided by each component's category. It is evident that in correspondence of a generic realization the more significant contribution comes always from non-structural components, followed by structural elements and contents. Note that in no simulation the structure is collapsed and never irreparability is reached, so the total replacement cost is never observed. The area beneath the total repair cost curve (dashed curve in Figure 83-a) correspond to the fictitious total amount of money required to repair the structure over 500 realizations, and it is equal to 346 M$. Accordingly, even if non-structural components are still the main source of repairing costs, the beneficial effect of low-damage technology is evident, given the significant reduction of the overall repair cost. The area beneath the repair cost curve corresponding to structural and non-structural components, contents and demolition/reconstruction contributions is compared to the total area, providing the pie chart of Figure 83-b. Data observed confirm that the main part of repair costs is attributed to non-structural components, which cover a percentage of 51% of the total, followed by structural components (29%) and contents (20%).

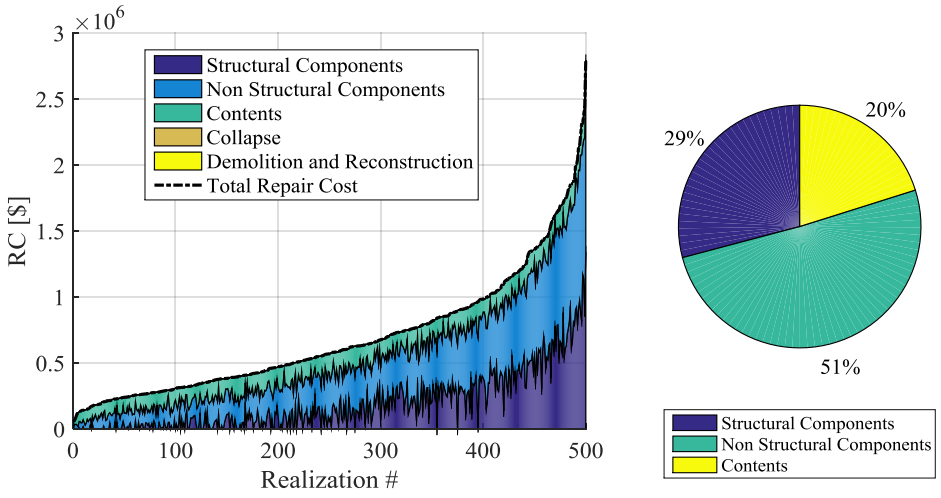

(a) (b)

Figure 83: a) Repair cost over realizations - LD-HYB system; b) Contribution of different categories to the overall repair cost (346 M$) for LD-HYB system

The Mean Damage Factor (MDF) of RC is 0.69 M$, the Scenario Expected Loss (SEL) is 0.57 M$ and the Scenario Upper Loss (SUL) is 1.36 M$. The characteristic PML value (PML_k) is 1.69 M$.

Repair costs are binned and shown in the bar plot of Figure 84. The Cumulative Distribution Function (CDF) of Repair Cost is given in Figure 85, while Figure 86 shows the CDF of RCR. The probability of loss, expressed as the probability of exceeding a certain RCR value, given the intensity measure, is plotted in Figure 87.

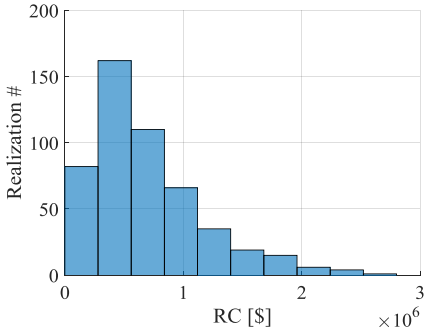

Figure 84 Binned repair costs resulting from the Intensity-based loss estimation analysis of the LD-HYB system

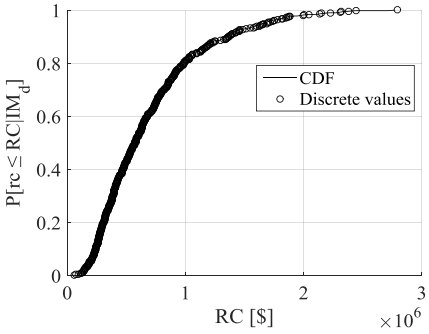

Figure 85 Cumulative distribution function of repair cost (RC) - LD-HYB system

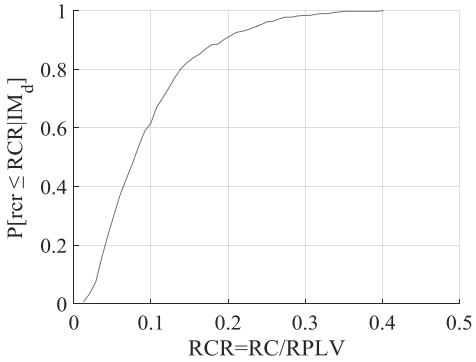

Figure 86 Cumulative distribution function of repair cost ratio (RCR) - LD-HYB system

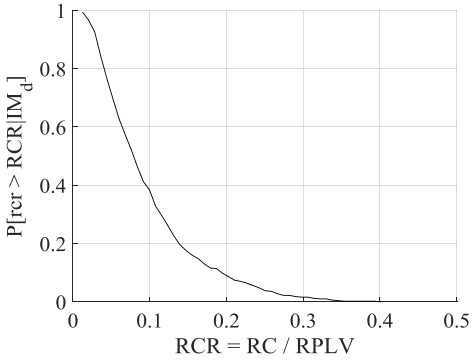

Figure 87 Probability of loss - LD-HYB system

From the analysis of plots from Figure 83 to Figure 87, it is evident that loss due to non-structural components is significantly decreased, upgrading considerably the overall structural performance in terms of losses.

5.6 The case-study structure designed as a dissipative Braced Frame (BF) system

The case-study building is designed assuming a dissipative Braced Frame (BF) configuration as seismic technology. In particular energy dissipation will be provided by steel shear links (SL) supported by tubular braces, described at §5.1.2.

The typical deformed shape of this structural typology is illustrated in Figure 88.

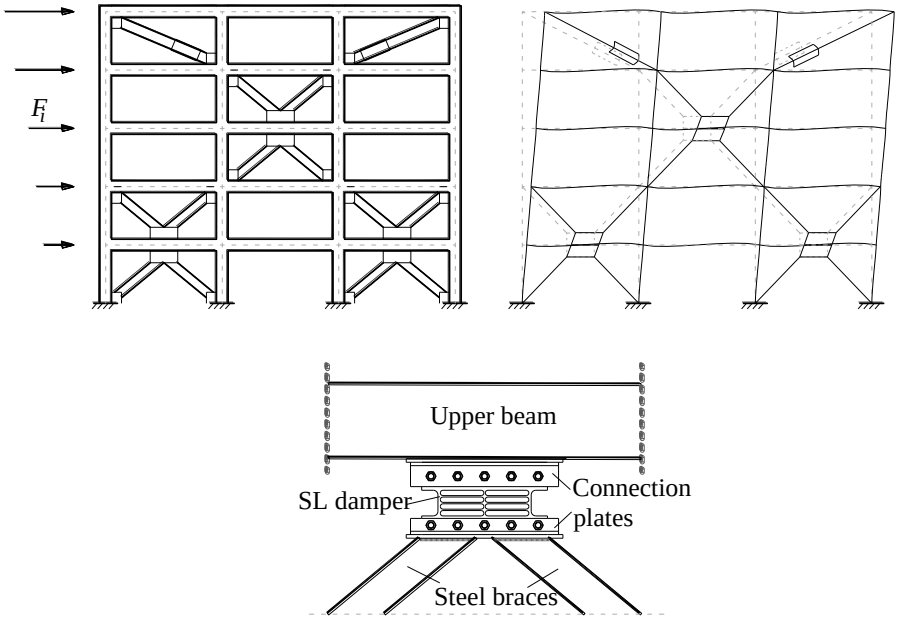

Figure 88 Typical deformed shape and beam-dissipative brace connection of the BF system adopting SL dampers

Beams and columns transversal sections are respectively 300x400 mm and 500x500 mm, so significantly lower than MRF and HYB case-study systems. Indeed seismic action is now withstand by dissipative braces, so allowing beams and columns to be designed only for gravitational loads,

having the accuracy of verifying columns against eventual traction axial stresses induced by braces.
The following sub-sections describe the application of the DDBD to the BF case-study and its main results, outputs of dynamic non-linear analysis, definition of fragility curve and finally the development of the intensity-based loss analysis.

5.6.1 Materials

Concrete class is C25/30 and steel reinforcement is B450C, as for the MRF case-study (§ 5.3.1). Structural steel adopted for braces is S275, while American ASTM A36 mild steel is used for SL dampers, produced in South America.

5.6.2 Application of DDBD

The Direct Displacement-Based Design (DDBD) is applied to the HYB system according to the procedure proposed in Nuzzo et al. (2018) and addressed to Appendix B. The bare frame's behaviour is supposed elastic in order to avoid structural damage, while the design target drift is 0.5%, that means a relative displacement of 0.016 m. The corresponding base shear is 504 kN and it is distributed along the height proportionally to the first mode shape, generating forces, shear, displacements and stiffnesses at each storey indicated in Table 26. Arranging permanent and live loads in the seismic combination, seismic masses of 426 tons and 248 tons have been respectively defined for levels 1 to 4 and for last level (note that masses indicated in Table 26 refers to the single frame).

Table 26 Bare frame mechanical properties

Level	Mass	h_i	F_i	$d_{i,absolute}$	$d_{i,relative}$	$K_{F,i}$	$V_{F,i}$
-	ton	m	kN	m	m	kN/m	kN
1	213	3.2	39	0.009	0.009	58384	504
2	213	6.4	78	0.025	0.016	28875	465
3	213	9.6	117	0.041	0.016	24314	387
4	213	12.8	156	0.053	0.012	21893	270
5	124	16	114	0.061	0.008	14409	114

The bare frame equivalent stiffness is K^*_F =8282 kN/m. The equivalent DB damping ratio is calculated through equation (B.3), supposing a first tentative value of r^*_{DB}=0.04, that corresponds to mean experimental value observed for SL specimens. This design choice will be verified successively. Differently the design equivalent DB ductility is set to μ^*_{DB}=3, which is a quite precautionary value considering ductility capacity of steel dampers. This design choice will prevent unsatisfied checks concerning dissipative braces maximum deformation. Although, if DB demand in the final braced frame structure will be too low, this value should be increased and the whole procedure iterated again. A first tentative value of the equivalent BF damping ratio should be supposed, for example in the range of 10-15%, which corresponds to the minimum bound of values for structures equipped with dissipative braces. In this way, entering in the reduced ADRS curve in correspondence of the equivalent SDOF target displacement, it is possible to determine the equivalent base shear of the BF system, $V^*_{PP,BF}$. At this point it is possible to apply equations (B.4) and (B.2), evaluate analytically the equivalent BF damping ratio and iterate its calculation until convergence between two consecutive values is observed. Values obtained from the last iteration are given in Table 27.

Table 27 Last iteration of the evaluation of the equivalent BF damping ratio

r_{DB}	μ_{DB}	$d^*_{v,DB}$	ξ^F_v	ξ^{DB}_h	$V^*_{PP,DB}$	ξ^{BF}_h
-	-	m	%	%	kN	%
0.04	3	0.015	5	38	1372	33

Applying equations (B.8) and (B.9) it is possible to determine the equivalent design capacity curve of BF system and, consequently, the equivalent DB design capacity curve as well. After calculating a value of α=7.6, forces and stiffnesses for BF and DB systems are determined (Table 28). Corresponding equivalent SDOF capacity curves are plotted in Figure 89.

Table 28 F, BF and DB design capacity curves

	F	BF	DB
V^*_y [kN]	168	1438	1270
V^*_{PP} [kN]	504	1875	1372
K^* [kN/m]	8282	70961	62679
K^*_{py} [kN/m]	8282	10789	2507

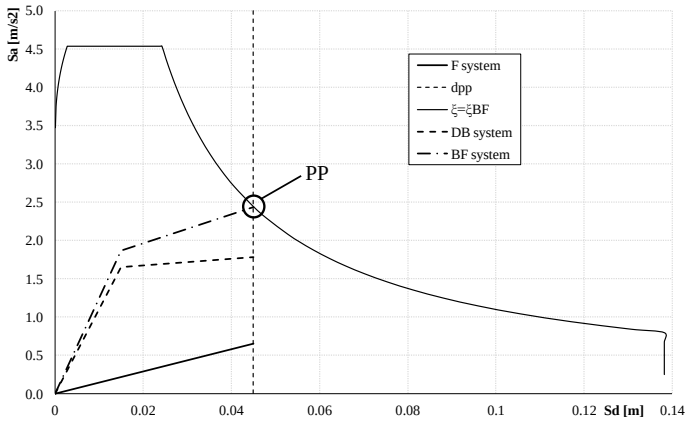

Figure 89 Definition of final Frame (F), Damped Brace (DB) and Braced Frame (BF) capacity curves

Applying equations (B.10) and (B.11) mechanical properties of dissipative braces in correspondence of each storey i are determined and given in Table 29.

Table 29 Dissipative braces' mechanical properties in correspondence of each storey

Level	$K_{DB,i}$ [kN/mm]	$V_{y,DB,i}$ [kN]
1	442	1270
2	219	1172
3	184	975
4	166	680
5	109	286

At this step it is necessary to match these design values with real dissipative braces, that in the specific case-study consist in tubular braces supporting SL dampers. Considering demanding yielding forces given in Table 29, it is believed recommendable that at the first two floors two bays are braced, in order to split the force to be provided in two dampers. With this in mind, the braces configuration given in Figure 90 is chosen, thus limiting transmission of vertical traction forces to columns. This generates the adoption of diagonal braces at last floor in correspondence of two bays, and alternation of V-braces and chevron-braces in correspondence of other floors.

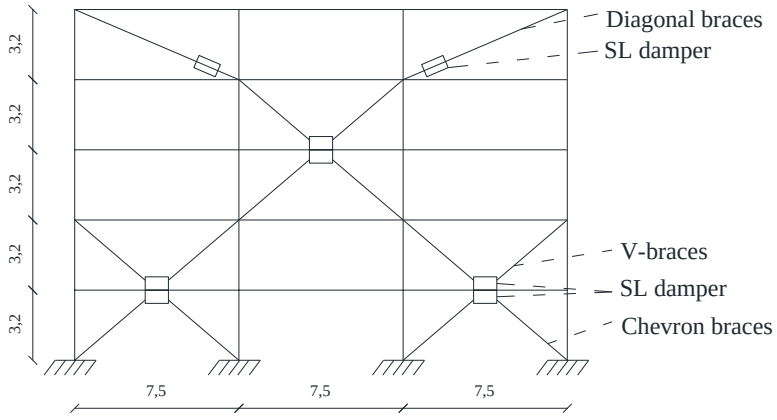

Figure 90 Dissipative braces' configuration

SL dampers' geometry is chosen in order to satisfy design yielding forces. In particular, fixing horizontal and vertical stiffeners dimensions, that

behaved satisfactorily during past experimental tests avoiding premature buckling phenomena (Nuzzo et al. 2017), the width B and thickness t_w of dissipative windows have to be identified. Geometries are roughly established and shown in Figure 91, based on analytical formulation suggested in Nuzzo et al. 2018.

Level	width B [mm]	thickness t_w [mm]	SL B_t_w
1	600	5	SL 60_5
2	550	5	SL 55_5
3	750	6	SL 75_6
4	650	5	SL 65_5
5	300	2	SL 30_2

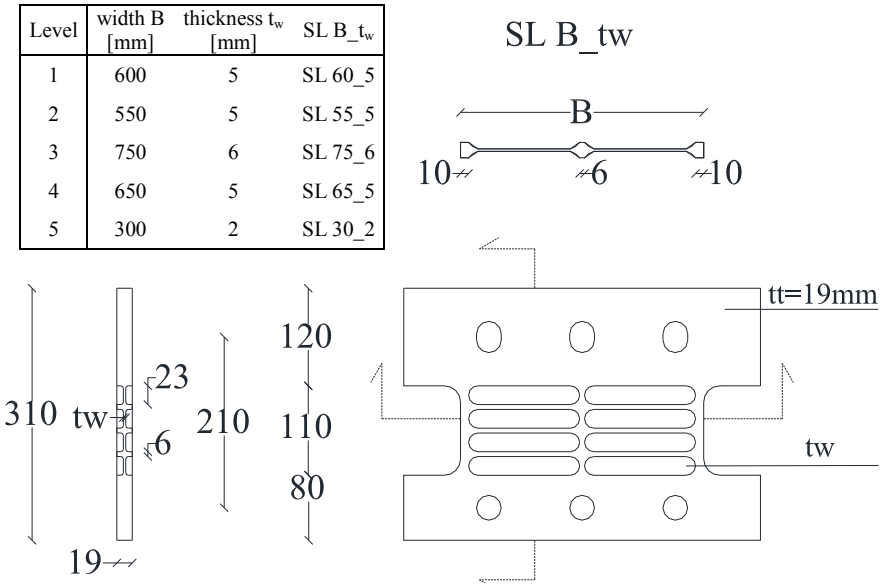

Figure 91 Shear Link geometry

Consequently, SL elastic stiffness at the j-th bay and i-th storey $K_{SL,j,i}$ is defined, and so it is possible to determine support braces' dimensions generating the brace elastic stiffness $K_{b,j,i}$ that, in series with $K_{SL,j,i}$ can provide the required design elastic stiffness in correspondence of the j-th bay at the i-th storey (Figure 92), according to the following equation:

$$K_{DB,j,i}=\frac{K_{B,j,i}\cdot K_{SL,j,i}}{K_{B,j,i}+K_{SL,j,i}} \tag{32}$$

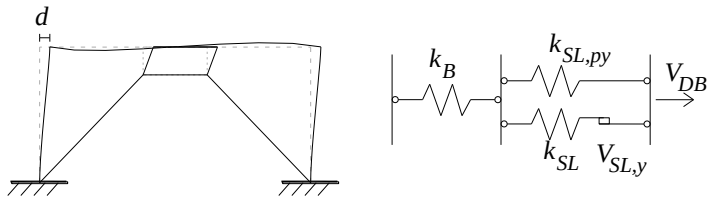

Figure 92 Damped brace given by damper SL and braces B In series

Finally, knowing SL post-to-pre yielding stiffnesses ratio $r_{SL,j,i}$, it is possible to evaluate the dissipative brace post-yielding stiffness:

$$K_{DB,py,j,i}=\frac{K_{B,j,i}\cdot\left(r_{SL,j,i}\cdot K_{SL,j,i}\right)}{K_{B,j,i}+r_{SL,j,i}\cdot K_{SL,j,i}} \tag{33}$$

Note that for chevron braces and V-braces K_b must be multiplied by 2 in previous equations.

Final dissipative braces' mechanical properties in the j-th bay and i-th level are summarized in Table 30.

Table 30 Dissipative braces' mechanical properties in correspondence of each j-th braced bay at i-th level

Level	$V_{y,DB,j,i}$ [kN]	$k_{DB,j,i}$ [kN/mm]	$k_{DB,py,j,i}$ [kN/mm]	$r_{DB,j,i}$
1	635	221	27	0.12
2	586	109	22	0.20
3	975	184	30	0.16
4	680	166	27	0.16
5	143	55	9	0.08

At this point it is necessary to validate if the initial tentative value of r^*_{DB} is coherent with the real distribution of $r_{DB,j,i}$ obtained in Table 30. Applying equation (B.12), a value of $r^*_{DB}=0.12$ is determined, so very different from the initial value supposed, equal to 0.04. Consequently it is necessary to iterate again introducing the new value of r^*_{DB}. After a couple of iterations the final converging value is $r^*_{DB}=0.135$. Main results of the

last iteration of the procedure are reported in Table 31 to Table 33 and in Figure 93. The final value of α is 6.9.

Table 31 Last iteration of the evaluation of the equivalent BF damping ratio for converging value of r^*_{DB}=0.135

r^*_{DB}	μ_{DB}	$d^*_{y,DB}$	ξ^F_v	ξ^{DB}_h	$V^*_{PP,DB}$	ξ^{BF}_h
-	-	m	%	%	kN	%
0.135	3	0.015	5	29	1466	27

Table 32 F, BF and DB design capacity curves for converging value of r^*_{DB}=0.135

	F	BF	DB
V^*_y [kN]	168	1322	1154
V^*_{PP} [kN]	504	1969	1466
K^* [kN/m]	8282	65230	56948
K^*_{py} [kN/m]	8282	15970	7688

Table 33 Dissipative braces' mechanical properties in correspondence of each j-th braced bay at i-th level for converging value of r^*_{DB}=0.135

Level	$V_{y,DB,j,i}$ [kN]	$k_{DB,j,i}$ [kN/mm]	$k_{DB,py,j,i}$ [kN/mm]	$r_{DB,j,i}$
1	577	201	27	0.13
2	532	99	23	0.23
3	886	167	31	0.18
4	618	151	27	0.18
5	130	50	9	0.17

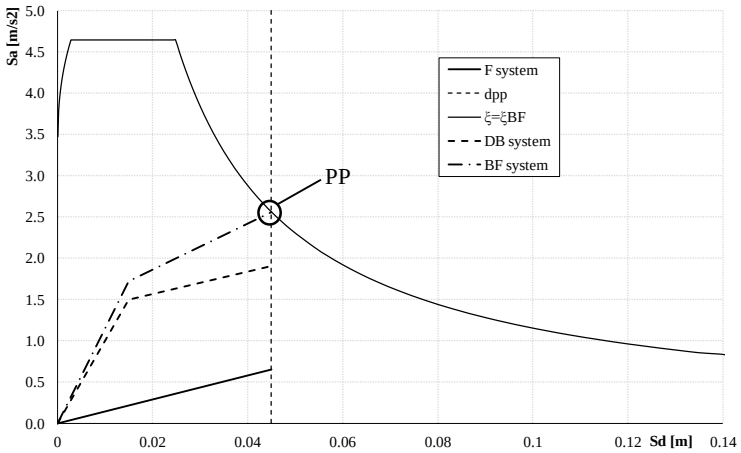

Figure 93 Definition of capacity curves for converging value of r^*_{DB}=0.135

The minimum area of braces' transversal section is determined through equation (32) after SLs dimensions have been chosen. Tubular diagonals are then selected from commercial standard elements (Table 34) respecting this requirement and verifying that buckling resistance (determined in the respect of Eurocode 8 - part 1) is higher than the axial force acting in each brace, which can be assumed as the axial component of the SL damper's yielding force.

Table 34 Tubular sections and buckling resistance

Level	d x s	$N_{b,Rd}$
-	mm x mm	kN
1	273 x 5.6	1113
2	168.3 x 4.0	391
3	219.1 x 5.9	875
4	219.1 x 5.0	745
5	219.1 x 4	365

Considering the real dimensions of supporting braces, initial and post-yielding stiffnesses of dissipative braces are calculated again and final results are shown in Table 35.

Table 35 Final dissipative braces elastic and post-yielding stiffnesses

Level	$K_{SL,j,i}$ [kN/mm]	$K_{B,j,i}$ [kN/mm]	$r_{SL,j,i}$	$K_{DB,j,i}$ [kN/mm]	$K_{DB,py,j,i}$ [kN/mm]	$r_{DB,j,i}$
1	750	141	0.04	205	27	0.13
2	700	62	0.04	105	23	0.22
3	900	119	0.04	188	31	0.17
4	800	101	0.04	161	28	0.17
5	250	61	0.04	49	9	0.18

Finally, the initial choice of the μ^*_{DB} value is checked through equation (B.13) and (B.14), according to which values of $\mu_{DB,i}$ are calculated, verifying that they are lower than the maximum admissible capacity of the device. In the specific case-study the maximum demand ductility in SL dampers according to the design procedure is μ=15 at second floor, lower than the maximum capacity, experimentally observed around 25.

5.6.3 Structural design and modeling

Beams and columns steel reinforcement quantity is chosen as a consequence of internal actions coming from the DDBD. Final configurations are represented in Figure 94.

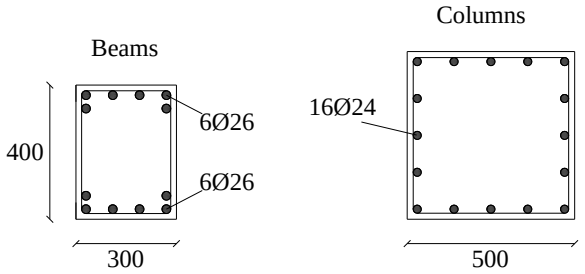

Figure 94 Beams and columns cross sections - BF system

Beams and columns are modelled in Opensees (McKenna 1997) as “elasticBeamColumn” elements, verifying successively that yielding is never achieved in any of them. Dissipative braces are modeled as "twoNodeLink" elements characterized by "uniaxialMaterial Steel01", that requires the definition of initial stiffness, yielding force and post-to-pre yielding stiffnesses ratio. Yielding forces of Table 33 and elastic stiffnesses of Table 35 are defined in the horizontal direction, thus the axial components have to be defined and implemented in the FEM model. Note also that in correspondence of chevron or V-braces these mechanical properties should be divided by the effective number braces, that is two, since they can be considered as two springs working in parallel. Moreover the braces' ends connected to upper beams are released with respect to the vertical direction in order to account for the presence of slotted holes, opportunely designed to avoid the transmission of axial actions to beams.

5.6.4 Dynamic non-linear analysis

The first vibrational period of the 2D BF system is T_1=0.55s. Dynamic nonlinear analysis are performed in correspondence of the set of records introduced in paragraph 5.2.3. An OpenSees-Matlab code is created in order to both check the structural design and get EDP quantities needed for the loss estimation analysis. The displacement profile envelope in correspondence of each record is plotted in Figure 95, showing also the mean trend.

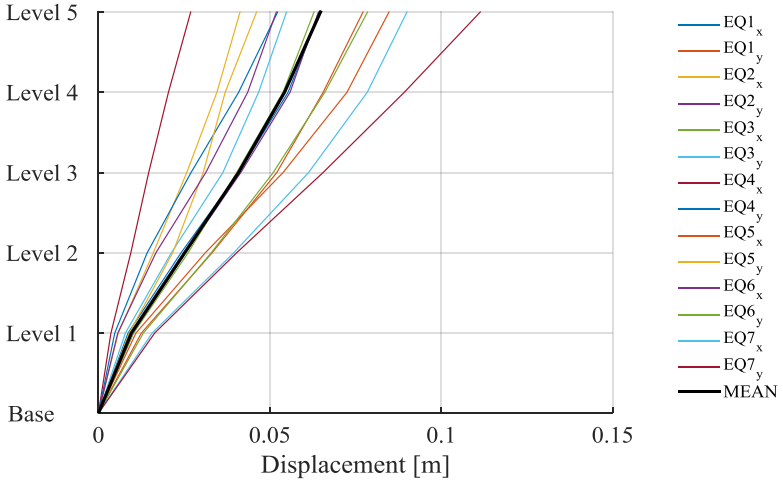

Figure 95 Displacement profile envelope of BF system

It is verified that in correspondence of beams and columns the mean of maximum internal actions over the 14 records is never greater than elements' yielding moment.

EDPs required for the loss estimation analysis are IDR, PFA and RIDR. In particular, the maximum in correspondence of each record is selected and recalled in the following tables and figures.

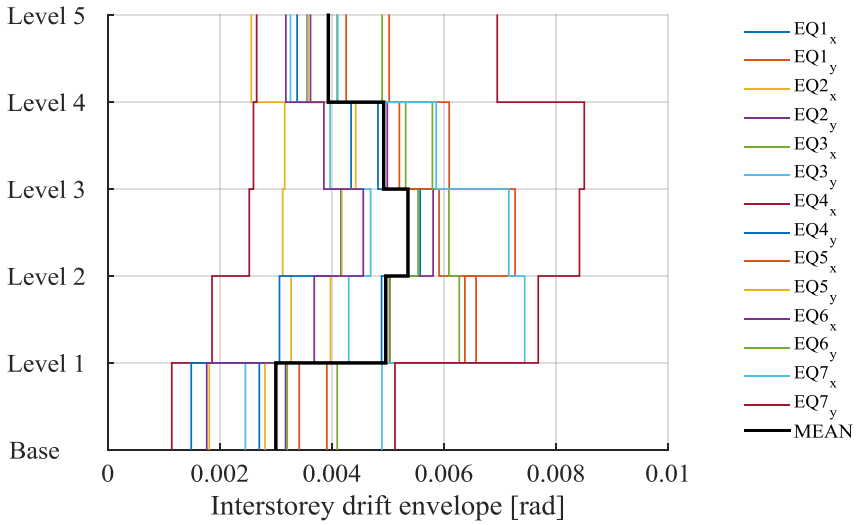

Figure 96 IDR envelope of BF system

Table 36 Maximum IDR values of BF system

Level	Base-1	1-2	2-3	3-4	4-5
EQ1x	0.27%	0.49%	0.56%	0.48%	0.34%
EQ1y	0.34%	0.64%	0.73%	0.61%	0.50%
EQ2x	0.18%	0.33%	0.31%	0.32%	0.26%
EQ2y	0.32%	0.50%	0.58%	0.50%	0.36%
EQ3x	0.32%	0.50%	0.55%	0.53%	0.41%
EQ3y	0.25%	0.43%	0.47%	0.40%	0.33%
EQ4x	0.11%	0.19%	0.25%	0.26%	0.27%
EQ4y	0.15%	0.31%	0.42%	0.43%	0.36%
EQ5x	0.39%	0.66%	0.59%	0.52%	0.43%
EQ5y	0.28%	0.40%	0.42%	0.44%	0.36%
EQ6x	0.18%	0.37%	0.46%	0.39%	0.32%
EQ6y	0.41%	0.63%	0.61%	0.58%	0.49%
EQ7x	0.49%	0.74%	0.72%	0.59%	0.41%
EQ7y	0.51%	0.77%	0.84%	0.85%	0.70%
MEAN	**0.30%**	**0.50%**	**0.54%**	**0.49%**	**0.39%**

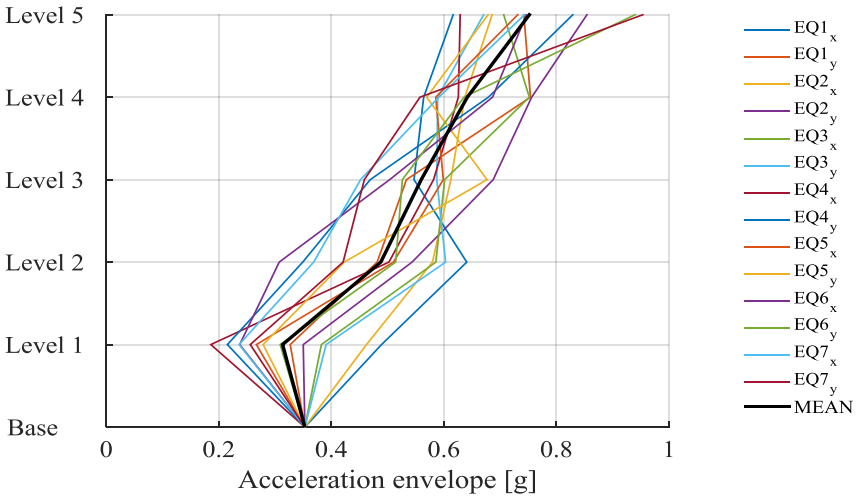

Figure 97 PFA envelope of BF system

Table 37 PFA values of BF system (in g)

Level	Ground	1	2	3	4	5
EQ1x	0.35	0.49	0.64	0.55	0.56	0.62
EQ1y	0.35	0.33	0.48	0.53	0.75	0.74
EQ2x	0.35	0.46	0.58	0.61	0.64	0.69
EQ2y	0.35	0.35	0.54	0.69	0.76	0.85
EQ3x	0.35	0.38	0.59	0.60	0.75	0.71
EQ3y	0.35	0.39	0.60	0.59	0.59	0.67
EQ4x	0.35	0.19	0.50	0.58	0.63	0.63
EQ4y	0.35	0.22	0.35	0.47	0.68	0.83
EQ5x	0.35	0.27	0.51	0.60	0.59	0.73
EQ5y	0.35	0.28	0.42	0.68	0.57	0.68
EQ6x	0.35	0.24	0.31	0.50	0.69	0.75
EQ6y	0.35	0.31	0.51	0.53	0.64	0.94
EQ7x	0.35	0.24	0.37	0.45	0.59	0.74
EQ7y	0.35	0.26	0.42	0.46	0.56	0.95
MEAN	**0.35**	**0.31**	**0.49**	**0.56**	**0.64**	**0.75**

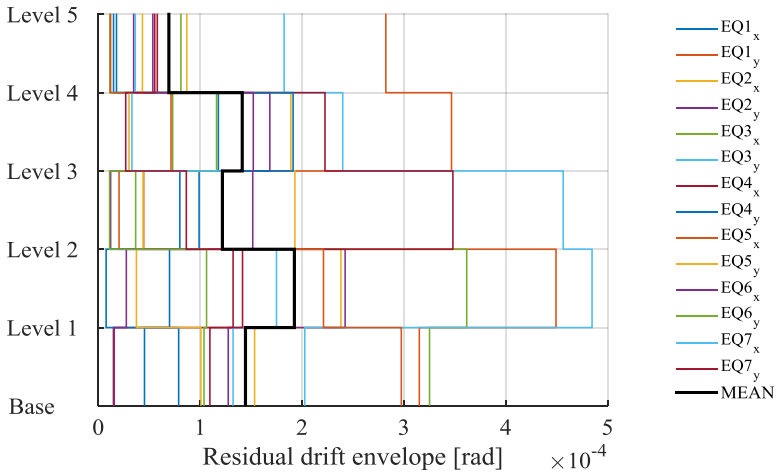

Figure 98 RIDR envelope of BF system

Table 38 Maximum RIDR values of BF system

Level	Base-1	1-2	2-3	3-4	4-5
EQ1x	0.00%	0.01%	0.01%	0.01%	0.00%
EQ1y	0.03%	0.03%	0.00%	0.04%	0.03%
EQ2x	0.01%	0.02%	0.02%	0.02%	0.02%
EQ2y	0.01%	0.02%	0.00%	0.02%	0.01%
EQ3x	0.00%	0.01%	0.00%	0.04%	0.03%
EQ3y	0.02%	0.02%	0.05%	0.05%	0.02%
EQ4x	0.01%	0.02%	0.03%	0.01%	0.00%
EQ4y	0.00%	0.02%	0.01%	0.00%	0.01%
EQ5x	0.00%	0.01%	0.00%	0.02%	0.03%
EQ5y	0.00%	0.00%	0.00%	0.00%	0.01%
EQ6x	0.00%	0.02%	0.02%	0.00%	0.00%
EQ6y	0.01%	0.01%	0.00%	0.01%	0.01%
EQ7x	0.00%	0.00%	0.01%	0.02%	0.01%
EQ7y	0.01%	0.00%	0.01%	0.01%	0.01%
MEAN	**0.01%**	**0.01%**	**0.01%**	**0.02%**	**0.01%**

5.6.5 IDA analysis and fragility curve

Incremental Dynamic Analysis (IDA) are performed employing the 42 records introduced in §5.2.3 and adopting IDR as EDP. Resulting IDA curves are plotted in Figure 99. The fragility curve, given in Figure 100, is constructed selecting the IM values that cause collapse and plotting the relative Cumulative Distribution Function (CDF). In particular the attainment of failure is considered when an IDR value of 0.8% is reached.

This value represents the attainment of an interstorey displacement of 25 mm, which is estimated to be distributed between the SL damper and steel braces in the ratio of 20:5. Indeed the maximum allowable deformation that SL dampers can admit is experimentally demonstrated to be 20 mm.

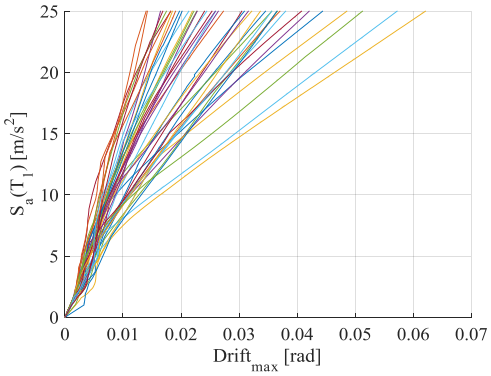

Figure 99 IDA curves for BF system

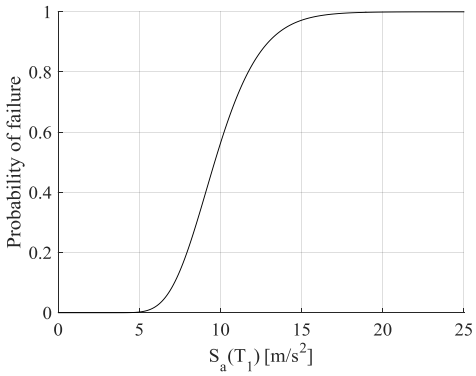

Figure 100 Fragility curve for BF system

5.6.6 Structural fragility components

Structural fragility components adopted for the BF system concern both beam-column joint and SL dampers. Beam-column joint fragility component adopted is the same used for the MRF system, so more details are provided at §5.3.6. As far as SL dampers are concerned, no fragility curves exist in literature. In appendix H of FEMA P-58-1 (2012), several methodologies for the development of fragility curves are proposed. Among them, the one better suiting the specific case is the Actual Demand Data derivation method, usable when data are available from m individual specimen tests, and each tested specimen experienced the damage state of interest at a known value of demand, d_i. The fragility parameters to be defined are the median value of the demand at which the damage state is likely to initiate and the value of the random dispersion, respectively derived as follows:

$$\mu = e^{\left(\frac{1}{m}\sum_{i=1}^{m} \ln d_i\right)} \quad (34)$$

$$\beta = \sqrt{\left(\frac{1}{m\text{-}1}\sum_{i=1}^{m}\left(\ln\frac{d_i}{\mu}\right)^2\right)} \quad (35)$$

In the specific case of SL dampers, experimental results of recent cyclic tests performed in Naples (Nuzzo et al. 2017) can be employed (more details are given in Appendix A). Considering that SL devices are designed so that buckling is never reached if not when the damper is already severely damaged, the only damage state identified is when the SL undergoes a deformation corresponding to its maximum capacity. Actually, if under a moderate earthquake a SL, which is designed to yield for very small values of displacement, is significantly deformed but not collapsed, anyway it would be substituted. For this reason the damage state is selected to be at the attainment of the 75% of the SL's deformation capacity. The Engineering Demand Parameter (EDP) selected to represent SL damage state is the IDR. Actually, the measure observed in experimental tests was the relative deformation of the devices, so it is necessary to convert it into the EDP. It is satisfactorily admissible that when SL dampers are yielded, given that their post-yielding stiffness is significantly lower than support braces' elastic stiffness, IDR corresponds to the relative deformation within dissipative devices. With this assumption, IDR corresponding to the attainment of the maximum deformation capacity of specimens can be easily derived dividing the experimental observations (SL's relative displacement) by the interstorey height of the case-study structure. The definition of fragility parameters is given in Table 39, while the final fragility curve is plotted in Figure 101. The cost for the realization of a singular device is estimated to be around 300 $, considering the cost per kg of steel according to Italian price list for Central regions (Prezzario Regione Umbria, 2014), including labor cost. The repair intervention after a seismic event, consisting in the substitution

of dampers, is assumed equal to the cost of the device itself increased of the 30%. Actually the structural architecture has to be defined so that SL dampers result located in easily accessible locations, so not requiring any further significant cost for the substitution intervention. Considering also an increment of the cost per device in the case in which a very small number (2) of elements have to be substituted, the final economic consequence function of Figure 102 is determined.

Table 39 Definition of fragility parameters for SL dampers

specimen #	$d_{i,collapse}$ [mm]	$d_{i,collapse}/h$ [rad]	3/4 $d_{i,collapse}/h$ [rad]	μ [rad]	β
1	20.3	0.0063	0.0048		
2	22.8	0.0071	0.0053		
3	20	0.0063	0.0047		
4	19	0.0059	0.0045	0.0049	0.11
5	20.7	0.0065	0.0049		
6	19	0.0059	0.0045		
7	25.8	0.0081	0.0060		

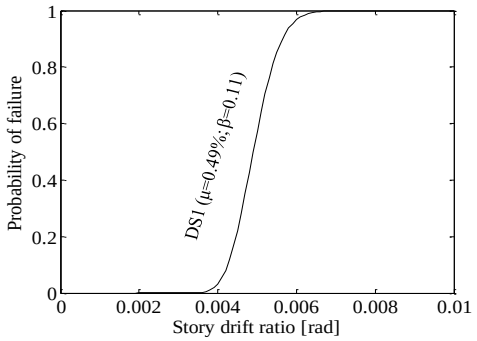

Figure 101 Fragility curve of SL damper

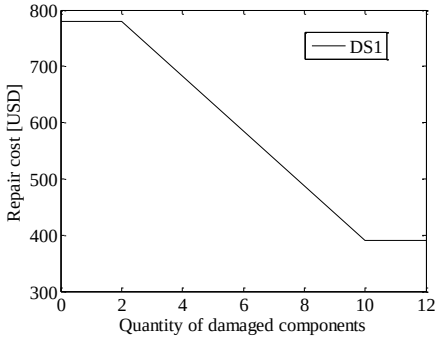

Figure 102 Economic consequence function of SL damper

5.6.7 Loss estimation analysis and results

In order to perform the loss estimation analysis it is necessary to evaluate the total replacement cost of the facility. As already introduced in §5.2.4, the construction cost of BF system is estimated starting from MRF's one

and opportunely increasing it according to the comparison of both systems structural costs. In particular the construction cost of the only structural part of the BF building (concrete, steel reinforcement, structural steel of braces and SL dampers), including cost of labor, is estimated through the use of Central Italy construction price list (Bollettino ufficiale della Regione Umbria, 2014) to be 161'371 $. The total replacement cost is assumed to be 2551 $/m^2, that corresponds to a total of 7.75 M$, considering the total area of 506 m^2 and the number of levels (which is 6 considering also the ground floor).

The intensity-based loss estimation analysis is performed and final results are herein addressed.

Repair Costs (RC) corresponding to each realization of the Monte Carlo simulation are plotted in Figure 103-a, showing also the amount of repair costs provided by each component's category. It is evident that in correspondence of a generic realization the more significant contribution comes from non-structural components, followed by contents and structural elements. Note that in no simulation the structure is collapsed and never irreparability is reached, so the total replacement cost is never observed. The area beneath the total repair cost curve (dashed curve in Figure 103-a) correspond to the fictitious total amount of money required to repair the structure over 500 realizations, and it is equal to 269 M$. The area beneath the repair cost curve corresponding to structural and non-structural components, contents and demolition/reconstruction contributions is compared to the total area, providing the pie chart of Figure 103-b. Data observed confirm that the main part of repair costs is attributed to non-structural components, which cover a percentage of 67% of the total, followed by contents (27%) and structural components (6%). It is interesting to observe that the cost attributed to structural elements is significantly reduced, confirming that beam-column joints are preserved from damage. The very low cost of SL devices also has a positive impact on this result.

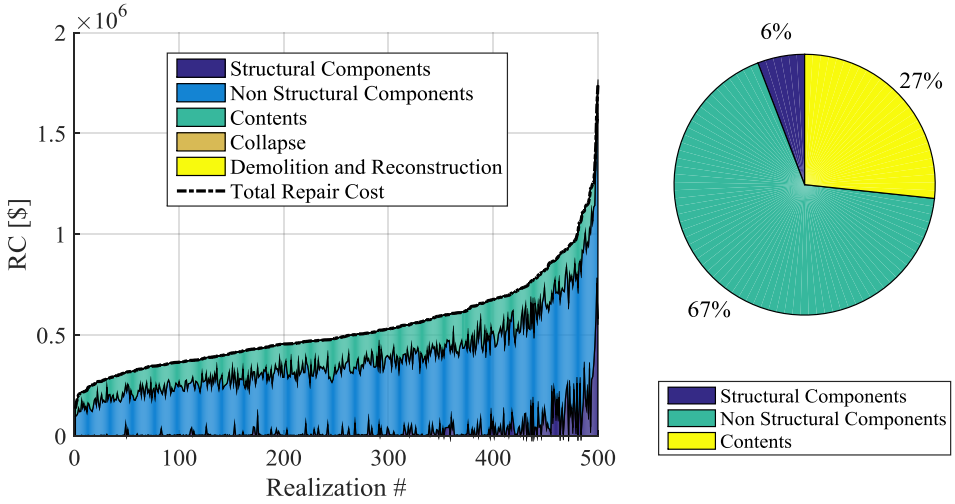

(a) (b)

Figure 103: a) Repair cost over realizations - BF system; b) Contribution of different categories to the overall repair cost (269 M$) for BF system

The Mean Damage Factor (MDF) of RC is 0.54 M$, the Scenario Expected Loss (SEL) is 0.49 M$ and the Scenario Upper Loss (SUL) is 0.83 M$. The characteristic PML value (PML_k) is 0.95 M$.

Repair costs are binned and shown in the bar plot of Figure 104. The Cumulative Distribution Function (CDF) of Repair Cost is given in Figure 105, while Figure 106 shows the CDF of repair cost over the total RPLV, that is RCR. The probability of loss, expressed as the probability of exceeding a certain RCR value, given the intensity measure, is plotted in Figure 107.

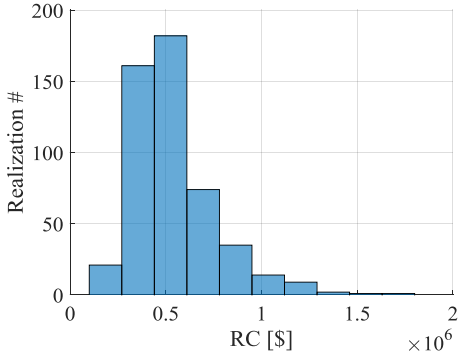

Figure 104 Binned repair costs resulting from the Intensity-based loss estimation analysis of the BF system

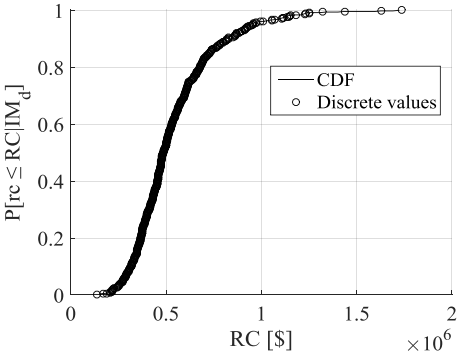

Figure 105 Cumulative distribution function of repair cost (RC) - BF system

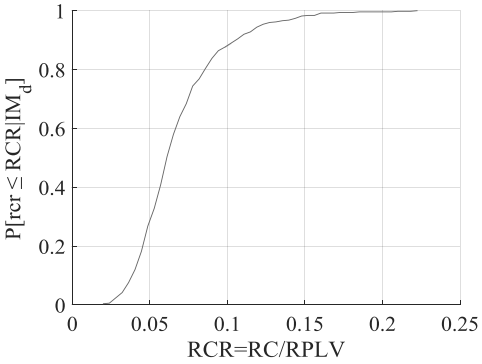

Figure 106 Cumulative distribution function of repair cost ratio (RCR) - BF system

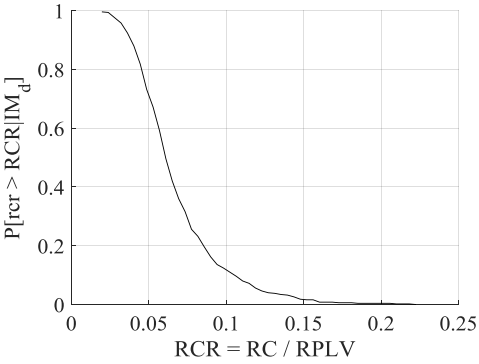

Figure 107 Probability of loss - BF system

5.7 The case-study structure designed as a Base Isolated (BI) system

The last case-study analyzed concerns the building designed assuming Base Isolation (BI) system as seismic technology. In particular High Damping Rubber Bearing (HDRB) devices are assumed for the specific case-study. As for previous systems, only external frames are considered seismic resistant. Accordingly, the central columns are supposed to be laying on simple rollers.

The typical configuration and deformed shape of this structural typology are illustrated in Figure 108.

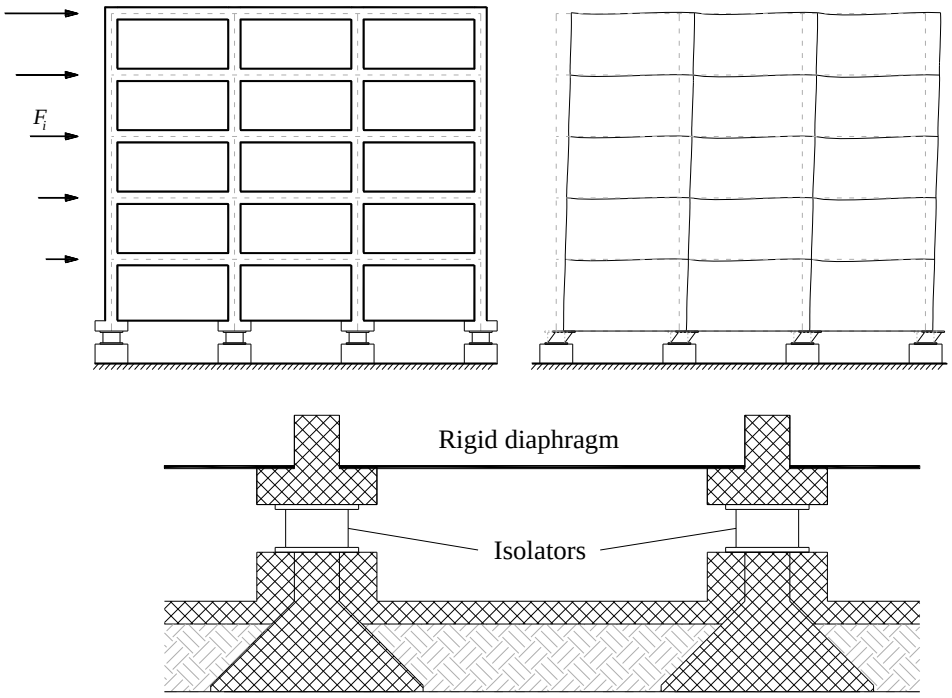

Figure 108 Typical BI system configuration and deformed shape

Beams and columns transversal sections are respectively 300x500 mm and 400x400 mm. Indeed, similarly to the BF configuration, beams and columns can be designed only for gravitational loads, given that the presence of the base isolation system decouples the ground movement caused by the seismic action from the superstructure.

The following sub-sections describe the application of the DDBD to the BI case-study and its main results, outputs of dynamic non-linear analysis, definition of fragility curve and finally the development of the intensity-based loss analysis.

5.7.1 Materials

Concrete class is C25/30 and steel reinforcement is B450C, as for the MRF case-study (§ 5.3.1). HDRBs are made of soft rubber, characterized by shore shear elasticity modulus G=0.4 MPa and equivalent viscous damping ξ=10-15% at shear deformation γ=1.

5.7.2 Application of DDBD

The Direct Displacement-Based Design (DDBD) is applied to the BI system according to the procedure provided by Cardone et al. 2009 and recalled in Appendix C. The selected design drift is 0.4%, in order to avoid structural damage. The preliminary design provides a value of the equivalent isolation system's displacement D_d=0.285 m, in correspondence of the choice of the base isolation system's damping ratio ξ_{is}=15% and a period T_{is}=3.53s. The BI structure's equivalent SDOF design displacement is Δ_d=0.307 m, while the equivalent damping ratio is 14%, adopting a value of the superstructure damping ratio ξ_s=2%, as commonly assumed for BI structures given their lower involvement into deformation.
The DDBD results are herein summarized.

Table 40 Application of DDBD to the BI system

D_d	Δ_d	ξ_{is}	ξ_s	ξ_{bi}	η	T_{eq}	K_{eq}	Base Shear	K_{is}
[m]	[m]	[%]	[%]	[%]		[s]	[kN/m]	[kN]	[kN/m]
0.285	0.307	15	2	14.05	0.72	3.30	8580	2634	9253

The base shear is divided by the number of seismic lateral frames and then distributed along the levels, obtaining lateral forces given in Table 41. Note that, differently from previous analyzed case-study systems, internal frames contribute to lateral resistance given the isotropic behaviour of adopted isolators. In particular, differently from external frames characterized by four HDRBs, i.e. one per column, in correspondence of each internal frame there are two HDRBs, i.e. at the base of the two

external columns, while the internal columns are laying on simple rollers. Consequently the base shear acting in correspondence of each external frame is 1/3 of that in output from the DDBD procedure.

Table 41 Lateral forces distributed along levels - BI system

Level	Δ_i [m]	m_i [tons]	$m_i\Delta_i$ [-]	F_i [kN]
5	0.321	250	80	**97**
4	0.319	424	135	**164**
3	0.315	424	134	**161**
2	0.308	424	130	**158**
1	0.297	424	126	**152**
Base	0.285	424	121	**146**
		2371	726	**878**

Descending internal actions are employed to preliminary dimension beams and columns longitudinal reinforcement.

5.7.3 BI system structural section definition and modeling

Beams and columns steel reinforcement quantity is chosen as a consequence of internal actions coming from the DDBD. Final configurations are represented in Figure 109.

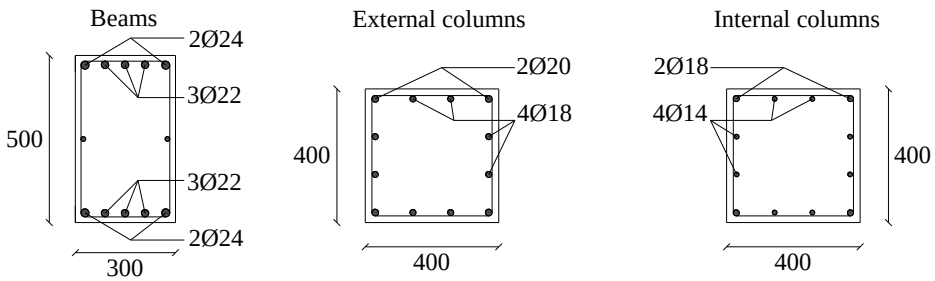

Figure 109 Beams and Columns in BI systems

Final mechanical characteristics adopted for elastomeric isolators are given in Table 42. Note that the total stiffness is lower than the design parameter in output from the DDBD procedure (Table 40). Actually the preliminary design resulted too conservative, yielding a design

displacement in correspondence of isolators of almost 0.3 m. The design has been optimized in accordance to results of dynamic nonlinear analysis, as it will be introduced in the next paragraph, demonstrating that a displacement capacity of 0.2 m is sufficiently satisfactory. Isolators with this capacity have been selected from an Italian catalogue (Fip - industriale), yielding the geometry described in Figure 110 and Table 42.

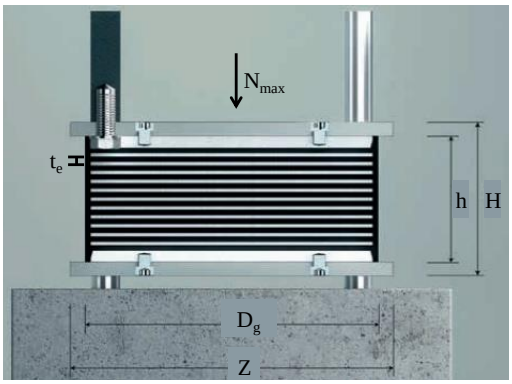

Figure 110 Elastomeric device's geoemtry - from Fip industriale catalogue

Table 42 Elastomeric isolators' mechanical characteristics

Device	#	D_g [mm]	t_e [mm]	h [mm]	H [mm]	Z [mm]	W [kg]	N_{max} [kN]	K_h [kN/m]	K_v [10^3 kN/m]	$K_{is,tot}$ [kN/m]	c [kNs/m]
SI-S 450/102	4	450	102	190	240	500	220	900	620	725	8640	105
SI-S 500/102	8	500	102	190	240	550	270	1420	770	1038		117

Beams and columns are modelled in Opensees (McKenna 1997) as “elasticBeamColumn” elements, verifying successively that yielding is never achieved in any of them. HDRB isolators are modelled as "zeroLength" elements at the base of columns, characterized by a viscous and a linear springs in parallel, provided with the horizontal stiffness K_h and the damping coefficient c given in Table 42.

5.7.4 Dynamic non-linear analysis

The first vibrational period of the 2D BI system is T_1=3.52 s and it mainly concerns, as expected, the isolation system. According to Italian code indications (NTC 2008), the fundamental period of vibration of a base isolated system should be at least $3T_{fb}$. In the specific case-study, the structure in analysis is a simple frame characterized by a relative high deformability, as observed from the MRF and HYB systems' modal investigation. Consequently, although quite high, the period observed in not very far from the minimum requirement. Even if the Italian code does not provide any upper limit of the base isolated structure's fundamental period, it is generally good practice to do not exceed the value of 4 seconds, in order to do not excessively amplify displacements. Tall buildings and peculiar constructions can obviously be exceptions.

Dynamic nonlinear analysis are performed in correspondence of the set of records introduced in paragraph 5.2.3. An OpenSees-Matlab code is created in order to both check the structural design and get EDP needed for the loss estimation analysis. The displacement profile envelope in correspondence of each record is plotted in Figure 111, showing also the mean trend.

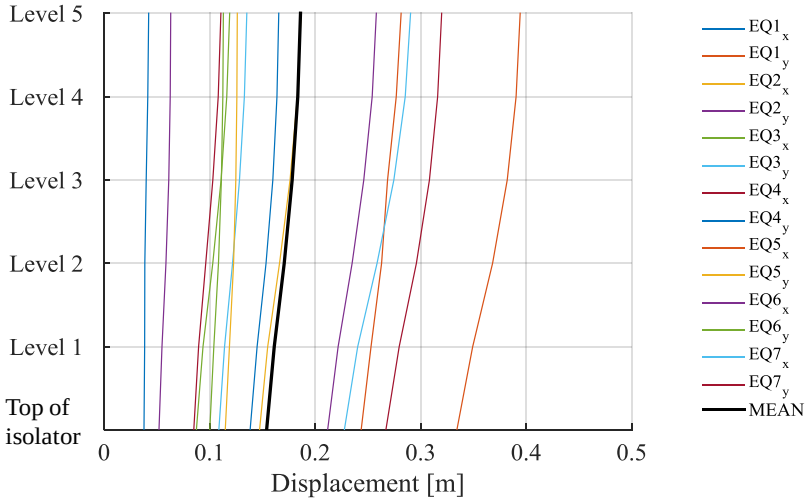

Figure 111 Displacement profile envelope of BI system

It is verified that in correspondence of beams and columns the mean of maximum internal actions over the 14 records is never greater than elements' yielding moment.

EDPs required for the loss estimation analysis are IDR, PFA and RIDR. In particular, the maximum in correspondence of each record is selected and recalled in the following tables and figures.

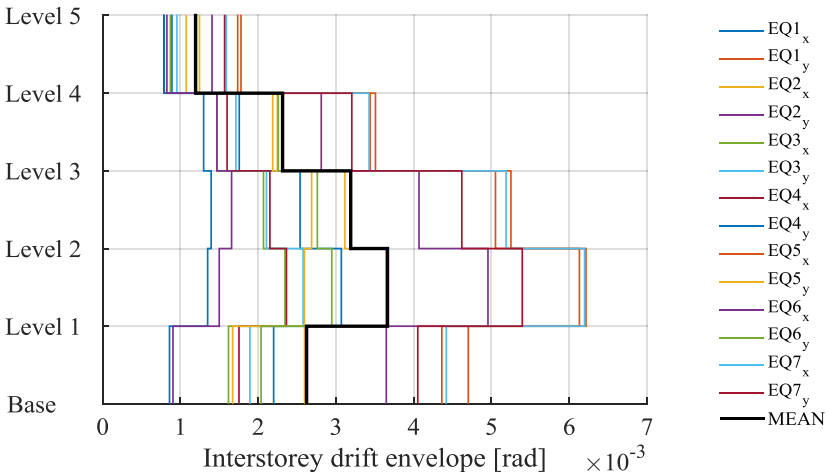

Figure 112 IDR envelope of BI system

Table 43 Maximum IDR values of BI system

Level	Base-1	1-2	2-3	3-4	4-5
EQ1x	0.22%	0.31%	0.25%	0.18%	0.09%
EQ1y	0.47%	0.61%	0.51%	0.34%	0.18%
EQ2x	0.26%	0.36%	0.31%	0.22%	0.11%
EQ2y	0.36%	0.50%	0.41%	0.28%	0.14%
EQ3x	0.16%	0.23%	0.21%	0.15%	0.09%
EQ3y	0.19%	0.26%	0.21%	0.17%	0.10%
EQ4x	0.18%	0.24%	0.22%	0.16%	0.08%
EQ4y	0.09%	0.14%	0.14%	0.13%	0.08%
EQ5x	0.44%	0.62%	0.53%	0.35%	0.17%
EQ5y	0.17%	0.26%	0.27%	0.22%	0.12%
EQ6x	0.09%	0.15%	0.17%	0.15%	0.08%
EQ6y	0.20%	0.29%	0.28%	0.23%	0.12%
EQ7x	0.44%	0.62%	0.52%	0.34%	0.16%
EQ7y	0.41%	0.54%	0.46%	0.32%	0.16%
MEAN	**0.26%**	**0.37%**	**0.32%**	**0.23%**	**0.12%**

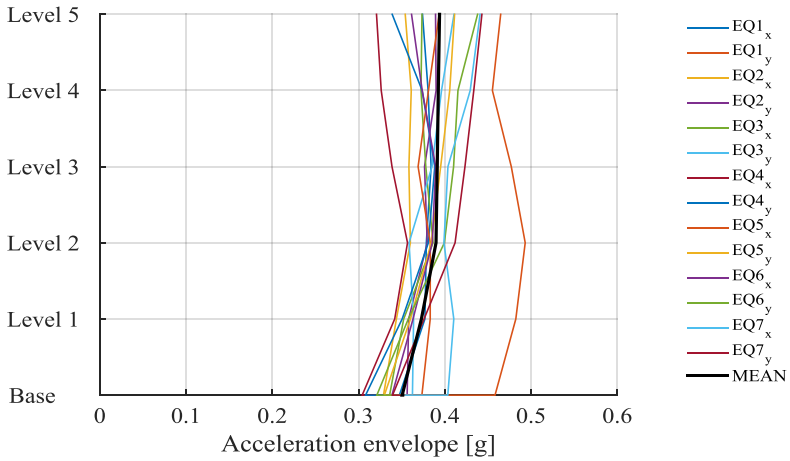

Figure 113 PFA envelope of BI system

Table 44 PFA values of BI system (in g)

Level	Ground	1	2	3	4	5
EQ1x	0.35	0.38	0.38	0.38	0.38	0.37
EQ1y	0.35	0.48	0.49	0.48	0.46	0.46
EQ2x	0.35	0.34	0.36	0.36	0.36	0.35
EQ2y	0.35	0.36	0.38	0.38	0.39	0.39
EQ3x	0.35	0.35	0.39	0.38	0.37	0.37
EQ3y	0.35	0.36	0.36	0.39	0.40	0.41
EQ4x	0.35	0.34	0.36	0.34	0.33	0.32
EQ4y	0.35	0.35	0.38	0.39	0.37	0.34
EQ5x	0.35	0.38	0.38	0.37	0.38	0.39
EQ5y	0.35	0.36	0.38	0.40	0.41	0.41
EQ6x	0.35	0.36	0.39	0.39	0.37	0.36
EQ6y	0.35	0.36	0.40	0.41	0.42	0.44
EQ7x	0.35	0.41	0.40	0.40	0.43	0.44
EQ7y	0.35	0.38	0.41	0.42	0.43	0.44
MEAN	**0.35**	**0.37**	**0.39**	**0.39**	**0.39**	**0.39**

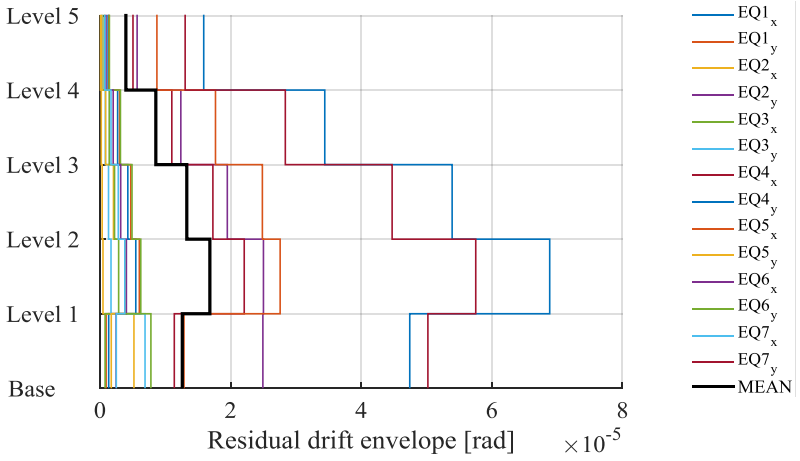

Figure 114 RIDR envelope of BI system

Table 45 Maximum residual drift values of BI system

Level	Base-1	1-2	2-3	3-4	4-5
EQ1x	0.000%	0.000%	0.000%	0.001%	0.000%
EQ1y	0.000%	0.000%	0.000%	0.001%	0.000%
EQ2x	0.000%	0.000%	0.000%	0.000%	0.001%
EQ2y	0.001%	0.001%	0.002%	0.003%	0.002%
EQ3x	0.000%	0.000%	0.000%	0.001%	0.000%
EQ3y	0.000%	0.000%	0.000%	0.000%	0.001%
EQ4x	0.001%	0.001%	0.002%	0.002%	0.001%
EQ4y	0.002%	0.003%	0.005%	0.007%	0.005%
EQ5x	0.001%	0.002%	0.002%	0.003%	0.001%
EQ5y	0.000%	0.000%	0.000%	0.000%	0.000%
EQ6x	0.000%	0.000%	0.000%	0.000%	0.000%
EQ6y	0.000%	0.000%	0.000%	0.000%	0.001%
EQ7x	0.000%	0.000%	0.000%	0.000%	0.000%
EQ7y	0.001%	0.003%	0.004%	0.006%	0.005%
MEAN	**0.000%**	**0.001%**	**0.001%**	**0.002%**	**0.001%**

According to Italian seismic code (NTC 2008), base isolators have to be verified in correspondence of seismic records characterized by a probability of occurrence of 2% in 50 years. Consequently a new records' selection has been derived, providing events detailed in Table 46.

The mean relative displacement of HDRB elements, evaluated as the average value of maximum deformations registered for each of the selected records (Figure 115), is lower than the deformation capacity of 200 mm (the mean-maximum demand is 182 mm).

Table 46 Set of 7 spectro-compatible records

#	Waveform ID	EQ ID	Earthquake Name	Mw	PGA_x [g]	PGA_y [g]	Scale Factor x	Scale Factor y
1	242	111	Eastern Fukushima Pref	6.6	0.19	0.18	2.21	2.34
2	139	51	Southern Iwate Prefecture	6.9	0.30	0.22	1.41	1.91
3	438	83	Parkfield	6	0.14	0.23	3.00	1.85
4	422	72	Friuli 1st shock	6.4	0.32	0.35	1.35	1.23
5	146	54	S Suruga Bay	6.2	0.42	0.26	1.02	1.65
6	464	99	Northridge	6.7	0.29	0.23	1.47	1.83
7	421	46	Irpinia	6.9	0.18	0.16	2.42	2.68

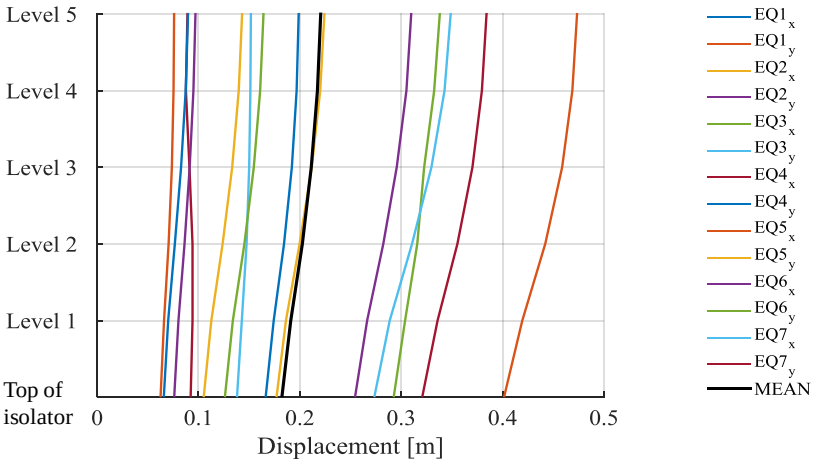

Figure 115 Displacement profile of BI system in correspondence of events with probability of occurrence of 2% in 50 years

5.7.5 IDA analysis and fragility curve

Incremental Dynamic Analysis (IDA) are performed employing the 42 records introduced at §5.2.3 and adopting the base displacement, that is the displacement at the top of isolators, as EDP. Resulting IDA curves are plotted in Figure 116. The fragility curve, given in Figure 117, is constructed selecting the IM values that cause collapse and plotting the relative Cumulative Distribution Function (CDF). In particular the attainment of failure is considered when the isolators maximum displacement of 200 mm is achieved. Indeed the supplier provides devices designed so to prevent other type of failure, such as buckling. Moreover,

given the symmetrical structural system, no eccentricity problem are expected in the structure.

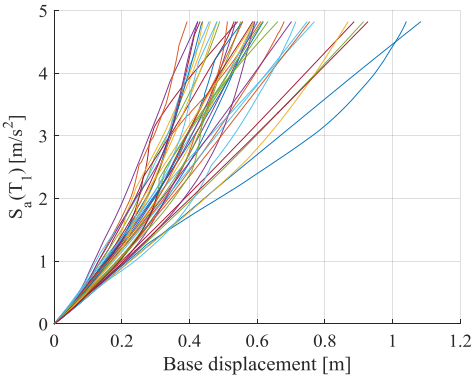

Figure 116 IDA curves for BI system

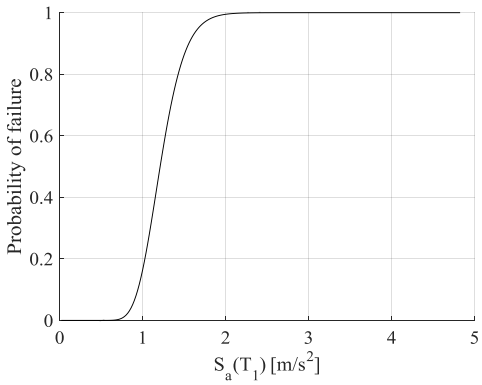

Figure 117 Fragility curve for BI system

5.7.6 Structural fragility components

Structural fragility components adopted for the BI system concern both beam-column joint and isolators. Beam-column joint fragility component adopted is the same used for the MRF system, so more details are provided at §5.3.6. As far as isolators are concerned, there are in literature many studies concerning the evaluation of the whole base isolated structure's probability of failure (Huang et al. 2010, Dang et al. 2015, Ali et al. 2014, Kotrotsou et al. 2015, Castaldo et al. 2017, Mansouri et al. 2017), but none of them explicitly investigating isolators' fragility curves. In appendix H of FEMA P-58-1 2012, several methodologies for the development of fragility curves are proposed. The most accurate of them uses experimental tests data, as the Actual Demand Data adopted for SL damper's fragility curve derivation. Actually in literature there is a wide number of experimental results that could be employed to this aim, but this detailed study is not object of interest of the present work of thesis. Differently, FEMA P-58-1 also suggests the Derivation method, usable

when no experimental data are available but it is possible to model the behavior and analytically estimate the level of demand at which the damage state of interest is expected to occur. In particular, knowing the capacity of the component, Q, defined in terms of a specific demand parameter, the median capacity μ is taken as 0.92Q, and the logarithmic standard deviation as β=0.4. So in the specific case-study, given the maximum allowable displacement of employed isolators, that is 200 mm, the median capacity is approximated to the value of 184 mm. The final fragility curve is plotted in Figure 118.

The cost for the retrofit intervention and substitution of the eventually damaged isolator is estimated on the basis of price list of Sicilian Region (Gazzetta Ufficiale della Regione Sicilia, 2013) to be 5760 $. It is comprehensive of the unloading of the existing elements through the use of hydraulic jack, insertion of the new device and release of the structure. It is common practice to place isolators in easy accessible locations, so no significant additional costs are expected for the isolator's substitution.

The final economic consequence function of Figure 119 is determined.

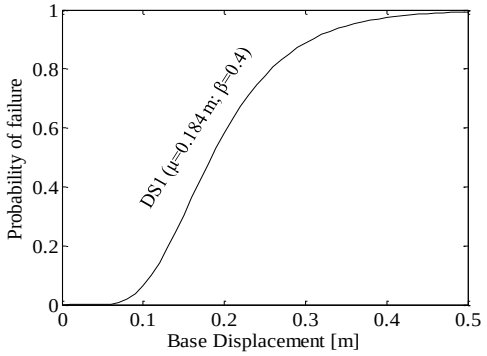

Figure 118 Fragility curve of elastomeric isolators with 200 mm displacement capacity

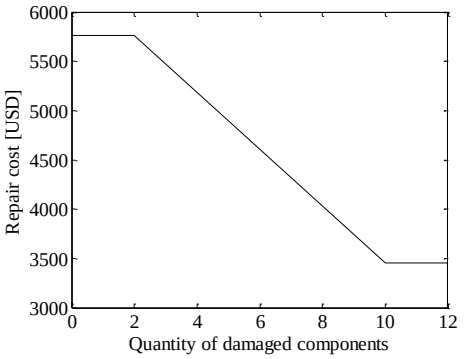

Figure 119 Economic consequence function of elastomeric isolators

5.7.7 Loss estimation analysis and results

In order to perform the loss estimation analysis it is necessary to evaluate the total replacement cost of the facility. As already introduced in §5.2.4, the construction cost of BI system is estimated starting from MRF's one and opportunely increasing it according to the comparison of both systems structural costs. Moreover it is necessary to account also for the increased cost due to the use of deformable services, which have to allow the important displacements characterizing base isolated structures.

The construction cost of the only superstructure of the BI building (concrete, steel reinforcement), including cost of labor, is estimated through the use of Central Italy construction price list (Bollettino ufficiale della Regione Umbria, 2014) to be 64'490 $. The cost for the supply and installation operation of each isolator is estimated on the basis of price list of Sicilian Region (Gazzetta Ufficiale della Regione Sicilia, 2013), suggesting a cost of 109 $/dm^3 plus the 2% for labor cost, for a total of 46'747 $. The cost of rollers to be placed in correspondence of the four central columns is roughly considered equal to 2500 $ each. The incidence of services for an office building is estimated to be the 25% of the total. Moreover, in the case of flexible installations a further increment of 15% is assumed. Considering the MRF system as comparison, the final BI system's total replacement cost is 2'975 $/m^2, that corresponds to a total of 9.04 M$, considering the total area of 506 m^2 and the number of levels (which is 6 considering also the ground floor).

Finally, intensity-based loss estimation analysis is performed.

Repair Costs (RC) corresponding to each realization of the Monte Carlo simulation is plotted in Figure 120-a, showing also the amount of repair costs provided by each component's category. It is evident that in correspondence of a generic realization the more significant contribution comes from non-structural components, followed by contents and structural elements. Note that in no simulation the structure is collapsed and never irreparability is reached, so the total replacement cost is never

observed. The area beneath the total repair cost curve (dashed curve in Figure 120-a) correspond to the fictitious total amount of money required to repair the structure over 500 realizations, and it is equal to 161 M$. The area beneath the repair cost curve corresponding to structural and non-structural components, contents and demolition/reconstruction contributions is compared to the total area, providing the pie chart of Figure 120-b. Data observed confirm that the main part of repair costs is attributed to non-structural components, which cover a percentage of 52% of the total, followed by contents (36%) and structural components (12%). It is interesting to observe that the cost attributed to structural elements is significantly reduced, confirming that beam-column joints are preserved from damage.

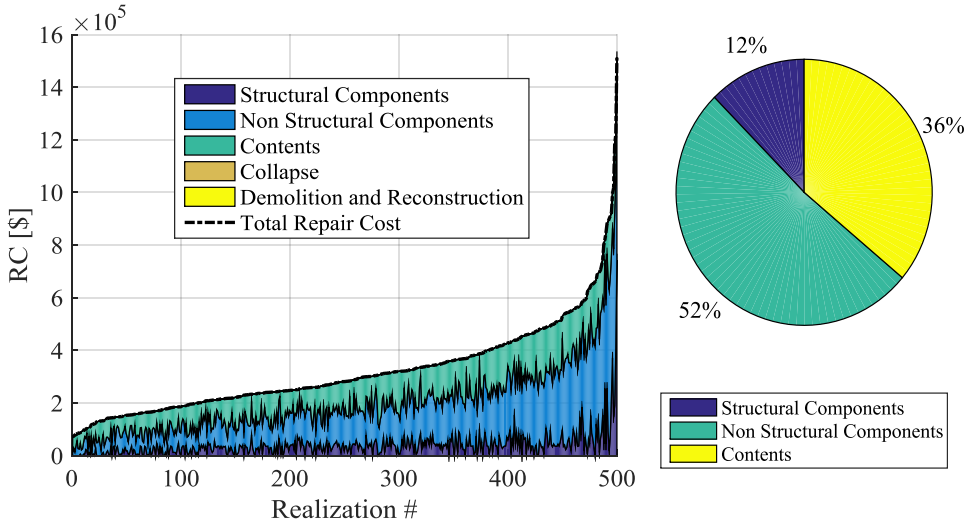

(a) (b)

Figure 120: a) Repair cost over realizations - BI system; b) Contribution of different categories to the overall repair cost (161 M$) for BI system

The Mean Damage Factor (MDF) of RC is 0.32 M$, the Scenario Expected Loss (SEL) is 0.28 M$ and the Scenario Upper Loss (SUL) is 0.53 M$. The characteristic PML value (PML_k) is 0.63 M$.

Repair costs are binned and shown in the bar plot of Figure 121. The Cumulative Distribution Function (CDF) of Repair Cost is given in Figure 122, while Figure 123 shows the CDF of RCR. The probability of loss, expressed as the probability of exceeding a certain repair cost ratio, given the intensity measure is plotted in Figure 124.

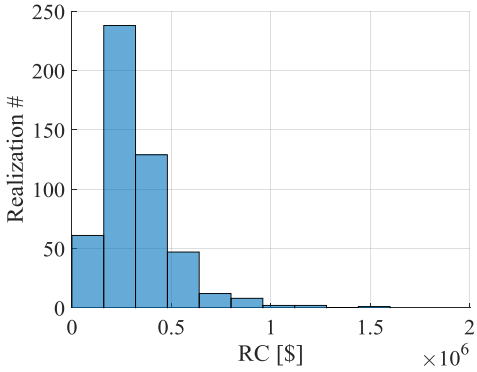

Figure 121 Binned repair costs resulting from the Intensity-based loss estimation analysis of the BI system

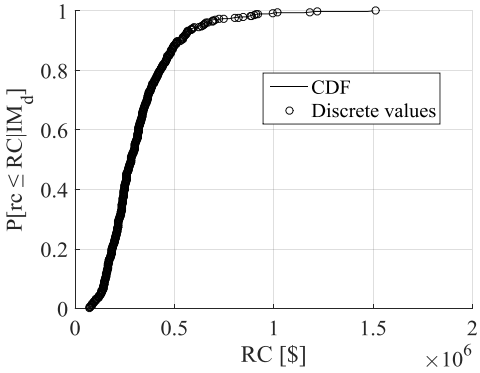

Figure 122 Cumulative distribution function of repair cost (RC) - BI system

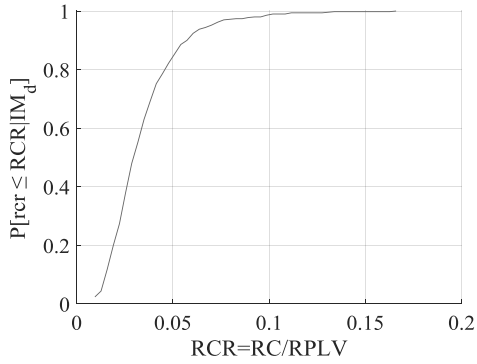

Figure 123 Cumulative distribution function of repair cost ratio (RCR) - BI system

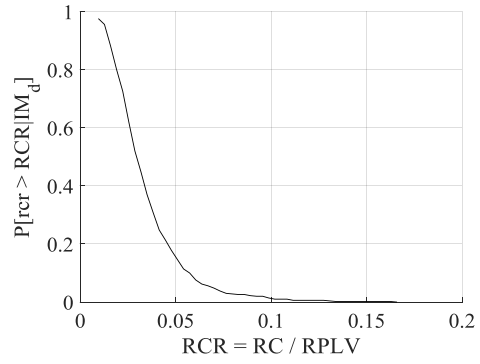

Figure 124 Probability of loss - BI system

5.8 Loss-based comparison of the five alternative structural systems

In the present section analyzed seismic technologies, namely MRF, HYB, LD-HYB, BF and BI systems, are compared, both recalling some main results observed as output of the dynamic non-linear analysis and loss estimation assessments.

5.8.1 Non-linear dynamic response

The main outputs of the dynamic non-linear analysis performed in correspondence of each seismic system are compared. In particular, mean displacement, IDR, PFA and RIDR envelopes are shown from Figure 125 to Figure 128. From the displacement envelope it is evident that BF system is the most rigid, having a mean top displacement of 7 cm, while HYB structure is subjected to a mean top displacement of around 16 cm and MRF and BI systems of 18 cm. Also, note that BI system mean base displacement is slightly higher than 15 cm. From the analysis of mean IDR envelops, it is evidenced that MRF and HYB systems are subjected to a comparable interstorey deformation, with a maximum value of around 1.5% at the first level. Conversely, BF system's maximum IDR is slightly higher than 0.5% at the third level, that is the design value. Finally IDR values measured in correspondence of the BI system are coherent with the technology adopted, being always very small, with a peak value at the second level of 0.4%.

From the analysis of PFA envelopes, it is evident that the ground value corresponds to the PGA, then, as a mean trend, amplified along the height of the structure. Only BF system represents an exception, presenting a mean reduced PFA at the first level, and significant amplifications at other levels (maximum value is 0.75g at the last level). MRF and HYB technologies present similar trends of PFA, while in BI system amplifications are very small, always keeping the value below 0.4g.

Finally, the analysis of RIDR envelopes is very explicative for what concerns the main drawback of MRF solutions: it presents residual drifts higher than all other cases, with maximum values of 0.085%. This result contributes to generate some of the Monte Carlo simulations yielding irreparability conditions in the loss analysis, as observed in §5.3.7.

BI system is expected to behave linearly, thus providing zero residual drifts. Differently, in the HYB solution residual drifts are null thanks to the re-centering action provided by post-tensioning cables. Finally, the BF technology yields negligible RIDR as well.

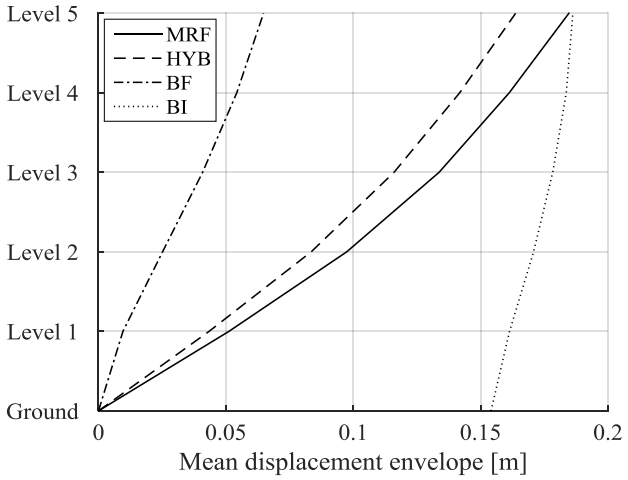

Figure 125 Comparison of displacement profile envelopes in correspondence of MRF, HYB, BF and BI systems

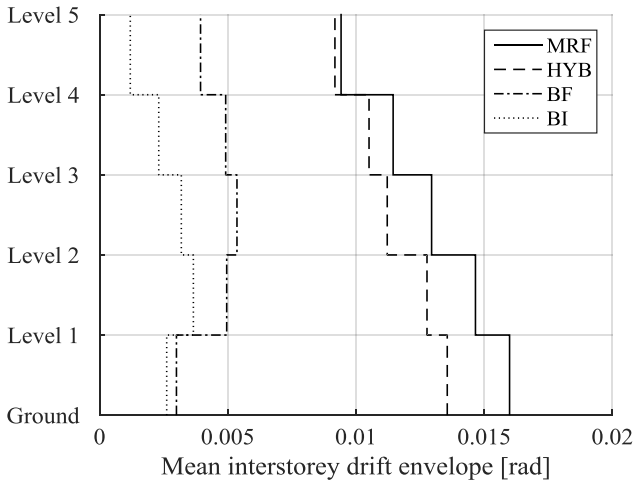

Figure 126 Comparison of IDR profile envelopes in correspondence of MRF, HYB, BF and BI systems

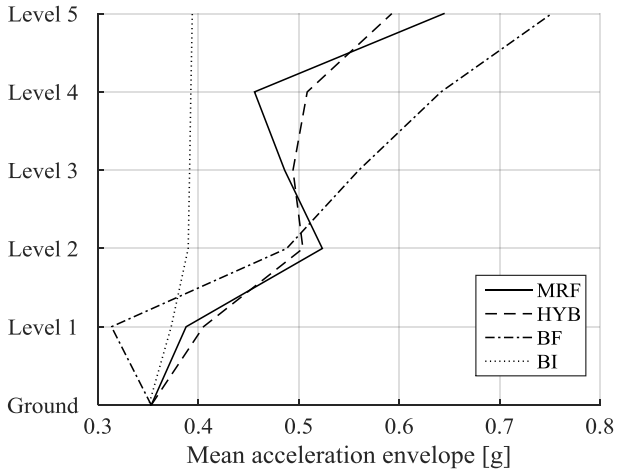

Figure 127 Comparison of PFA profile envelopes in correspondence of MRF, HYB, BF and BI systems

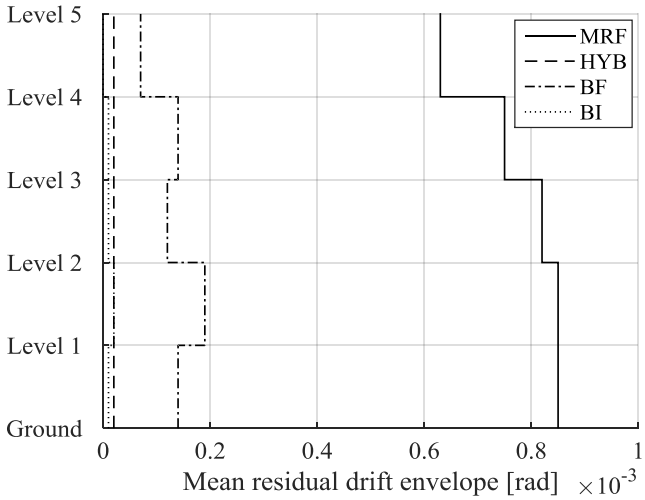

Figure 128 Comparison of RIDR profile envelopes in correspondence of MRF, HYB, BF and BI systems

5.8.2 Loss performance

Finally, loss performance of the different seismic technologies studied, namely MRF, HYB, LD-HYB, BF and BI, are compared. The values of RPLV and RC_{tot}, that is the fictitious repair cost obtained summing the results of all the numerical simulations, are summarized in Table 47 for all systems.

Table 47 RPLV and RC_{tot} of MRF, HYB, LD-HYB, BF and BI technologies

	MRF	HYB	LD-HYB	BF	BI
RPLV [M$]	6.61	6.90	6.90	7.75	9.04
RC_{tot} [M$]	821	590	346	269	161

In Figure 129 and Figure 130 the trend of RC and RCR over the Monte Carlo simulations are shown: there is a significant gap between MRF's overall repair costs, RC_{tot}, and all the other solutions. In particular, it emerges that the adopted alternative seismic technologies allow to

progressively reduce losses, if considered in the following order: HYB, LD-HYB, BF and BI.

Moreover, the MRF system it is the only presenting some Monte Carlo realizations in which RC=RPLV, both because exceeding the maximum loss threshold of 0.5 or for the achievement of irreparability conditions due to high RIDR values.

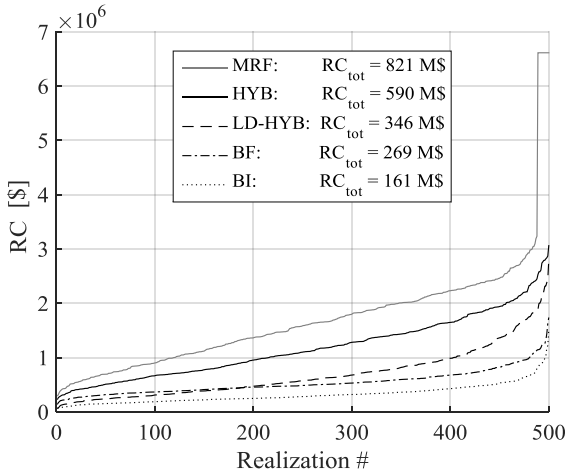

Figure 129 Repair Cost (RC) over Monte Carlo simulations for all analyzed seismic technologies

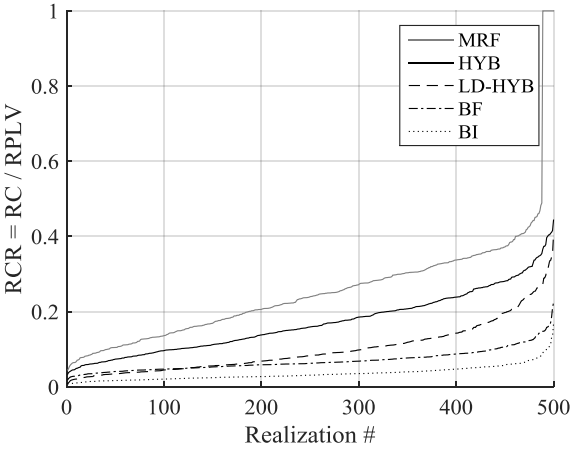

Figure 130 Repair Cost Ratio (RCR) over Monte Carlo simulations for all analyzed seismic technologies

Although, the most significant contribution that makes a difference between MRF and other technologies is represented by structural components. Indeed, Figure 131 shows that structural components RC bar of MRF system is more than doubled with respect to the closest one, given by HYB system. Differently, MRF system's RC given by non-structural components are slightly higher than HYB case-study, due to MRF slightly higher IDR values. This is the main reason leading to the employment of the LD-HYB technology: indeed, the re-centering dissipative rocking solution, even if significantly reducing structural damage, is still a quite deformable system. Accordingly, it is expectable that non-structural RCs are similar to MRF system ones. In particular, as evidenced by Figure 132, main source of non-structural losses comes from glass curtain wall and gypsum partitions, that are IDR sensitive. Instead, the adoption of low-damage non-structural components significantly reduces this contribution of loss, as evidenced by LD-HYB system's loss performances. The adoption of the BF seismic solution drastically reduces the structural economic losses, given that this technology is designed for drifts of 0.5%, against drifts of 2% of MRF or HYB systems, thus avoiding bare frame's non-linear behavior. Actually, the contribution of loss due to structural components is provided, in this specific case, by both beam-column connections and SL dampers: Figure 133 shows that both this contributions are very small. Non-structural components' damage of the BF system is similar to LD-HYB due to the significant lower IDR values involved. Finally, BI system shows that structural components contribution to loss, given by beam-column connections and isolators, is comparable to BF system: in particular, as evidenced by Figure 133, beam-column connections generate a practically null loss, while loss due to isolators, still very small, is higher than SLs simply because steel dampers are cheaper than HDRB devices. Non-structural components' losses of the BI system are the lowest among the five technologies compared, given that both IDR and PFA demands are smaller. The

analysis of losses due to damage of contents shows a comparable trend for all the technologies, with a reduction in the case of BI system (Figure 134).

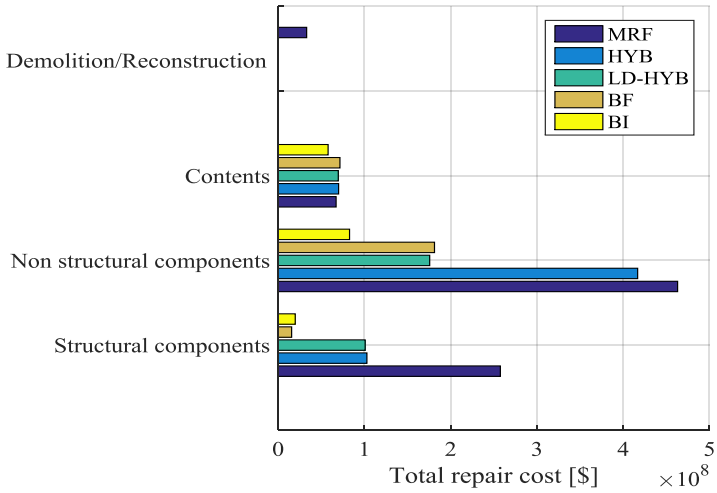

Figure 131 Comparison of different source of losses for MRF, HYB, LD-HYB, BF and BI technologies

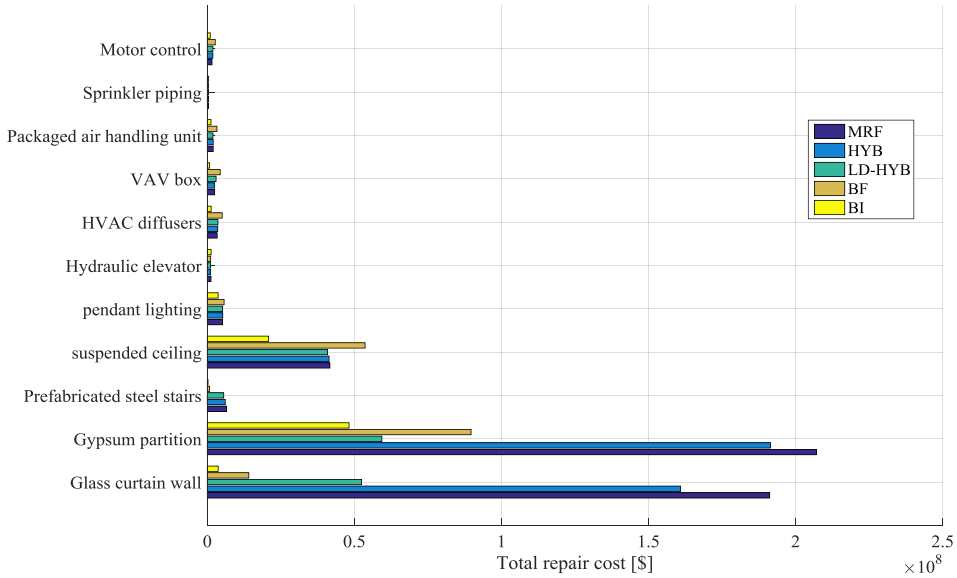

Figure 132 Comparison of non-structural components losses for MRF, HYB, LD-HYB, BF and BI technologies

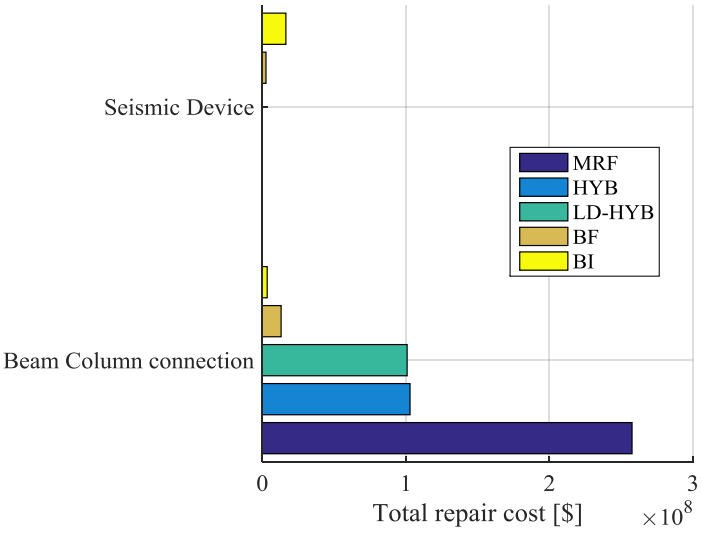

Figure 133 Comparison of structural components losses for MRF, HYB, LD-HYB, BF and BI technologies

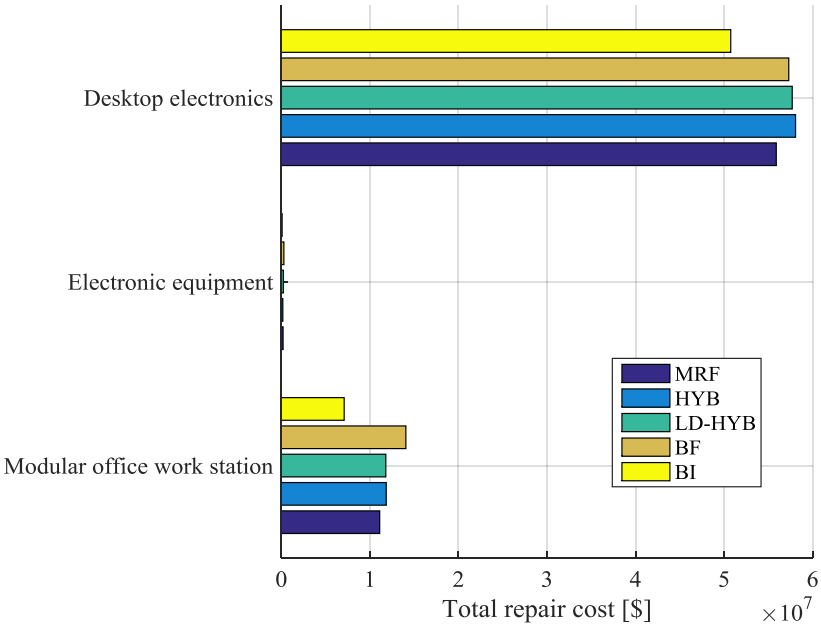

Figure 134 Comparison of contents losses for MRF, HYB, LD-HYB, BF and BI technologies

Finally, the CDF of RC and RCR for the five seismic technologies analyzed are compared in Figure 135 and Figure 136, while corresponding loss curves are given in Figure 137. The beneficial effect of alternative seismic solutions in reducing losses is evident.

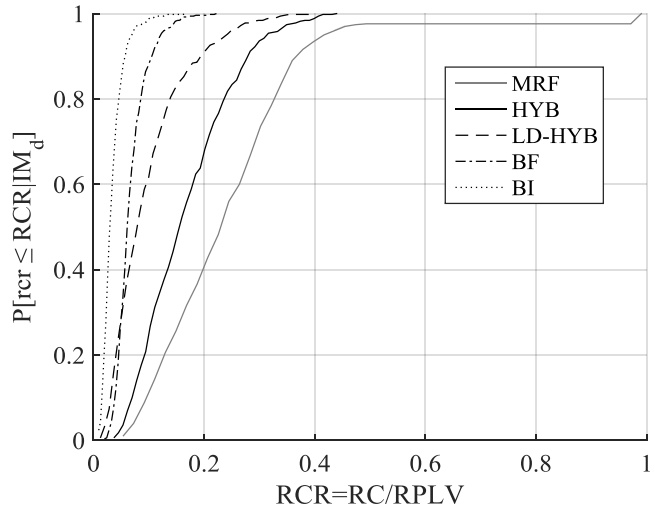

Figure 135 Comparison of CDF in terms of RC for MRF, HYB, LD-HYB, BF and BI technologies

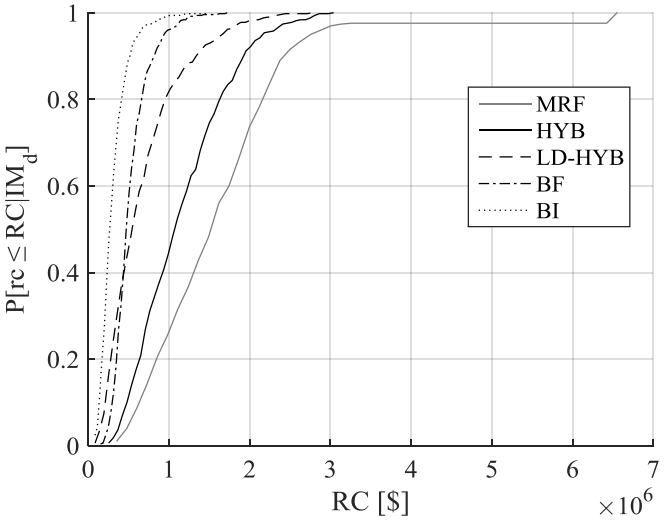

Figure 136 Comparison of CDF in terms of RCR for MRF, HYB, LD-HYB, BF and BI technologies

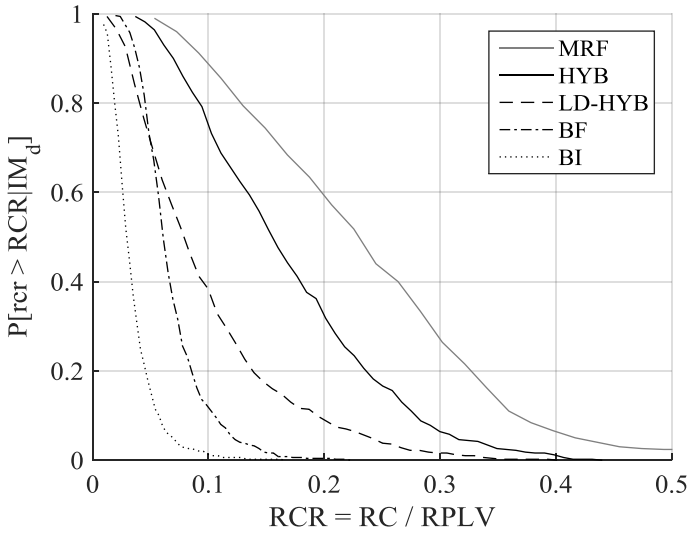

Figure 137 Comparison of loss curves in terms of RCR for MRF, HYB, LD-HYB, BF and BI technologies

From the analysis of these plots it is interesting to compare Mean Damage Factors (MDF) and particular PML quantities, namely the Scenario Expected Loss (SEL), the Scenario Upper Loss (SUL) and the characteristic value (PML_k), respectively corresponding to the RC median value and the RC 90° and 95° percentiles of non-exceedance. The above quantities are selected both in terms of RC and RCR, and are given in Table 48 and Figure 138 and in Table 49 and Figure 139, respectively. The great advantage corresponding to the reduced losses gained passing from a MRF system to different types of low-damage technologies is evident. Note that, as the system's performance in terms of loss arises, the distance between upper percentiles, MDF and SEL values is reduced.

Table 48 MDF, SEL, SUL and PML_k results in terms of RC for MRF, HYB, LD-HYB, BF and BI technologies

	MRF	HYB	LD-HYB	BF	BI
MDF [M$]	1.69	1.18	0.69	0.54	0.32
SEL [M$]	1.59	1.10	0.57	0.49	0.28
SUL [M$]	2.46	1.94	1.36	0.83	0.53
PML_k [M$]	2.82	2.20	1.69	0.95	0.63

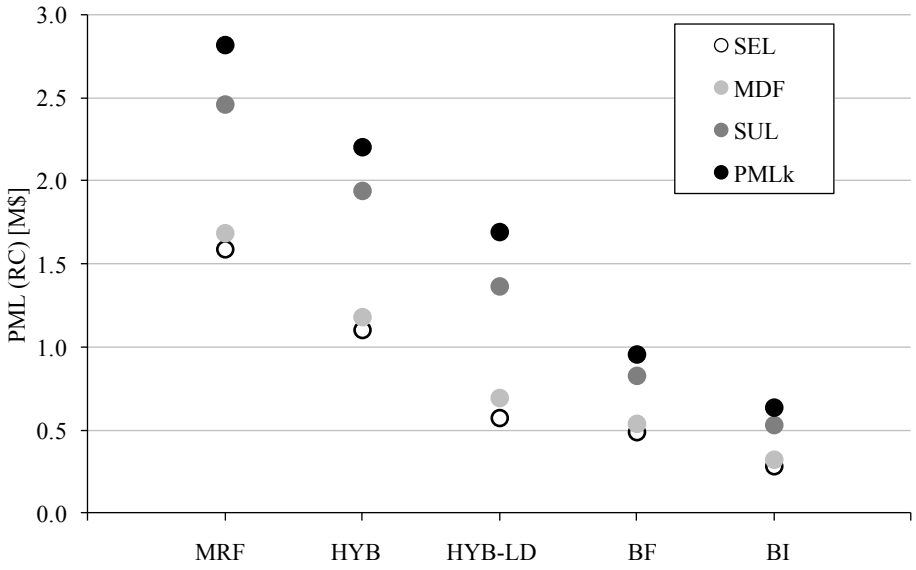

Figure 138 Comparison of MDF, SEL, SUL and PML_k results in terms of RC for MRF, HYB, LD-HYB, BF and BI technologies

Table 49 MDF, SEL, SUL and PML_k results in terms of RCR for MRF, HYB, LD-HYB, BF and BI technologies

	MRF	HYB	LD-HYB	BF	BI
MDF [-]	0.25	0.17	0.10	0.07	0.04
SEL [-]	0.24	0.16	0.08	0.06	0.03
SUL [-]	0.37	0.28	0.20	0.11	0.06
PML_k [-]	0.43	0.32	0.25	0.12	0.07

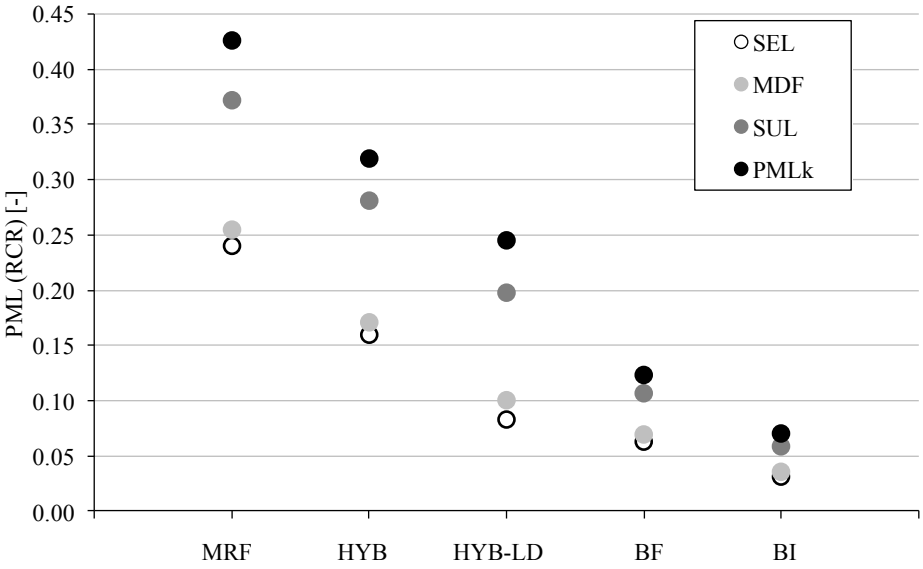

Figure 139 Comparison of MDF, SEL, SUL and PML_k results in terms of RCR for MRF, HYB, LD-HYB, BF and BI technologies

5.8.3 Analysis in the view of a loss performance matrix

This section is addressed to the analysis and comparison of the five seismic technologies, namely MRF, HYB, LD-HYB, BF and BI, in the qualitative loss performance matrixes proposed in Figure 25 and corresponding to basic, essential/hazardous or critical safety facility's objectives for a fixed intensity level. In the perspective of realizing a cost-based design, a performance goal corresponding to a maximum characteristic PML value, in terms of RCR, equal to 0.3 is set, that means attempting to design a building able to provide a maximum RC equal to 30% of the total RPLV at the occurrence of the design earthquake, with a maximum probability of being exceeded of 5%. Considering the loss performance matrixes, shown again from Figure 140 to Figure 142, overlapped with the case studies loss curves, the imposed design loss limits correspond, at least, to a medium, low and unacceptable design

performance level supposing a basic, essential or critical facility, respectively.

Once the design loss performance goal is set, the capacity of the different systems of achieving it can be analyzed. As reported in Table 49, MRF and HYB systems would not be able to satisfy the required loss performance objective, given that the PML_k values are respectively 0.43 and 0.32. Differently, LD-HYB, BF and BI technologies, yielding respectively 0.25, 0.12 and 0.07 PML_k values, are able to accomplish the design objectives. More in detail, if a basic facility is supposed, the BI and BF systems would provide an ideal design, while the LD-HYB case-study would correspond to a high performance level, then evolving in a medium performance level in the hypothesis of an essential/hazardous facility. Differently, for the same occupancy level, BF and BI systems would still correspond to an ideal design. Finally, supposing a critical safety building, the LD-HYB and BF technologies would provide low and high performance levels, respectively. Conversely, the BI system would always yield an ideal design, given the corresponding low repair costs.

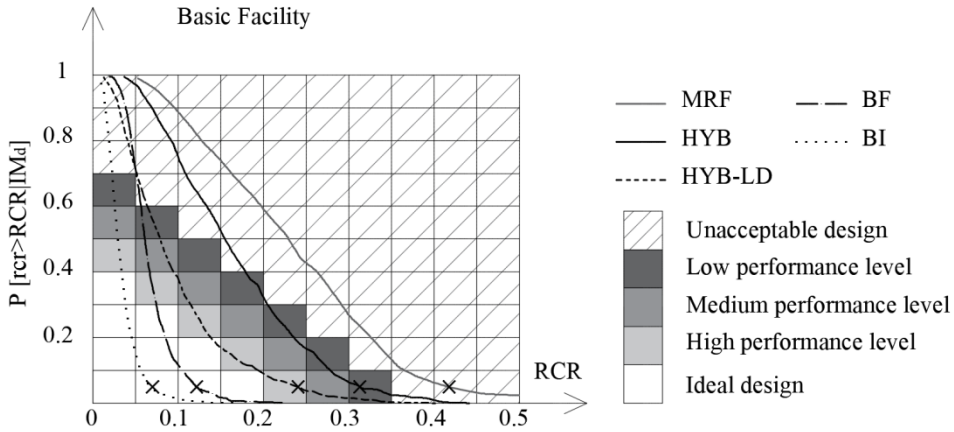

Figure 140 MRF, HYB, LD-HYB, BF and BI loss curves overlapped on a qualitative loss performance matrix for a basic objective

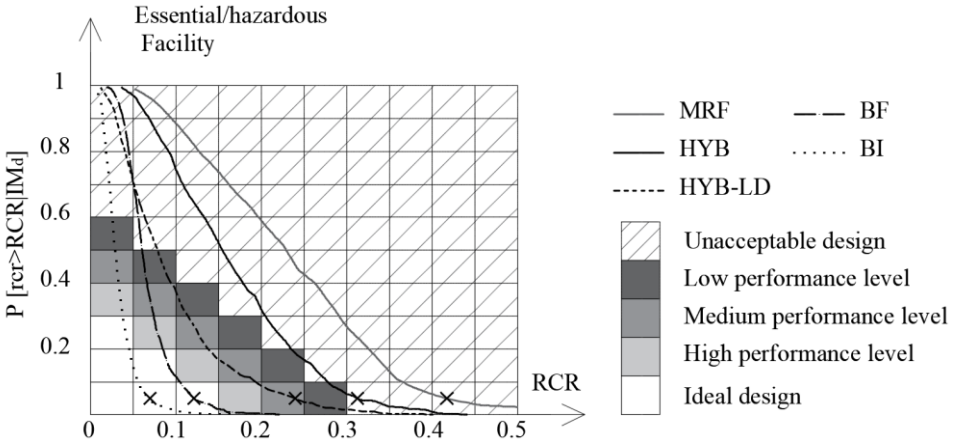

Figure 141 MRF, HYB, LD-HYB, BF and BI loss curves overlapped on a qualitative loss performance matrix for an essential/hazardous objective

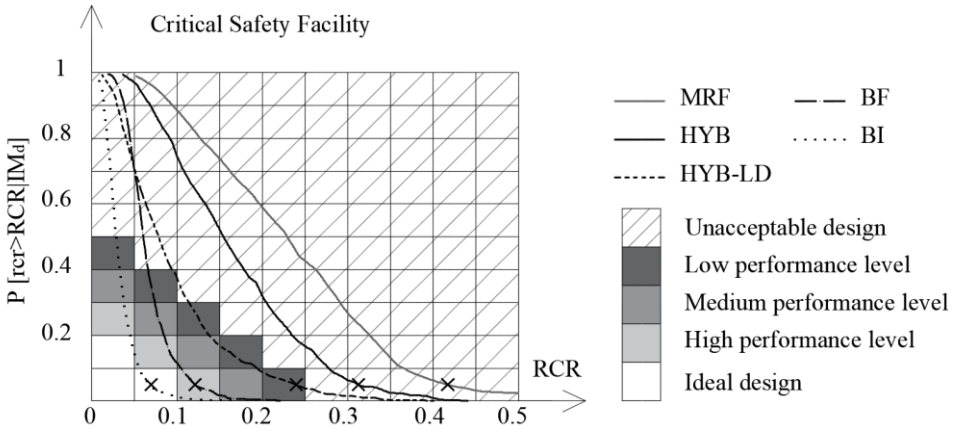

Figure 142 MRF, HYB, LD-HYB, BF and BI loss curves overlapped on a qualitative loss performance matrix for a critical safety objective

It is worthwhile to mention that RCR values of each technology are obtained dividing repair costs due to the design seismic event by the corresponding RPLV, that is progressively higher passing from the MRF to the BI systems (Figure 143). Consequently, this could misrepresent the results observed in the plots above. In order to appreciate the incidence of higher RPLV values on the output analysis in terms of RCR instead of RC, the characteristic value of both loss parameters for the analyzed seismic

technologies are shown in Figure 144 and Figure 145, indicating the reduction achieved by each alternative system with respect to MRF (percentages in brackets). It emerges that the loss enhancement gained passing from the traditional MRF system to low-damage technologies presents differences between 2% and 7%, if analyzed in terms of RC or RCR. In conclusion, the alteration of results due to the comparison of structural systems characterized by different RPLV does not significantly modify results, although it is recommendable to take this factor into account.

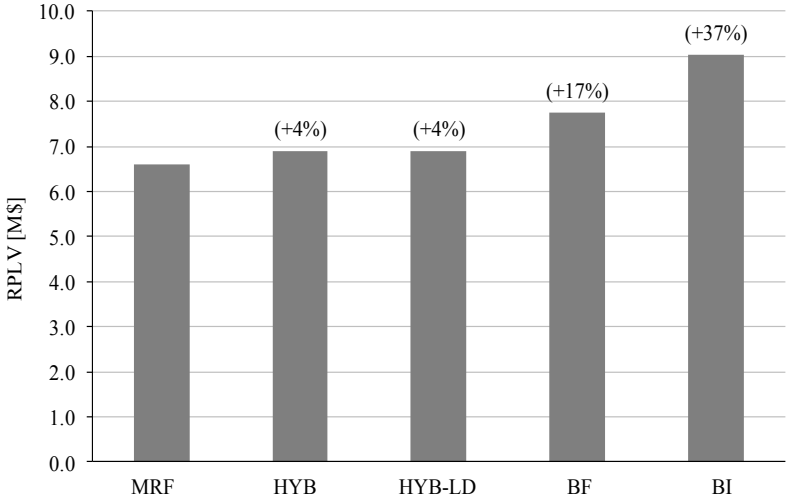

Figure 143 Comparison of analyzed seismic technologies RPLV (percentage in brackets represent the increase of RPLV corresponding to each alternative system with respect to MRF)

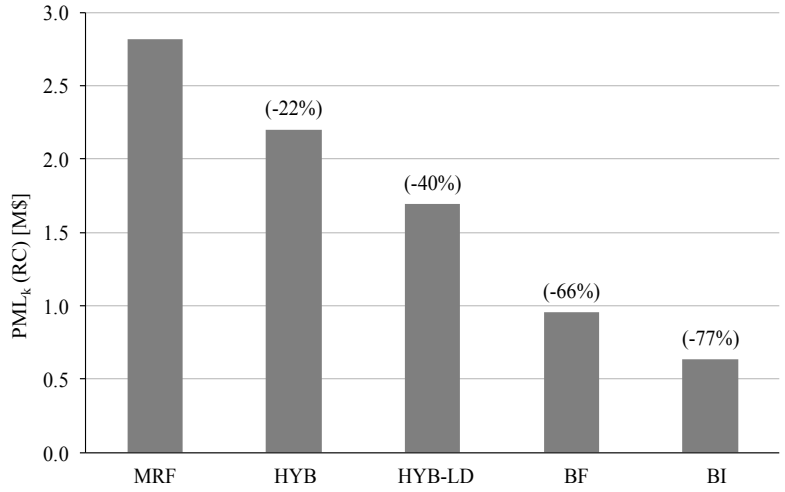

Figure 144 Comparison of PML_k values of RC in correspondence of each seismic technology (percentage in brackets represent the reduction achieved, in terms of characteristic value, by each alternative system with respect to MRF)

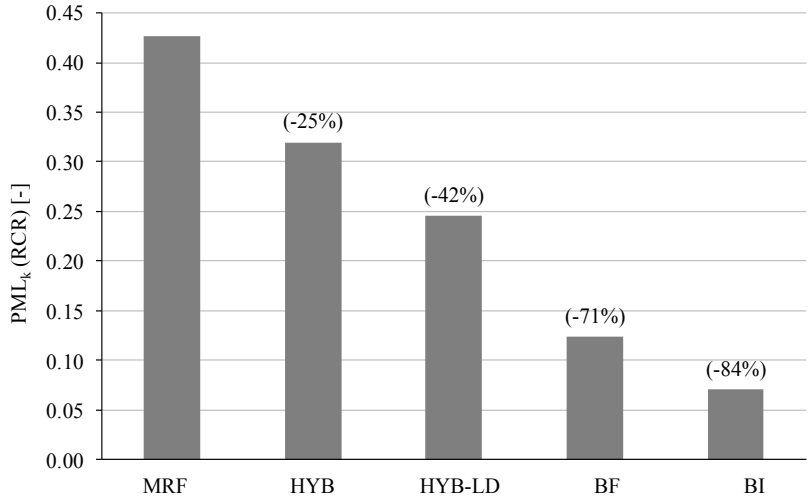

Figure 145 Comparison of PML_k values of RCR in correspondence of each seismic technology (percentage in brackets represent the reduction achieved, in terms of characteristic value, by each alternative system with respect to MRF)

Finally, Construction Cost (C_c) and characteristic Probable Maximum Loss PML_k are compared in Figure 146. From the plot the ascending and

descending trends of C_c and PML_k are evident. Again the percentage of increased C_c and decreased PML_k values of the alternative technologies with respect to MRF system are indicated in brackets. It emerges that the drawback of initially paying more for the adoption of a low-damage control system is generally largely counterbalanced by the significantly lower characteristic repair cost values, generated in correspondence of the design seismic intensity.

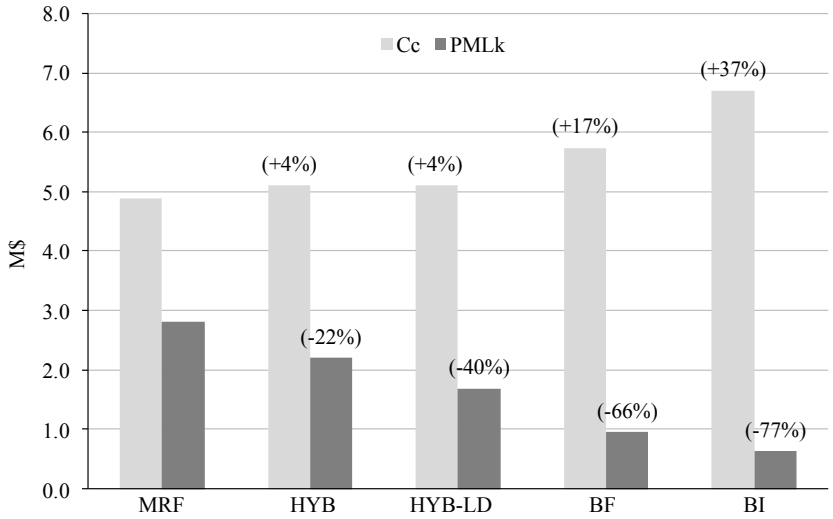

Figure 146 Comparison of Construction Cost (C_c) and characteristic Probable Maximum Loss (PML_k) for each technology

In conclusion, the loss-based comparison of the alternative seismic solutions for the analyzed case-study structure has demonstrated that, if PML values in correspondence of the design earthquake would be taken into account as initial designing parameters, the adoption of low-damage technologies would significantly enhance achievable loss performances.

CONCLUSIONS

In this work of thesis a new approach in the Performance Based Earthquake Engineering (PBEE) framework has been proposed, introducing a loss performance matrix, in the attempt of associating expected repair costs induced by earthquakes to seismic design performance levels. In earthquake engineering it is common practice to adopt the PBEE framework, where performance objectives are defined depending on the earthquake intensity level (return period) and the building's occupancy and/or importance level. This standard approach intends to pursue a balance between economic, political, social and technical features. However, critical issues emerged from past severe seismic events' lessons: numerous ordinary buildings, designed for a Life Safety performance level under a 500yrs earthquake events, were deemed irreparable. The business interruption (downtime), together with the need to demolish and rebuild structures generated high consequence costs. These observations highlighted the importance of controlling structural damage in the PBEE framework. To this aim, a correlation between structural performance level and repair costs induced by seismic events is proposed. Indeed, the classification of different performance levels through direct losses definition would be univocal, all-encompassing of damages relative to structural components, non-structural components and contents if properly evaluated, and univocally understood by non-technical stakeholders, such as owners, insurers and decision-makers.

A 3D loss performance matrix has been presented in Chapter 3, which represents an evolution of the traditional PBEE. Its axes respectively show the seismic Intensity Measure (IM), the probability of loss, corresponding to the probability of exceeding a certain level of loss given a seismic intensity, and the Repair Cost Ratio (RCR), that is the repair cost (RC) over the total

RePLacement Value (RPLV) of the building/facility, for a given IM. Defining RCR and its probability of exceedance practically means defining the probable Maximum Loss (PML), that is, therefore, briefly indicated as new performance measure. RCR values are limited to the value of 0.5, considered as the loss threshold over which it is deemed economically convenient to demolish and re-build the structure. The loss ratio is the result of the loss estimation analysis performed for the newly designed structure, under a certain seismic intensity, to obtain a defined performance level. In this work, PML has been chosen as performance measure due to its less computationally demanding evaluation with respect to EAL and the more clear meaning to the designer/stakeholder.

Given a seismic intensity, according to different combinations of RCR and corresponding probability of loss, different performance levels are distinguished, ranging from an ideal towards an unacceptable design. The qualitative shape of the loss performance matrix has been illustrated in this thesis, discussing the expected trend of repair cost ratio as a function of performance level and earthquake intensity.

In the perspective of suggesting a multi-objective loss performance matrix, several performance goals are customized according to the seismic intensity IM and the facility's social importance. It has been outlined that there is a diagonal correspondence between loss performance objectives, building's importance level and intensity measure: indeed the loss thresholds identifying loss performance levels of a basic facility designed for a low IM correspond to the same limits for an essential/hazardous facility designed for an intermediate IM, as well as to a critical safety facility designed for a severe IM. In the same way as the traditional PBEE, the design of a specific facility could require different loss indicator levels according to the severity of the seismic entity.

An important advantage achieved employing loss indicators, as in the proposed framework, is that they are continuum parameters, thus allowing wide ranges of design options, differently from the discrete performance levels of the traditional PBEE.

The employment of the proposed multi-objective loss performance matrix well suits with the application of a cost based-design framework, proposed in this thesis, according to which a pre-defined loss performance objective is set, and

seismic design is considered satisfactory only if the imposed loss requirement is achieved. In particular, the methodology starts with a prompt seismic design of the facility through a Direct Displacement-Based Design (DDBD) approach, that can better associate design parameters to expected damage with respect to a Force-Based Design (FBD) method. After imposing a PML design limit, an intensity-based loss estimation analysis has to be performed, thus evaluating the loss curve under the design IM, providing the probability of exceeding a certain RCR value, given IM. This curve can be overlapped into the loss performance matrix, finally allowing the designer to read if the loss performance goals are achieved or not. If not, the structural design parameters has to be more conservative and the whole DDBD-loss assessment procedure has to be iterated again.

In Chapter 5 the comparison of alternative low-damage solutions via loss estimation approach is performed adopting a 5-storey 3-bay commercial office building as case-study structure. In particular, five different technologies, traditional cast-in-situ Moment Resisting Frame (MRF), re-centring dissipative rocking system (HYB), HYB system adopting low-damage non-structural components (LD-HYB), dissipative Braced Frame (BF) employing shear link dampers, and base isolation (BI) with high damping rubber bearing, are employed for the seismic design of the same building for a Life Safety performance level under a 500yrs earthquake event. In particular, a DDBD approach is adopted for each structural solution, considering design drifts of 2% for MRF and HYB systems, 0.5% for BF structure and 0.4% for BI technology. While consolidated DDBD methods for MRF and HYB systems exist today, a specific DDBD methodology for dissipative braced frames has been proposed in Appendix B. Literature proposals of DDBD for base isolated structures have been adopted.

Through the implementation of dynamic nonlinear analysis mean trend of maximum displacements, Interstorey Drifts Ratio (IDR), Peak Floor Acceleration (PFA) and Residual Interstorey Drifts Ratio (RIDR) are evaluated. As expected, displacement envelopes show that BF system is the most rigid, having a mean top displacement of 7 cm, while HYB structure is subjected to a mean top displacement of around 16 cm and MRF and BI systems of 18 cm.

Also, it has been shown that BI system's mean base displacement is slightly higher than 15 cm. From the analysis of mean IDR envelopes, it has been evidenced that MRF and HYB systems are subjected to a comparable interstorey deformation, with a maximum value of around 1.5% at the first level. Conversely, BF system's maximum IDR is slightly higher than 0.5% at the third level, that is the design value. Finally, IDR values measured in correspondence of the BI system are coherent with the technology adopted, being always very small, with a peak value at the second level of 0.4%.

The system suffering higher PFA values is the BF system, due to its higher stiffness. MRF and HYB technologies present similar trends of PFA, while in BI system amplifications are limited, always keeping the value below 0.4g.

Finally, the analysis of RIDR envelopes has highlighted the main concern of MRF solutions, since presenting residual drifts significantly higher than all other cases, with maximum values of around 0.1%. This result contributed to generate some of the Monte Carlo simulations yielding irreparability conditions in the loss analysis. BI system, behaving linearly, has provided zero residual drifts. Differently, in the HYB solution residual drifts were null thanks to the re-centering action provided by post-tensioning cables. Finally, the BF technology yielded negligible RIDR as well.

The main scope of this investigation is the analysis of the loss performances of the innovative seismic control technologies with respect to the traditional MRF system, considering the rate of increase of the Construction Cost, and finally exploring if it is worthwhile when compared to the reduced repair costs at the occurrence of the design earthquake. Adopted fragility components and relative cost consequences are the same for all analyzed systems, except for the specific structural component corresponding to the particular technology. In particular, a fragility curve has been developed for shear link dampers used in the BF system, employing recent experimental tests results. Moreover, in the LD-HYB solution curtain wall and internal partition fragility curves are different from other systems, since corresponding to low-damage elements.

Losses in terms of RC are finally evaluated performing intensity-based loss analysis in correspondence of the design seismic hazard, through PACT software. It emerged that the adopted alternative seismic technologies allowed to

progressively reduce losses, with respect to MRF solution, if considered in the following order: HYB, LD-HYB, BF and BI. Damage and consequent losses caused by structural components, non-structural components and contents are distinguished for each technology. It was outlined that non-structural components are always the most significant contributors to losses, for all systems. Structural elements' damage in the MRF solution has determined RC more than doubled with respect to all other technologies. Differently, MRF system's RC given by non-structural components are slightly higher than HYB case-study, due to MRF slightly higher IDR values. This is the main reason leading to the employment of the LD-HYB technology: indeed, the re-centring dissipative rocking solution, even if significantly reducing structural damage, is still a quite deformable system. Accordingly, it is expectable that non-structural RCs are similar to MRF system's ones. In particular, main source of non-structural losses came from glass curtain wall and gypsum partitions, that are IDR sensitive. Instead, the adoption of low-damage non-structural components has significantly reduced this contribution to loss, as evidenced by LD-HYB system's loss performances. The adoption of the BF seismic solution has drastically reduced the structural economic losses, given that this technology has been designed for drifts of 0.5% against drifts of 2% of MRF or HYB systems, thus avoiding bare frame's non-linear behavior. Non-structural components' damage of the BF system is similar to LD-HYB due to the significant lower IDR values involved. Finally, BI system has shown that structural components contribution to loss, given by beam-column connections and isolators, is comparable to BF system: in particular, beam-column connections generate a practically null loss, while loss due to isolators, still very small, is higher than SLs simply because steel dampers are cheaper than HDRB devices. Non-structural components losses of the BI system are the lowest among the five technologies compared, given that both IDR and PFA demands are smaller. The analysis of losses due to damage of contents shows a comparable trend for all the technologies, with a reduction in the case of BI system.

Defining RCR allows to take into account also the initial required investment associated to each system. Loss curves are finally compared, highlighting the beneficial effect of adopting alternative seismic control systems in reducing

losses. Each technology is placed in the new loss performance matrix and specific PML quantities are observed, namely the Scenario Expect Loss (SEL), corresponding to the median value of loss, the Mean Damage Factor (MDF), that is the average, the Scenario Upper Loss (SUL) and the characteristic PML value (PML_k), corresponding to the 90° and 95° percentiles respectively. The great advantage corresponding to the reduced losses gained passing from a MRF system to HYB, LD-HYB, BF and BI different technologies is evident. It has been proven that, as the system's performance in terms of loss arises, the distance between upper percentiles, MDF and SEL values is reduced.

In the perspective of realizing a cost-based design setting the performance goal corresponding to a maximum characteristic PML value, in terms of RCR, equal to 0.3, it emerged that MRF and HYB systems were not able to satisfy the required loss performance objective, given the corresponding PML_k values respectively of 0.43 and 0.32. Differently, LD-HYB, BF and BI technologies, yielding respectively 0.25, 0.12 and 0.07 PML_k values, accomplished the design objectives. More in detail, supposing a basic facility, the BI and BF systems would provide an ideal design, while the LD-HYB case-study would correspond to a high performance level, then evolving in a medium performance level in the hypothesis of an essential/hazardous facility. Differently, for the same occupancy level, BF and BI systems would still correspond to an ideal design. Finally, supposing a critical safety building, the LD-HYB and BF technologies would provide low and high performance levels, respectively. Conversely, the BI system would always yield an ideal design, given the corresponding low repair costs.

In order to appreciate the incidence of higher RPLV values on the output analysis in terms of RCR instead of RC, the characteristic value of both loss parameters for the analyzed seismic technologies have been investigated, highlighting the reduction achieved by each alternative system with respect to MRF. It was outlined that the loss enhancement gained passing from the traditional MRF system to low-damage technologies presented differences between 2% and 7%, if analyzed in terms of RC or RCR. In conclusion, the alteration of results due to the comparison of structural systems characterized by different RPLV did not significantly modify results.

Finally, Construction Costs (C_c) and characteristic repair costs (PML_k) of each technology have been compared, highlighting that the drawback of initially paying more for the adoption of a low-damage control system has been largely counterbalanced by the significantly lower characteristic repair cost values, generated in correspondence of the design seismic intensity.

In conclusion, this work of thesis has proposed an integrated multi-objective loss performance matrix attempting to directly include losses within the design framework, through a cost-based approach. Its application to traditional and innovative seismic control technologies has highlighted the alteration of economic convenience of the first with respect to the others. Indeed, even if the construction cost of the MRF system is always lower than other structural typologies, the repairing activities costs are, conversely, always higher. As a matter of fact, the conventional MRF system, opportunely seismically designed according to current code prescriptions, has generated significant repair costs in case of occurrence of the seismic event in correspondence of which the structure was designed. The HYB solution allowed to limit damage and enhance seismic structural performance with a small increase of initial cost. Although, in order to limit also its non-structural damage it has been necessary to adopt low-damage curtain walls and internal partitions, further enhancing performance in terms of economic losses. Braced frame and base isolated systems allowed to significantly reduce losses, but unavoidably generating higher construction costs.

These results provide interesting considerations about limits of performance-based design framework, which has been outlined not considering both economic losses caused by structural and non-structural damage and significant performance enhancement that can be achieved adopting alternative low-damage technologies.

The use of this new loss performance matrix could imply that seismic design might not necessarily be carried out in order to limit a specific EDP, as it is in the traditional PBEE, rather it pursues pre-defined level of economic losses associated to a certain level of confidence. In more practical terms, a combination of an EDP-based design approach (i.e. Displacement-Based

Design) and loss-based charts/spectra would allow to integrate the two approaches and enhance the current mechanical-based approach with some more explicit economic considerations.

The implementation of the proposed cost-based design framework within the multi-objective loss performance matrix environment, currently presents some limitations, if not some interesting cause for reflection of future research developments.

First of all, it is necessary to promote the procedure from an iterative design approach (looking for the system satisfying pre-defined loss performance levels), that is more similar to a cost-based assessment, towards a more reliable methodology promptly yielding the desired loss indicators. To this aim, it would be very useful to provide relations correlating design parameters to loss indicators, so allowing a pre-dimensioning of the structure directing the final seismic solution towards the satisfaction of required loss performances. Moreover, the provision of design parameters - DVs relations should be differentiated for different seismic technical solutions, in order to provide a wide range of choice to the designer on one hand, and to promote the use of alternative low-damage solutions on the other hand. As a matter of fact, today in some countries, such as Italy, the implementation of alternative seismic control systems is generally not preferred to the traditional (capacity design) structures, due to their higher initial costs. On the contrary, if losses caused by the occurrence of design seismic events would be accounted for, the economic advantages of the low-damage technologies would stand out.

A further insight to be investigated consists in the definition of the allowable socio-economic limits identifying the loss performance levels in the multi-objective matrixes. Indeed, the trend assumed in the present thesis is qualitative, but it should be characterized as the result of a wide socio-economic study, that lies outside engineering expertise and the scope of this thesis.

As far as the loss estimation analysis is concerned, it would be unreasonable to realize specific studies for each fragility component in the context of the designing stage, since it would be extremely time-consuming. Differently, a wide database of fragility curves covering common typologies of components

should be formulated and made available to designers for a prompter implementation of the loss analysis.

Also the identification of all the structural, non-structural components and contents that could be susceptible of damage can be quite onerous in terms of time. Although, in the perspective of performing structural design in the Building Information Modeling (BIM) environment, the definition of performance groups could become much easier. In particular, an integration of fragility components database within BIM platform would significantly simplify the loss estimation process, thus representing an interesting and valuable future development.

APPENDIX A

Experimental investigation of low cost steel shear links for seismic energy dissipation

This section describes the experimental investigation on a newly designed steel shear link (SL) for seismic protection of civil structures. It is a low-cost hysteretic device, realized from a single steel plate where variable thickness is given through milling, that already found several applications in South America for both new constructions and seismic retrofit of existing buildings. Even small variation of device's geometry can significantly modify its mechanical behavior, both in terms of strength and initial stiffness. Such SL dampers are very appealing thanks to their flexibility in terms of design solutions.

SL device is conceived to be connected to the main frame through bolted connections and mounted on a supporting brace. In particular, the presence of slotted holes on one edge of the damper avoids the transmission of axial stress by the upper frame beam. A couple of equal specimens for 5 different geometries has been tested, for a total of 10 tests. Two different boundary configurations have been considered, analyzing results of fully-tightened or not fully-tightened bolts in correspondence of slotted holes. Both monotonic and hysteretic mechanical responses have been investigated performing 3 monotonic and 7 cyclic tests. The set-up system is properly designed to resist high force up to 1000kN, accordingly to the capacity of largest specimens. This appendix presents main experimental results and data processing concerning analysis of deformation process, hardening behavior and collapse. Main features of the control devices are highlighted, above all, the high dissipative capability that is

mainly due to the particular shape of the steel damper which leads to a high buckling resistance.

A.1Experimental campaign

The Shear Link damper has been investigated through an experimental program carried out at the laboratory of Department of Structures for Engineering and Architecture, University of Naples (Italy). The testing machine has an axial hydraulic actuator with a capacity of 2500 kN in tension and 3000 kN in compression, with a stroke of 150 mm. The machine has a rigid basement, where four vertical steel columns are founded. The actuator is attached to the columns through a rigid frame that can move from 60 to 400 cm from the base level. A total of 10 specimens (Figure 147) of 5 different geometries were tested, disposing of 2 samples for each typology. Each specimen is indicated in the following as SL X_Y, where X is the web width in cm, while Y is the dissipative windows thickness in mm. Total height (310 mm), height of the web (110 mm) and thickness of the plate (19 mm) are the same for all the devices (they are reported once in Figure 147 with reference to the device SL 30_3). The thickness of the dissipative windows is 3 or 5 mm. The web width is 300, 400 or 500 mm.

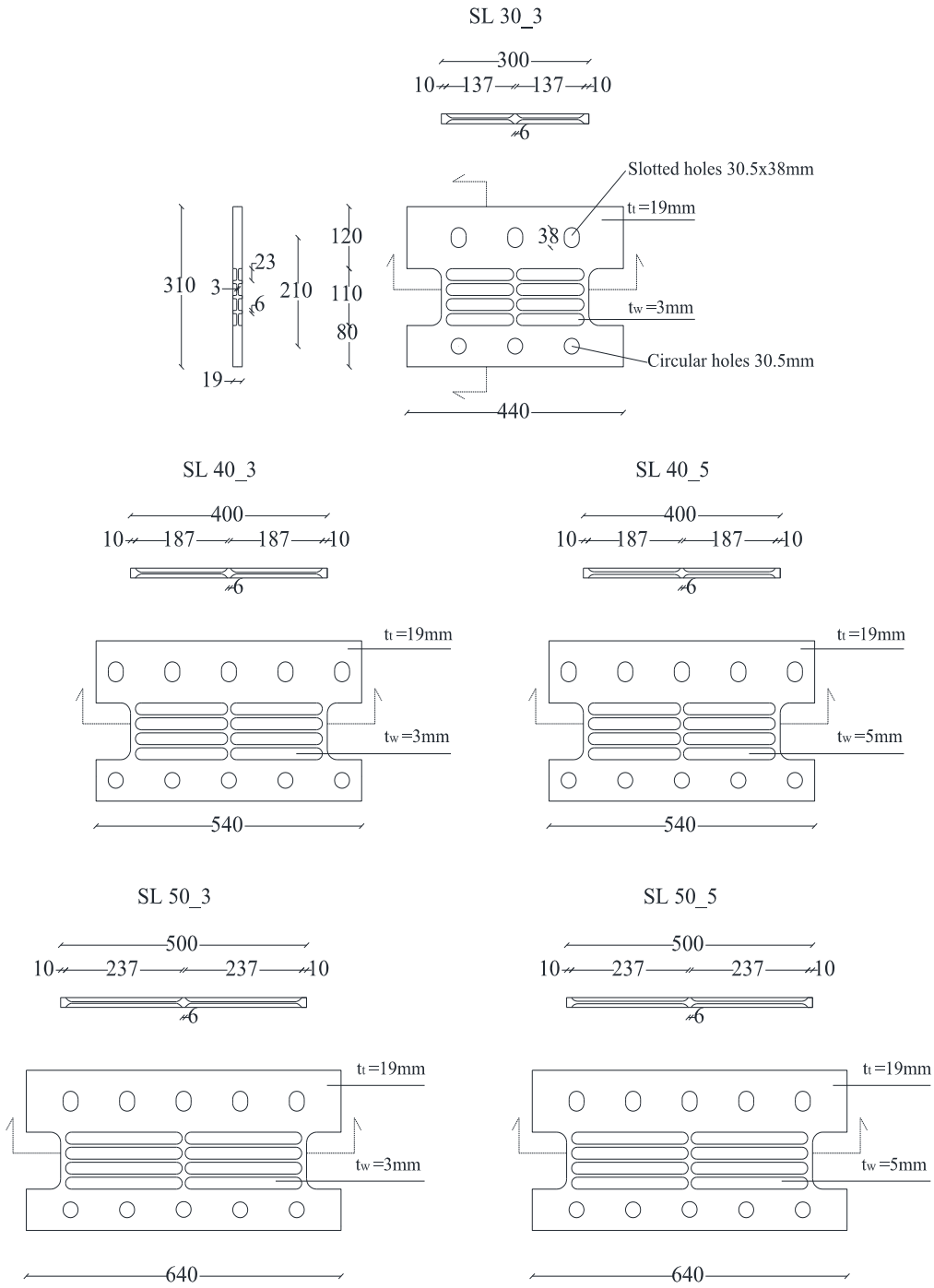

Figure 147 Geometry of the specimens (dimensions in mm)

The connection is given by M30 high strength bolts. On one side of the device there are circular 30.5mm holes, while on the other side 30.5x38mm slotted holes have been realized. The small tolerance of 0.5mm is to reduce slippage movements during the tests that can affect the overall response. The number of bolts is 10 for all the specimens, except for the smallest (SL 30_3), for which it is 6. Bolts in circular holes have been always fully tightened with a torque of 2800Nm to achieve a fixed configuration without slippage. Differently, bolts in slotted holes have been fully tightened in some configurations, indicated as FF (Fixed-Fixed), while in other cases they have not been tightened at all, obtaining the FNF (Fixed-Not Fixed) configuration. This allows understanding the role of the boundary conditions in determining the mechanical response of the device. In particular, the slotted holes, as said above, had been thought to avoid axial stress in the device due to deflection of the beam under gravity loads. At the same time, however, the cyclic behavior of the device is affected by slotted holes due clearances. Actually, due to free or restrained rotations at slotted holes, the device can be roughly thought as a cantilever in the FNF configuration and as fixed at both ends in the FF configuration, respectively (Figure 148).

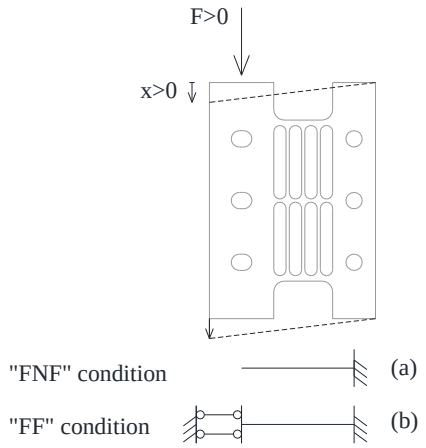

Figure 148 Boundary conditions for SLB devices and sign convention for force (F) and displacements (x)

The following Table 50 displays for each test the geometry of the device, the number of the sample (1 or 2), the type of test (cyclic or monotonic) and the tightening configuration of bolts on the slotted holes (FF or FNF).

Table 50 SL test program

Test #	Device	Sample	Test	Tightening configuration
1	SL 30_3	1	Cyclic	FF
2		2	Cyclic	FNF
3	SL 40_3	1	Cyclic	FF
4		2	Monotonic	FF
5	SL 40_5	1	Cyclic	FNF
6		2	Monotonic	FNF
7	SL 50_3	1	Cyclic	FF
8		2	Cyclic	FNF
9	SL 50_5	1	Monotonic	FNF
10		2	Cyclic	FNF

As can be derived from Table 50, for two devices (type SL30_3 and SL50_3), samples #1 and #2 have been used to investigate the role of boundary conditions (FF or FNF) with the same load protocol (cyclic). Samples #1 and #2 in the other cases have been used to assess the different performance of the same device under monotonic and cyclic loads.

Monotonic tests were performed with a constant velocity of 0.05 mm/s of the actuator. Cyclic tests have been done according to the displacement time-history described in Table 51 and Figure 149.

Specimens were made of American ASTM A36 mild steel plates. Two tensile tests (Figure 150) were conducted to determine yielding stress (σ_y), yielding strain (ε_y), ultimate stress (σ_u), ultimate strain (ε_u) and Young modulus (E_s), as given in Table 52. Other material's mechanical properties have been derived: shear yielding stress has been calculated as $\sigma_y/\sqrt{3}$, shear modulus as $E/(2(1+\nu))$, where the adopted Poisson modulus ν is 0.3; finally shear strain at yielding γ_y has been determined as τ_y/G. Stress-strain curve is shown in Figure 151 only for tensile test 1, given that curve relative to test 2 is practically overlapped.

Table 51 Cyclic load history

No. of cycles	Amplitude	Velocity
[-]	[mm]	[mm/s]
3	1	0.05
3	2	0.05
3	5	0.1
3	10	0.2
3	15	0.3
3	20	1
3	30	1
3	40	1
3	50	1

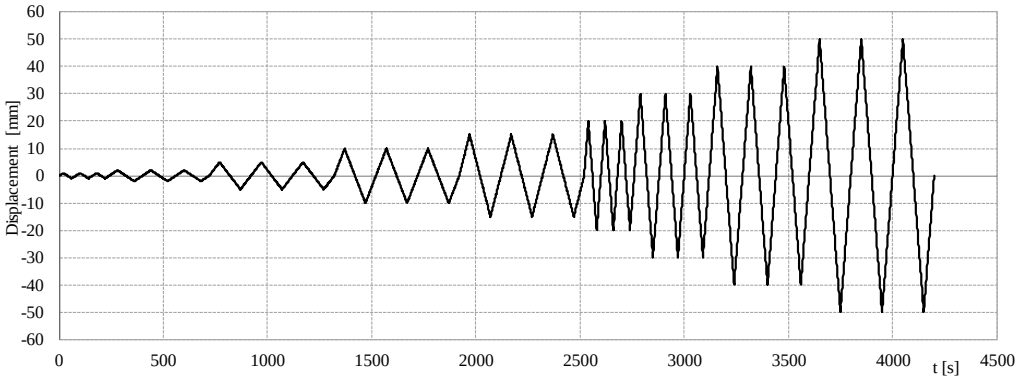

Figure 149 Cyclic load history

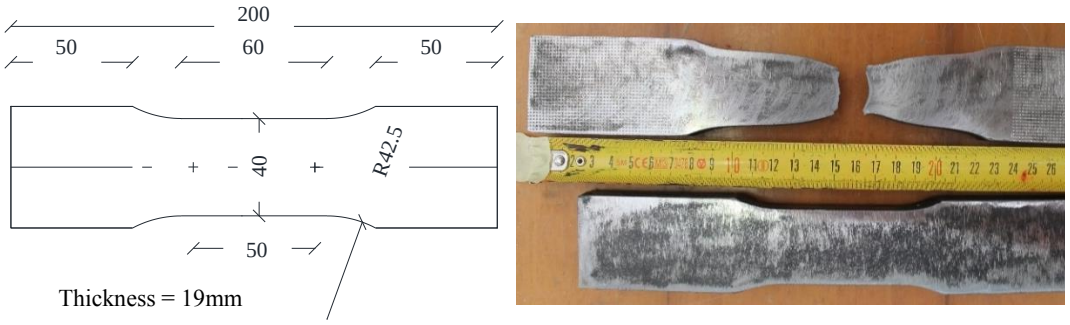

Figure 150 Tensile test specimen

Table 52 Tensile test output results

Sample	Test #	σ_y [MPa]	ε_y [%]	σ_u [MPa]	E_s [MPa]	ε_u [%]	τ_y [MPa]	G [MPa]	γ_y [%]
19 mm A36	1	342	0.17%	448	200786	16.5	197	77225	0.26%
19 mm A36	2	342	0.17%	447	200126	16.5	197	76971	0.26%
19 mm A36	Average	342	0.17%	447	200456	16.5	197	77098	0.26%

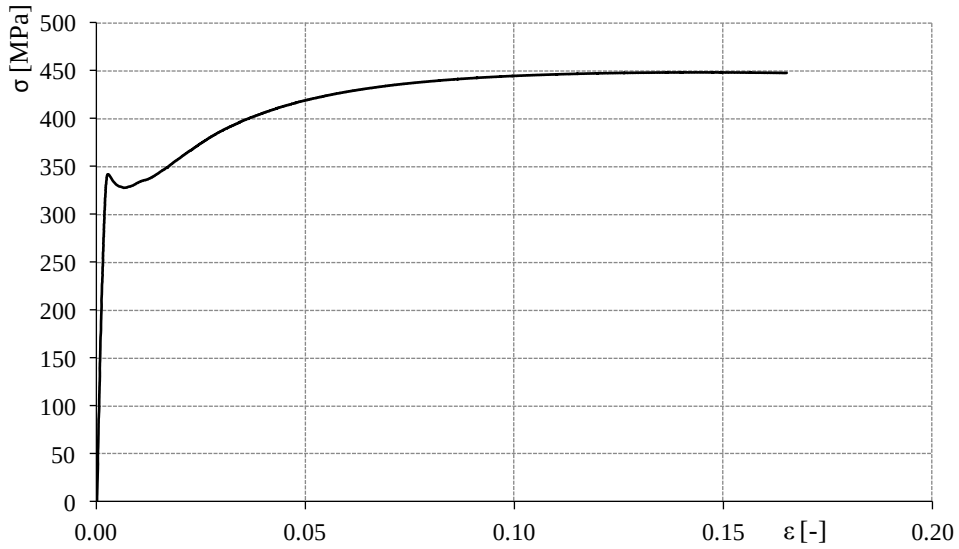

Figure 151 Stress-strain tensile test for steel

A.2Experimental set-up and measurement

The experimental set-up is composed by a complex system of steel plates, partially welded and bolted, designed to resist a maximum force of 1000kN. It is characterized by a total height of about 2m and 0.75mx0.67m plane dimensions. Plane and vertical sections of the set-up are given respectively in Figure 152 and Figure 153, while in Figure 154 front and lateral pictures are shown.

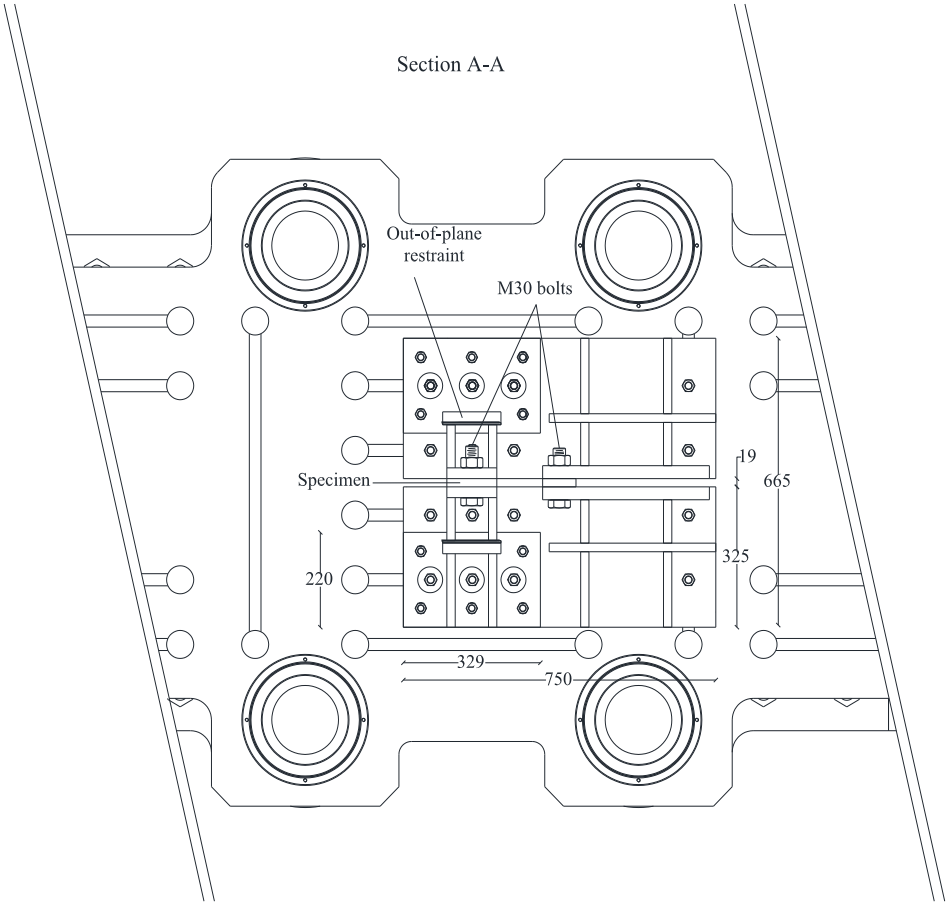

Figure 152 Experimental set-up plan view – section A-A (dimensions are in mm)

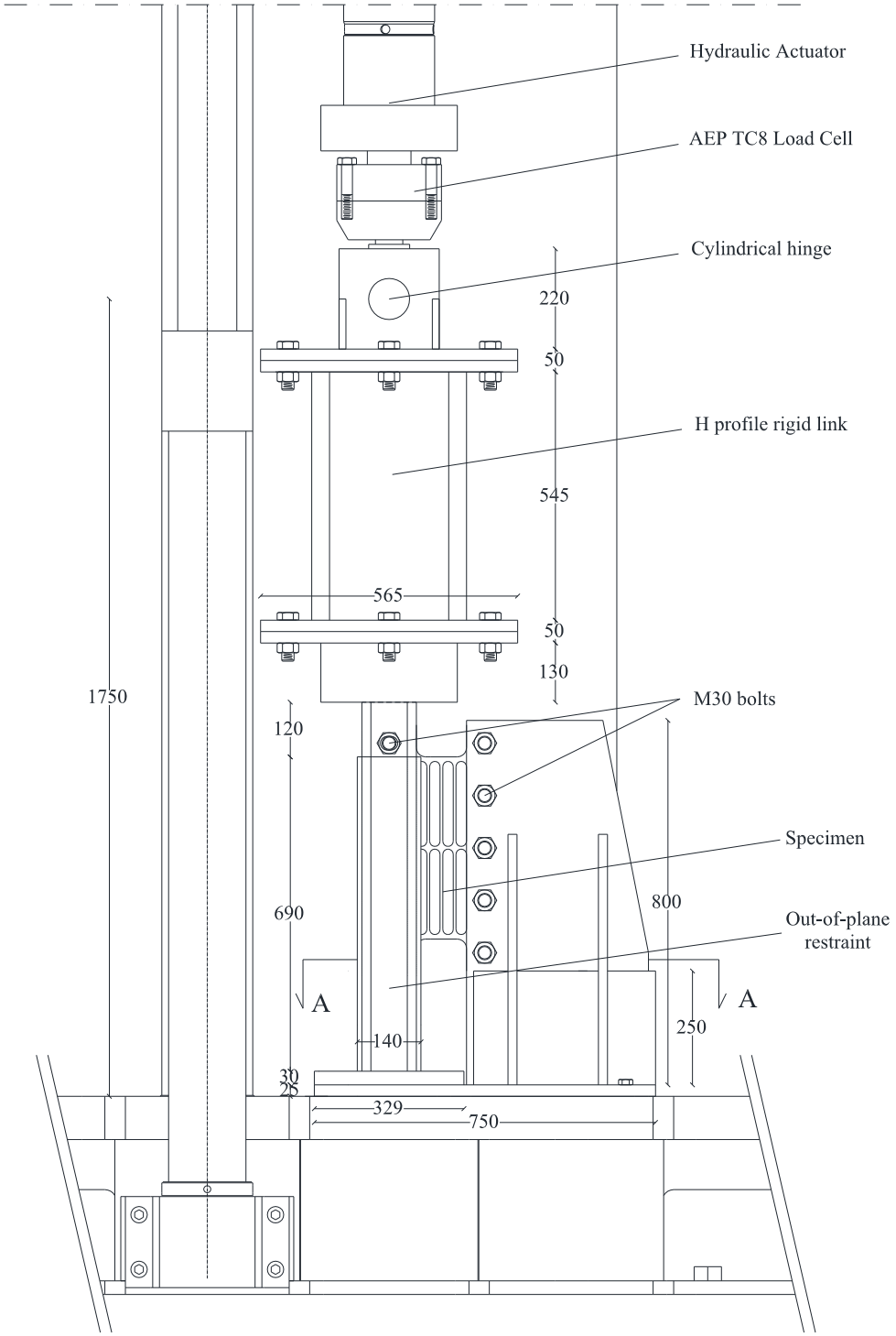

Figure 153 Experimental set-up frontal view (dimensions are in mm)

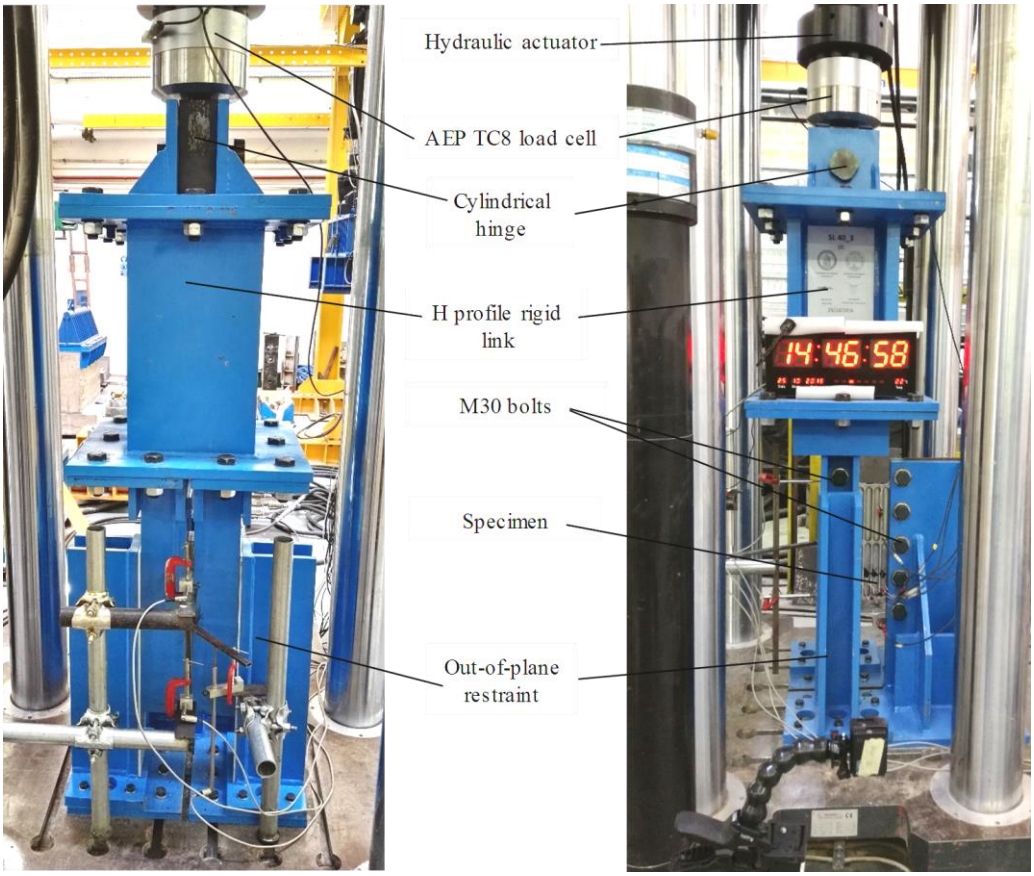

Figure 154 Experimental set-up: lateral (left) and frontal (right) views

A cylindrical hinge connects the set-up to the machine, so avoiding the transmission of bending moment to the actuator and preventing potential damage of the latter. Moreover, in order to control and limit horizontal forces transferred to the actuator, an extension of the whole set-up height was necessary. In particular, it consists of a 0.545m height and 0.31mx0.34m transversal dimensions H profile designed to behave as a rigid link. The whole system has high stiffness (thickness of steel plates is between 20mm and 30mm) to ensure the effective transmission of the force from the set-up to the specimen. Connections between the specimens and the set-up are realized through M30 high strength bolts. One side of the device is loaded by the actuator through the set-up system, while the other side is connected to stiff steel plates directly fixed to the basement of the machine, simulating a fixed restraint. The geometry of the set-up has also been designed in order to avoid flexural-torsional buckling of the

device, also limiting eccentricities between the specimen and the actuator. Moreover, a specific out-of-plane restraint (Figure 155) was placed on the transversal side of the specimen, so preventing any undesirable movement. In order to limit friction during vertical movement, teflon layers were applied on vertical surfaces of restraints. These additional constraints, which would not actually be installed for real applications, were positioned for precautionary purposes, i.e. to prevent damage to the machine and to people working around it. However for none of the tests carried out they were really called to react.

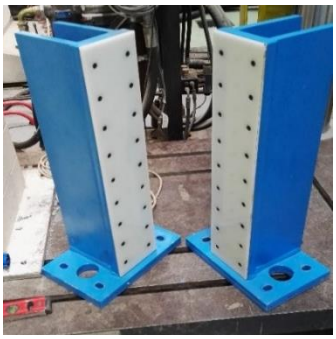

Figure 155 Out-of-plane restraints

Sensors for measurement of force, displacements and strains are briefly presented in Table 53. All tests were conducted at room temperature. Data were sampled at 100 Hz.

Table 53 Measurement instruments properties

Instrument	**Company**	**Model**	**Range**	**Max voltage [V]**	**Sensitivity [mV/V]**
Load cell	AEP	TC8.212.R4	± 1000 kN	15	2
LVDT V1	HBM	WA	± 50 mm	2.5	80
LVDT V2		WA	± 10 mm		
LVDT H1		WA	± 10 mm		
LVDT H2		WA	± 10 mm		
LVDT H3		WA	± 10 mm		
LVDT H4		WA	± 10 mm		
Strain gauges	KYOWA CO. LTD	KFG-6-120-C1-11	-	-	12

A load cell is located at the top of the set-up just under the head of the actuator, to provide the effective value of the applied load F. The LVDT placement (Figure 156) was defined in order to measure all significant displacements, thus

permitting a filtering of components arising from rigid body motion due to set up flexibility and clearances at the connections. The distances between horizontal LVDTs on the two faces, indicated as L1 and L2 in Figure 156 (b), vary in the ranges 320-500mm and 445-670mm respectively, depending on the geometry of specimens. The need to provide instruments also on the right face was conceived after analyzed Test #1 output results, when only LVDT V1, H3, H4 had been used.

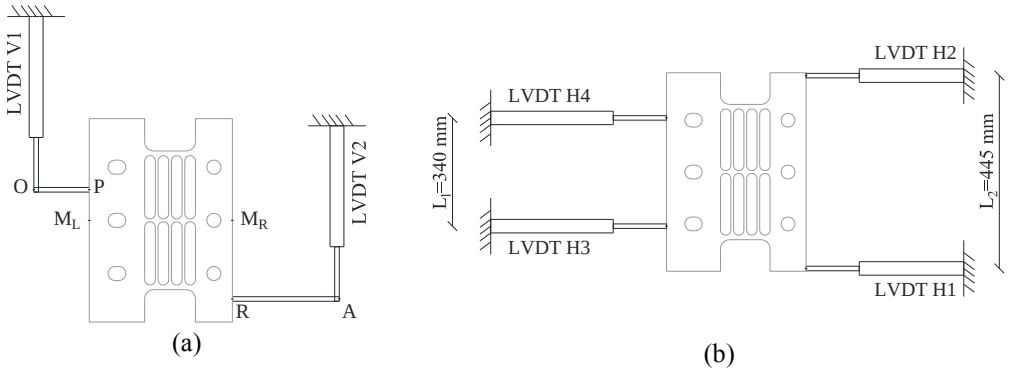

Figure 156 LVDT configuration on test #2 for measurement of vertical (a) and horizontal (b) displacements

Vertical displacement components of points of the left (ML) and right (MR) side of the device have been derived starting from registrations coming from horizontal and vertical LVDTs, on the base of pure geometrical considerations. Displacement demand x to the device is calculated as the instantaneous difference of the above vertical movements. In addition to LVDTs, n°6 strain gauges (sg) were used to measure local deformation. Number four sg were positioned on the windows with an inclination of 45°, while the other two were placed at the bottom and top stiffeners in horizontal configuration (Figure 157).

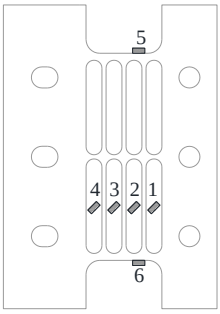

Figure 157 Strain gauges configuration

A.3Output results

Results in terms of force-displacements (*F*-*x*) response are shown in Figure 158 for all 10 tests. It is worth noting that *F* and *x* have the meaning described in the previous section, except for test #1, where not all the LVDTs were installed and *x* simply represents absolute vertical displacement of point M_L in Figure 156 (a).

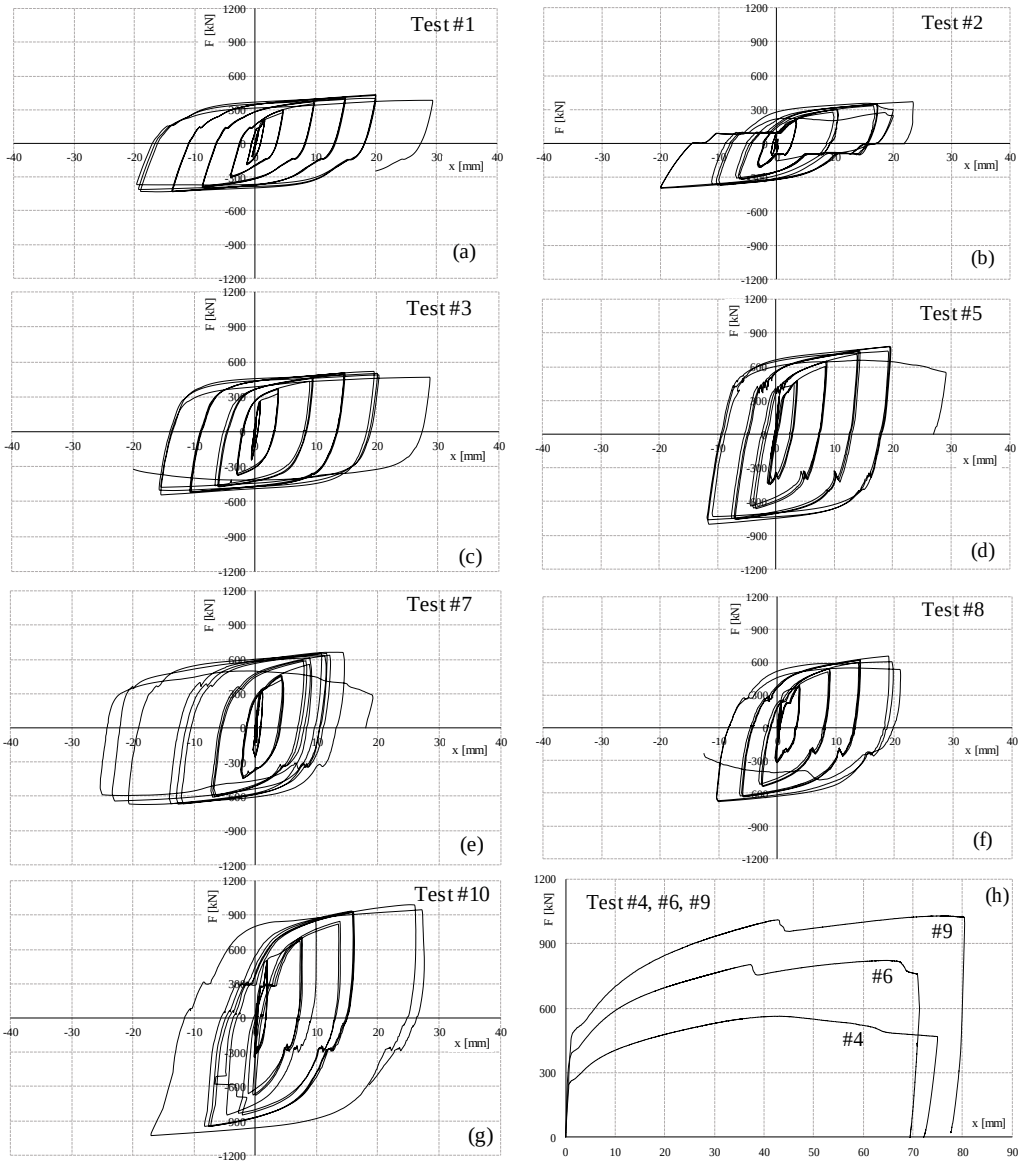

Figure 158 F-x curves for all specimens

Smoother curves are those related to tests performed in the FF configuration (#1, 3, 4, 7), as expected. The others referred to FNF tests are more irregular due to the sliding of bolts within the slotted holes. Too large, unexpected zero-force displacements have been registered for test #2, highlighting something did not perfectly work during that test, probably due to an incorrect tightening of the bolts at the end of the device that had to be fully fixed.

A very stiff initial elastic behavior is observed for all the tests and stable hysteretic loops are obtained up to ±20 mm in all cases. Differently from previous SL generations hysteretic loops keep the same level of strength up to failure, not exhibiting significant softening. It is worth noting that capacity force of specimens with the same geometry but thicknesses of dissipative windows varying from 3 to 5mm increases of about 50% (e.g. compare test #3 and #5, #4 and #6, #7 and #10). Loops are not symmetric, particularly in case of FNF configuration: during unloading and reloading phases residual deformations are stored due to slippage at the connections. This is also confirmed by comparing displacement of the actuator (x_{act}) and that of the device (x), for test #7 and #8 (Figure 159). The displacement demand x to the device gradually deviates from displacement of the actuator x_{act}, especially in the case of FNF configuration, as expected. Displacement x_{act} is larger than x until the device is far from failure (i.e. up to values for x_{act} less than 15 mm, t=2520s). After that, the trend is inverted, with higher displacement of the device due to significant, irreversible damage.

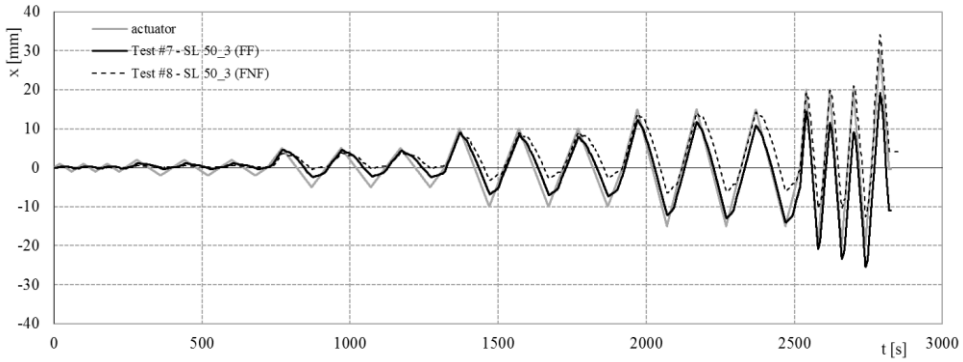

Figure 159 Applied displacement versus recorded relative displacement

The same SL device provided almost the same maximum peak force for both cyclic and monotonic tests (Figure 160, Figure 161 and Figure 162). However, they occurred for different amount of displacement. Actually, the envelope of the loops registered for cyclic tests provided higher values of force with respect to the monotonic test on the same device (such hardening phenomenon will be addressed in the following sections).

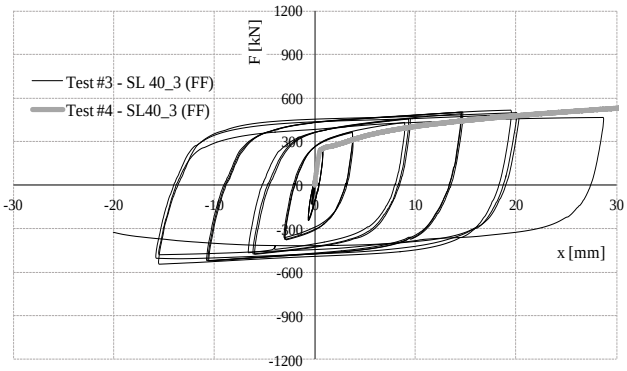

Figure 160 Cyclic and monotonic F-x curves for specimen SL 40_ 3

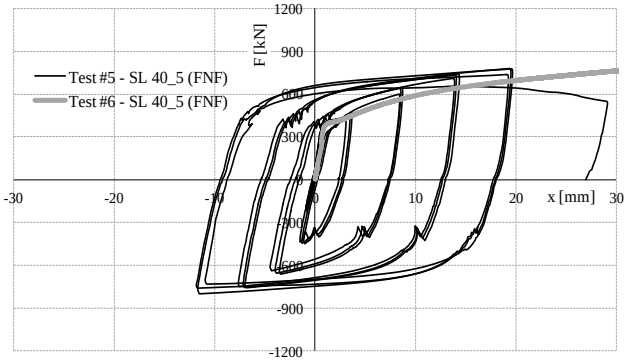

Figure 161 Cyclic and monotonic F-x curves for specimens SL 40_5

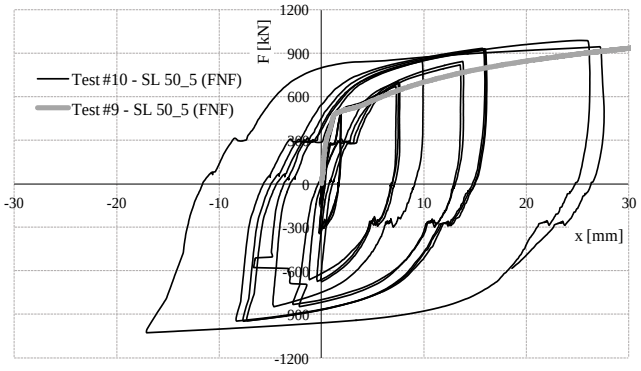

Figure 162: Cyclic and monotonic F-x curves for specimens SL 50_5

As far as the failure mechanism is concerned, two different phenomena were mainly observed under monotonic and cyclic load, respectively. During all cyclic tests, at displacement level around ±20 mm a tearing break was generated

at the top stiffener and rapidly propagated throughout the specimen until break (Figure 163). In this case, only when tearing practically affected most of the device's width, local buckling at the windows could be observed in some cases.

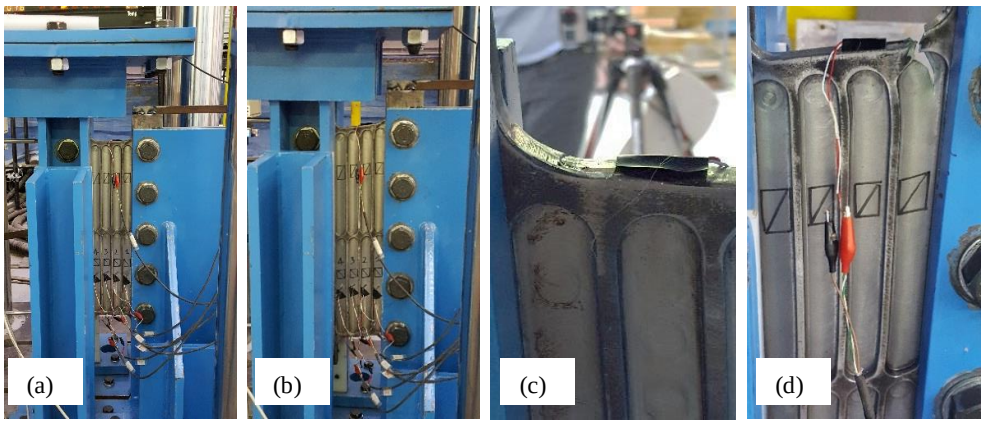

Figure 163 Cyclic test # 10 damage scenario: a) initial condition, b) yielded phase, c) onset of tearing, d) distribution of tearing

Differently from cyclic test where cyclic degradation and residual deformation are expected to reduce ductility, higher levels of deformation were reached during the monotonic test. For a displacement level around 40 mm, a global buckling phenomenon was generated, involving almost all the windows and including internal stiffeners (Figure 164). In this case just at the onset of buckling (tests #6, 9) or by end of the test (test #4) some tearing in the top stiffener was observed.

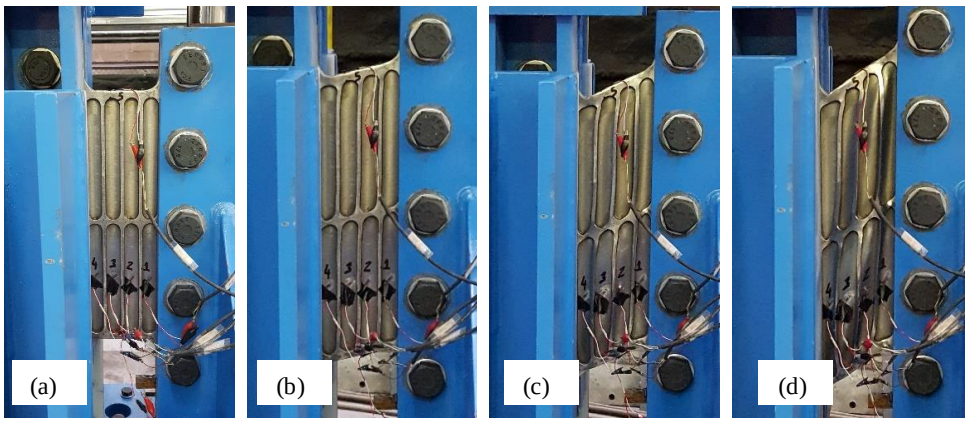

Figure 164 Monotonic test # 4 damage scenario: a) initial condition, b) yielded phase, c) onset of buckling, d) global buckling

A.4Processing and discussion of experimental results

The output results of the 10 tests have been deeply analysed to identify the main mechanical properties of each tested device and study performance under different tightening and loading conditions. Furthermore in this paragraph analytical formulation to roughly predict SLs experimental behavior are suggested and compared to observed results.
The parameters in this analysis come from a bi-linear idealization of the non-linear behaviour of SLs (Figure 165). More in detail, they are:

F_y	yielding force;
k_{el}	elastic stiffness secant at yielding point;
k_{pl}/k_{el}	plastic to elastic stiffness ratio;
F_{max}	peak force;
F_{max}/F_y	maximum hardening ratio;
d_{max}	displacement corresponding to peak force;
$\xi_{eq}=E_D/(4\pi E_S)$	equivalent damping ratio at ± 20 mm;
k_{eq}	equivalent stiffness at ± 20 mm;

where ED and ES are the energy dissipated in one cycle, given by the area enclosed in the loop, and the strain energy stored in the system, respectively, both evaluated at a displacement of ± 20 mm. The plastic stiffness is determined in correspondence of a displacement of 20 mm. Table 54 below shows results for all the analysed specimens.

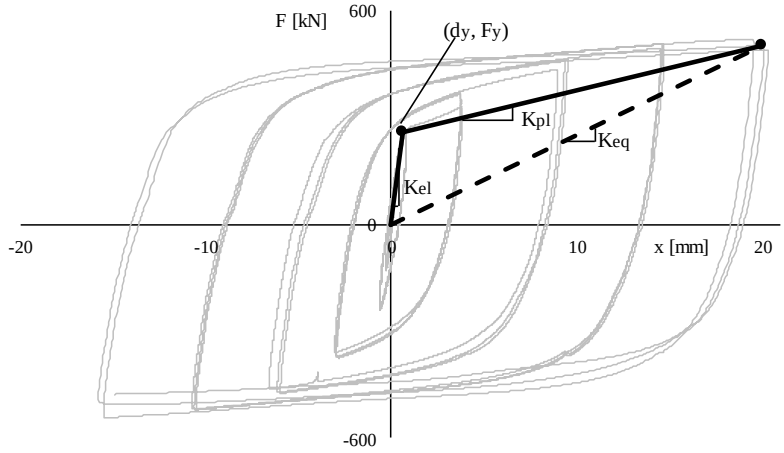

Figure 165 Bi-linear idealization of the non-linear SLs behavior

Table 54 Experimental SLs mechanical parameters

Test #	SL	Sample	Test	Tightening configuration	F_y [kN]	k_{el} [kN/mm]	k_{pl}/k_{el}	F_{max} [kN]	F_{max} / F_y	d_{max} [mm]	ξ_{eq} [%]	k_{eq} [kN/mm]
1	**30_3**	1	Cyclic	FF	188	250	5%	434	2.3	20.3	48	20
2		2	Cyclic	FNF	160	240	4%	396	2.5	22.8	48	26
3	**40_3**	1	Cyclic	FF	260	420	3%	517	2.0	20	52	28
4		2	Monotonic	FF	250	450	3%	563	2.3	43.6	-	-
5	**40_5**	1	Cyclic	FNF	400	500	4%	800	2.0	19	49	50
6		2	Monotonic	FNF	370	500	3%	803	2.2	37.3	-	-
7	**50_3**	1	Cyclic	FF	340	550	3%	671	2.0	20.7	53	37
8		2	Cyclic	FNF	315	500	4%	676	2.1	19	47	45
9	**50_5**	1	Monotonic	FNF	480	700	3%	1030	2.1	42.8	-	-
10		2	Cyclic	FNF	500	680	4%	1029	1.9	25.8	41	80

Due to different boundary conditions, it can be observed that SLs in FF configuration usually provide higher values of initial stiffness and yielding force than FNF case, although with no significant discrepancy. From the comparison of SLs under different loading conditions, it emerges that initial elastic stiffness at yielding point is generally similar, with slightly higher values in monotonic tests. Contrarily registered yielding force values are higher for cyclically loaded samples, as already highlighted in Figure 160 to Figure 162.

Even if in seismic loading condition SL device obviously undergoes cyclic behavior, the sense of analyzing its monotonic performance stands in the necessity of numerically modeling dampers within a structure, particularly in the case of performing a static pushover analysis. For this reason, authors believe it can be interesting to compare F-x monotonic curves with the skeleton curve extrapolated from corresponding cyclic tests.

Hysteretic behavior has been analyzed in order to get skeleton path and compare it to the result of correspondent monotonic curves. Kato et al. (1973) observed that the stress-strain relation of steel bars under cyclic loading can be decomposed into skeleton part, softened part and elastically unloaded part. The same procedure has been applied to force-displacement experimental curves of specimens SL40_3_1 (test #3), SLB40_5_1 (test #5) and SL50_5_2 (test #10), but for sake of shortness only test #3 plot is shown in Figure 166, stretching its hysteretic loops in one sequence for each sign domain until degrading behavior is observed and differentiating the three parts mentioned above. The segments indicated as "Skeleton part" represent the load path exceeding the stress level attained in the previous cycle: connecting them in each domain, the positive and negative skeleton curves are obtained. On the other hand, the loading path covering a level of stress already attained in the previous cycle turns out to be softened: this is the result of Bauschinger effect, which consists in the reduction of material's yield stress when the direction of deformation is reversed after plastic regime has been reached (Mahato et al. 2014). Since the loading path in all the tests starts in the positive domain, the negative skeleton curves are significantly softened with respect to the positive ones. It is worth to note that the unloaded part follows the initial elastic path in all the loops.

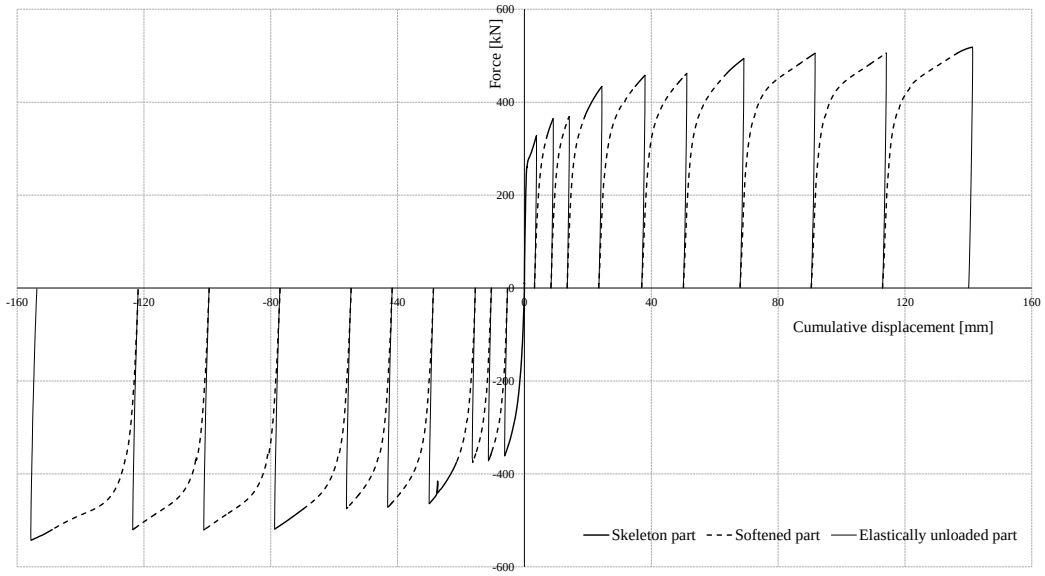

Figure 166 Decomposition of test #3 cyclic curve into skeleton, Bauschinger (softned) and elastically unloaded parts

The decomposition of the cyclic curve into the skeleton and Bauschinger parts allows to formulate several considerations. First of all the skeleton path can be interestingly compared to the monotonic test performed on the same device. In particular only the positive skeleton is compared to the monotonic curve since the negative skeleton initial stiffness is affected by softening due to Bauschinger effect. As demonstrative example, Figure 167 shows positive skeleton and monotonic curves relative to SL40_5 device: it emerges that initial stiffness predicted by the positive skeleton curve is quite satisfactory, while after yielding the monotonic curve is always lower. This behavior, consistent with results observed in previous experimental investigations on steel material (Nakashima 1995, Shi et al. 2011) is attributed to hardening effect. Quantification of hardening effect is very important because it significantly affects energy dissipation capacity of hysteretic devices. The gap between monotonic and positive skeleton curves after yielding can be indicated as hardening factor (H_f), around 4% for specimen SL40_3 and 7% for specimens SL40_5 and SL50_5. Scaling positive skeleton curves by H_f, a quite good agreement with monotonic curves is obtained. It is interesting to note that the hardening factor is consistent with the ratio between yielding forces observed respectively in cyclic and monotonic tests. This confirms that hardening effect is more significant in cyclic loading conditions than in monotonic ones: the ratio between the force corresponding to 20mm displacement and the yielding force varies in the range 1.9-2.5 for cyclic tests (see Table 54), while it is 1.8-1.9 for monotonic tests.

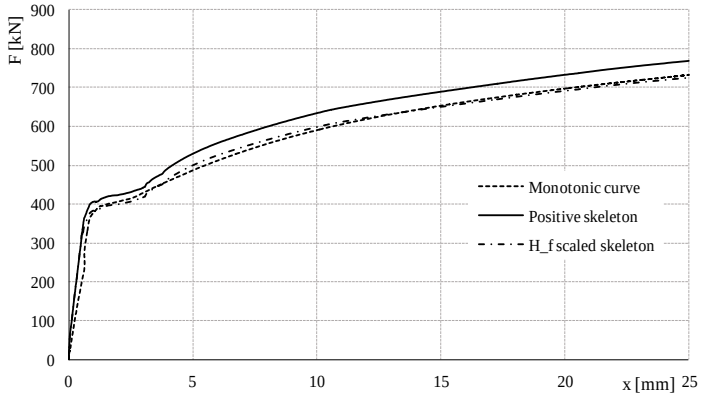

Figure 167 Comparison between monotonic and skeleton curves for SL40_5 device

The decomposition of the cyclic curve can also be adopted in order to do energetic considerations and compute the ultimate energy absorption capacity as the sum of the areas respectively enclosed by skeleton and Bauschinger parts (Akiyama et al. 1995, Benavent-Climent et al. 1998). Benavent-Climent (2007) proposed an energy-based damage model defining energy capacity through the above mentioned method. Furthermore, each of the two parts can be considered representative of different fracture mechanisms (Cahis 2000). Kato et al. (1973) observed that ductile fracture, described by the skeleton part, is independent by fatigue fracture, represented by the Bauschinger part, since hysteresis loops at constant stress amplitude do not contribute to form the skeleton curve. This observation is confirmed also in Figure 166 where it is evident that only the first of the three cycles at constant amplitude provide a contribution to characterize the skeleton part. In the three specimens analyzed above the ultimate displacement in the cyclic test is always lower than the monotonic one. This can justify a failure mechanism produced by fatigue in cyclic tests, where, as a matter of fact, tearing on top stiffeners was observed, whereas in monotonic tests crisis of the device was always caused by buckling of dissipative windows at a larger displacement.

In order to obtain effective parameters for simplified linear model of SL devices, equivalent damping and stiffness have been estimated for any cycle amplitude in the range 2÷20 mm (Figure 168). As a consequence of stable hysteretic behavior, a general increasing trend of equivalent damping is observed, in spite of decreasing stiffness. At a displacement amplitude of 5mm equivalent damping is already higher than 30%. for all devices . For the sake of brevity, only values at ± 20 mm are displayed in Table 54: at this deformation level ξ_{eq} is always higher than 40%, in some cases around 50%. This is definitely consistent with results coming from similar experimental test performed in the past (Chan et al. 2008, Teruna et al. 2015). As far as tightening mode is concerned, damping ratio for FNF configuration resulted to be slightly lower (maximum reduction 10%) than that achieved in FF condition, as expected due to clearances and slippage at slotted holes. Post-elastic stiffness is no larger than 3% and 5% of the initial stiffness in monotonic and cyclic tests respectively, with a mean value of k_{pl}/k_{el} over the 10 tests of 4%.

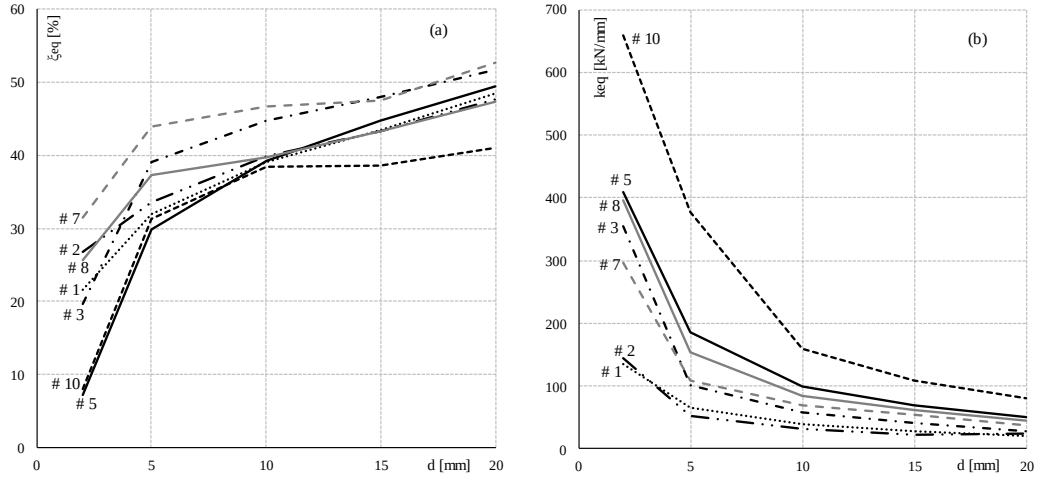

Figure 168 Equivalent damping (a) and stiffness (b) in the range 2÷20 mm cycle amplitude

Some attempts to define analytical formulations aimed at predicting the devices' mechanical behavior were carried out as follows, particularly referring to yielding force and initial stiffness. Further insights will be made as future developments of this work.

Yielding force was estimated starting from the knowledge of the yielding shear stress τ_y of steel (Table 52) and of the web area A_w:

$$F_{y,a}=\tau_y A_w \tag{A.1}$$

Table 55 shows the comparison between experimental (mean value between the two prototypes of the same SL) and analytical values of yielding force ($F_{y,m}$ and $F_{y,a}$), highlighting a very good agreement of the two results. This suggests an easy way to predict the reaction force at yield of any SL device, starting from geometric information and knowing the yielding stress of the material.

Table 55 Analytical prediction of yielding force

SLB	σ_y [mPa]	τ_y [MPa]	A_w [mm^2]	$F_{y,m}$ [kN]	$F_{y,a}$ [kN]	$F_{y,a}$ / F_y
30_3	342	197	900	174	178	1.0
40_3			1200	255	237	0.9
40_5			2000	385	395	1.0
50_3			1500	328	296	0.9
50_5			2500	490	494	1.0

Considering a pure shear behavior, SLs initial stiffness has been evaluated as $k_{a,V}=GA_w/h$, where h is the web height, and compared to mean experimental values kel,m of those in Table 54 for the two prototypes of the same SL (Table 56).

Table 56 Analytical prediction of elastic stiffness

SLB	G [MPa]	h [mm]	A_w [mm^2]	$k_{el,m}$ [kN/mm]	$k_{a,V}$ [kN/mm]	$k_{a,V}$ / k_{el}
30_3	77098	110	900	245	631	2.6
40_3			1200	435	841	1.9
40_5			2000	500	1402	2.8
50_3			1500	525	1051	2.0
50_5			2500	690	1752	2.5

The analytical stiffness $k_{a,V}$ usually provides higher values with respect to $k_{el,m}$, being in the ratio of 1.9÷2.8. Overestimation is expected, due to additional flexibility given by flexural behaviour and clearance at connections. In addition, k_{el} in Table 54 has been estimated as the secant stiffness at yielding point. As a first approximation, the expected elastic stiffness can be calculated as $k_{a,V}$ to be properly reduced by a coefficient 2.4.

A.5Analysis of deformation

The deformation process has been investigated exploiting information provided by strain guauges. Supposing that dissipative windows deform in a pure shear mode, shear strain γ' can be evaluated from the axial strain ε detected along a 45° oriented direction (see strain gauges #1 to #4, Figure 157) as $\gamma'=2\varepsilon$. Shear strain measured at yielding in correspondence of the four sg #1 to #4 of each specimen are given in Table 57: last row shows the average trend for each

dissipative window, evidencing generally increasing values from fixed end to loaded side of the device. The mean shear strain registered on the four windows for each specimen are given in γ'_{av} column, while the overall average is evidenced in bold and it is equal to 0.26%, corresponding to the experimental value determined from the tensile test on the material. From this analysis of deformation it emerges that in correspondence of F_y all windows are already beyond the yielding point, resulting in a quite uniform distribution of deformation.

Table 57 Experimental shear strain at yielding

Test #	SL	Sample	γ_1	γ_2	γ_3	γ_4	γ'_{av}
1	**30_3**	1	0.0015	0.0021	0.0037	0.0021	0.0023
2		2	0.0023	0.0016	0.0018	0.0018	0.0019
3	**40_3**	1	0.0013	0.0019	0.0057	0.0028	0.0029
4		2	0.0014	0.0057	0.0114	0.0027	0.0053
5	**40_5**	1	0.0024	0.0025	0.0024	0.0026	0.0025
6		2	0.0018	0.0020	0.0020	0.0015	0.0018
7	**50_3**	1	0.0029	0.0025	0.0022	0.0019	0.0024
8		2	0.0025	0.0026	0.0024	0.0021	0.0024
9	**50_5**	1	NA	0.0022	0.0025	0.0026	0.0024
10		2	0.0014	0.0021	0.0023	0.0026	0.0021
AVERAGE			0.0020	0.0025	0.0036	0.0023	**0.0026**

*note: NA = Not Available data

The above analysis is based on the hypothesis of pure shear behavior up to yielding. In attempt to validating this condition, an analysis of relative rotation between the two sides of specimens was conducted: mean values at yielding and in correspondence of the maximum force over the ten tests are respectively $6 \cdot 10^{-4}$ rad and $1.58 \cdot 10^{-2}$ rad, so highlighting that in the elastic range flexural behavior was not significant. A further validation of this consideration comes from estimation of the flexural relative displacement at yielding for the three monotonic tests (tests #4, #6 and #9) and its comparison with the total yielding displacement x_y. In particular, from the elastic theory, flexural relative displacement $x_{y,flex}$ for a cantilever (FNF configuration) and a fixed-fixed (FF configuration) beam can be estimated as $Fl^3/3EI$ and $Fl^3/12EI$, respectively. From Table 58 component $x_{y,flex}$ is around 1% for FF configuration and 12-16% for FNF configuration, thus confirming that shear is controlling deformation during elastic behavior.

Table 58 Displacement at yielding point for monotonic tests

Test #	**Tightening configuration**	x_y **[mm]**	$x_{y,flex}$ **[mm]**	$x_{y,flex} / x_y$
4	FF	0.56	0.01	1%
6	FNF	0.74	0.12	16%
9	FNF	0.69	0.08	12%

APPENDIX B

Displacement-based design approach for dissipative braced structures

This section describes an iterative Displacement-Based Design framework for structures equipped with dissipative braces, indicated in the following as Braced Frame (BF). Starting from the approach suggested by Mazza and Vulcano (2014), a comprehensive design procedure with a direct and intuitive reference to effective parameters of damping braces was found out.

A BF system can be considered the equivalent of two springs in parallel, given respectively by the bare frame (F) and damped brace systems (DB), which contribute to define the overall capacity curve. The adoption of dissipative braces has the main aim of conveying energy dissipation, thus damaging, out from structural elements. For this reason the design target displacement d_{PP} should be governed by F system's performance to be pursued. Then, since F and DB systems are in parallel, BF system's target displacement will be the same. The proposed design method mainly works in the ADRS space, aiming to define the performance point (PP) to be achieved and the desired BF capacity curve that can satisfy the specific design requirements. In order to identify PP, it is necessary to know which is the force corresponding to the target displacement, depending on the equivalent damping ratio ξ_{eq}^{BF}. The framework suggests a methodology to characterize PP and BF capacity curve based on literature equations and initial engineering judgment assumptions. Successively, knowing F capacity curve after pre-dimensioning of structural elements, it is possible to build the DB capacity curve as difference of BF and F. Finally it is possible to

characterize mechanical properties of dissipative braces at each storey adopting a proportionality to bare frame's lateral properties. At the end of the framework, if F system's contribution to the overall BF capacity curve is not enough, delivering main involvement to DB system and leading to dissipative braces of excessive dimensions, the all framework should be iterated again increasing beams and columns dimensions.

The proposed design procedure, synthetically introduced above, can be distributed into several steps, as indicated in the flowchart of Figure 169, each of which is widely described through the following sub-sections.

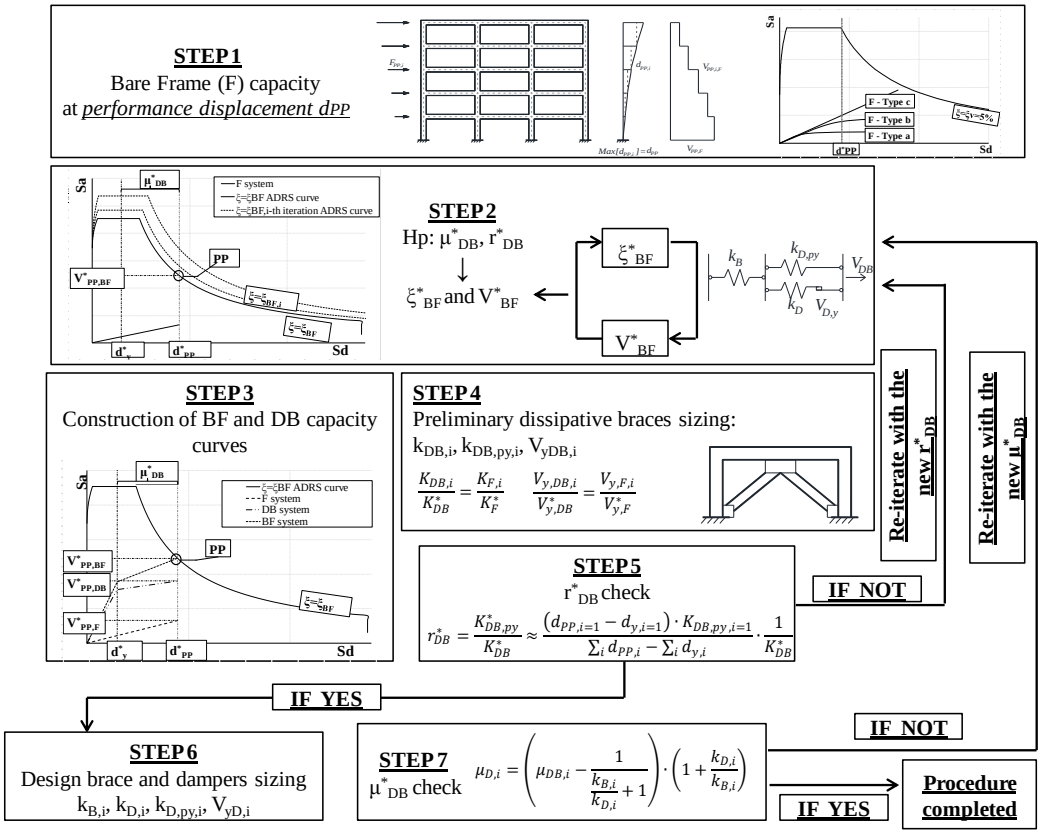

Figure 169 Flowchart of the displacement-based design procedure for dissipative braced systems

B.1 Step 1. Dimensioning of F System

The step 1 of the proposed design framework consists in the definition of beams and columns section dimensions. The pre-dimensioning of structural elements can be performed for gravitational loads, verifying the maximum deflection in beams and the maximum axial force in columns. At this step, in order to identify the BF system's target displacement, it is necessary to establish the behavior of F system in case of seismic event, which could be:

- Type a - dissipative: in this case the formation of plastic hinges within beams' ends and at the base of ground floor columns is allowed. This choice would lead to a less expensive construction because part of energy dissipation would be provided by F system. Moreover, allowing F system's yielding would arise the target displacement, thus a probable lower force would correspond to it, limiting dissipative braces dimensions. The cons of this design assumption is that the structure would experience damage after a seismic event, consequently generating significant repair costs and recovering time.
- Type b - partially dissipative: in this case again plastic hinges' formation is allowed, but limiting their rotation to a repairable limit state, that means allowing damage which can be repaired within a reasonable cost. This line of research is still open since it brings some main issues not yet solved, such as the definition of the repairable limit state. A possible approach is to apply an iterative cost-based design methodology, as proposed in Nuzzo et al. (2018), to be concluded when repair costs, output of a loss estimation analysis, satisfies the maximum allowed design threshold. Although, given the numerous efforts in studying and suggesting new technologies able to absorb seismic energy and prevent structural damaging, it is recommendable, if economically feasible, to employ them.
- Type c - elastic: in this case no plastic hinges are allowed to form. In correspondence of the PP the bare frame is supposed to be in the elastic field, thereby completely avoiding structural damage. This is the most expensive solution among the three cases in terms of construction cost, but it allows important savings if repair costs and recovering time after

the design seismic event's occurrence are considered. Moreover in this case the braced structure can be considered re-centering due to elastic behavior, thus avoiding residual drifts.

Once the F system's seismic behavior has been defined, it is possible to choose the target displacement d_{PP} to be achieved. In case of dissipative behavior, codes' indications for capacity design structures can be assumed, while for partially dissipative systems the repair limit displacement has to be identified. Differently, for elastic structures a target displacement limiting damage to non-structural elements could be chosen, belonging to the range 0.5-1% of interstorey drifts.
Successively, the base shear F_h generating a maximum interstorey drift equal to the target displacement on F system is distributed along the height, according to the following equation:

$$F_i = F_h \cdot \frac{W_i \cdot z_i}{\sum W_i \cdot z_i} \tag{B.1}$$

where W_i is the seismic weight of the i-th storey and z_i is its height. In this case F_h can be indicated as the base shear in correspondence of the target displacement in F system, $F_h = V_{PP,F}$.

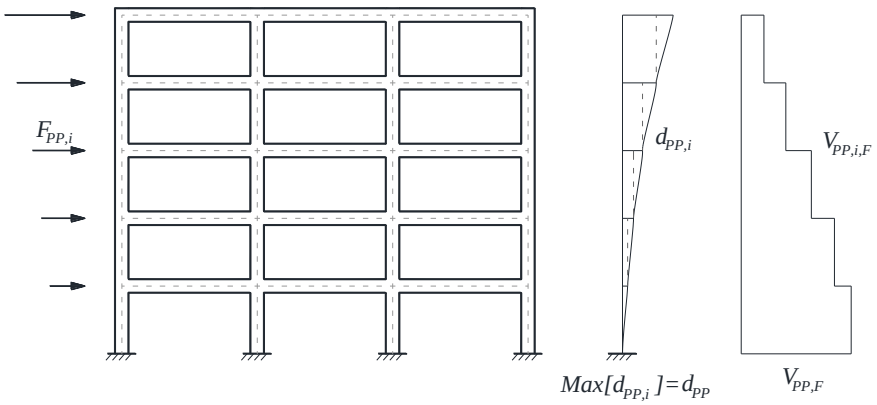

Figure 170 Distribution of relative displacements and shear forces at the target displacement in F system

At the end of this step the bare frame capacity curve is known, and it can be represented in the ADRS space after converting it to the equivalent single-degree-of-freedom-system and indicating its base shear at PP and elastic stiffness respectively as $V^*_{PP,F}$ and K^*_F. The equivalent SDOF roof displacement at PP is d^*_{PP}. The elastic ADRS curve is defined according to the seismic design intensity.

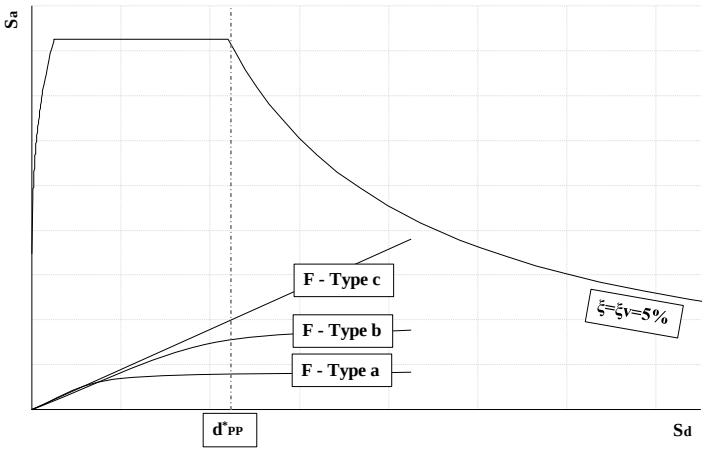

Figure 171 Step 1: definition of F system capacity curve

The proposed design procedure is applicable independently from the choice of the F system's behavior (type a, b or c). Although, for the sake of simplicity, the linear behavior is assumed in the following steps.

B.2 Step 2. Evaluation of the performance point

At the end of the previous step the target displacement and the F system capacity curve have been defined, but the PP is still unknown because the performance base shear of the equivalent BF system, $V^*_{PP,BF}$, depends from the design ADRS curve. Consequently it is necessary to evaluate the equivalent BF damping ratio, that can be calculated through the expression suggested by Mazza and Vulcano (2014):

$$\xi_{eq}^{BF}=\xi_v^F+\frac{\xi_h^F\cdot V^*_{PP,F}+\xi_h^{DB}\cdot V^*_{PP,DB}}{V^*_{PP,F}+V^*_{PP,DB}} \tag{B.2}$$

where

- ξ_v^F is the equivalent viscous damping ratio of F system, and it is assumed equal to 5%;
- ξ_h^F is the F equivalent hysteretic damping ratio and is equal to zero if F system is supposed elastic;
- ξ_h^{DB} is the DB equivalent hysteretic damping ratio and can be calculated as (Dwairi et al. 2007):

$$\xi_h^{DB}=63.7\cdot\frac{(\mu_{DB}^*-1)\cdot(1-r_{DB}^*)}{\mu_{DB}^*\cdot[1+r_{DB}^*\cdot(\mu_{DB}^*-1)]} \quad (B.3)$$

  In the above equation μ_{DB}^* and r_{DB}^* respectively correspond to equivalent DB ductility and post to pre-yielding stiffnesses ratio. These parameters are unknown and should be supposed by the designer based on engineering judgment, considering expected behavior of the dissipative system. As it will be clarified at step 5, the equivalent post to pre-yielding stiffnesses ratio r_{DB}^* will be verified at the end of the procedure, once effective braces' stiffnesses will have been defined.
- $V_{PP,F}^*$ is the equivalent F base shear at PP and it has been determined at step 1;
- $V_{PP,DB}^*$ is the equivalent DB base shear at PP, and it can be determined as the difference between the equivalent BF and F base shear values:

$$V_{PP,DB}^*=V_{PP,BF}^*-V_{PP,F}^* \quad (B.4)$$

  Note that the equivalent BF base shear is unknown as well, and it can be determined by the intersection of the design ADRS spectrum with the target displacement. Consequently, since the aim of this step is to evaluate the design spectrum, the BF equivalent damping ratio should be defined iteratively starting from a reasonable value according to the expected dissipative behavior (e.g. 10% or higher).

At the end of step 2 target displacement, F system's capacity curve, equivalent BF base shear and design ADRS spectrum are defined. Moreover, since a value

of equivalent DB ductility has been supposed, equivalent yielding displacement can be deducted as

$$d_y^* = d_{y,DB}^* = d_{y,BF}^* = \frac{d_{PP}^*}{\mu_{DB}^*} \tag{B.5}$$

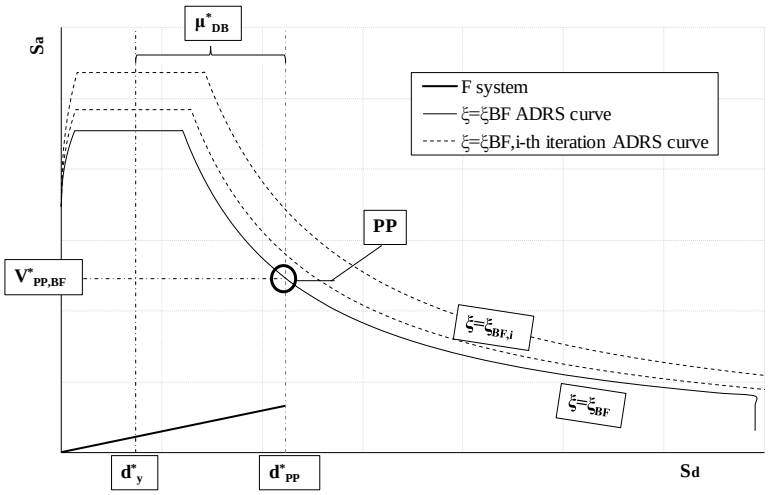

Figure 172 Step 2: definition of performance point PP

B.3 Step 3. Construction of BF capacity curve

In order to build BF capacity curve, it is necessary to evaluate the DB to F equivalent elastic stiffnesses ratio:

$$\alpha = \frac{K_{DB}^*}{K_F^*} \tag{B.6}$$

In equation (B.6) K^*_{DB} is the equivalent damped brace elastic stiffness, and it is still unknown. However, it is possible to demonstrate that starting from the simple equation

$$V_{PP,BF}^* = V_{y,BF}^* + K_{BF,py}^* \cdot \left(d_{pp}^* - d_y^*\right) \tag{B.7}$$

where $V^*_{y,BF}$ and $K^*_{DB,py}$ are respectively the BF equivalent yielding force and post-yielding stiffness, the parameter α can be evaluated as:

$$\alpha=\left(\frac{V^*_{PP,BF}}{K^*_F}-d^*_{pp}\right)\cdot\frac{1}{d^*_y+r^*_{DB}\cdot\left(d^*_{pp}-d^*_y\right)} \tag{B.8}$$

Once α has been estimated, it is possible to calculate the equivalent BF post-yielding stiffness as

$$K^*_{BF,py}=K^*_F+r^*_{DB}\cdot\alpha\cdot K^*_F \tag{B.9}$$

At this point, knowing the equivalent yielding displacement, the PP and the BF equivalent post-yielding stiffness it is possible to construct the BF capacity curve. Then, as difference between BF and F systems' performances at yielding point and at PP, the DB capacity curve can be derived as well.

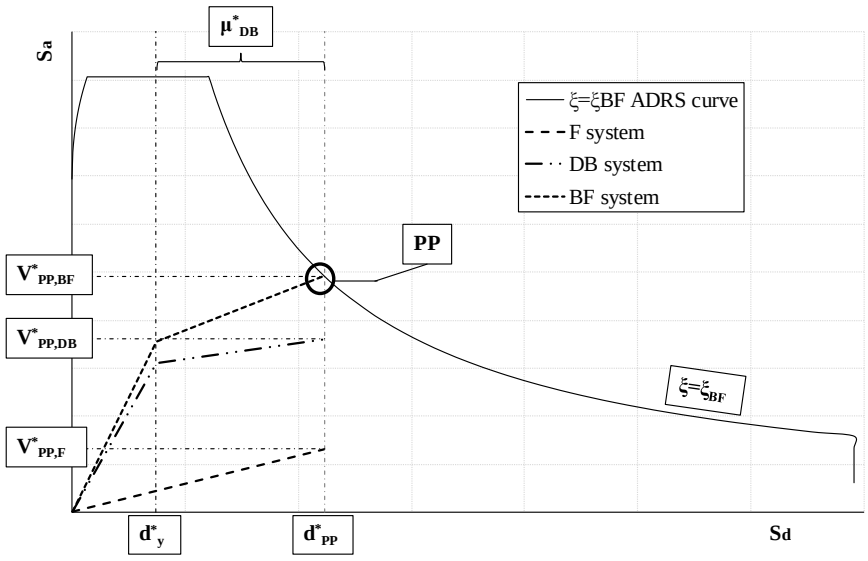

Figure 173 Step c: definition of BF and DB capacity curves

B.4 Step 4. Preliminary sizing of dissipative braces

Finally, once the equivalent yielding force and equivalent elastic stiffness of DB system are known, it is possible to distribute them at each floor of the real structure assuming the proportionality to F system's mechanical properties distribution:

$$\frac{K_{DB,i}}{K^*_{DB}} = \frac{K_{F,i}}{K^*_F} \tag{B.10}$$

$$\frac{V_{y,DB,i}}{V^*_{y,DB}} = \frac{V_{y,F,i}}{V^*_{y,F}} \tag{B.11}$$

where $K_{DB,i}$, $K_{F,i}$, $V_{y,DB,i}$ and $V_{y,F,i}$ are respectively horizontal elastic stiffnesses and yielding forces of dissipative braces and bare frame at the i-th storey. The post yielding stiffness at each storey, $K_{DB,py,i}$, can be evaluated multiplying the elastic DB stiffness at that storey by the post to pre yielding stiffnesses ratio of the real dissipative brace, $r_{DB,i}$, supposed to be known once the designer has chosen the dissipative brace system to adopt.

B.5 Step 5. Design check

At this point it is recommended to check if initial assumption about r^*_{DB} is coherent with real dissipative brace parameters, $r_{DB,i}$, verifying the satisfaction of the following equation:

$$r^*_{DB} = \frac{K^*_{DB,py}}{K^*_{DB}} \approx \frac{(d_{PP,i=1} - d_{y,i=1}) \cdot K_{DB,py,i=1}}{\sum_i d_{PP,i} - \sum_i d_{y,i}} \cdot \frac{1}{K^*_{DB}} \tag{B.12}$$

where $d_{PP,i}$ is the relative displacement of the i-th story at the performance point, and it is known from step 1 of the design procedure, while $d_{y,i}$ is the yielding relative displacement of the i-th story, and it can be calculated from the ratio $V_{y,DB,i}/K_{DB,i}$. If equation (B.12) is verified, the initial value assumed for r^*_{DB} can be considered satisfactory, otherwise it is necessary to iterate again the design procedure from step 2, assuming the new value of r^*_{DB} determined from equation (B.12).

Finally, it is necessary to check if the ductility of each equivalent dissipative $\mu_{DB,i}$ is coherent with the initial design assumption μ^*_{DB}, verifying the following equation:

$$\mu_{D,i} = \left(\mu_{DB,i} - \frac{1}{\frac{k_{B,i}}{k_{D,i}} + 1} \right) \cdot \left(1 + \frac{k_{D,i}}{k_{B,i}} \right) \tag{B.13}$$

where

$$\mu_{DB,i} = \frac{d_{PP,i}}{V_{y,DB,i} / k_{DB,i}} \tag{B.14}$$

Note that in the case in which the bare frame F is linear, the value of each dissipative brace's ductility $\mu_{DB,i}$ is constant and equal to $\mu^*_{DB,i}$.

If final mechanical properties of a single dissipative brace element are too demanding, it is possible to brace more bays at the i-th storey: in this case all dissipative braces at that floor would be working in parallel, then each elastic stiffness and yielding force would be given by the total equally divided by the number of elements adopted. If braces dimensions are still too large, it probably means that contribution provided by F system to the total BF performance is too low: it is necessary to increase beams and columns section's dimensions so that to relieve DB system. Alternatively, it is possible to modify target displacement, downgrading F system's performance to a more damageable construction.

Finally, once $K_{DB,i}$ and $V_{y,DB,i}$ of each dissipative brace have been determined, the design framework can be verified performing a pushover analysis of the braced frame system, so comparing desired BF capacity curve with the real one. The equivalent BF damping ratio can be calculated in correspondence of PP through Jacobsen's formula (Chopra 1997) and compared to the value obtained through equation (B.2). In this way it is possible to determine the real design ADRS curve and cross it with the numerical capacity curve, verifying if they meet at PP.

After the dimensioning of dissipative braces and the validation of the method through the pushover curve, dissipative braces have to be verified in terms of maximum deformation, while beams and columns in terms of stresses. Note that structures equipped with dissipative braces could suffer severe tension stress in columns. In order to limit this detrimental effect, a proper configuration of braces should be adopted within the structure. Moreover, also limiting dimensions of structural elements can reduce forces in correspondence of them.

APPENDIX C

Direct displacement-based design approach for base isolated structures

An important contribution to Direct Displacement-based Design method for Base Isolated (BI) structures is provided by Cardone et al. 2009, both for elastomeric and friction systems. The procedure is herein briefly summarized for rubber bearings. Conceptually the method is constructed from the observation that the superstructure and the isolation system, converted into the respectively equivalent Single Degree of Freedom Systems (SDOF), are subjected to the same force since they work as springs in series. Consequently, the method starts from the rough evaluation of the capacity curve of the superstructure system, which is linear in the hypothesis of new structures. Once it is known, it is possible to enter in the Acceleration Displacement Response Spectrum (ADRS), reduced of a damping ratio value compatible with the type of isolation system adopted, and read the design displacement value D_d of the isolation system in correspondence of the design force deducted from the superstructure's capacity curve (see Figure 174). In particular the base isolation system's design displacement D_d can be chosen in correspondence of a combination of damping ratio ξ_{is} and period T_{is} values respectively between ranges of admissible values, that corresponds to a pair of parameters falling within the red area of Figure 174.

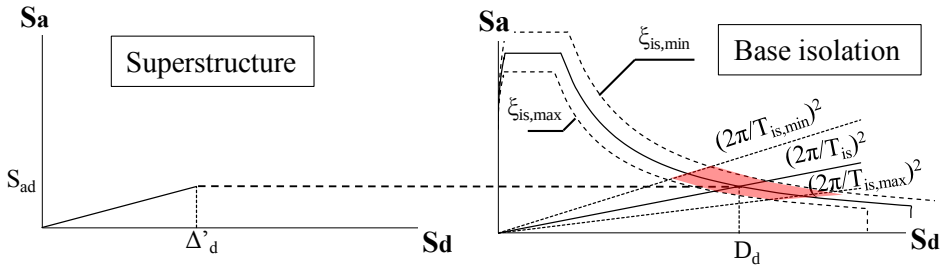

Figure 174 DDBD approach for base isolated systems - after Cardone et al. 2009

The capacity curve of the superstructure can be constructed after the choice of some characteristics, in particular:

- geometry, including beam and columns sections, according to functional and/or aesthetics requirements and non-seismic load conditions;
- design drift θ_d, to be chosen according to the level of protection from damage to be provided to the superstructure: in case of new buildings, a value between 0.3-0.5% should be adopted;
- rough estimation of the fundamental period of vibration of the equivalent fixed base structure, according to approximated formulations (e.g. $T_{fb}=0.075H^{3/4}$ for reinforced concrete frames of total height H);
- rough estimation of the design acceleration in correspondence of the superstructure, according to the following equation:

$$S_{ad}=\Delta'_d\cdot(k_{fb}/m'_e) \qquad (C.1)$$

where Δ'_d is the design displacement of the superstructure, k_{fb} and m'_e are respectively the elastic stiffness and the mass of the equivalent fixed base structure. Analytical expressions for the determination of the above parameters are detailed in Cardone et al. (2009).

At the end of this first preliminary design phase the method provides the isolators design displacement D_d, the equivalent damping ratio ξ_{is} and the period of vibration of the base isolated system T_{is}. At this step, it is possible to determine the equivalent SDOF system of the base isolated structure, determining its design displacement Δ_d and equivalent mass according to the

well known expressions (15) and (16) given at §4.4.1, where now the target displacement profile is described by the equation:

$$\Delta_i = D_d + \theta_d \cdot \frac{h_1}{100 \cdot \Phi_1} \cdot \Phi_i \qquad \text{(C.2)}$$

where Φ_i describes the displacement pattern according to the relation

$$\Phi_i = \cos\left[\frac{1}{I_r} \cdot \left(1 - \frac{h_i}{H}\right) \cdot \frac{\pi}{2}\right] - \cos\left[\frac{1}{I_r} \cdot \frac{\pi}{2}\right] \qquad \text{(C.3)}$$

in which H is the total height of the building, h_i the i^{th} interstorey height and I_r is the ratio between the effective period of vibration of the base isolation system T_{is} and the fundamental period of vibration of the fixed base building T_{fb}. At this point it is possible, as for traditional DDBD, enter into the design displacement response spectrum and read the equivalent period of vibration of the base isolated system. The equivalent damping ratio can be determined through the equation:

$$\xi_{eq} = \left[\xi_{is} \cdot D_d + \xi_s \cdot \left(\Delta_d - D_d\right)\right] / \Delta_d \qquad \text{(C.4)}$$

Finally, the equivalent stiffness and the base shear V_b can be determined as for the traditional DDBD. The base isolation stiffness can be calculated through equation:

$$K_{is} = V_b / D_d \qquad \text{(C.5)}$$

REFERENCES

Ali A., Hayah N.A., Kim D., Cho S.G. (2014). Probabilistic seismic assessment of base-isolated NPPS subjected to strong ground motions of Tohoku earthquake. Journal of Nuclear Engineering and Technology, Vol.46 no.5, October 2014. http://dx.doi.org/10.5516/net.09.2014.030

Alirezaei M., Noori M., Tatari O., Mackie K.R., Elgamal A. (2016). BIM-Based Damage Estimation of Buildings under Earthquake Loading Condition. Procedia Engineering 145 (2016) 1051 – 1058

Almufti, I., M. Willford (2013). Resilience-based earthquake design (REDi) Rating System. http://www.arup.com/Publications/REDi_Rating_System.aspx.

Almufti I., Willford M. (2014). The REDiTM rating system: a framework to implement resilience-based earthquake design for new buildings. Proceedings of 10th U.S. National Conference on Earthquake Engineering NCEE, Alaska, July 2014.

Akiyama H., Takahashi M., Shi Z. (1995). Ultimate energy absorption capacity of round −shape steel rods subjected to bending. J. Struct. Constr. Eng, AIJ, vol. 475, pp. 145–154.

Applied Technology Council (1996). Seismic evaluation and retrofit of existing concrete buildings. ATC-40, California.

Applied Technology Council (2011). Guidelines for Seismic Performance Assessment of Buildings, ATC-58, Redwood City, California.

Aslani H, Miranda M (2005). Probabilistic earthquake loss estimation and loss disaggregation in buildings. Blume Earthquake Engineering Center, Report No. 157, Stanford University

Baker J.W., Cornell C.A. (2006). Vector-valued ground motion intensity measures for probabilistic seismic demand analysis. Pacific Earthquake Engineering research Center, University of California, Berkeley 2006

Baker J.W., Cornell C.A. (2008). Uncertainty propagation in probabilistic seismic loss estimation. Structural Safety, 30 pag 236-252.

Baker J.W., Cremen G., Giovinazzi S., Seville E. (2016). Benchmarking FEMA P-58 performance predictions against observed earthquake data – A preliminary evaluation for the Canterbury earthquake sequence. Proceedings of NZSEE Conference.

Bazzurro P., Cornell C.A. (2002). Vector-valued probabilistic seismic hazard analysis (VPSHA). Proceedings of the 7th US National Conference on Earthquake Engineering, pp. 21-25

Beetham T. (2013). Simplified Displacement-Based performance assessment of retrofit alternatives for decision making. Master Degree in Earthquake Enineering, University of Pavia, Italy.

Benavent Climent A., Oh S.-H., Akiyama H. (1998). Ultimate energy absorption capacity of slit-type steel plates subjected to shear deformations. J. Struct. Constr. Eng, vol. No. 503, p. 139−147.

Benavent-Climent A. (2007). An energy-based damage model for seismic response of steel structures. Earthq. Eng. Struct. Dyn.

Bergman D.M., Goel S.C. (1987). Evaluation of cyclic testing of steel-plate devices for Added Damping And Stiffness," Rep. UMCE 87-10, Univ. Michigan.

Bollettino ufficiale della Regione Umbria. Elenco regionale dei prezzi e dei costi minimi della manodopera per lavori edili, impianti tecnologici, infrastrutture a rete, lavori stradali e impianti sportivi per l'esecuzione di opere pubbliche - Edizione 2014. Elenco regionale dei costi per la sicurezza dei lavoratori - Edizione 2014. Deliberazione della giunta regionale n.1371, 31 Ottobre 2014, (in Italian).

Bovo M., Bucci G.M., Savoia M. (2017). Comparison between seismic performance of different design philosophies by means of loss assessment analysis. Proceedings of XVII Conference ANIDIS - L'ingegneria sismica in Italia. Pistoia, Italy, September 2017.

Bozzo L.M., Cahís X., Torres L. (1998). A shear type energy dissipator for the protection of masonry infill walls. Proceedings of the Sixth U.S. National Conference on Earthquake Engineering, Seattle (Washington).

Bozzo L.M., Barbat A.H. (1999). Diseño sismorresistente de edificios. Técnicas convencionales y avanzadas. Barcelona: Editorial Reverte, 1999, (in Spanish).

Bradley B.A. (2009). User manual for SLAT: seismic loss assessment tool version 1.14", Research report 2009-01

Bradley B.A., Dhakal R.P., Cubrinovski M., MacRae G.A., Lee D.S. (2009). Seismic loss estimation for efficient decision making. Bulletin of the New Zealand society for earthquake engineering, Vol. 42, No 2, June 2009

Cutfield M.R., Ma Q.T., Ryan K.L. (2014). Cost-benefit analysis of base isolated and conventional buildings: a case-study. Proceedings of NZSEE Conference.

Cahís X., Bozzo L.M., Torres L., Foti D. (1997). An energy dissipating device for seismic protection of masonry infill walls. In ANIDIS procedia - Taormina.

Cahis X. (2000). Desarrollo de un nuevo disipador de energía para diseño sismorresistente. Análisis numérico y validación experimental de su comportamiento. Doctoral thesis (in Spanish) - Universitat Politècnica de Catalunya, (in Spanish).

Cardone D., Palermo G., Dolce M. (2009). Direct Displacement-Based Design of buildings with different seismic isolation systems. Journal of Earthquake Engineering 14:163-191

Castaldo P., Amendola G., Palazzo B. (2017). Seismic fragility and reliability of structures isolated by friction pendulum devices: seismic reliability-based design (SRBD). Earthquake Engineering and Structural Dynamics 2017; 46:425–446. DOI: 10.1002/eqe.2798

Chan R.W.K., Albermani F. (2008). Experimental study of steel slit damper for passive energy dissipation. Eng. Struct., vol. 30, no. 4, pp. 1058–1066.

Choi J., Abebe D.Y. (2013). Hysteresis Characteristics of Shear Panel Damper using SLY120. In APCBEE procedia, pp. 370–375.

Chopra A.K. (1997). Dynamics of structures: theory and application to earthquake engineering. Prentice-Hall Ltd., Englewood Cliffs, NJ.

Christopoulos C., Pampanin S., Priestley M.J.N. (2003). Performance-based seismic response of frame structures including residual deformations. part I: single-degree of freedom systems. Journal of Earthquake Engineering and Structural Dynamics 2003; Vol. 7, n° 1, pp. 97–118

Christopoulos C., Pampanin S. (2004). Towards performance-based seismic design of MDOF structures with explicit consideration of residual deformations. ISET Journal of Earthquake Technology, Vol. 41, No. 1, March 2004, pp. 53-73.

Christopoulos C., Filiatrault A. (2006). Principles of Passive Supplemental Damping and Seismic Isolation. IUSS Press, vol. 133, no. 8. p. 1192.

Christopoulos C., Filiatrault A. (2006). Principles of passive supplemental damping and seismic isolation. IUSS PRESS, Pavia, Italy.

Cimellaro G.P., Terzic V., Mahin S. (2015). Quantification of resilience improvements for critical facilities through advanced technologies. Proceedings of the 12th International Conference on Applications of Statistics and Probability in Civil Enginering (ICASP12). Vancouver, Canada, July 2015.

Clark P., Aiken I., Kasai K., Ko E., Kimura I. (1999). Design procedures for buildings incorporating hysteretic damping devices. Proceedings of 68th Annual Convention SEAOC, 1999, pp. 355–371.

Collegio degli ingegneri ed architetti di Milano. Prezzi per tipologie edilizie. DEI (in Italian).

Cordova P.P, Mehanny S.S.F., Deierlein G.G., Cornell C.A. (2001). Development of new seismic intensity measure and probabilistic design procedure. Proceedings of the 3rd U.S.-Japan Workshop on Performance-Based Seismic Design Methodology for Concrete Buildings, 2001

Cornell C A, Krawinkler H (2000). Progress and Challenges in Seismic Performance Assessment. *PEER Center News*, Vol. 3, No. 2.

Cosenza E., Manfredi G., Ramasco R. (1993). The use of damage functionals in earthquake engineering: a comparison between different methods. Earthquake engineering and structural dynamics, vol. 22, 855-868.

Dang Y., Han J.P., Li Y.T. (2015). Analysis of the seismic performance of isolated buildings according to Life-Cycle Cost. Journal of Computational intelligence and Neuroscience (Hindawi), Vol. 2015, Article ID 195042.

De Iuliis M, Petti L, Palazzo B (2008). Semi-active control of structures by using early warning seismic network information. Proceedings 4th European conference of structural control, p 367–374. ISBN: 9785904045104.

De Mare G., Morano P. (2002). La stima del costo delle opere pubbliche. Utet, Torino. Capitoli 1 e 2 (in Italian).

Del Vecchio C., Di Ludovico M., Pampanin S., Prota A. (2017). Actual versus predicted repair costs: case studies on RC buildings damaged by L'Aquila earthquake. Proceedings of 16th World Conference on Earthquake Engineering. Santiago, Chile.

Dhakal R.P. (2011). Structural design for earthquake resistance: past, present and future. Report to the Canterbury Earthquake Royal Commission. August 2011

DM 65 del 07/03/2017. Linee guida per la classificazione del rischio sismico in Italia – SismaBonus, (in Italian).

Dwairi H.M., Kowlsky M.J., Nau J.M. (2007). Equivalent damping in support of direct displacement-based design. J Earthquake Engineering 11:512-530.

Eads L., Miranda E., Lignos D.G. (2015). Average spectral acceleration as an intensity measure for collapse risk assessment. Earthquake Engineering and Structural Dynamics, 44(12), pp2057-2073.

Eastman C., Teicholz P., Sacks R., Liston K. (2011). BIM Handbook. A guide to building information modeling for owners, managers, designers, engineers and contractors. John Wiley & Sons, Inc.

Eurocode 0 “Basis of structural design” (2002), European Standard EN 1990. Brussels, 1990

Eurocode 8 “Design of structures for earthquake resistance—Part 1: General rules, seismic actions and rules for buildings”, European Standard EN 1998-1, Brussels, 2003

FEMA 273 (1996). NEHRP guidelines for the seismic rehabilitation of buildings. U.S. Federal Emergency Management Agency.

FEMA 274 (1996). NEHRP commentary on the guidelines for the seismic rehabilitation of buildings. U.S. Federal Emergency Management Agency.

FEMA P-58-1 (2012). Seismic performance assessment of buildings Volume 1 – Methodology.

FEMA P-58-2 (2012). Seismic performance assessment of building Volume 2 – Implementation guide.

FIP INDUSTRIALE S.r.l. leading technologies, Padova (Italy), http://www.fipindustriale.it

Fitzgerald K., Haselton C., Baker J., Cook D. (2016). Fragility Functions for the Precast Hybrid Moment Frame System. Background document for FEMA P-58 Fragility Function Creation, Haselton Baker Risk Group, March 2016

Garro Espinoza A. (2017). Cost-benefit evaluation of post-tensioned rocking-dissipative concrete buildings. Master degree, IUSS school (Pavia).

Ghobarah A. (2015). On drift limits associated with different damage levels. https://www.researchgate.net/publication/272353679

Gray M.G., Christopoulos C., Packer J.A. (2014). Cast Steel Yielding Brace System for Concentrically Braced Frames: Concept Development and Experimental Validations. J. Struct. Eng., vol. 140, no. 4, p. 4013095.

Haselton C.B., Baker J.W., Liel A.B., Dierlein G.G. (2009). Accounting for ground-motion spectral shape characteristics in structural collapse assessment through an adjustment for epsilon. Journal of Structural Engineering, 137(3), 332-344

Huang Y.N., Whittaker A.S., Luco N. (2010). Seismic performance assessment of base-isolated safety-related nuclear structures. Journal of Earthquake Engineering and Structural Dynamics 2010; 39:1421–1442

Hurtado F., Bozzo L. M. (2008). Numerical and experimental analysis of a shear-link energy dissipator for seismic protection of buildings. Proceedings of the 14th World Conference on Earthquake Engineering, 2008.

Iervolino I., Cornell C.A. (2005). Record selection for nonlinear seismic analysis of structures. Earthquake spectra, Vol.21 No.3., pp. 685-713, 2005

Iervolino I., Manfredi G., Cosenza E. (2006). Ground-motion duration effects on nonlinear strucutral response. Earthquake Engineering and Structural Dynamics, 35: 21-38.

Iervolino I., Manfredi G. (2008), A review of ground motion record selection strategies for dynamic structural analysis, Modern testing techniques for structural systems, pp 131-163

Iervolino I., Galasso C., Cosenza E. (2009). REXEL: computer aided record selection for code-based seismic structural analysis, Bulletin of Earthquake Engineering, 8:339-362, 2010. DOI 10.1007/s10518-009-9146-1

Kam W.Y., Pampanin S., Palermo A., Carr A.J. (2010). Self-centering structural systems with combination of hysteretic and viscous energy dissipations. Journal of Earthquake Engineering and Structural Dynamics 2010; 39:1083–1108

Kam W.Y., Pampanin S. (2012). Revisiting performance-based seismic design in the aftermath of the Christchurch 2010-2011: raising the bar to meet societal expectations. *Proceedings of World Conference on Earthquake Engineering*, Lisboa, Portugal.

Kanda K, Kobori T, Ikeda Y, Koshida H (1994). The development of a ‘‘Pre-arrival transmission system for earthquake information” applied to seismic response controlled structures. Proceedings of the 1st World conference on structural control, TA-3, p. 23–32.

Kato B., Akiyama H., Yamanouchi Y. (1973). Predictable properties of material under incremental cyclic loading. IABSE Reports Work. Comm., vol. 13, pp. 119–124.

Kelly JM (1999). The role of damping in seismic isolation. Earthquake Engineering and Structural Dynamics, 28(1):3–20.

Kobori T., Miura Y., Fukuzawa E. (1992). Development and application of hysteresis steel dampers. Proceedings of Earthquake Enginnering, Tenth World Conference, pp. 2341–2346.

Kotrotsou E., Aktas Y.D., Ioannou I. (2015). Seismic reliability of elastomeric base isolators. Proceedings of SECED 2015 Conference on Earthquake Risk and Engineering towards a Resilient World. 9-10 July 2015, Cambridge, UK.

Krawinkler H. (2002). A general approach to seismic performance assessment. Proceedings of International Conference on Advances and New Challenges in Earthquake Engineering Research, Hong Kong.

Krawinkler H., Miranda E. (2004). Performance-Based Earthquake Engineering. Chapter 9 from Earthquake Enginnering. From Engineering Seismology to Performance-Based Engineering. Edited by Bozorgnia Y. and Bertero V.V.. ICC 2004.

Ligabue V. (2015). Cost-effectiveness of alternative retrofit options to support decision making. PhD dissertation, University of Bologna, Italy.

Liu Y., Aoki T., Shimoda M. (2013). Strain Distribution Measurement of a Shear Panel Damper Developed for Bridge Structure. J. Struct., vol. 11.

Mahato J.K., De P.S., Sarkar A., Kundu A., Chakraborti P.C. (2014). Effect of prestrain and stress rate on bauschinger effect of monotonically and cyclically deformed ofhc copper. Procedia Eng., vol. 74, pp. 368–375.

Maia L., Mêda P., Freitas J.G. (2015). BIM methodology, a new approach - case-study of structural elements creation. Procedia Engineering 114 (2015) 816 – 823.

Mansouri I., Ghodrati Amiri G., Wan Hu J., Khoshkalam M., Soori S., Shahbazi S. (2017). Seismic Fragility Estimates of LRB Base Isolated Frames Using Performance-Based Design. Shock and Vibration, Volume 2017, Article ID 5184790, https://doi.org/10.1155/2017/5184790.

Marriott D.J., Pampanin S., Bull D., Palermo A. (2009). A probabilistic seismic loss assessment of advanced post-tensioned precast bridge systems. Proceedings NZSEE Conference.

Mayes R., Wetzel N., Weaver B., Tam K., Parker W., Brown A., Pietra D. (2013). Performance based design of buildings to assess damage and downtime and implement a rating system, *Bulletin of the New Zealand society for earthquake engineering*, Vol. 46, No 1.

Mazza F., Vulcano A. (2014). Displacement-based design procedure of damped braces for the seismic retrofitting of r.c. framed buildings. Bulletin of Earthquake Engineering, 13:2121-2143.

McKenna F.T. (1997). Object-oriented finite element programming: frameworks for analysis, algorithms and parallel computing. PhD dissertation, University of California, Berkeley (US)

Memari, A. M., Shirazi, A. and Kremer, P. A., (2007). Static Finite Element Analysis of Architectural Glass Curtain Walls Under In-Plane Loads and Corresponding Full-Scale Test. Structural Engineering and Mechanics Journal, Vol. 25, No. 4, pp. 365-382.

Miano A., Jalayer F., Prota A. (2016). Cloud to IDA: a very efficient solution for performing Incremental Dynamic Analysis. Conference paper, October 2016

Miranda E., Aslani H. (2002). Building-Specific loss estimation methodology. Report to PEER.

Miranda E., Eads L., Davalos H., Lignos D. (2017). Assessment of the probability of collapse of structures during earthquakes. Proceedings of the 16th World Conference on Earthquake Engineering, Santiago, Chile.

Nakashima M. (1995). Strain-hardening behavior of shear panels made of low-yield steel. I: Test. J. Struct. Eng., vol. 121 (12), pp. 1742–1749.

Nuzzo I., Losanno D., Serino G., Bozzo Rotondo L.M. (2014). A Seismic-resistant Precast r. c. System equipped with Shear Link Dissipators for Residential Buildings. Second Intl. Conf. Adv. Civil, Struct. Environ. Eng., vol. 2, no. 1, pp. 249–254.

Nuzzo I., Caterino N., Maddaloni G., Occhiuzzi A. (2017). Smart hybrid isolation of a case-study highway bridge exploiting seismic early warning information. Journal of Engineering Structures, Vol. 147, pp. 134-147.

Nuzzo I., Losanno D., Caterino N., Serino G., Bozzo Rotondo L.M. (2017). Experimental investigation of low cost steel shear links for seismic energy dissipation. Journal of Engineering Structures, under review.

Nuzzo I., Caterino N., Pampanin S. (2018). A cost-based seismic design framework for reinforced concrete frame structures: comparison of conventional and innovative construction techniques. Earthquake Engineering and Structural Dynamics. In submission.

Nuzzo I., Losanno D., Caterino N. (2018). Simplified seismic design method for dissipative braced structures. Engineering Structures. In submission

Nuzzo I., Losanno D., Cilento F., Caterino N. (2018). Analytical and numerical modeling of a shear link device based on experimental tests. Engineering Structures. In submission

Occhiuzzi A, Grasso VF, Manfredi G (2004). Early warning systems from a structural control perspective. Proceedings 3rd European conference on structural control.

Occhiuzzi A, Iervolino I, Manfredi G (2006). Feedforward control algorithms for seismic early warning systems. Proceedings 4th World conference on structural control and monitoring.

Occhiuzzi A, Caterino N, Maddaloni G (2008a). Exploitation of seismic early warning networks for structural control.Proceedigns 4th European conference on structural control.

Occhiuzzi A, Caterino N, Maddaloni G (2008b). Structural control strategies for seismic early warning systems. Proceedings 14th World conference on earthquake engineering.

Pagni C.A:, Lowes L.N. (2006). Fragility functions for older reinforced concrete beam-column joints. Earthquake Spectra 22(1): 215-238.

Palermo, A., Pampanin, S., Buchanan, A.H. and Newcombe, M.P. (2005). Seismic Design of Multi-storey Buildings using Laminated Veneer Lumber (LVL). Proceedings, New Zealand Society for Earthquake Engineering Conference, Wairakei.

Pampanin S., Priestley M.J.N., Sritharan S. (2001). Analytical modeling of the seismic behavior of precast concrete frames designed with ductile connections. Journal of Earthquake Engineering, Vol. 5, N°3, pp 329-367.

Pampanin S., Christopoulos C., Priestley M.J.N. (2002). Residual deformations in the performance-based seismic assessment of frame structures. ROSE school, IUSS press, September 2002

Pampanin S., Christopoulos C., Priestley M.J.N. (2003). Performance-based seismic response of frame structures including residual deformations. part II: multi-degree of freedom systems. Journal of Earthquake Engineering and Structural Dynamics 2003; Vol. 7, n° 1, pp. 119-147

Pampanin S. (2005). Emerging Solutions for High Seismic Performance of Precast/Prestressed Concrete Buildings. Journal of Advanced Concrete Technology (ACT), invited paper for Special Issue on "High performance systems", Vol. 3 (2), pp. 202-223

Pampanin, S., Palermo, A., Buchanan, A., Fragiacomo, M., Deam, B. (2006). Code Provisions for Seismic Design of Multi-Storey Post-tensioned Timber Buildings, CIB Workshop, Florence, August.

Pampanin S. (2009). Alternative Performance-Based retrofit strategies and solutions for existing RC buildings. Series "Geotechnical, Geological, and Earthquake Engineering, Volume 10" Chapter 13 within the Book "Seismic Risk Assessment and Retrofitting - with special emphasis on existing low rise structures"- (Editors: A. Ilki, F. Karadogan, S. Pala and E. Yuksel) Publisher Springer, pp. 267-295.

Pampanin S., Marriott D., Palermo A., Bolognini D. (2010). Presss design handbook. New Zealand Concrete Society NZSE.

Pampanin S. (2012). Reality check and renewed challenges in earthquake engineering: implementing low-damage systems - from theory to practice. Bulletin of New Zealand Society for Earthquake Engineering (NZSEE), Vol. 45, n° 4, December 2012

Park Y.J., Ang A.H.-S. (1985). Mechanistic seismic damage model for reinforced concrete, Journal of structural engineering, Vol. 111, n° 4, April 1985.

Paulay, T. and Priestley, M.J.N. (1992). Seismic Design of Reinforced Concrete and Masonry Buildings. John Wiley & Sons, Chichester, UK.

Pnevmatikos NG, Kallivokas LF, Gantes CJ (2004). Feed-forward control of active variable stiffness systems for mitigating seismic hazard in structures. Engineering Structures, 26:471–83. http://dx.doi.org/10.1016/j.engstruct.2003.11.003.

Popov E.P., M.D. Engelhardt (1988). Seismic eccentrically braced frames. J. Constr. Steel Res.

Prezzario Unico del Cratere del Centro Italia (2016). Ordinanza n°7 del Commissario del Governo per la Ricostruzione del 14/12/2016 (in Italian).

Priestley M.J.N. (1991). Overview of the PRESSS Research Programme PCI Journal. Vol.36, No.4, pp.50-57.

Priestley M.J.N. (1996). The PRESSS Program Current Status and Proposed Plans for Phase III. PCI Journal, Vol. 41, No. 2, pp. 22-40.

Priestley M.J.J. (1998). Displacement-Based approaches to rational limit states design of new structures. Keynote lecture at the 11th European Conference on Earthquake Engineering, Paris (France), 1998.

Priestley M.J.N., Sritharan S., Conley J.R., Pampanin S. (1999). Preliminary results and conclusions from the PRESSS five-story precast concrete test building. PCI Journal, 44(6), 42-67.

Priestley M.J.J. (2000). Performance Based Seismic Design. Proceedings of 12th World Conference on Earthquake Engineering.

Priestley M.J.J. (2002). Direct Displacement-Based Design of precast/prestressed concrete buildings. PCI, 6.

Priestley, M.J.N.; Calvi, G.M.; Kowalski, M.J. (2007). Diplacement Based Seismic Design of Structures. IUSS Press, Pavia, Italy.

Rai D.C., Wallaces B.J. (1998). Aluminium shear-links for enhanced seismic resistance. Earthq. Eng. Struct. Dyn., vol. 27, pp. 315–342.

Ramirez, C. M. and Miranda, E. (2009). Building specific loss estimation methods & tools for simplified performance-based earthquake engineering. Technical Report No. 171, John A. Blume Earthquake Engineering Center, http://blume.stanford.edu, Stanford University.

Ruiz-Garcia J., Negrete M. (2009). Drift-based fragility assessment of confined masonry walls in seismic zones. Engineering Structures 31: 170-181.

Saborío Romano D., Welch D.P., Sullivan T.J., Landi L. (2017). Comparison of loss assessment using refined analysis and simplified DDBA approach for an existing building in Italy. Proceedings of 16th World Conference on Earthquake Engineering. Santiago Chile.

Sahoo D.R., Rai D.C. (2010). Seismic strengthening of non-ductile reinforced concrete frames using aluminum shear links as energy-dissipation devices. Eng. Struct., 2010.

SEAOC Blue Book (1959). Recommended lateral force requirements and commentary. Seismology Commitee, Structural Engineers Association of California, First Edition.

SEAOC (1995). Vision 2000 - Performance-Based Seismic Engineering of buildings. Structural Engineers Association of California, Sacramento, California, USA.

Shi Y., Wang M., Wang Y. (2011). Experimental and constitutive model study of structural steel under cyclic loading. J. Constr. Steel Res., vol. 67, no. 8, pp. 1185–1197.

Shibata A., Sozen M. (1976). Substitute structure method for seismic design in reinforced concrete. Journal, Structural Division, ASCE Vol. 102 (6).

Shome N., Cornell C.A. (1998). Normalization and scaling accelerograms for nonlinear structural analysis. Proceedings of the 6th US National Conference on Earthquake Engineering, Seattle (WA), 1998

Shome N., Cornell C.A., Bazzurro P., Carballo J.E. (1998). Earthquakes, records and nonlinear responses, Earthquake Spectra, 14(3), pp. 469-500

Smerzini C., Paolucci R. (2013). SIMBAD: a database with Selected Input Motions for displacement-based Assessment and Design – 3rd release, Research Project DPC - RELUIS 2010-2013, Politecnico di Milano, January 2013

Soong TT, Spencer BF (2002). Supplemental energy dissipation: state-of-the-art and state-of-the-practice. Engineering Structure, 24:243–59.

Spizzuoco M., Calabrese A., Serino G. (2014). Innovative low-cost recycled rubber-fiber reinforced isolator: experimental tests and Finite Element Analyses. Engineering Structures, 76: 99-111.

Sporn B., Pampanin S. (2013). A "retrofit" solution for Force-Based Design: eliminating the need for iteration and initial period estimation. New Zealand Society for earthquake Engineering, Wellington (NZ), 2013.

Stone W.C., Taylor A.W. (1993). Seismic performance of circular bridge columns designed in accordance with AASHTO/CALTRANS standards. NIST building science series 170, February1993.

Sullivan, T. J. and Calvi, G. M. (2011). Considerations for the seismic assessment of buildings using the direct displacement-based assessment approach. Proceedings of the 2011 ANIDIS Conference, Bari 2011.

Symans M.D., Charney F.A., Whittaker A.S., Constantinou M.C., Kircher C.A., Johnson M.W. (2008) Energy Dissipation Systems for Seismic Applications: Current Practice and Recent Developments. J Struct Eng ASCE/JANUARY 2008/ DOI: 10.1061/(ASCE)0733-9445134:1(3).

Tasligedik AS, Pampanin S, Palermo A (2014) Low-damage seismic solutions for non-structural drywall partitions. Bull Earthq Eng 13(4):1029–1050

Tsai K.C., Chen H.W., Hong C.P., Su Y.F. (1993). Design of steel triangular plate energy absorbers for seismic-resistant construction. Earthq. Spectra, vol. 9:3, pp. 505–528.

U.S. Resiliency Council Building Ratings, www.usrc.org

Vamvatsikos D., Cornell C.A. (2002) Incremental dynamic analysis, Earthquake Engineering and Structural Dynamic, 31(3): 491-514.

Vamvatsikos D., Cornell C.A. (2002) The incremental dynamic analysis and its application to performance-based earthquake engineering. Proceedings of the 12th European Conference on Earthquake Engineering, London (UK).

Vitiello U., Asprone D., Di Ludovico M., Prota A. (2016). Life-Cycle Cost optimization of the seismic retrofit of existing RC structures. Bulletin of Earthquake Engineering, DOI 10.1007/s10518-016-0046-x

Vitiello U., Asprone D., Di Ludovico M., Prota A. (2016). BIM supporting economic optimization of seismic retrofit of existing structures. Proceedings of the Fifth International Symposium on Life-Cycle Civil Engineering - Life-Cycle of Engineering Systems: Emphasis on Sustainable Civil Infrastructure. Delft, The Netherlands, October 2016.

Welch D.P., Sullivan T.J., Calvi G.M., (2012). Towards a Direct Displacement-Based Loss Assessment methodology for RC frame buildings. Proceedings of the 15th World Conference on Earthquake Engineering, Lisboa, Portugal 2012.

Welch D.P., Sullivan T.J., Calvi G.M., (2014). Developing direct displacement-based procedures for simplified loss assessment in performance-based earthquake engineering. Journal of Earthquake Engineering, 18:290-322.

Whittaker A.S., Bertero V.V., Thompson C.L., Alonso L.J. (1991). Seismic Testing of Steel Plate Energy Dissipation Devices. Earthq. Spectra, vol. 7, no. 4, pp. 563–604.

Williams M.S., Sexsmith R.G. (1995). Seismic damage indices for concrete structures: a state-of-art review. Earthquake Spectra, vol. 11, n° 2, May 1995

Yang T.Y., Moehle J., Stojadinovic B., Der Kiureghian A. (2009). Seismic performance evaluation of facilities: methodology and implementation. Journal of structural engineering ASCE.

Yeo G.L., Cornell C.A. (2005). Stochastic characterization and decision bases under time-dependent aftershock risk in performance-based earthquake engineering. Report to PEER.